

A MATHEMATICAL MODEL FOR  
THE NONDETERMINISTIC ANALYSIS  
OF A MARINE RISER

TRACY CLARK TUCKER



LIBRARY  
NAVAL POSTGRADUATE SCHOOL  
MONTEREY, CALIF. 93940

T147299









A MATHEMATICAL MODEL FOR THE  
NONDETERMINISTIC ANALYSIS OF A MARINE RISER

BY

TRACY CLARK TUCKER

B.S., United States Naval Academy, 1960  
B.C.E., Rensselaer Polytechnic Institute, 1962  
M.S., University of Illinois, 1965

THESIS

Submitted in partial fulfillment of the requirements  
for the degree of Doctor of Philosophy in Civil Engineering  
in the Graduate College of the  
University of Illinois at Urbana-Champaign, 1972

Urbana, Illinois

T147299

LIBRARY

NAVAL POSTGRADUATE SCHOOL

MONTEREY, CALIF. 93940

A MATHEMATICAL MODEL FOR THE  
NONDETERMINISTIC ANALYSIS OF A MARINE RISER

BY

TRACY CLARK TUCKER

B.S., United States Naval Academy, 1960  
B.C.E., Rensselaer Polytechnic Institute, 1962  
M.S., University of Illinois, 1965

THESIS

Submitted in partial fulfillment of the requirements  
for the degree of Doctor of Philosophy in Civil Engineering  
in the Graduate College of the  
University of Illinois at Urbana-Champaign, 1972

Urbana, Illinois



Thesis  
T846

## ACKNOWLEDGMENTS

The author wishes to express his sincere appreciation to his advisor, Professor J. P. Murtha, for his invaluable guidance, suggestions, and encouragement during the course of this research. Acknowledgment is also extended to the Department of the Navy for the opportunity to pursue higher education and to the staffs of the Computing Services Office and the Civil Engineering Systems Laboratory for their assistance in the use of computer facilities. Special acknowledgment is expressed to Mrs. Joyce Sterner for her excellent preparation of the manuscript. Finally, the author wishes to thank his wife, Linda, whose patience and understanding made this task infinitely easier.



## TABLE OF CONTENTS

Chapter		Page
1	INTRODUCTION . . . . .	1
	1.1 The Marine Riser Problem . . . . .	1
	1.2 Importance of the Problem . . . . .	3
	1.3 Summary of Previous Work . . . . .	4
	1.4 Objective and Scope . . . . .	6
	1.5 Notation. . . . .	8
2	A MATHEMATICAL MODEL OF THE MARINE RISER. . . . .	14
	2.1 General . . . . .	14
	2.2 The Finite Difference Structural Model. . . . .	14
	2.3 Validity of the Finite Difference Structural Model . . . . .	19
	2.4 Tests of the Finite Difference Model of a Constant Tension Beam. . . . .	21
	2.5 Comparison of Riser Finite Difference Model Results With Other Approximate Solutions . . . . .	32
	2.6 Selection of Number of Nodes in the Finite Difference Model . . . . .	35
3	THE STATIC RESPONSE OF A MARINE RISER TO RANDOM WAVE FORCES . . . . .	36
	3.1 General . . . . .	36
	3.2 Method of Solution . . . . .	36
	3.3 Fluid Kinematic Spectra. . . . .	41
	3.4 Wave Force Spectra . . . . .	58
	3.5 Response Spectra . . . . .	65
	3.6 Sample Problem. . . . .	69
4	THE DYNAMIC RESPONSE OF A MARINE RISER TO RANDOM WAVE FORCES . . . . .	72
	4.1 General . . . . .	72
	4.2 Equation of Motion for Dynamic Riser Problem. . . . .	73
	4.3 The Riser Eigenvalue Problem - Natural Frequencies and Mode Shapes. . . . .	82
	4.4 Solution of the Equations of Motion. . . . .	88
	4.5 Derivation of Response Spectral Density Functions. . . . .	95
	4.6 Damping . . . . .	109





Chapter	Page
4.7	Variances and Covariances of Time Derivatives of Random Normal Coordinates . . . . . 117
4.8	Calculation of Standard Deviations of Relative Velocities . . . . . 118
5	THE DYNAMIC RESPONSE OF A MARINE RISER TO COMBINATIONS OF RANDOM WAVE FORCES, RANDOM TOP OFFSET, AND DETERMINISTIC CURRENT FORCES . . . . . 126
5.1	General . . . . . 126
5.2	Response to Random Wave Forces and Steady Current Forces . . . . . 126
5.3	Riser Response to Random Top Offset. . . . . 142
5.4	Total Response to Current, Waves, and Top Offset . . . . . 144
6	SAMPLE PROBLEMS . . . . . 146
6.1	General . . . . . 146
6.2	Riser Response to Random Waves Alone . . . . . 147
6.3	Riser Response to Random Waves and Steady Deterministic Current. . . . . 151
7	CONCLUSIONS AND RECOMMENDATIONS FOR FURTHER STUDY. . . . . 154
7.1	Conclusions. . . . . 154
7.2	Recommendations for Further Study . . . . . 156
	LIST OF REFERENCES . . . . . 158
	TABLES . . . . . 161
	FIGURES . . . . . 167
Appendix	
A	ANALYTICAL SOLUTION FOR THE DEFLECTED SHAPE OF A SIMPLE BEAM CAUSED BY A WAVE INERTIA FORCE DISTRIBUTION. . . . . 239
B	ANALYTICAL SOLUTIONS FOR THE DEFLECTED SHAPES OF A CONSTANT TENSION BEAM CAUSED BY WAVE DRAG AND INERTIA FORCE DISTRIBUTIONS . . . . . 242
C	SEA SURFACE ELEVATION SPECTRA . . . . . 248
VITA	. . . . . 255



## LIST OF TABLES

Table		Page
2.1	COMPARISON OF MARINE RISER NATURAL FREQUENCIES . . . . .	161
2.2	COMPARISON OF SERIES AND FINITE DIFFERENCE SOLUTIONS . . . . .	162



## LIST OF FIGURES

Figure		Page
1.1	Typical Marine Riser Installation . . . . .	167
1.2	Free Body Diagram of Deflected Riser . . . . .	168
1.3	Forces on Element of Riser Length . . . . .	169
2.1	Node Numbering Scheme . . . . .	170
2.2	Definition Sketch of Constant Tension Beam . . . . .	170
2.3	Frequency Ratios for Finite Difference Model of Constant Tension Beam . . . . .	171
2.4	Spatial Variation of Inertia Force. . . . .	172
2.5	Spatial Variation of Drag Force. . . . .	172
2.6	Definition Sketch of Simple Beam Subjected to Inertia Force . . . . .	173
2.7	Midspan Deflection Ratios for Simple Beam . . . . .	174
2.8	Schematic Representation of Lumped-Smeared Force Model . . . . .	175
2.9	Sketches Used in Derivation of Lumped-Smeared Force Model . . . . .	176
2.10a	End Rotation Ratios, Inertia Force, $kh = .01$ . . . . .	177
2.10b	End Rotation Ratios, Inertia Force, $kh = 10$ . . . . .	178
2.10c	End Rotation Ratios, Inertia Force, $kh = 100$ . . . . .	179
2.10d	End Rotation Ratios, Inertia Force, $kh = 10^5$ . . . . .	180
2.11a	Midspan Deflection Ratios, Inertia Force, $kh = .01$ . . . . .	181
2.11b	Midspan Deflection Ratios, Inertia Force, $kh = 10$ . . . . .	182
2.11c	Midspan Deflection Ratios, Inertia Force, $kh = 100$ . . . . .	183
2.11d	Midspan Deflection Ratios, Inertia Force, $kh = 10^5$ . . . . .	184





Figure	Page
2.12a	End Rotation Ratios, Drag Force, $kh = .01$ . . . . . 185
2.12b	End Rotation Ratios, Drag Force, $kh = 10$ . . . . . 186
2.12c	End Rotation Ratios, Drag Force, $kh = 100$ . . . . . 187
2.12d	End Rotation Ratios, Drag Force, $kh = 10^5$ . . . . . 188
2.13a	Midspan Deflection Ratios, Drag Force, $kh = .01$ . . . . . 189
2.13b	Midspan Deflection Ratios, Drag Force, $kh = 10$ . . . . . 190
2.13c	Midspan Deflection Ratios, Drag Force, $kh = 100$ . . . . . 191
2.13d	Midspan Deflection Ratios, Drag Force, $kh = 10^5$ . . . . . 192
2.14	Natural Frequencies of Vertical Marine Riser, $G_T = 1.0$ . . . . . 193
2.15	Perturbation Parameter. . . . . 194
3.1	Definition Sketch of Sea Surface Elevation . . . . . 195
3.2	Typical Sea Surface Elevation Spectrum . . . . . 195
3.3	Water Velocity Spectra. . . . . 196
3.4	Water Acceleration Spectra . . . . . 197
3.5	Root Mean Square Water Velocity Profiles. . . . . 198
3.6a	Static Bottom Rotation Spectrum for Ten Knot Wind Velocity. . . . . 199
3.6b	Static Bottom Rotation Spectrum for Twenty Knot Wind Velocity. . . . . 200
3.6c	Static Bottom Rotation Spectrum for Thirty Knot Wind Velocity. . . . . 201
3.6d	Static Bottom Rotation Spectrum for Forty Knot Wind Velocity . . . . . 202
3.7a	Effect of Wind Velocity on Mean Square Static Bottom Rotation . . . . . 203



Figure	Page
3.7b Effect of Wind Velocity on Root Mean Square Static Bottom Rotation . . . . .	203
4.1 Comparison of Fundamental Frequencies, $G_T = 1.0$ . . . .	204
4.2 Comparison of Fundamental Frequencies, $G_T = 1.2$ . . . .	205
4.3 Natural Frequencies of Typical Marine Riser, $G_T = 1.0$ . . . . .	206
4.4 Natural Frequencies of Typical Marine Riser, $G_T = 1.2$ . . . . .	207
4.5 Variation of Horizontal Reaction with Bottom Rotation of Riser . . . . .	208
4.6 Schematic Representation of Damping in Marine Riser . . . . .	209
5.1 Variation of Mean Bottom Rotation with Mean Top Offset . . . . .	210
5.2 Variation of Bottom Rotation Variance with Top Offset Variance . . . . .	211
6.1 Standard Deviation of Wave-Induced Bottom Rotation Versus Wind Velocity . . . . .	212
6.2 Bottom Rotation Spectrum Induced by 13 Knot SMB Spectrum . . . . .	213
6.3 Bottom Rotation Spectra Induced by 20 Knot PM Spectrum. . . . .	214
6.4 Bottom Rotation Spectra Induced by 25 Knot PM Spectrum. . . . .	215
6.5 Bottom Rotation Spectra Induced by 30 Knot PM Spectrum. . . . .	216
6.6 Variation of Damping Ratio with Depth, 30 Knot PM Spectrum. . . . .	217
6.7 Variation of Damping Ratio with Wind Velocity, 609 Ft Riser . . . . .	217
6.8 Profiles of Standard Deviation of Relative Water Velocity for 30 Knot PM Spectrum . . . . .	218





Figure		Page
6.9	Standard Deviation of Wave-Induced Bottom Rotation Versus Energy Density . . . . .	219
6.10	Comparison of SMB and PM Spectra . . . . .	220
6.11	Effect of Energy Density on Wave-Induced Bottom Rotation . . . . .	221
6.12	Standard Deviation of Maximum Wave-Induced Bending Moment . . . . .	222
6.13	Bottom Rotation Spectrum Produced by 20 Knot PM Spectrum. . . . .	223
6.14	Bottom Rotation Spectrum Produced by 30 Knot PM Spectrum. . . . .	224
6.15	Modal Contributions to Standard Deviation of Deflection . . . . .	225
6.16	Modal Contributions to Standard Deviation of Bending Moment . . . . .	226
6.17	Bottom Rotation Statistics for 609 ft Riser with 30 Knot, PM Waves and Uniform Current . . . . .	227
6.18	Effect of Uniform Current Velocity on Damping Ratio. . . . .	228
6.19	Effect of Uniform Current on Hydraulic Damping Coefficients . . . . .	229
6.20	Effect of Uniform Current on Standard Deviation of Relative Water Velocity . . . . .	230
6.21	Effect of Uniform Current on Deflection . . . . .	231
6.22	Effect of Uniform Current on Bending Moments . . . . .	232
6.23	Effect of Wind Driven Current on Bottom Rotation . . . . .	233
6.24	Effect of Wind Driven Current on Damping Ratios . . . . .	234
6.25	Comparison of Velocity Profiles. . . . .	235
6.26	Effect of Wind Driven Current on Hydraulic Damping Coefficients . . . . .	236



Figure		Page
6.27	Effect of Wind Driven Current on Deflection. . . . .	237
6.28	Effect of Wind Driven Current on Bending Moment . . . .	238
C.1	Sea Surface Elevation Spectra, 20 Knot Wind. . . . .	251
C.2	Sea Surface Elevation Spectra, 30 Knot Wind. . . . .	252
C.3	Sea Surface Elevation Spectra, 40 Knot Wind. . . . .	253
C.4	Average Energy Densities for Three Wave Spectra . . . .	254



## Chapter 1

### INTRODUCTION

#### 1.1 The Marine Riser Problem

##### 1.1.1 Description of the Marine Riser System

A marine riser is a long, slender pipe used in offshore drilling operations. Extending from a fixed or floating platform at the sea surface to a wellhead connection at the seafloor, the riser contains the drill string, which it guides and supports, and the drilling mud, which it returns to the surface for reuse. Figure 1.1 depicts a typical riser installation.

Risers with outside diameters of less than two feet are commonly used in water several hundred feet deep.<sup>1-3</sup> Such a long, slender structure tends to buckle under its own weight unless it is supported in some manner. To prevent buckling and reduce deflections, a tension force, which is usually somewhat greater than the total submerged weight of the riser system, is applied at the surface end of the riser.

Near the upper end of the riser, there is normally a slip joint which permits lengthening and shortening of the riser to compensate for changes in water depth caused by tides and waves. At the bottom end, where the riser connects to the blowout preventer, there is a flexible ball joint which permits some angular rotation without excessive bending when misalignment occurs.

In addition to its own weight and the supporting tension, the riser is also subjected to the hydrodynamic forces of currents and water waves and to stresses resulting from the relative lateral displacement of the riser ends, which occurs when the surface platform drifts off station.



### 1.1.2 The Riser Differential Equation

Figure 1.2 is a free body diagram of the deflected riser showing the coordinate system employed in this thesis and the loads involved in the problem. All applied loads and deflections are assumed to be coplanar.

The governing differential equation, which is derived by applying the equations of static equilibrium to the element of riser length shown in Fig. 1.3, is

$$\frac{d^2}{dx^2} \left( EI \frac{d^2 y}{dx^2} \right) - \frac{d}{dx} \left( T(x) \frac{dy}{dx} \right) = p(x) \quad (1.1)$$

where

- $E$  = the modulus of elasticity of the riser material
- $I$  = the moment of inertia of the riser cross section
- $T(x)$  = the axial tension in the riser
- $p(x)$  = the lateral force per unit length of the riser

Summation of forces in the vertical direction yields

$$\frac{dT(x)}{dx} = w(x) \quad (1.2)$$

where

$w(x)$  = the submerged weight of the riser system per unit length.

For risers considered herein,  $E$ ,  $I$ , and  $w$  are constant and Eq. 1.1 reduces to

$$EI \frac{d^4 y}{dx^4} - T(x) \frac{d^2 y}{dx^2} - w \frac{dy}{dx} = p(x) \quad (1.3)$$

When the lateral force intensity is time dependent, the response is also time dependent, and the equation of equilibrium is





$$m \frac{\partial^2 y}{\partial t^2} + c(x) \frac{\partial y}{\partial t} + EI \frac{\partial^4 y}{\partial x^4} - T(x) \frac{\partial^2 y}{\partial x^2} - w \frac{\partial y}{\partial x} = p(x, t) \quad (1.4)$$

in which  $m$  is the riser system mass per unit length and  $c(x)$  is a damping function.

In a structural sense, the marine riser is simply a tension beam whose axial tension varies along its length. Because of the varying tension, the governing differential equation does not possess a closed form solution. Therefore, in the structural analysis of the marine riser, it is necessary to employ an approximate method of solution.

## 1.2 Importance of the Problem

In riser installations, it is necessary to limit the bottom rotation to a few degrees.<sup>3,4</sup> The maximum rotation must be less than that permitted by the design of the ball joint, which is usually about ten degrees. It is seldom possible, however, to attain such a rotation without producing excessive stresses in the riser. Moreover, in most installations, if the rotation is more than a few degrees, the drill pipe rubs against the riser, the ball joint, the blowout preventer, and the well casing resulting in wear which is great enough to constitute failure.<sup>3</sup>

Bottom rotation is controlled, in part, by the positioning system used to keep the surface support platform on station. Whether a conventional mooring system or a dynamic positioning system is used, accurate information describing the behavior of the riser in its operating environment is needed for proper design of the system.

Offshore drilling operations are expensive. The failure of a marine riser system results not only in the loss of costly hardware, but also in the loss of considerable productive time which is valued in thousands



of dollars per day. Thus, there is much practical significance in any method of analysis which leads to a better understanding of riser behavior under random environmental loads and reduces the risk of unexpected failure.

Published methods of riser analysis consider the effects of current, top offset, and top tension, but often ignore dynamic wave loads. Because the marine riser is a long, flexible structure, its fundamental period of vibration is typically on the order of a few seconds. Ocean waves generally have periods ranging from six to thirty seconds. Hence, it is not uncommon for one or more of the riser natural periods to be in the range of wave periods, where the dynamic response is significantly greater than the static response. Neglecting the dynamic nature of the wave forces may result in unacceptable error in response calculations.

Even when wave forces are considered, the approach used in published analyses is to calculate deterministically the response to a design wave of a given height and frequency. Anyone who has seen the ocean will agree that unlike a simple design wave, real waves are extremely complex and highly irregular. A more realistic alternative to the design wave approach is to treat the wave forces as the random physical phenomenon which they are and calculate the random response caused by these forces. Such an approach is used in this thesis.

### 1.3 Summary of Previous Work

There are two separate areas of previous research which form a basis for this thesis. The first of these is the development of approximate methods of analyzing beams with varying axial tension. Fischer and Ludwig<sup>4</sup> utilized the infinite power series method to calculate the response of a marine riser to a static current force and constant top deflection. This



approach was also employed by Huang and Dareing<sup>5</sup> to determine the natural frequencies of beams with variable tension. Frohrib and Plunkett<sup>6</sup> used a perturbation solution to determine the natural frequencies of a drill string. Finite difference methods were employed in the analysis of the drilling riser which was to have been used in Project Mohole<sup>7,8</sup> and have been utilized in the study of marine risers up to 1,300 feet long for offshore oil drilling.<sup>9</sup> Because the finite difference method permits a simple transformation of the governing differential equation into matrix form, a form which is convenient for machine computation, that method is used here for the calculation of riser response to random environmental forces.

The second body of previous research to which this thesis is indebted is the development of models which accurately describe the random nature of ocean waves and the random forces they cause on submerged objects. Excellent comprehensive summaries of this development have been given by Pierson<sup>10</sup> and Neumann and Pierson.<sup>11</sup> Some of the more noteworthy milestones will be mentioned here. Fundamental to this development was the work of Rice<sup>12</sup> on the statistical properties of Gaussian processes. The demonstration by Pierson and others<sup>10</sup> that the sea surface is essentially a Gaussian random process paved the way for the applications of Rice's work to the study of ocean waves. Longuet-Higgins<sup>13</sup> showed that the random wave heights for a narrow band spectrum have a Rayleigh probability distribution. From this early theoretical work and oceanographic observations, several models were formulated for the spectral density function of the sea surface elevation.<sup>14-16</sup>

A significant extension of the work on ocean wave spectra was accomplished by Borgman,<sup>17,18</sup> who derived expressions for the spectral



density functions of ocean wave forces on piles and demonstrated their validity by comparison with observed force spectra. Borgman's work opened the door to treatment of the response of ocean structures to wave forces as a random vibration problem. Such an approach was used by Foster<sup>19</sup> and Malhotra and Penzien,<sup>20,21</sup> who adapted Borgman's model to the nondeterministic analysis of offshore towers; such an approach is also used in this thesis in the nondeterministic analysis of marine risers.

#### 1.4 Objective and Scope

The objective of this thesis is to develop a mathematical model for predicting the random dynamic response of a marine riser to a combination of random wave forces, deterministic steady current forces, and random operational movement of the surface support platform. Wave induced platform motion is not included in the model.

The finite difference method is used to transform Eq. 1.3 into the matrix form

$$[K]_{n \times n} \{y\}_{n \times 1} = \{p\}_{n \times 1} \quad (1.5)$$

where

$[K]$  = a stiffness matrix whose elements are derived by application of difference equations at each of  $n$  nodes along the riser axis

$\{y\}$  = a vector of node deflections

$\{p\}$  = a vector of force intensities at the nodes

While it is expected that the accuracy of the finite difference model depends on the number of nodes used in the model, there is no way to determine a priori how many nodes must be used to accurately represent the real structure.





In Chapter 2, the effect of the number of nodes on model accuracy is investigated, and criteria are established for selecting the number of nodes.

Treatment of the riser problem in this thesis differs from published methods of analysis in that the wave forces and top offset are considered to be Gaussian, stationary random variables. It is shown that the riser response is also a Gaussian, stationary random variable, whose probability density function is thus completely determined by the mean and variance. Because the mean response can be set to zero by a transformation of coordinates, knowledge of the response variance is sufficient to make probability calculations. The response variance is obtained by integrating the response spectral density function with respect to frequency. Thus, one objective of this thesis is to develop expressions for the spectral density functions of response parameters which result from a random sea represented by the oceanographer's sea surface elevation spectrum.

Initially, only the response caused by random waves is considered. In Chapter 3, static response spectral density functions are derived, and examples are given to show how nondynamic effects influence riser response. Dynamic response spectral density functions resulting from waves alone are derived in Chapter 4. Modification of the hydrodynamic forces by wave structure interaction is considered. The model is completed in Chapter 5 where dynamic response spectral density functions caused by a combination of random waves and a steady deterministic current are derived, and the influence of random top offset on response variance is determined. In Chapter 6, the results of several sample calculations are used to show the effects of various problem parameters on the response.



## 1.5 Notation

Each symbol used in this thesis is defined where it first appears in the text. For ease of reference, the notation is summarized here.

[B] transformation matrix relating random moments to normal coordinates

$C_a$  coefficient equal to  $C_I \rho \frac{\pi D^2}{4}$

$C_u$  coefficient equal to  $\frac{1}{2} C_D \rho D$

$C_D$  drag coefficient

$C_I$  inertia coefficient

$[C_0]$  modal damping matrix

$[C^*]$  diagonalized modal damping matrix

D riser outside diameter

E modulus of elasticity

$E[]$  expectation operator

$E^*$  energy density per unit sea surface area

$\{E\}$  error vector

F probability distribution function

$G_T$  top tension ratio

$G_L$  length ratio



$H$	wave height
$H(\Omega)$	complex frequency response function
$I$	moment of inertia of riser cross section
$[J]$	transformation matrix relating random moments to deflections
$[K]$	riser stiffness matrix
$L$	riser length
$L^*$	parameter equal to $\frac{L^4}{(n+1)^4 EI}$
$\tilde{L}$	wave length
$M(x,t)$	random bending moment in riser
$P(x,t)$	random hydrodynamic force intensity
$P_0(x,t)$	force intensity equivalent to top offset
$\{P^*\}$	vector of random modal forces
$p$	probability
$R(\cdot)$	correlation function
$S(\Omega)$	one-sided spectral density function
$\dot{S}(\Omega)$	two-sided spectral density function
$T$	axial tension in riser
$T_L$	tension at top end of riser



$T_0$	tension at bottom end of riser
$T^*$	parameter equal to $\frac{TL^2}{(n+1)^2EI}$
$U(x,t)$	random horizontal water particle displacement caused by waves
$\dot{U}(x,t)$	horizontal component of random water particle velocity due to waves
$V(x,t)$	horizontal component of wave induced water particle displacement with respect to structure
$\dot{W}(x,t)$	random vertical component of water particle velocity due to waves
$Y(x,t)$	random horizontal deflection of riser due to waves and current
$\bar{Y}(x,t)$	random horizontal deflection of riser due to top offset
$\hat{Y}(x,t)$	total random horizontal deflection of riser
$Y_{top}(t)$	random top offset
$\{b\}$	vector of influence coefficients relating top offset to riser deflections
$[c]$	structure damping matrix
$[\tilde{c}]$ , $\{\tilde{c}\}$	equivalent linear damping matrices
$[c_e]$	environmental damping matrix
$e$	base of natural logarithms





$f$	probability density function
$g$	gravitational constant, $32.2 \text{ ft/sec}^2$
$h$	water depth
$\hat{h}$	impulse response function
$i$	$\sqrt{-1}$
$ic, jc$	subscripts of spectral components
$k$	wave number
$m$	mass of riser system per unit length
$m_e$	effective mass of riser system and surrounding water
$n$	number of nodes in finite difference model
$nc$	number of spectral components
$ni, nj, nk, nl$	subscripts on riser model nodes
$nm$	number of natural modes in solution
$p(x,t)$	lateral force intensity on riser
$\{\tilde{p}\}$	vector of force intensities due to lateral loads and top offset
$\tilde{q}$	spatial wave force modifier
$r, s$	subscripts on natural modes
$t$	time



$t_d$	duration of environmental conditions
$\dot{u}(x,t)$	horizontal component of water particle velocity
$\dot{u}_c$	steady current velocity
$\ddot{u}(x,t)$	horizontal component of water particle acceleration
$v_w$	wind velocity
$w$	submerged weight of riser system per unit length
$w^*$	a parameter equal to $\frac{wL^3}{2(n+1)^3EI}$
$x$	vertical coordinate
$y$	horizontal coordinate
$\Gamma(\Omega)$	power transfer function
$\theta_0(t)$	random bottom rotation
$\Lambda$	ratio of finite difference solution to analytical solution
$\sum$	summation operator
$\phi$	velocity potential
$\psi$	random phase angle
$\Omega$	spectral frequency
$\alpha$	ratio of current velocity to standard deviation of relative water velocity with respect to structure



$\beta$	internal friction damping ratio
$\gamma$	unit weight of water
$\delta$	Dirac delta function
$\zeta$	total damping ratio
$\eta(t)$	sea surface elevation
$\mu$	mean value; tension beam parameter equal to $\sqrt{T/EI}$
$\nu$	radius of gyration of area under spectral density function
$\xi$	dummy time variable
$\rho$	mass density of water
$\sigma$	standard deviation
$\sigma^2$	variance
$\tau$	time lag
$\phi$	mode shape
$\omega$	natural frequency of riser

Each dot over a symbol indicates a derivative with respect to time. Thus,  $\ddot{U}(x,t)$  is the horizontal component of random water acceleration caused by waves.



## Chapter 2

### A MATHEMATICAL MODEL OF THE MARINE RISER

#### 2.1 General

In this chapter, the governing differential equation of the marine riser is transformed into matrix form using the method of finite differences. This mathematical model of the structure is then tested by comparing the results of finite difference analysis to known exact solutions and published approximate solutions, and the number of nodes necessary to accurately model the structure is determined. In the process of establishing the validity of the finite difference structural model, a modified wave force model is also evolved and tested.

#### 2.2 The Finite Difference Structural Model

In the finite difference method, a continuous structure having an infinite number of degrees of freedom is represented by a mathematical model having a finite number of degrees of freedom. The differential equation of the continuous structure is transformed into a system of simultaneous algebraic equations by substituting difference equations for the derivatives in the differential equation at each of a finite number of discrete points or nodes along the riser length.

Consider the riser to be divided into  $n+1$  increments of equal length,  $\Delta x = \frac{L}{n+1}$ , joined by  $n$  interior nodes as shown in Fig. 2.1. Nodes 0 and  $n+1$  are at the bottom and top ends of the riser respectively, and nodes  $-1$  and  $n+2$  are imaginary nodes located a distance  $\Delta x$  below the bottom and above the top. The finite difference model is formed by writing





Eq. 1.3 at each of the interior nodes and replacing the derivatives with standard central difference equations.<sup>22</sup>

$$(\Delta x)^4 \frac{d^4 y}{dx^4} = y_{ni-2} - 4y_{ni-1} + 6y_{ni} - 4y_{ni+1} + y_{ni+2} \quad (2.1)$$

$$(\Delta x)^2 \frac{d^2 y}{dx^2} = y_{ni-1} - 2y_{ni} + y_{ni+1} \quad (2.2)$$

$$2(\Delta x) \frac{dy}{dx} = -y_{ni-1} + y_{ni+1} \quad (2.3)$$

Multiplication of each term of Eq. 1.3 by

$$\frac{(\Delta x)^4}{EI} = \frac{(\Delta x)^2}{EI} \frac{L^2}{(n+1)^2} = \frac{\Delta x}{EI} \frac{L^3}{(n+1)^3} = \frac{L^4}{EI(n+1)^4} \quad (2.4)$$

results in

$$\begin{aligned} (\Delta x)^4 \frac{d^4 y}{dx^4} - \frac{T}{EI} \frac{L^2}{(n+1)^2} (\Delta x)^2 \frac{d^2 y}{dx^2} - \frac{wL^3}{2(n+1)^3 EI} (2\Delta x) \frac{dy}{dx} \\ = \frac{PL^4}{(n+1)^4 EI} \end{aligned} \quad (2.5)$$

The substitution of Eqs. 2.1, 2.2, and 2.3 into Eq. 2.5 yields

$$\begin{aligned} y_{ni-2} - 4y_{ni-1} + 6y_{ni} - 4y_{ni+1} + y_{ni+2} \\ - T_{ni}^* (y_{ni-1} - 2y_{ni} + y_{ni+1}) \\ - w^* (-y_{ni-1} + y_{ni+1}) = p_{ni} L^* \end{aligned} \quad (2.6)$$

where

$$T_{ni}^* = \frac{T(x_{ni})L^2}{(n+1)^2 EI} \quad (2.7a)$$



$$w^* = \frac{wL^3}{2(n+1)^3EI} \quad (2.7b)$$

$$L^* = \frac{L^4}{(n+1)^4EI} \quad (2.7c)$$

$$p_{ni} = p(x_{ni}) \quad (2.7d)$$

and  $x_{ni}$  is the  $x$  coordinate of node  $ni$ . The terms of Eq. 2.6 may be conveniently rearranged so as to combine coefficients of the node deflections.

$$\begin{aligned} y_{ni-2} + [-4 - T_{ni}^* + w^*]y_{ni-1} + [6 + 2T_{ni}^*]y_{ni} \\ + [-4 - T_{ni+1}^* + w^*]y_{ni+1} + y_{ni+2} = p_{ni}L^* \end{aligned} \quad (2.8)$$

When Eq. 2.8 is applied at each of the nodes, there result  $n$  simultaneous linear algebraic equations in  $n+4$  unknown deflections.

The number of unknown deflections is reduced to  $n$  by application of the four boundary conditions. At the lower end of the riser,  $x = 0$ , the deflection and moment are zero.

$$y_0 = 0 \quad (2.9a)$$

$$\begin{aligned} M(0) &= -EI \frac{d^2y_0}{dx^2} \\ &= -EI \frac{1}{(\Delta x)^2} [y_{-1} - 2y_0 + y_1] = 0 \end{aligned}$$

Therefore,

$$y_{-1} = -y_1 \quad (2.9b)$$

The top deflection,  $y_{n-1} = y_{top}$ , which is the lateral displacement of the surface support platform, is considered as an input parameter and therefore



not an unknown, and the top moment is taken as zero.

$$M_{\text{top}} = -EI \frac{d^2 y}{dx^2} \Big|_{x=h} = 0$$

From Eq. 2.2,

$$\frac{d^2 y}{dx^2} \Big|_{x=h} = \frac{1}{(\Delta x)^2} [y_n - 2y_{\text{top}} + y_{n+2}] = 0$$

Therefore, the deflection of the imaginary node  $n+2$  is

$$y_{n+2} = 2y_{\text{top}} - y_n \quad (2.10)$$

Equations 2.8, 2.9, and 2.10 are conveniently expressed in matrix form,

$$[K]_{n \times n} y_{n \times 1} = \{P\}_{n \times 1} \quad (2.11)$$

The stiffness matrix,  $[K]$ , is a five-term banded matrix whose nonzero elements are

$$K_{1,1} = \frac{1}{L^*} (5 + 2T_1^*) \quad (2.12a)$$

$$K_{n,n} = \frac{1}{L^*} (5 + 2T_n^*) \quad (2.12b)$$

$$K_{ni,ni} = \frac{1}{L^*} (6 + 2T_{ni}^*), \quad ni = 2, n-1 \quad (2.12c)$$

$$K_{ni,ni-1} = \frac{1}{L^*} (-4 - T_{ni}^* + w^*), \quad ni = 2, n \quad (2.12d)$$

$$K_{ni,ni+1} = \frac{1}{L^*} (-4 - T_{ni}^* - w^*), \quad ni = 1, n-1 \quad (2.12e)$$



$$K_{ni,ni+2} = \frac{1}{L^*}, \quad ni = 1, n-2 \quad (2.12f)$$

$$K_{ni,ni-2} = \frac{1}{L^*}, \quad ni = 3, n \quad (2.12g)$$

Elements of the vector  $\{y\}$  are the node displacements, and  $\{\tilde{p}\}$  is a vector of load intensities in which

$$\begin{aligned} \tilde{p}_{n1} &= p_{ni} & ni &= 1, n-2 \\ \tilde{p}_{n-1} &= p_{n-1} - \frac{y_{top}}{L^*} \\ \tilde{p}_n &= p_n + (2 + T_n^* + w^*) \frac{y_{top}}{L^*} \end{aligned} \quad (2.13)$$

The riser axial tension, which is used to compute  $T_{ni}^*$ , is determined by integrating Eq. 1.2. The tension at coordinate  $x$  is

$$T(x) = T_0 + wx \quad (2.14)$$

where  $T_0$ , the axial tension at the lower end of the riser, is given by

$$T_0 = T_L - wL \quad (2.15)$$

and  $T_L$  is the axial tension at the surface.

Equations 2.11, 2.12, and 2.13 describe the finite difference model of the marine riser in matrix form. It is of interest to compare this model with the finite difference model used by Butler, et al.,<sup>7</sup> for engineering studies of the Project Mohole drilling riser. The formulation of the Mohole model was somewhat different from the formulation of the model presented herein. For the Mohole riser, axial tension was considered to be constant





between nodes, and changes in tension were concentrated at the nodes. The Mohole model was also derived for the general case of variable EI, which could have been done here by applying the finite difference equations to Eq. 1.1 instead of Eq. 1.3. When the Mohole riser equations are written for the case of constant EI, they are identical to those derived herein.

## 2.3 Validity of the Finite Difference Structural Model

In subsequent chapters of this thesis, the finite difference structural model is used as a component of a larger mathematical model for calculating the riser response to random wave forces. The validity of this larger mathematical model depends, in part, on the validity of the finite difference structural model. Therefore, before the finite difference model is applied, it is prudent to consider the question, "How well does the model represent the continuous riser system?"

In judging the validity of the finite difference model, two criteria are of particular interest. Because normal mode superposition is used in the dynamic analysis of the riser, its natural frequencies and mode shapes must be determined. The first criterion, then, is that the natural frequencies and mode shapes of the finite difference model must be reasonably close to the actual natural frequencies and mode shapes of the continuous riser structure. To be effective, the finite difference model must also give node deflections, rotations, and moments which do not differ significantly from the actual deflections, rotations, and moments. Therefore, the second criterion is that the deflected shape of the finite difference model must reasonably approximate the deflected shape of the actual riser. Since the random forces in the riser problem are those produced by ocean waves, it is especially important to study the accuracy of the deflected shape of the model



when the applied force distribution is that which is typical of ocean waves.

In order to form a judgment as to how well the finite difference model meets these two criteria, a standard for comparison is needed. The obvious standard is an analytical solution, if it exists. However, the marine riser has no closed-form solution, and therefore some other standard must be sought.

One approach to testing the validity of the finite difference model is to perform the tests on a structure similar to the riser, but having an analytical solution which can be used as the standard for comparison. This approach is used in Section 2.4, where a constant tension beam is modeled by the method of finite differences. The validity of this model is tested by comparing the natural frequencies, mode shapes, and deflected shapes of the model with the corresponding analytical solutions to the constant tension beam. In the process of testing the deflected shape of the model under wave loads, an improved wave force model is developed and tested.

While validity tests of the finite difference method with the constant tension beam as a test structure are certainly worthwhile, some tests of the riser finite difference model are also definitely in order. In the absence of a closed-form solution to the riser equation, the only standard for comparison is the results of other approximate methods of analysis. In Section 2.5, the natural frequencies and deflected shapes of the riser finite difference model are compared to other published solutions.



## 2.4 Tests of the Finite Difference Model of a Constant Tension Beam

### 2.4.1 Formation of the Finite Difference Model

The constant tension beam, which is shown in Fig. 2.2, is identical to the marine riser with one exception. Because  $dT/dx = 0$ , the governing differential equation of the constant tension beam is

$$EI \frac{d^4 y}{dx^4} - T \frac{d^2 y}{dx^2} = p(x) \quad (2.16)$$

It follows that the stiffness matrix for the finite difference model of the constant tension beam is identical to that given by Eqs. 2.12 for the riser except that  $T^*$  is a constant and

$$K_{ni,ni-1} = K_{ni,ni+1} = \frac{1}{L} (-4 \quad -T^*) \quad (2.17)$$

### 2.4.2 Tests of Natural Frequencies and Mode Shapes

#### Finite Difference Solution

The natural frequencies and mode shapes of the finite difference model are found by letting the force intensity vector of Eq. 2.11 represent the d'Alembert forces, all other externally applied forces being zero.

$$\{\tilde{p}\} = -m \frac{\partial^2}{\partial t^2} \{y(x,t)\} \quad (2.18)$$

in which  $m$  is the mass per unit length of the riser system. Application of the method of separation of variables leads to the characteristic equation,

$$[K] \{y\} = m\omega^2 \{y\} \quad (2.19)$$

Solutions to Eq. 2.19 are the natural frequencies,  $\omega_r$ ,  $r = 1, 2, \dots, n$  and mode shapes,  $\{\phi^{(r)}\}$ , of the finite difference model.



## Analytical Solution

The analytical solution for the natural frequency and shape of the  $r^{\text{th}}$  mode of a constant tension beam is<sup>23</sup>

$$\omega_r = r^2 \frac{\pi^2}{L^2} \sqrt{\frac{EI}{m} + \frac{TL^2}{r^2 \pi^2 m}} \quad (2.20)$$

$$\phi^{(r)}(x) = \sin \frac{r\pi x}{L} \quad (2.21)$$

It is convenient to use the following two dimensionless parameters in this study as well as in the riser analysis which follows. Let

$$G_L = \frac{wL^3}{EI} = \text{the length ratio}$$

and

$$G_T = \frac{T_L}{wL} = \text{the top tension ratio}$$

Then Eq. 2.20 may be rewritten

$$\omega_r = r^2 \frac{\pi^2}{L^2} \sqrt{1 + \frac{G_L G_T}{r^2 \pi^2}} \cdot \sqrt{\frac{EI}{mL^4}} \quad (2.22)$$

Equation 2.22 is the standard against which the natural frequencies of the finite difference model are to be compared.

## Comparison of Finite Difference and Analytical Solutions

The natural frequencies and mode shapes of the finite difference model of the constant tension beam were calculated by using the University of Illinois Department of Computer Science System 360 Library routine EIGENP.





This routine computes the eigenvalues of a real, general matrix using the QR double-step method and computes the eigenvectors by inverse iteration.<sup>24</sup>

Comparison of the finite difference and analytical solutions was made for finite difference models having 3, 5, 7, 11, 15, 19, 23, and 31 equally spaced interior nodes. In all cases, the first five modes were compared except for the model having only three interior nodes and thus only three natural modes. A top tension ratio of 0.5 was used to approximate a riser whose average tension is one-half of the total submerged weight. Length ratios of 8 and 1000, which are typical of risers located in shallow and moderately deep water, were used in the comparison. The accuracy of the finite difference model is expressed by the frequency ratio, which is simply the natural frequency of the finite difference model divided by the actual natural frequency.

The results of the frequency comparison are shown in Fig. 2.3. As expected, the accuracy of the finite difference model improves as the number of nodes in the model increases. Also, the accuracy of the model is better for lower mode numbers than higher ones. It is significant that the finite difference model frequencies are more accurate for high  $G_L$  than for low  $G_L$ . As the length ratio increases, the structure becomes less like a beam and more like a vibrating string, which is apparently more suitable for finite difference analysis than a beam. Because  $G_L$  is proportional to the water depth cubed, the finite difference model does a better job of predicting frequencies in deep water than it does in shallow water. Finally, although the actual number of nodes which one uses depends upon the accuracy desired, it is significant that the accuracy of the first three frequencies is 99 percent or better for the 31-node model.



The agreement between the mode shapes of the finite difference model and the analytical solution is even better than the agreement between the frequencies. For each of the models tested, the first five mode shapes were normalized and the ratio of the deflection at each node to the corresponding analytical deflection was calculated. In all the models this ratio was 1.000 at every node.

### 2.4.3 Tests of Deflected Shape Under Wave Loads

#### Wave Force Distributions

The second criterion for judging the validity of the finite difference model is that the deflected shape of the model under a given loading must reasonably approximate the actual deflected shape of the structure under the same loading. Because the model will be used to calculate the riser response to wave forces, a logical force distribution for the validity tests is one which is typical of water waves. The expression commonly used for the wave force on a vertical circular cylinder is Morrison's formula,<sup>25</sup>

$$p(x,t) = C_D \frac{1}{2} \rho D |\dot{u}| + C_I \rho \frac{\pi D^2}{4} \ddot{u} \quad (2.23)$$

where

$p(x,t)$  = the wave force per unit length

$C_D$  = a dimensionless drag coefficient

$C_I$  = a dimensionless inertia coefficient

$\rho$  = the mass density of the water

$D$  = the outside diameter of the riser

$\dot{u}(x,t)$  = the horizontal component of water particle velocity

$\ddot{u}(x,t)$  = the horizontal component of water particle acceleration



According to Eq. 2.23, the hydrodynamic force consists of two components, a drag force which is a function of water particle velocity and an inertia force which is a function of water particle acceleration.

Water particle velocities and accelerations for use in Eq. 2.23 are given by several wave theories found in the literature. Linear or Airy theory, which is derived for small amplitude waves, is used in this study. According to linear wave theory,<sup>26</sup> the horizontal component of water particle velocity is

$$\dot{u} = \frac{1}{2} H \frac{gk}{\Omega} \frac{\cosh(kx)}{\cosh(kh)} \sin(ky - \Omega t) \quad (2.24)$$

in which

$H$  = the wave height measured from crest to trough

$g$  = gravitational acceleration (32.2 ft/sec<sup>2</sup>)

$k$  = the wave number equal to  $2\pi/L$

$L$  = the wave length

$h$  = the water depth

$\Omega$  = the circular frequency of the wave

In linear theory, convective acceleration is neglected as small, and the water particle acceleration is the time derivative of the water particle velocity.<sup>26</sup>

$$\ddot{u} = \frac{\partial \dot{u}}{\partial t} = -\frac{1}{2} H g k \frac{\cosh(kx)}{\cosh(kh)} \cos(ky - \Omega t) \quad (2.25)$$

Of immediate interest is the spatial variation of the drag and inertia forces. From Eqs. 2.25 and 2.23, it is evident that the spatial variation of the inertia force is given by

$$q(x) = \frac{\cosh(kx)}{\cosh(kh)} \quad (2.26)$$



where  $q(x)$  is the ratio of the force intensity at coordinate  $x$  to the force intensity at the surface. Similarly, from Eqs. 2.24 and 2.23, it follows that the spatial variation of the drag force is

$$q(x) = \frac{\cosh^2(kx)}{\cosh^2(kh)} \quad (2.27)$$

The spatial variation of inertia and drag forces for representative values of  $kh$  is shown in Figs. 2.4 and 2.5. This spatial variation is completely defined by the parameter  $kh$ , which may assume a range of values. As the water depth decreases,  $kh$  approaches zero and the forces approach a uniform distribution. An upper limit on wave number may be determined with the help of linear wave theory which provides the following relationship between wave circular frequency, wave number, and water depth.

$$\omega^2 = gk \tanh(kh) \quad (2.28)$$

For large values of  $kh$ , the hyperbolic tangent approaches unity and

$$k = \frac{\omega^2}{g} \quad (2.29)$$

With a wave circular frequency of  $\pi/3$  radians per second, which corresponds to a six second wave period, Eq. 2.29 yields a wave number of  $.034 \text{ feet}^{-1}$ . Therefore, an upper limit on  $kh$  is  $.034 h$ , where  $h$  is in feet.

#### Comparison of Finite Difference and Analytical Solutions for Wave Inertia Force Deflections

In this section, the finite difference deflections are compared to the analytical deflections of a simple beam subjected to the force given by Eq. 2.26. The problem is sketched in Fig. 2.6, and the analytical solution is derived in Appendix A. Finite difference model deflections are





obtained by premultiplying both sides of Eq. 2.11 by  $[K]^{-1}$ ,

$$\{y\} = [K]^{-1} \{p\} \quad (2.30)$$

in which

$$p_{n1} = \frac{\cosh(kx_{n1})}{\cosh(kh)} \quad (2.31)$$

and  $[K]$  is the stiffness matrix of the constant tension beam with  $T^*$  set to zero. A measure of the accuracy of the finite difference model is  $\Lambda_y$ , the ratio of the node deflections computed by finite differences to the corresponding analytical deflections.

The variation of midspan deflection ratio,  $\Lambda_{y(L/2)}$ , with  $kh$  is shown in Fig. 2.7 for finite difference models having 3, 7, 15, and 31 equally spaced nodes. (It is helpful to remember that the number of length increments is one more than the number of nodes.) For values of  $kh$  less than 3, the finite difference model yields results which are in good agreement with the analytical solution. In this region, errors are conservative and tend to decrease as  $n$  increases. As  $kh$  increases above 3, the finite difference model becomes increasingly less accurate, although accuracy is improved somewhat by increasing  $n$ . Even with as many as 31 nodes, the error of the finite difference model is greater than 10 percent for  $kh$  greater than 37. In essence, the model acts as a filter which removes those loads for which  $kh$  is large.

If the model is to be useful in deep water where large values of  $kh$  occur, then it is obvious that a very large number of nodes must be used to accurately depict the force which, for large values of  $kh$ , decays rapidly with distance below the surface. For economy of computation, it is necessary to limit the number of nodes. Thus, it is evident that an alternate force model is needed--one which accurately predicts the deflected shape,



even for large  $kh$ , without requiring an excessively large number of nodes. Such a model is developed in Section 2.4.4.

#### 2.4.4 The Lumped-Smeared Force Model

A force model which does not require a large number of nodes for satisfactory accuracy is the lumped-smeared force model shown schematically in Fig. 2.8. The lumped-smeared force intensity,  $\hat{q}_{ni}$ , is obtained by calculating concentrated reactions to the distributed force,  $q(x)$ , at each node and then distributing or smearing the total concentrated reaction at each node over the region halfway to adjacent nodes.

Consider a section of the structure between nodes  $ni-1$  and  $ni+1$  shown in Fig. 2.9a. Let  $Q_{ni,R}$  and  $Q_{ni,L}$  be the concentrated reactions at node  $ni$ . Summation of moments about node  $ni-1$  in Fig. 2.9c yields

$$Q_{ni,L} = \frac{n+1}{h} \int_{x_{ni-1}}^{x_{ni}} (x - x_{ni-1}) q(x) dx \quad (2.32)$$

Similarly, summation of moments about node  $ni+1$  in Fig. 2.9d results in

$$Q_{ni,R} = \frac{n+1}{h} \int_{x_{ni}}^{x_{ni+1}} (x_{ni+1} - x) q(x) dx \quad (2.33)$$

The lumped-smeared force intensity at node  $ni$  is, by definition,

$$\begin{aligned} \hat{q}_{ni} = \frac{n+1}{h} [Q_{ni,L} + Q_{ni,R}] &= \left[ \frac{n+1}{h} \right]^2 \left[ \int_{x_{ni}}^{x_{ni+1}} [x_{ni+1} - x] q(x) dx + \int_{x_{ni-1}}^{x_{ni}} [x - x_{ni-1}] q(x) dx \right] \end{aligned} \quad (2.34)$$

It is evident that the lumped-smeared model preserves the total force on the structure.



### Lumped-Smeared Inertia Force

The lumped-smeared inertia force intensity at node  $n_i$  is found by substituting Eq. 2.26 into Eq. 2.34. Integration of the resulting expression leads to

$$\begin{aligned} \dot{q}_{n_i} = & \frac{(n+1)^2}{(kh)^2 \cosh(kh)} [\cosh(kx_{n_i-1}) - 2 \cosh(kx_{n_i}) \\ & + \cosh(kx_{n_i+1})] \end{aligned} \quad (2.35)$$

### Lumped-Smeared Drag Force

To obtain the lumped-smeared drag force intensity at node  $n_i$ , Eq. 2.27 is substituted into Eq. 2.34. After integration and simplification, there results

$$\begin{aligned} q_{n_i} = & \frac{1}{8 \cosh^2(kh)} \left[ \left[ \frac{n+1}{kh} \right]^2 [\cosh(2kx_{n_i-1}) \right. \\ & \left. - 2 \cosh(2kx_{n_i}) + \cosh(2kx_{n_i+1})] + 4 \right] \end{aligned} \quad (2.36)$$

### Tests of Deflected Shape Using Lumped-Smeared Wave Force Model

The analytical solutions for the deflections and end rotation of a constant tension beam under the inertia and drag forces of Eqs. 2.26 and 2.27 are derived in Appendix B. The corresponding finite difference solutions are obtained from Eq. 2.30 with the stiffness matrix defined by Eqs. 2.12 and 2.17 and elements of the force intensity vector given by Eqs. 2.35 and 2.36. The validity of the combined finite difference structural model and the lumped-smeared force model is measured by the parameter  $\Delta$ , defined as the ratio of node deflection or rotation calculated with the model to the



corresponding deflection or rotation given by the analytical solution. Hence,  $\Lambda_{\theta_0}$  is the rotation ratio at  $x = 0$  and  $\Lambda_{y(L/2)}$  is the midspan deflection ratio.

In comparing the two solutions, the problem parameters have been chosen so that the constant tension beam approximates, as nearly as possible, typical riser installations in the ocean. Accordingly, the load distribution parameter,  $kh$ , is varied from .01 to  $10^5$ , the former value corresponding to a practically uniform load and the latter corresponding to a practically concentrated load very near the right end of the beam. Appropriate values of the parameter  $L$ , which appears in the analytical solution, are selected by noting that  $L$  may be written as a function of the riser parameters  $G_L$  and  $G_T$ .

$$L = \sqrt{\frac{T}{EI}} = \frac{1}{L} \sqrt{G_L G_T}$$

The length ratio,  $G_L$ , of the constant tension beam is varied from 8 to 8000, a range which includes length ratios of typical riser installations. The top tension ratio,  $G_T$ , of a riser is usually one or slightly larger. For this constant tension beam study, a ratio of  $\frac{T}{WL} = 0.5$  is used to approximate the average tension in a riser with a top tension ratio of 1.0.

Some results of the comparison between the finite difference solution with the lumped-smeared force model and the analytical solution are shown in Figs. 2.10 through 2.13. Figures 2.10 and 2.11 show the variation of  $\Lambda_{\theta_0}$  and  $\Lambda_{y(L/2)}$  with number of nodes in the finite difference model for the inertia force distribution of Eq. 2.26, for length ratios of 8, 216, 1000, and 8000, and for load distributions parameters,  $kh$ , of 0.1, 10, 100, and 100,000. The same information is shown in Figs. 2.12 and 2.13 for the drag force distribution of Eq. 2.27.





As expected, the accuracy of the finite difference model with the lumped-smeared force system improves when the number of nodes is increased. Better accuracy with more nodes was also shown in Fig. 2.7 for the finite difference structural model without the lumped-smeared force model. Unlike Fig. 2.7, however, Figs. 2.10 through 2.13 show no significant loss of accuracy as the parameter  $kh$  increases. Even when the applied force is essentially a concentrated force very close to the end of the beam, as it is when  $kh$  is  $10^5$ , the finite difference, lumped-smeared model yields results which are accurate to within one percent when ten or more nodes are used. Thus, the lumped-smeared force model corrects the main disadvantage of the unmodified finite difference model--its inability to accurately represent the force distribution for all values of  $kh$ .

The lumped-smeared model has another significant characteristic. Except for small values of  $kh$ , as would be encountered in shallow water, the model displays a marked increase in accuracy as length ratio increases even when only a few nodes are used. This is particularly evident in the case of the end deflection ratios for  $G_L = 1000$  and  $8000$ . Even for a model with three nodes, when  $G_L = 8000$  and  $kh$  is equal to or greater than 10, the error in end rotation is very small. Because the length ratio increases with the water depth cubed, the finite difference model with the lumped-smeared force system becomes increasingly accurate as water depth increases.

With the assumption that the validity of the finite difference, lumped-smeared model for the constant tension beam is indicative of its validity for the marine riser, it may be concluded that the model is an acceptable method of representing the effect of wave drag and inertia forces on the riser structure.



## 2.5 Comparison of Riser Finite Difference Model Results With Other Approximate Solutions

Although there is no closed-form riser solution to which the riser finite difference model results may be compared, there are published approximate solutions which will serve as a standard for comparison. The literature includes approximate solutions for the natural frequencies as well as the static deflections of a marine riser.

### 2.5.1 Comparison of Natural Frequencies

The natural frequencies and mode shapes of the finite difference model of the marine riser were found by solving Eq. 2.19 with  $[K]$  given by Eqs. 2.12. Calculations were made by using the routine EIGENP which is described in Section 2.4.2.

Huang and Dareing<sup>5</sup> have solved the characteristic differential equation of the marine riser,

$$\frac{d^4 y}{dx^4} - \frac{T(x)}{EI} \frac{d^2 y}{dx^2} - \frac{w}{EI} \frac{dy}{dx} - \omega^2 \frac{m}{EI} y(x) = 0 \quad (2.37)$$

using the infinite power series method, with  $y$  expanded into a power series in  $x$ .

$$y = \sum_{j=0}^{\infty} c_j x^j \quad (2.38)$$

They calculated the first three natural frequencies of pipes having linear tension variation and several end conditions, one of which corresponds to a marine riser with zero bottom tension. Table 2.1 is a comparison of the first three eigenvalues as given by Huang and Dareing and as calculated by the finite difference model with thirty-one equally spaced nodes. In all



cases, the finite difference model frequencies are slightly lower than, but very close to, the series solution.

Another approach to the solution of Eq. 2.37 is used by Frohrib and Plunkett<sup>6</sup> who employ a perturbation method. Again, a power series is used, but instead of powers of  $x$ , the series is in powers of the perturbation parameter,

$$\alpha = \sqrt{\frac{EI}{wL^3}} = \frac{1}{\sqrt{G_L}}$$

Solution is obtained by setting coefficients of like powers of  $\alpha$  equal to zero.

Figure 2.14 is a comparison of the first three natural frequencies of a marine riser with zero bottom tension as calculated by the finite difference method, the series method of Huang and Dareing, and the perturbation method of Frohrib and Plunkett. Twenty-three equally spaced nodes were used for the finite difference solutions. The finite difference model and the series method give virtually identical results for all length ratios from zero to 1000. The perturbation solution agrees with the other two solutions for length ratios greater than 200. For lower values of  $G_L$ , the perturbation parameter used by Frohrib and Plunkett increases rapidly, as shown in Fig. 2.15. As in any perturbation solution, the results become less accurate as the magnitude of the perturbation parameter increases.

The favorable agreement of the finite difference model frequencies with those of the series and perturbation solutions suggests that the former method is an acceptable one, at least for the first few modes of vibration and the range of length ratios studied.



### 2.5.2 Comparison of Responses to Steady Current Forces

Fischer and Ludwig<sup>4</sup> solved Eq. 1.3 using the infinite power series method and presented their results in dimensionless form in a series of figures. From these figures may be calculated the top and bottom rotations, maximum moment, and top shear for a given top offset and two load distributions. These two load distributions correspond to a uniform current and a linearly varying current with bottom current velocity equal to one half of the top current velocity.

For the purposes of comparing the finite difference model with the series solution of Fischer and Ludwig, a test riser was selected having the following characteristics.

D	=	20 inches
Wall thickness	=	0.438 inches
L	=	600 feet
E	=	$29 \times 10^6$ pounds per square inch
w	=	248 pounds per foot

Five combinations of top tension, lateral current load, and top offset were investigated. Solutions for each of the five cases were obtained both by using the figures of Fischer and Ludwig and the finite difference model with various numbers of nodes. Two finite difference models were considered, one with equally spaced nodes and the second with unequally spaced nodes. In the latter model, the node spacing in the center half of the riser is twice as long as the node spacing in the end quarters. The results for the five examples are given in Table 2.2.

The two finite difference models yield results which are in close agreement with the series solution of Fischer and Ludwig. The agreement





improves as the number of nodes in the finite difference model increases, and even with as few as seventeen nodes, the agreement is very close.

## 2.6 Selection of Number of Nodes in the Finite Difference Model

The number of nodes used in the finite difference model should strike a balance between economy and accuracy. The use of more nodes than are needed for the accuracy desired wastes costly machine computation time, but the use of too few nodes may produce unacceptably inaccurate results.

While this thesis does not profess to give definitive criteria for selecting the number of nodes, the results of Sections 2.4 and 2.5 do provide useful guidance in the absence of better criteria. Because the lumped-smeared force model so effectively represents wave force distributions, the controlling criteria for selection of the number of nodes will usually be the accuracy with which the natural frequencies must be obtained. If the riser length ratio and the number of natural modes to be considered is known, Fig. 2.3 may be used to choose the number of nodes which correspond to the desired accuracy of the natural frequencies. Figures 2.10 through 2.13 should also be checked to insure that the accuracy of the lumped-smeared force model is also acceptable for the number of nodes selected.



## Chapter 3

### THE STATIC RESPONSE OF A MARINE RISER TO RANDOM WAVE FORCES

#### 3.1 General

In Chapter 2, a mathematical model of the marine riser was derived by applying the method of finite differences to the riser differential equation, and a lumped-smeared model was developed to represent the wave force intensities at the nodes of the finite difference model. In this and subsequent chapters, these models are used to determine riser response to random wave forces. Consideration of dynamic effects is deferred until Chapter 4, so that in this chapter attention may be focused on the nondynamic effects which influence riser response.

It will be shown that the random wave force may be considered to be a stationary, zero mean, Gaussian random process. Riser response parameters, the bottom rotation, deflections, and bending moments, which are linear functions of the wave force intensity, are also zero mean, Gaussian random processes because the class of Gaussian random variables is closed under linear operations.<sup>27</sup> Thus, while it will not be possible to determine the exact response of the riser at a particular time, the model should make it possible to calculate the probability that the response will not exceed some tolerable level.

#### 3.2 Method of Solution

As a typical response parameter, consider the random bottom rotation,  $\theta_0(t)$ . (In this thesis, a random variable is represented by a capital



letter\*, and the corresponding lower case letter denotes the state variable or range variable of the random variable). The probability that the bottom rotation does not exceed some allowable value,  $\theta_a$ , is given by

$$P(|\theta_0| \leq \theta_a) = \int_{-\theta_a}^{\theta_a} f_{\theta_0}(\theta) d\theta \quad (3.1)$$

in which  $f_{\theta_0}$  is the probability density function. For a Gaussian bottom rotation, the probability density function is

$$f_{\theta_0}(\theta) = \frac{1}{\sqrt{2\pi} \sigma_{\theta_0}} \exp \left[ -\frac{(\theta - \mu_{\theta_0})^2}{2\sigma_{\theta_0}^2} \right] \quad (3.2)$$

where

$\sigma_{\theta_0}^2$  = the variance of the bottom rotation

$\sigma_{\theta_0}$  = the standard deviation of the bottom rotation

$\mu_{\theta_0}$  = the mean value of the bottom rotation

From Eq. 3.2 it is seen that the probability density function of a Gaussian random variable is completely defined by its mean and variance. The mean values can be conveniently set to zero by a transformation of coordinates. Therefore, if it is possible to calculate the variance of the response, then it is also possible to determine the probability associated with a specific level of response.

---

\* Not all capitalized variables are random variables, however. For example,  $I$ , the moment of inertia of the riser cross section and  $E$ , the modulus of elasticity, are considered to be deterministic.



By definition, the variance is the second central moment of a random variable.

$$\sigma_{\theta_0}^2 = E [\theta_0 - \mu_{\theta_0}]^2 \quad (3.3)$$

where  $E [ ]$  denotes the operation of taking the mathematical expectation.

For a zero mean random variable, the variance is the mean square value,

$$\sigma_{\theta_0}^2 = E [\theta_0^2] \quad (3.4)$$

Suppose that a time record of the bottom rotation,  $\theta_0(t)$ , were available. Because the variation of bottom rotation with time is a random process, this record would be just one realization of an infinite collection of possible records. This collection is called the ensemble, and the single record is called a sample function.

One of the statistical quantities which could be calculated from the ensemble is the autocorrelation function,  $R_{\theta_0}$ , which, by definition, is given by

$$R_{\theta_0\theta_0}(t_1, t_2) = E [\theta_0(t_1) \theta_0(t_2)] \quad (3.5)$$

The autocorrelation function is the ensemble average of the product of the random response at times  $t_1$  and  $t_2$ . If the random process is stationary, then the autocorrelation function is invariant with a shift in time.

$$\begin{aligned} R_{\theta_0\theta_0}(t_1, t_2) &= R_{\theta_0\theta_0}(t_2 - t_1) \\ &= R_{\theta_0\theta_0}(\tau) \\ &= E [\theta_0(t) \theta_0(t + \tau)] \end{aligned} \quad (3.6)$$





Equation 3.6 states that the autocorrelation function is independent of time and depends solely on the time lag,  $\tau$ . If the time lag is set to zero and the random process has a zero mean, then the autocorrelation function is identically equal to the variance.

$$R_{\theta_0\theta_0}(0) = E[\theta_0(t)\theta_0(t)] = \sigma_{\theta_0}^2 \quad (3.7)$$

Thus, if the autocorrelation function is known, the variance, and hence the probability density function, may be determined.

The autocorrelation function is defined in the time domain. It is often convenient to shift from the time domain to the frequency domain by means of a Fourier transformation. By the Wiener-Khintchine theorem,<sup>27</sup> the result of a Fourier transformation of the autocorrelation function of a stationary random process is the spectral density function,  $\hat{S}_{\theta_0\theta_0}(\Omega)$ ,

$$\hat{S}_{\theta_0\theta_0}(\Omega) = \frac{1}{2\pi} \int_{-\infty}^{\infty} R_{\theta_0\theta_0}(\tau) e^{-i\Omega\tau} d\tau \quad (3.8)$$

where  $\Omega$  is the frequency in radians per second and  $i = \sqrt{-1}$ . Conversely, the autocorrelation function is the Fourier transform of the spectral density function.

$$R_{\theta_0\theta_0}(\tau) = \int_{-\infty}^{\infty} \hat{S}_{\theta_0\theta_0}(\Omega) e^{i\Omega\tau} d\Omega \quad (3.9)$$

Equations 3.7 and 3.9 suggest an alternate method of calculating the variance.

$$\begin{aligned} \sigma_{\theta_0}^2 &= R_{\theta_0\theta_0}(0) = \int_{-\infty}^{\infty} \hat{S}_{\theta_0\theta_0}(\Omega) e^{i\Omega 0} d\Omega \\ &= \int_{-\infty}^{\infty} \hat{S}_{\theta_0\theta_0}(\Omega) d\Omega \end{aligned} \quad (3.10)$$



The variance is seen to be the area under the spectral density function of a zero mean stationary random process. Thus, if the response spectral density function is known, then the variance may be determined.

Throughout this thesis,  $\hat{S}(\Omega)$  is used to denote a two-sided spectrum, which is defined for both positive and negative frequencies and is an even function of frequency. An equivalent way of representing the same spectrum is as a one-sided spectrum,  $S(\Omega) = 2 \hat{S}(\Omega)$ . The one-sided spectrum, which is nonzero for positive frequencies only, is more efficient for numerical integration.

In Sections 3.3, 3.4 and 3.5, a mathematical model is developed for determining the static response spectral density functions,  $S_{\theta_0\theta_0}(\Omega)$ ,  $S_{Y_{n1}Y_{n1}}(\Omega)$ , and  $S_{M_{n1}M_{n1}}(\Omega)$ . The subscript  $n1$  refers to node  $n1$  of the structural model,  $Y_{n1}(\tau)$  is the random deflection of node  $n1$ , and  $M_{n1}(t)$  is the random moment at node  $n1$ . The input to the model is the oceanographer's description of the random sea surface, the one-dimensional sea surface elevation spectral density function,  $S_{\eta\eta}(\Omega)$ , where  $\eta(t)$  is the random elevation of the sea surface above mean water level, as shown in Fig. 3.1. (Although  $\eta$  is a random variable, it is represented by a lower case symbol in this thesis in order to agree with the notation commonly used in the literature). The static response spectral density function is obtained from the sea surface elevation spectral density function through a series of intermediate relationships. These intermediate steps, which are developed next, are

1. Calculation of the fluid kinematic spectral densities from the sea surface elevation spectral density by means of linear wave theory,



2. Calculation of wave force spectral densities from fluid kinematic spectral densities by means of the Morrison force formula, Eq. 2.23, and the lumped-smeared force model developed in Chapter 2.
3. Calculation of the static response spectral density from the wave force spectral density by means of the finite difference model developed in Chapter 2.

Steps 1 and 2, which are treated in Sections 3.3 and 3.4, are based on the work of Borgman.<sup>17,18</sup> Because details of the derivation are not widely available, they are included here.

### 3.3 Fluid Kinematic Spectra

The four fluid kinematic spectral density functions which are used in the calculation of wave force spectral densities are

$$S_{\dot{U}_{nk} \dot{U}_{n\ell}}(\Omega)$$

$$S_{\dot{U}_{nk} \ddot{U}_{n\ell}}(\Omega)$$

$$S_{\ddot{U}_{nk} \dot{U}_{n\ell}}(\Omega)$$

$$S_{\ddot{U}_{nk} \ddot{U}_{n\ell}}(\Omega)$$

where

$\dot{U}_{nk}(t)$  = the horizontal component of the random water particle velocity at node  $nk$

$\ddot{U}_{nk}(t)$  = the horizontal component of random water particle acceleration at node  $nk$



It is only necessary to derive an expression for  $S_{\dot{U}_{nk} \dot{U}_{nl}}(\Omega)$  as a function of the sea surface elevation spectrum,  $S_{\eta\eta}(\Omega)$ , because, as will be demonstrated, the remaining three spectra are readily obtained from  $S_{\dot{U}_{nk} \dot{U}_{nl}}(\Omega)$ .

In this thesis, the sea surface elevation spectral density function is one-sided and defined in such a way that the area under the spectrum is equal to the variance of the sea surface elevation. In the literature, there appear several formulas for the spectral density of either the wave height or the sea surface elevation for fully developed seas. Because these spectra are not all defined in the same manner, one must use extreme care in using them for engineering analyses. Three of the more commonly used sea surface elevation spectra are described in Appendix C.

### 3.3.1 Derivation of Expressions for Random Water Velocity and Acceleration

For deterministic analyses, linear wave theory is often used to calculate the fluid velocities and accelerations associated with water waves. For the nondeterministic model developed here, linear wave theory is used to relate the fluid kinematic spectra to the surface elevation spectrum,  $S_{\eta\eta}(\Omega)$ . In order to apply linear wave theory, it is first necessary to establish a relationship between the random sea surface elevation,  $\eta(t)$ , and the sea surface elevation spectral density,  $S_{\eta\eta}$ . Such a relationship may be found by using energy considerations and the spectral decomposition theorem.

The average total energy per unit surface area of the sea,  $E^*$ , may be determined from the sea surface elevation spectrum,  $S_{\eta\eta}$ . It can be shown that<sup>26</sup>

$$E^* = \gamma \sigma_{\eta}^2 \quad (3.11)$$





where

$\gamma$  = the unit weight of the water

$\sigma_n^2$  = the variance of the sea surface elevation

Because the mean value of  $\eta$  is zero, by definition, the variance is the area under the spectral density curve.

$$\sigma_n^2 = \int_0^{\infty} S_{\eta\eta}(\Omega) d\Omega \quad (3.12)$$

Combining Eq. 3.11 and 3.12 yields

$$E^* = \gamma \int_0^{\infty} S_{\eta\eta}(\Omega) d\Omega \quad (3.13)$$

Consider a typical sea surface elevation spectrum shown in Fig. 3.2. Let the spectrum be divided into  $nc$  frequency components, each of size  $\Delta\Omega$ . It is assumed that the sea surface elevation is a stationary random process, which, by the spectral decomposition theorem<sup>2,6</sup> is the sum of an infinite number of sinusoidal components. Thus the random sea surface elevation may be expressed by

$$\eta = \lim_{\substack{nc \rightarrow \infty \\ \Delta\Omega \rightarrow 0}} \sum_{ic=1}^{nc} \frac{H_{ic}}{2} \sin(k_{ic}y - \Omega_{ic}t + \psi_{ic}) \quad (3.14)$$

where

$ic$  = an index denoting a component of the frequency spectrum

$H_{ic}$  = the wave height of component  $ic$

$k_{ic}$  = the wave number of component  $ic$

$\psi_{ic}$  = a random phase angle



Let the random phase angles be independent with probability density functions given by

$$\begin{aligned} f_{\psi}(\psi) &= \frac{1}{2\pi} & 0 \leq \psi \leq \pi \\ &= 0 & \text{otherwise} \end{aligned} \quad (3.15)$$

Further, let the wave height of sinusoidal component  $ic$  be related deterministically to the contribution to total energy density at frequency  $\omega_{ic}$ . Pierson<sup>10</sup> shows that by the central limit theorem, the sea surface elevation which results from these assumptions converges in quadratic mean to a Gaussian random process.

Let  $\Delta E_{ic}^*$  be the contribution of sinusoidal component  $ic$  to the total average energy per unit surface area. Then,

$$E^* = \sum_{ic=1}^{nc} \Delta E_{ic}^* \quad (3.16)$$

The average energy per unit surface area of a sinusoidal wave with height  $H$  is given by<sup>26</sup>

$$E^* = \frac{\gamma}{8} H^2 \quad (3.17)$$

Therefore, the energy contribution of sinusoidal component  $ic$  is

$$\Delta E_{ic}^* = \frac{\gamma}{8} H_{ic}^2 \quad (3.18)$$

Equation 3.13 may also be written

$$E^* = \gamma \lim_{\substack{nc \rightarrow \infty \\ \Delta\Omega \rightarrow 0}} \sum_{ic=1}^{nc} S_{\eta_{ic}} \Delta\Omega \quad (3.19)$$



From Eqs. 3.16 and 3.19, an alternate expression for the contribution of sinusoidal component  $i_c$  to total average energy per unit surface area is

$$\Delta E_{i_c}^* = \gamma S_{nn_{i_c}} \Delta \Omega \quad (3.20)$$

Equations 3.18 and 3.20 yield the following expression for the wave height of sinusoidal component  $i_c$  in terms of the sea surface elevation spectral density at  $\Omega_{i_c}$ .

$$H_{i_c} = 2 \sqrt{2 S_{nn_{i_c}} \Delta \Omega} \quad (3.21)$$

When Eq. 3.21 is substituted into equation 3.14, there results

$$\eta = \sum_{i_c=1}^{nc} \sqrt{2 S_{nn_{i_c}} \Delta \Omega} \sin (k_{i_c} y - \Omega_{i_c} t + \psi_{i_c}) \quad (3.22)$$

In the limit as  $\Delta \Omega$  approaches zero and  $nc$  approaches infinity, Eq. 3.22 becomes

$$\eta = \int_0^{\infty} \sqrt{2 S_{nn} d\Omega} \sin (ky - \Omega t + \psi) \quad (3.23)$$

The next step in the development of the relationship between  $S_{nn}(\Omega)$  and  $\dot{S}_{U_{nk} \dot{U}_{n\ell}}(\Omega)$  is the application of linear wave theory to determine an expression for random velocity potential  $\Phi(x,y,t)$ , which is defined in such a way that

$$\dot{U} = - \frac{\partial \Phi}{\partial y} = \text{the random water particle velocity in the } y \text{ (horizontal) direction}$$

$$\dot{W} = - \frac{\partial \Phi}{\partial x} = \text{The random water particle velocity in the } x \text{ (vertical) direction}$$



The assumption of incompressible, irrotational flow and continuity requirements lead to Laplace's equation,

$$\nabla^2 \phi = 0 \quad (3.24)$$

The velocity potential is determined by solving Eq. 3.24 and applying the following boundary conditions. At  $x = 0$ ,

$$-\frac{\partial \phi}{\partial x} = 0 \quad (3.25a)$$

At  $x = h + \eta$

$$\eta = \frac{1}{g} \frac{\partial \phi}{\partial t} \quad (3.25b)$$

and

$$-\frac{\partial \phi}{\partial x} = \frac{\partial \eta}{\partial t} \quad (3.25c)$$

Equation 3.25a states that the water velocity component perpendicular to the ocean bottom is zero at the ocean bottom. Equation 3.25b, which is obtained from Bernoulli's equation, states that the pressure is equal to zero on the free surface. Equation 3.25c is a mathematical statement of the condition that particles on the free surface stay there (the vertical component of water particle velocity at the free surface equals the time rate of change of the surface elevation). In linear wave theory, it is assumed that the wave amplitudes are so small that satisfying Eqs. 3.25b and 3.25c at the mean water level,  $x = h$ , is nearly the same as satisfying them at  $x = h + \eta$ . Thus the last two boundary conditions become

$$\eta = \frac{1}{g} \left. \frac{\partial \phi}{\partial t} \right|_{x=h} \quad (3.26a)$$





and

$$-\left. \frac{\partial \phi}{\partial x} \right|_{x=h} = \frac{\partial \eta}{\partial t} \quad (3.26b)$$

A solution which satisfies Eqs. 3.24 and 3.25a is

$$\phi = \sum_{i=1}^{nc} C_{iC} \cosh(k_{iC}x) \cdot \cos(k_{iC}y - \Omega_{iC}t + \psi_{iC}) \quad (3.27)$$

$C_{iC}$  is a coefficient which is determined by substituting Eqs. 3.22 and 3.27 into Eq. 3.26a.

$$C_{iC} = \frac{g}{\Omega_{iC}} \sqrt{2S_{nn_{iC}} \Delta \Omega} \frac{1}{\cosh(k_{iC}h)} \quad (3.28)$$

Substitution of Eq. 3.28 into Eq. 3.27 produces the linear wave theory solution for the random velocity potential.

$$\begin{aligned} \phi = & \sum_{i=1}^{nc} \frac{g}{\Omega_{iC}} \sqrt{2S_{nn_{iC}} \Delta \Omega} \frac{\cosh(k_{iC}x)}{\cosh(k_{iC}h)} \\ & \cdot \cos(k_{iC}y - \Omega_{iC}t + \psi_{iC}) \end{aligned} \quad (3.29)$$

In the limit, as  $\Delta \Omega$  approaches zero and  $nc$  approaches infinity,

$$\begin{aligned} \phi = & \int_0^{\infty} \frac{g}{\Omega} \sqrt{2S_{nn}(\Omega) d\Omega} \frac{\cosh(kx)}{\cosh(kh)} \\ & \cdot \cos(ky - \Omega t + \psi) \end{aligned} \quad (3.30)$$

Substitution of Eqs. 3.22 and 3.29 into Eq. 3.26b leads to the following useful relationship.

$$\Omega_{iC}^2 = g k_{iC} \tanh(k_{iC}h) \quad (3.31)$$



The horizontal component of random water particle velocity is obtained by differentiating the velocity potential with respect to  $y$ .

$$\begin{aligned}\dot{U} &= -\frac{\partial \Phi}{\partial y} \\ &= \int_0^{\infty} \frac{kg}{\Omega} \sqrt{2S_{nn}} d\Omega \frac{\cosh(kx)}{\cosh(kh)} \cdot \sin(ky - \Omega t + \Psi) \quad (3.32)\end{aligned}$$

The horizontal component of water particle acceleration is the derivative of the particle velocity with respect to time.

$$\frac{D\dot{U}}{Dt} = \frac{\partial \dot{U}}{\partial t} + \dot{U} \frac{\partial \dot{U}}{\partial y} + \dot{W} \frac{\partial \dot{U}}{\partial x} \quad (3.33)$$

The last two terms of Eq. 3.33 are convective acceleration terms which may be ignored as being small compared to the temporal acceleration,  $\frac{\partial \dot{U}}{\partial t}$ .<sup>2.6</sup>

$$\begin{aligned}\ddot{U} = \frac{\partial \dot{U}}{\partial t} &= - \int_0^{\infty} kg \sqrt{2S_{nn}} d\Omega \frac{\cosh(kx)}{\cosh(kh)} \\ &\cdot \cos(ky - \Omega t + \Psi) \quad (3.34)\end{aligned}$$

### 3.3.2 Correlation Functions of Random Water Particle Velocity

Because the random water particle velocity is a linear function of the zero mean, Gaussian, stationary random sea surface elevation, the water particle velocity is also a zero mean, Gaussian, stationary random process. Therefore, the correlation function of the water velocity at nodes  $nk$  and  $n\ell$  is independent of time,  $t$ , and is a function only of the time lag,  $\tau$ . By applying Eq. 3.32, the correlation function may be written



$$\begin{aligned}
R_{\dot{U}_{nk} \dot{U}_{n\ell}}(\tau) &= E [\dot{U}_{nk}(t) \dot{U}_{n\ell}(t + \tau)] \\
&= E \left[ \int_{\Omega=0}^{\infty} \frac{gk}{\Omega} \sqrt{2S_{nn}} d\Omega \frac{\cosh(kx_{nk})}{\cosh(kh)} \right. \\
&\quad \cdot \sin(kY_{nk} - \Omega t + \psi) \cdot \int_{\Omega'=0}^{\infty} \frac{gk'}{\Omega'} \sqrt{2S'_{nn}} d\Omega' \\
&\quad \cdot \frac{\cosh(k'x_{n\ell})}{\cosh(k'h)} \sin(k'Y_{n\ell} - \Omega' (t + \tau) + \psi') \left. \right] \quad (3.35)
\end{aligned}$$

The right hand side of Eq. 3.35 contains four random variables -  $Y_{nk}$  and  $Y_{n\ell}$ , the random deflections of nodes  $nk$  and  $n\ell$  and  $\psi$  and  $\psi'$ , the random phase angles. The random node deflections may be eliminated from Eq. 3.35 by assuming that the node deflections are small compared to the wave length of ocean waves. This assumption is reasonable if the deflections are on the order of a few feet, because typical ocean wave lengths are on the order of a few hundred feet. Another way of stating the assumption is that the deflections are so small compared to the wave lengths that the water velocity and acceleration at the undeflected riser node points is essentially the same as the water velocity and acceleration at the deflected node points.

By definition of the expectation operator, the correlation function of Eq. 3.35 is



$$\begin{aligned}
\dot{R}\dot{U}_{nk}\dot{U}_{n\ell} = & \int_{\psi=-\infty}^{\infty} \int_{\psi'=-\infty}^{\infty} \left[ \int_{\Omega=0}^{\infty} \frac{gk}{\Omega} \sqrt{2S_{nn}} d\Omega \frac{\cosh(kx_{nk})}{\cosh(kh)} \right. \\
& \cdot \sin(-\Omega t + \psi) \cdot \int_{\Omega'=0}^{\infty} \frac{gk'}{\Omega'} \sqrt{2S'_{nn}} d\Omega' \frac{\cosh(k'x_{n\ell})}{\cosh(k'h)} \\
& \left. \cdot \sin(-\Omega'(t + \tau) + \psi') \right] \cdot f_{\psi\psi'}(\psi, \psi') d\psi d\psi' \quad (3.36)
\end{aligned}$$

in which  $f_{\psi\psi'}$ , the joint probability density function of the statistically independent random phase angles  $\psi$  and  $\psi'$ , is

$$\begin{aligned}
f_{\psi\psi'}(\psi, \psi') &= f_{\psi}(\psi) f_{\psi'}(\psi') \\
&= \frac{1}{4\pi^2}, \quad 0 \leq \psi \leq 2\pi, \quad 0 \leq \psi' \leq 2\pi \\
&= 0, \quad \text{otherwise} \quad (3.37)
\end{aligned}$$

Equation 3.36 may be rewritten in a more convenient form by interchanging the order of integration with respect to phase angle and circular frequency and by changing the limits of integration with respect to phase angle so as to exclude the region where  $f_{\psi\psi'}$  is zero. When this is done the result is

$$\begin{aligned}
\dot{R}\dot{U}_{nk}\dot{U}_{n\ell}(\tau) &= \int_{\Omega=0}^{\infty} \int_{\Omega'=0}^{\infty} 2 \frac{g^2 k k'}{\Omega \Omega'} \sqrt{S_{nn} S'_{nn}} d\Omega d\Omega' \frac{\cosh(kx_{nk})}{\cosh(kh)} \frac{\cosh(k'x_{n\ell})}{\cosh(k'h)} \\
&\cdot \int_{\psi=0}^{2\pi} \int_{\psi'=0}^{2\pi} \sin[-\Omega t + \psi] \sin[-\Omega'(t + \tau) + \psi'] \\
&\cdot \frac{1}{4\pi^2} d\psi d\psi' \quad (3.38)
\end{aligned}$$





Consider the double integral with respect to phase angle which ends Eq. 3.38. If  $\Omega \neq \Omega'$ , the double integral reduces to two single integrals each of whose values is zero. Hence, Eq. 3.38 has a nonzero value only when  $\Omega = \Omega'$  and may be simplified to

$$\begin{aligned}
 R_{\dot{U}_{nk} \dot{U}_{n\ell}}(\tau) &= \int_{\Omega=0}^{\infty} 2 \left( \frac{gk}{\Omega} \right)^2 S_{nn}(\Omega) \frac{\cosh(kx_{nk}) \cosh(kx_{n\ell})}{\cosh^2(kh)} \\
 &\quad \cdot \frac{1}{4\pi^2} \int_{\psi=0}^{2\pi} \int_{\psi=0}^{2\pi} \sin[-\Omega t + \psi] \sin[-\Omega(t + \tau) + \psi] \\
 &\quad d\psi \, d\psi \, d\Omega
 \end{aligned} \tag{3.39}$$

The double integral with respect to random phase angle, which is easily evaluated by writing the product of the two sines as the sum of two cosines, equals  $2\pi^2 \cos(\Omega\tau)$ . Therefore, Eq. 3.39 reduces to

$$\begin{aligned}
 R_{\dot{U}_{nk} \dot{U}_{n\ell}}(\tau) &= \int_{\Omega=0}^{\infty} \left( \frac{gk}{\Omega} \right)^2 S_{nn}(\Omega) \frac{\cosh(kx_{nk}) \cosh(kx_{n\ell})}{\cosh^2(kh)} \\
 &\quad \cdot \cos(\Omega\tau) \, d\Omega
 \end{aligned} \tag{3.40}$$

By virtue of Eq. 3.7, the variance (if  $nk$  equals  $n\ell$ ) or covariance (if  $nk \neq n\ell$ ) of the water particle velocity may be obtained by setting  $\tau$  equal to zero in Eq. 3.40.

$$\begin{aligned}
 \sigma_{\dot{U}_{nk} \dot{U}_{n\ell}}^2 &= R_{\dot{U}_{nk} \dot{U}_{n\ell}}(0) \\
 &= \int_{\Omega=0}^{\infty} \left[ \left( \frac{gk}{\Omega} \right)^2 S_{nn}(\Omega) \frac{\cosh(kx_{nk}) \cosh(kx_{n\ell})}{\cosh^2(kh)} \right] d\Omega
 \end{aligned} \tag{3.41}$$



### 3.3.3 Spectral Density of Water Particle Velocity

The expression for  $\dot{S}_{\dot{U}_{nk}\dot{U}_{n\ell}}(\Omega)$  may be obtained by simply comparing Eqs. 3.10 and 3.41. It is apparent that  $\dot{S}_{\dot{U}_{nk}\dot{U}_{n\ell}}(\Omega)$  must be the expression in brackets in Eq. 3.41. A more rigorous derivation follows.

By definition, the spectral density function is the Fourier transform of the correlation function.

$$\tilde{\dot{S}}_{\dot{U}_{nk}\dot{U}_{n\ell}}(\Omega) = \frac{1}{2\pi} \int_{\tau=-\infty}^{\infty} R_{\dot{U}_{nk}\dot{U}_{n\ell}}(\tau) e^{-i\Omega\tau} d\tau \quad (3.42)$$

Substitution of Eq. 3.40 into Eq. 3.42 yields

$$\begin{aligned} \tilde{\dot{S}}_{\dot{U}_{nk}\dot{U}_{n\ell}}(\Omega) &= \frac{1}{2\pi} \int_{\tau=-\infty}^{\infty} g^2 \left[ \int_{\Omega'=0}^{\infty} \left( \frac{k'}{\Omega'} \right)^2 S_{\eta\eta}(\Omega') \right. \\ &\quad \cdot \left. \frac{\cosh(k'x_{nk}) \cosh(k'x_{n\ell})}{\cosh^2(k'h)} \cos(\Omega'\tau) d\Omega' \right] \\ &\quad \cdot e^{-i\Omega\tau} d\tau \end{aligned} \quad (3.43)$$

in which the prime notation indicates the wave number and frequency terms introduced by Eq. 3.40. Interchanging the order of integration in Eq. 3.43 leads to

$$\begin{aligned} \tilde{\dot{S}}_{\dot{U}_{nk}\dot{U}_{n\ell}}(\Omega) &= \frac{g^2}{2\pi} \int_{\Omega'=0}^{\infty} \left( \frac{k'}{\Omega'} \right)^2 S_{\eta\eta}(\Omega') \frac{\cosh(k'x_{nk}) \cosh(k'x_{n\ell})}{\cosh^2(k'h)} \\ &\quad \left\{ \int_{\tau=-\infty}^{\infty} \cos(\Omega'\tau) \cdot e^{-i\Omega\tau} d\tau \right\} d\Omega' \end{aligned} \quad (3.44)$$



Consider the expression in braces in Eq. 3.44. The solution of this integral, as given by Davenport and Root<sup>29</sup> is

$$\int_{-\infty}^{\infty} \cos(\Omega' \tau) e^{-i\Omega \tau} d\tau = \pi [\delta(\Omega + \Omega') + \delta(\Omega - \Omega')] \quad (3.45)$$

where  $\delta()$  is the Dirac delta function, defined as follows.

$$\begin{aligned} \int_a^b \delta(x) dx &= 1, & a < 0 < b \\ &= 0, & \text{otherwise} \\ \delta(x) &= 0, & x \neq 0 \\ &= \infty, & x = 0 \end{aligned}$$

It follows that Eq. 3.45 may be restated

$$\begin{aligned} \int_{-\infty}^{\infty} \cos(\Omega' \tau) e^{-i\Omega \tau} d\tau &= \pi, & \Omega' &= \pm \Omega \\ &= 0, & \text{otherwise.} \end{aligned} \quad (3.46)$$

Because of the nature of Eq. 3.46, the integral with respect to  $\Omega'$  in Eq. 3.44 is nonzero only when  $\Omega' = \pm \Omega$ . Therefore, Eq. 3.44 simplifies to

$$\dot{\mathbf{U}}_{nk} \cdot \dot{\mathbf{U}}_{nl}(\Omega) = \frac{1}{2} \left( \frac{gk}{\Omega} \right)^2 S_{nn}(|\Omega|) \frac{\cosh(kx_{nk}) \cosh(kx_{nl})}{\cosh^2(kh)} \quad (3.47)$$

and the corresponding one-sided spectrum for the horizontal component of water particle velocity is



$$\begin{aligned}
S_{\dot{U}_{nk}\dot{U}_{n\ell}}(\Omega) &= 2 \tilde{S}_{\dot{U}_{nk}\dot{U}_{n\ell}}(\Omega) \\
&= \left[ \left[ \frac{kg}{\Omega} \right]^2 \frac{\cosh(kx_{nk}) \cosh(kx_{n\ell})}{\cosh^2(kh)} \right] S_{\eta\eta}(\Omega), \\
&\quad 0 \leq \Omega < \infty \\
&= 0, \quad \Omega < 0
\end{aligned} \tag{3.48}$$

### 3.3.4 Other Fluid Kinematic Spectra

The spectral densities,  $S_{\dot{U}_{nk}\ddot{U}_{n\ell}}(\Omega)$ ,  $S_{\ddot{U}_{nk}\dot{U}_{n\ell}}(\Omega)$ , and  $S_{\ddot{U}_{nk}\ddot{U}_{n\ell}}(\Omega)$ , could be derived in the same manner as that used for  $S_{\dot{U}_{nk}\dot{U}_{n\ell}}(\Omega)$ , by writing the corresponding correlation functions, substituting Eqs. 3.32 and 3.34, and performing a Fourier transformation. A shorter derivation is possible, however, and will be used here.

To obtain  $S_{\dot{U}_{nk}\ddot{U}_{n\ell}}(\Omega)$  in terms of  $S_{\dot{U}_{nk}\dot{U}_{n\ell}}(\Omega)$ , it is only necessary to recognize that

$$\frac{\partial}{\partial \tau} \tilde{S}_{\dot{U}_{nk}\dot{U}_{n\ell}}(\Omega) = 0 \tag{3.49}$$

The substitution of Eq. 3.42 into Eq. 3.49 yields

$$\begin{aligned}
\frac{1}{2\pi} \int_{-\infty}^{\infty} \frac{\partial R_{\dot{U}_{nk}\dot{U}_{n\ell}}(\tau)}{\partial \tau} e^{-i\Omega\tau} d\tau \\
- i\Omega \cdot \frac{1}{2\pi} \int_{-\infty}^{\infty} R_{\dot{U}_{nk}\dot{U}_{n\ell}}(\tau) e^{-i\Omega\tau} d\tau = 0
\end{aligned} \tag{3.50}$$

The partial derivative of the correlation function is given by





$$\begin{aligned}
\frac{\partial}{\partial \tau} R_{\dot{U}_{nk} \dot{U}_{n\ell}}(\tau) &= \frac{\partial}{\partial \tau} E [\dot{U}_{nk}(t) \dot{U}_{n\ell}(t + \tau)] \\
&= E [\dot{U}_{nk}(t) \ddot{U}_{n\ell}(t + \tau)] \\
&= R_{\dot{U}_{nk} \ddot{U}_{n\ell}}(\tau)
\end{aligned} \tag{3.51}$$

which, when substituted into Eq. 3.50 results in

$$\begin{aligned}
&\frac{1}{2\pi} \int_{-\infty}^{\infty} R_{\dot{U}_{nk} \ddot{U}_{n\ell}}(\tau) e^{-i\Omega\tau} d\tau \\
&= i\Omega \frac{1}{2\pi} \int_{-\infty}^{\infty} R_{\dot{U}_{nk} \dot{U}_{n\ell}}(\tau) e^{-i\Omega\tau} d\tau
\end{aligned} \tag{3.52}$$

But the two Fourier transforms in Eq. 3.52 are, by definition, spectral density functions. Hence,

$$\tilde{S}_{\dot{U}_{nk} \ddot{U}_{n\ell}}(\Omega) = i\Omega \tilde{S}_{\dot{U}_{nk} \dot{U}_{n\ell}}(\Omega) \tag{3.53}$$

and for the one-sided spectrum,

$$S_{\dot{U}_{nk} \ddot{U}_{n\ell}}(\Omega) = i\Omega S_{\dot{U}_{nk} \dot{U}_{n\ell}}(\Omega) \tag{3.54}$$

In like manner by using the relationships

$$\frac{\partial}{\partial \tau} R_{\dot{U}_{nk} \dot{U}_{n\ell}}(\tau) = -R_{\ddot{U}_{nk} \dot{U}_{n\ell}}(\tau) \tag{3.55a}$$

$$\frac{\partial}{\partial \tau} R_{\ddot{U}_{nk} \dot{U}_{n\ell}}(\tau) = R_{\ddot{U}_{nk} \ddot{U}_{n\ell}}(\tau) \tag{3.55b}$$

and



$$\frac{\partial}{\partial \tau} \ddot{S}_{\dot{U}_{nk} \dot{U}_{n\ell}}(\Omega) = 0 \quad (3.55c)$$

it can be shown that

$$\ddot{S}_{\dot{U}_{nk} \dot{U}_{n\ell}}(\Omega) = -i\Omega \dot{S}_{\dot{U}_{nk} \dot{U}_{n\ell}}(\Omega) \quad (3.56a)$$

and

$$\ddot{S}_{\ddot{U}_{nk} \ddot{U}_{n\ell}}(\Omega) = \Omega^2 \dot{S}_{\dot{U}_{nk} \dot{U}_{n\ell}}(\Omega) \quad (3.56b)$$

### 3.3.5 Modification of the Input Sea Surface Elevation Spectrum by Linear Wave Theory

It has been shown that the fluid kinematic spectral density functions may be expressed in terms of the sea surface elevation spectral density. In a sense, the ocean acts as a linear filter whose input is the surface elevation spectrum and whose outputs are the fluid kinematic spectra at all locations,  $x$ , throughout the water column. In this thesis linear wave theory is used to model the effect of the ocean on the input spectrum.

A convenient way to regard the effect of the ocean on the input spectrum is to examine the power transfer function,  $\Gamma(\Omega)$ , which is defined as the ratio of the output spectral density to the input spectral density<sup>30</sup>

$$\Gamma(\Omega) = \frac{S_{\text{output}}(\Omega)}{S_{\text{input}}(\Omega)} \quad (3.57)$$

Consider the water velocity and acceleration spectral densities at node  $x_{nk}$  as outputs with the ocean acting as linear filter. These spectra may be expressed as products of an input spectral density and the appropriate power



transfer function.

$$S_{\dot{U}_{nk}\dot{U}_{nk}}(\Omega) = \Gamma_{\dot{U}}^*(x_{nk}, \Omega) \cdot S_{\eta\eta}(\Omega) \quad (3.58a)$$

$$S_{\ddot{U}_{nk}\ddot{U}_{nk}}(\Omega) = \Gamma_{\ddot{U}}^*(x_{nk}, \Omega) \cdot S_{\eta\eta}(\Omega) \quad (3.58b)$$

An examination of Eqs. 3.48 and 3.56b indicates that the two power transfer functions are

$$\Gamma_{\dot{U}}^*(x_{nk}, \Omega) = \left[ \frac{kg}{\Omega} \frac{\cosh(kx_{nk})}{\cosh(kh)} \right]^2 \quad (3.59a)$$

and

$$\begin{aligned} \Gamma_{\ddot{U}}^*(x_{nk}, \Omega) &= \Omega^2 \Gamma_{\dot{U}}^*(x_{nk}, \Omega) \\ &= \left[ \frac{kg \cosh(kx_{nk})}{\cosh(kh)} \right]^2 \end{aligned} \quad (3.59b)$$

Figures 3.3 and 3.4 demonstrate the manner in which the ocean modifies the input sea surface elevation spectral density. The input spectrum shown is that of Pierson and Moskowitz for a wind velocity of twenty knots and is given by Eq. C.4 of Appendix C. The power transfer functions and output kinematic spectra shown are for a water depth of six hundred feet and for distances below the surface of one, five, and ten percent of the total depth, that is, six, thirty, and sixty feet below the surface. Two distinct effects are seen in the figures. First, except for frequencies approaching zero, the output kinematic spectral densities decrease as distance below the surface increases. Secondly, except for locations very near



the surface, the ocean filters out the high frequency portion of the input sea surface elevation spectrum. This latter effect becomes more pronounced as distance below the surface increases. It may be concluded that the lower frequency components of the input spectrum influence the output kinematic spectra to greater distances below the surface than the higher frequency components do.

Figure 3.5 shows profiles of root mean square water velocity for various wind velocities, a water depth of six hundred feet, and the Pierson-Moskowitz sea surface elevation spectrum. Throughout the water column the root mean square water velocity, which is the square root of the integral of the water particle velocity spectral density function, increases with an increase in wind velocity. For a given wind velocity, the root mean square water velocity decreases as distance below the surface increases. This effect is caused by the reduction in spectral density and the removal of high frequency components of the input spectrum by the ocean as represented by linear wave theory.

### 3.4 Wave Force Spectra

In this section, the relationship between the fluid kinematic spectra developed in Section 3.3 and the wave force spectra is derived. The model used to express the random wave force intensity in terms of the fluid kinematic parameters is the nondeterministic version of Morrison's formula,<sup>25</sup>

$$P(x,t) = C_u \dot{U}|\dot{U}| + C_a \ddot{U} \quad (3.60)$$

where





$$C_u = C_D \frac{1}{2} \rho D \quad (3.61a)$$

and

$$C_a = C_I \rho \frac{\pi D^2}{4} \quad (3.61b)$$

In Eq. 3.60, the drag and inertia coefficients, mass density, and diameter are deterministic quantities, and the wave force intensity,  $P(x,t)$ , and fluid velocity and acceleration,  $\dot{U}$  and  $\ddot{U}$ , are random.

The random wave force is composed of a drag component which is a nonlinear function of the random water particle velocity and inertia component which is a linear function of the random water particle acceleration. The presence of the nonlinear velocity term complicates the solution because it precludes the use of a superposition technique.

#### 3.4.1 The Linearized Wave Force Model

The troublesome nonlinearity in the velocity term may be removed by the method of equivalent linearization, which is described in detail by Lin<sup>27</sup> and used by Borgman<sup>17,18</sup> and others<sup>19,20</sup> to linearize wave drag forces. The essence of the method is to replace the nonlinear term,  $\dot{U}|\dot{U}|$ , with a statistically linearized term,  $C \dot{U}$ , where  $C$  is a constant. The resulting random error,  $E$  is

$$E = \dot{U}|\dot{U}| - C \dot{U} \quad (3.62)$$

The coefficient  $C$  is determined such that the mean square value of the error is minimized.

$$\frac{\partial}{\partial C} [E(E^2)] = 0 \quad (3.63)$$



Because the operations of differentiation and determining the expected value are both linear, Eq. 3.63 may be written

$$E \left[ 2E \frac{\partial E}{\partial C} \right] = 0 \quad (3.64)$$

The substitution of Eq. 3.62 into Eq. 3.64 yields

$$- 2 E \left[ \dot{U}^2 | \dot{U} | \right] + 2 C \cdot E \left[ \dot{U}^2 \right] = 0 \quad (3.65)$$

Because  $\dot{U}$  is a zero mean random variable,  $E \left[ \dot{U}^2 \right] = \sigma_{\dot{U}}^2$ , the variance of the velocity. Therefore Eq. 3.65 may be written

$$C = \frac{E \left[ \dot{U}^2 | \dot{U} | \right]}{\sigma_{\dot{U}}^2} \quad (3.66)$$

The numerator of Eq. 3.66 is evaluated by noting that for  $\dot{U} < 0$ ,  $|\dot{U}| = -\dot{U}$ , and for  $\dot{U} > 0$ ,  $|\dot{U}| = \dot{U}$ . Hence,

$$\begin{aligned} E \left[ \dot{U}^2 | \dot{U} | \right] &= \int_{-\infty}^{\infty} \dot{u}^2 |\dot{u}| f_{\dot{U}}(\dot{u}) d\dot{u} \\ &= - \int_{-\infty}^0 \dot{u}^3 f_{\dot{U}}(\dot{u}) d\dot{u} \\ &\quad + \int_0^{\infty} \dot{u}^3 f_{\dot{U}}(\dot{u}) d\dot{u} \end{aligned} \quad (3.67)$$

where  $f_{\dot{U}}(\dot{u})$  is the normal probability density function given by

$$f_{\dot{U}}(\dot{u}) = \frac{1}{\sqrt{2\pi} \sigma_{\dot{U}}} e^{-\frac{\dot{u}^2}{2 \sigma_{\dot{U}}^2}} \quad (3.68)$$



Substitution of Eq. 3.68 into Eq. 3.67 and evaluation of the integrals leads to

$$E [\dot{U}^2 | \dot{U}] = \sqrt{\frac{8}{\pi}} \sigma_{\dot{U}}^3 \quad (3.69)$$

When Eq. 3.69 is substituted into Eq. 3.66, there results

$$C = \sqrt{\frac{8}{\pi}} \sigma_{\dot{U}} \quad (3.70)$$

The value of  $C$  determined by Eq. 3.70 minimizes the mean square random error,  $E$ , because

$$\begin{aligned} \frac{\partial^2}{\partial C^2} E (E^2) &= \frac{\partial}{\partial C} \{ E [2E \frac{\partial E}{\partial C}] \} \\ &= 2 E [\dot{U}^2] \\ &= 2 \sigma_{\dot{U}}^2 \end{aligned} \quad (3.71)$$

and the variance,  $\sigma_{\dot{U}}^2$ , must be nonnegative. The linearized version of the wave force equation may now be written

$$P(x,t) = C_{\dot{U}} \sqrt{\frac{8}{\pi}} \sigma_{\dot{U}} \dot{U}(x,t) + C_a \ddot{U}(x,t) \quad (3.72)$$

Because the random force intensity given by Eq. 3.72 is a linear function of the zero mean, Gaussian, stationary velocity and acceleration, the force intensity is also zero mean, Gaussian, and stationary.

#### 3.4.2 Correlation Function of the Random Wave Force Intensity

The correlation function of the random wave force intensity at node



$nk$ ,  $P_{nk}(t)$ , and the random wave force intensity at node  $n\ell$ ,  $P_{n\ell}(t)$ , is by definition

$$R_{P_{nk}P_{n\ell}}(\tau) = E [P_{nk}(t) P_{n\ell}(t + \tau)] \quad (3.73)$$

where

$$P_{nk}(t) = P(x_{nk}, t)$$

Substitution of Eq. 3.72 into Eq. 3.73 leads to

$$\begin{aligned} R_{P_{nk}P_{n\ell}}(\tau) = & C_u^2 \frac{8}{\pi} \sigma_{\dot{U}_{nk}} \sigma_{\dot{U}_{n\ell}} R_{\dot{U}_{nk}\dot{U}_{n\ell}}(\tau) \\ & + C_u C_a \sqrt{\frac{8}{\pi}} \sigma_{\dot{U}_{nk}} R_{\dot{U}_{nk}\ddot{U}_{n\ell}}(\tau) \\ & + C_u C_a \sqrt{\frac{8}{\pi}} \sigma_{\dot{U}_{n\ell}} R_{\ddot{U}_{nk}\dot{U}_{n\ell}}(\tau) \\ & + C_a^2 R_{\ddot{U}_{nk}\ddot{U}_{n\ell}}(\tau) \end{aligned} \quad (3.74)$$

### 3.4.3 Wave Force Spectral Densities

The wave force spectral density is obtained by taking the Fourier transform of the corresponding correlation function.

$$\tilde{S}_{P_{nk}P_{n\ell}}(\Omega) = \frac{1}{2\pi} \int_{-\infty}^{\infty} R_{P_{nk}P_{n\ell}}(\tau) e^{-i\Omega\tau} d\tau \quad (3.75)$$

Equation 3.75 may be expanded by substituting Eq. 3.74.





$$\begin{aligned}
\dot{S}_{P_{nk}P_{nl}}(\Omega) &= \frac{1}{2\pi} \int_{-\infty}^{\infty} \left\{ C_{\dot{U}}^2 \frac{8}{\pi} \sigma_{\dot{U}_{nk}} \sigma_{\dot{U}_{nl}} R_{\dot{U}_{nk}\dot{U}_{nl}}(\tau) \right. \\
&+ C_{\dot{U}} C_a \sqrt{\frac{8}{\pi}} \sigma_{\dot{U}_{nk}} R_{\dot{U}_{nk}\ddot{U}_{nl}}(\tau) \\
&+ C_{\dot{U}} C_a \sqrt{\frac{8}{\pi}} \sigma_{\ddot{U}_{nl}} R_{\ddot{U}_{nk}\dot{U}_{nl}}(\tau) \\
&\left. + C_a^2 R_{\ddot{U}_{nk}\ddot{U}_{nl}}(\tau) \right\} e^{-i\Omega\tau} d\tau \quad (3.76)
\end{aligned}$$

Interchanging the order of summation and integration in Eq. 3.76 leads to

$$\begin{aligned}
S_{P_{nk}P_{nl}}(\Omega) &= C_{\dot{U}}^2 \frac{8}{\pi} \sigma_{\dot{U}_{nk}} \sigma_{\dot{U}_{nl}} S_{\dot{U}_{nk}\dot{U}_{nl}}(\Omega) \\
&+ C_{\dot{U}} C_a \sqrt{\frac{8}{\pi}} \sigma_{\dot{U}_{nk}} S_{\dot{U}_{nk}\ddot{U}_{nl}}(\Omega) \\
&+ C_{\dot{U}} C_a \sqrt{\frac{8}{\pi}} \sigma_{\ddot{U}_{nl}} S_{\ddot{U}_{nk}\dot{U}_{nl}}(\Omega) \\
&+ C_a^2 S_{\ddot{U}_{nk}\ddot{U}_{nl}}(\Omega) \quad (3.77)
\end{aligned}$$

Equation 3.77 may be further simplified by employing Eqs. 3.54 and 3.56.

$$\begin{aligned}
S_{P_{nk}P_{nl}}(\Omega) &= \left[ C_{\dot{U}}^2 \frac{8}{\pi} \sigma_{\dot{U}_{nk}} \sigma_{\dot{U}_{nl}} + i\Omega C_{\dot{U}} C_a \sqrt{\frac{8}{\pi}} (\sigma_{\dot{U}_{nk}} - \sigma_{\dot{U}_{nl}}) \right. \\
&\left. + \Omega^2 C_a^2 \right] S_{\dot{U}_{nk}\dot{U}_{nl}}(\Omega) \quad (3.78)
\end{aligned}$$

Equations 3.78 and 3.48 constitute a mathematical link between the input to the problem - the surface elevation spectrum - and the spectral density function of the wave force intensities.



### 3.4.4 Introduction of the Lumped-Smeared Force Model

The accuracy of response calculations may be improved by incorporating the lumped-smeared force representation developed in Chapter 2 into the nondeterministic force model. Consider Eq. 3.78, which with the use of Eq. 3.48 may be written

$$\begin{aligned}
 S_{P_{nk}P_{n\ell}}(\Omega) = & \left[ C_u^2 \frac{8}{\pi} \sigma_{\dot{U}_{nk}} \sigma_{\dot{U}_{n\ell}} + i\Omega C_u C_a \sqrt{\frac{8}{\pi}} (\sigma_{\dot{U}_{nk}} - \sigma_{\dot{U}_{n\ell}}) \right. \\
 & + \Omega^2 C_a^2 \left. \right] \left[ \frac{kg}{\Omega} \right]^2 S_{\eta\eta}(\Omega) \\
 & \cdot \frac{\cosh(kx_{nk})}{\cosh(kh)} \cdot \frac{\cosh(kx_{n\ell})}{\cosh(kh)} \quad (3.79)
 \end{aligned}$$

The last two terms in Eq. 3.79, the fractions involving the hyperbolic cosines, represent the spatial variation of the random force intensity along the riser axis. The term  $\frac{\cosh(kx)}{\cosh(kh)}$  is also a spatial modifier for the inertia force, as indicated by Eq. 2.26. In the lumped-smeared force system, the ratio of hyperbolic cosines is replaced by the spatial modifier,  $\tilde{q}_{nk}(\Omega)$ , which is given by Eq. 2.35. The lumped-smeared force representation is introduced into the nondeterministic model by replacing the hyperbolic cosine ratios in Eq. 3.79 with the lumped-smeared spatial modifier,  $\tilde{q}_{nk}(\Omega)$ , of Eq. 2.35 resulting in



$$\begin{aligned}
S_{P_{nk} P_{n\ell}}(\Omega) = & \left[ c_u^2 \frac{8}{\pi} \sigma_{\dot{U}_{nk}} \sigma_{\dot{U}_{n\ell}} \right. \\
& + i\Omega c_u c_a \sqrt{\frac{8}{\pi}} (\sigma_{\dot{U}_{nk}} - \sigma_{\dot{U}_{n\ell}}) + c_a^2 \Omega^2 \left. \right] \\
& \left[ \frac{kg}{\Omega} \right]^2 \tilde{q}_{nk}(\Omega) \tilde{q}_{n\ell}(\Omega) S_{\eta\eta}(\Omega) \quad (3.80)
\end{aligned}$$

### 3.5 Response Spectra

The final step in the calculation of the nondeterministic static response of the riser is that relating the random wave forces to the random response. Response parameters of interest are the node deflections and moments and the bottom rotation of the riser. The approach adopted here is to first calculate the spectral densities of the node deflections and express the remaining response spectra in terms of these deflection spectra.

#### 3.5.1 Random Node Deflections

Let  $\{Y(t)\}$  be an  $n$  by 1 vector of random node deflections caused by the random wave forces,  $\{P(t)\}$ . The random deflections are related to the random force intensities by

$$[K] \{Y(t)\} = \{P(t)\} \quad (3.81)$$

in which the stiffness matrix  $[K]$  is defined by Eqs. 2.12. To obtain  $\{Y(t)\}$ , Eq. 3.81 is premultiplied by  $[K]^{-1}$ .

$$\{Y(t)\} = [K]^{-1} \{P(t)\} \quad (3.82)$$

A form of Eq. 3.82 which is useful for calculating the correlation functions



and spectral densities of the deflections is

$$Y_{ni}(t) = \sum_{nk=1}^n K_{ni,nk}^{-1} P_{nk}(t) \quad (3.83)$$

Because the node deflections are linear functions of the random force intensities, they are zero mean, Gaussian, and stationary.

By definition, the correlation function of the response at nodes  $ni$  and  $nj$  is given by

$$R_{Y_{ni}Y_{nj}}(\tau) = E[Y_{ni}(t)Y_{nj}(t+\tau)] \quad (3.84)$$

When Eq. 3.83 is substituted into Eq. 3.84 and the order of summation and expectation is interchanged, there results

$$R_{Y_{ni}Y_{nj}}(\tau) = \sum_{nk=1}^n \sum_{n\ell=1}^n K_{ni,nk}^{-1} K_{nj,n\ell}^{-1} R_{P_{nk}P_{n\ell}}(\tau) \quad (3.85)$$

The response spectral density is obtained by a Fourier transformation of the correlation function.

$$\tilde{S}_{Y_{ni}Y_{nj}}(\Omega) = \frac{1}{2\pi} \int_{-\infty}^{\infty} R_{Y_{ni}Y_{nj}}(\tau) e^{-i\Omega\tau} d\tau \quad (3.86)$$

Substituting Eq. 3.85 into Eq. 3.86 and interchanging the order of integration and summation leads to

$$S_{Y_{ni}Y_{nj}}(\Omega) = \sum_{nk=1}^n \sum_{n\ell=1}^n K_{ni,nk}^{-1} K_{nj,n\ell}^{-1} S_{P_{nk}P_{n\ell}}(\Omega) \quad (3.87)$$





Equation 3.87, together with Eq. 3.80 may be used to calculate the spectral density of the random static deflection resulting from the random sea described by the sea surface elevation spectrum,  $S_{\eta\eta}(\omega)$ .

### 3.5.2 Random Bottom Rotation

Consider the random bottom rotation,  $\theta_0(t)$ , defined as the slope of the deflection curve,  $Y(x,t)$ , at  $x = 0$ .

$$\theta_0(t) = \frac{\partial}{\partial x} Y(0,t) \quad (3.88)$$

By using Eq. 2.3, a finite difference version of Eq. 3.88 may be written,

$$\theta_0(t) = \frac{n+1}{2L} [-Y_{-1}(t) + Y_1(t)] \quad (3.89)$$

where  $Y_{-1}$  is the deflection of an imaginary node located a distance  $\frac{L}{n+1}$  below the riser bottom. Because the bending moment at the bottom of the riser is zero,  $Y_{-1}(t) = -Y_1(t)$ , as shown by Eq. 2.9b, and

$$\theta_0 = \frac{n+1}{L} Y_1(t) \quad (3.90)$$

The autocorrelation function of the bottom rotation is

$$R_{\theta_0\theta_0}(\tau) = E[\theta_0(t)\theta_0(t+\tau)] \quad (3.91)$$

which, after substitution of Eq. 3.90, becomes

$$R_{\theta_0\theta_0}(\tau) = \left(\frac{n+1}{L}\right)^2 R_{Y_1Y_1}(\tau) \quad (3.92)$$

A Fourier transformation of Eq. 3.92 yields



$$S_{\theta_0 \theta_0}(\Omega) = \left( \frac{n+1}{L} \right)^2 S_{Y_1 Y_1}(\Omega) \quad (3.93)$$

### 3.5.3 Random Bending Moments

Like the bottom rotation spectral density, the bending moment spectral density may be determined from the deflection spectral densities. Let  $M(x,t)$  be the wave-induced random bending moment at coordinate  $x$  and  $M_{ni}(t)$  be the random bending moment at node  $ni$ . From small deflection beam theory, the bending moment of the riser is related to the deflected shape,  $Y(x,t)$ , by

$$M(x,t) = -EI \frac{\partial^2 Y}{\partial x^2} \quad (3.94)$$

Equation 3.94 is transformed into finite difference form by introducing Eq. 2.2 for the second derivative.

$$M_{ni}(t) = - \left( \frac{n+1}{L} \right)^2 EI [ Y_{ni-1} - 2Y_{ni} + Y_{ni+1} ] \quad (3.95)$$

This transformation between random node deflections and random node moments is conveniently expressed in matrix form,

$$\{ M(t) \} = [ J ] \{ Y(t) \} \quad (3.96)$$

where  $[ J ]$  is an  $n$  by  $n$ , three term banded transformation matrix whose nonzero elements are

$$J_{ni,ni} = 2EI \left( \frac{n+1}{L} \right)^2, \quad ni = 1, n \quad (3.97a)$$

$$J_{ni,ni+1} = -EI \left( \frac{n+1}{L} \right)^2, \quad ni = 1, n-1 \quad (3.97b)$$

$$J_{ni,ni-1} = -EI \left( \frac{n+1}{L} \right)^2, \quad ni = 2, n \quad (3.97c)$$



A convenient form of Eq. 3.96, which takes account of the banded nature of  $[J]$ , is

$$M_{ni}(t) = \sum_{nk=ni-1}^{ni+1} J_{ni,nk} Y_{nk}(t) \quad (3.98)$$

The correlation function of the random moment at node  $ni$  and the random moment at node  $nj$  is

$$R_{M_{ni}M_{nj}}(\tau) = E[M_{ni}(t) M_{nj}(t + \tau)] \quad (3.99)$$

Substitution of Eq. 3.98 into Eq. 3.99 leads to

$$R_{M_{ni}M_{nj}}(\tau) = \sum_{nk=ni-1}^{ni+1} \sum_{n\ell=nj-1}^{nj+1} J_{ni,nk} J_{nj,n\ell} R_{Y_{nk}Y_{n\ell}}(\tau) \quad (3.100)$$

A Fourier transformation of both sides of Eq. 3.100 results in

$$S_{M_{ni}M_{nj}}(\Omega) = \sum_{nk=ni-1}^{ni+1} \sum_{n\ell=nj-1}^{nj+1} J_{ni,nk} J_{nj,n\ell} S_{Y_{nk}Y_{n\ell}}(\Omega) \quad (3.101)$$

### 3.6 Sample Problem

In this chapter, a model for calculating the response of a marine riser to random wave forces has been developed without consideration of dynamic effects. In order to illustrate the influence of nondynamic effects on the response, a sample problem has been solved with the use of this model.

The riser installation chosen for the sample problem has the following characteristics,



$$G_L = 216$$

$$D = 20 \text{ inches}$$

$$h=L = 609 \text{ feet}$$

$$E = 29 \times 10^6 \text{ pounds per square inch}$$

$$I = .0621 \text{ feet}^4$$

$$w = 248 \text{ pounds per foot}$$

The ratio of top tension to riser submerged weight is 1.2, and drag and inertia coefficients are 1.0 and 1.5 respectively. A finite difference model with 31 equally spaced nodes is used to represent the riser, and the random sea surface elevation is taken as that described by the Pierson-Moskowitz spectrum.

If the entire mathematical model is considered to be a linear system whose input is the sea surface elevation spectral density function and whose output is a response spectrum such as the bottom rotation spectral density, then the problem may be expressed as

$$S_{\theta_o\theta_o}(\omega) = \Gamma_{\theta_o}(\omega) \cdot S_{\eta\eta}(\omega) \quad (3.102)$$

where  $\Gamma_{\theta_o}(\omega)$  is the bottom rotation power transfer function of the system. From Eqs. 3.80, 3.87, and 3.93, it follows that the bottom rotation power transfer function is given by





$$\begin{aligned}
r_{\theta_0}(\Omega) = & \left[ \frac{n+1}{L} \right]^2 \left[ \frac{kg}{\Omega} \right]^2 \\
& \cdot \sum_{nk=1}^n \sum_{n\ell=1}^n K_{1,nk}^{-1} K_{1,n\ell}^{-1} \left[ \dot{c}_u^2 \frac{8}{\pi} \sigma_{\dot{u}_{nk}} \dot{u}_{n\ell} \right. \\
& + i\Omega \dot{c}_u \dot{c}_a \sqrt{\frac{8}{\pi}} (\sigma_{\dot{u}_{nk}} - \sigma_{\dot{u}_{n\ell}}) \\
& \left. + \dot{c}_a^2 \Omega^2 \right] \tilde{q}_{nk}(\Omega) \tilde{q}_{n\ell}(\Omega)
\end{aligned} \tag{3.103}$$

Figures 3.6a, 3.6b, 3.6c and 3.6d show the input sea surface elevation spectral density, the bottom rotation power transfer function, and the static bottom rotation spectral density for wind velocities of 10, 20, 30, and 40 knots. The variation of variance and standard deviation of the bottom rotation with wind velocity is shown in Fig. 3.7a and 3.7b.

In all cases, the bottom transfer function decreases markedly with increasing frequency. It may be concluded then that the effect of linear wave theory, the Morrison force formula, and the structural response to static wave loads, is to filter out the high frequency components of the sea surface elevation spectrum. This is illustrated in Fig. 3.6a through 3.6d where, in each case, the output bottom rotation spectrum has a narrower frequency band (is more sharply peaked) than the input sea surface elevation spectrum.

For low wind velocities, the static response of the riser is almost entirely a result of the inertia force. At a wind velocity of 30 knots, that part of the response caused by drag force is perceptible, and at a wind velocity of 40 knots, the effect of the drag force is appreciable. The rapid increase in the importance of the drag force at higher wind velocities is a consequence of its nonlinear nature.



## Chapter 4

### THE DYNAMIC RESPONSE OF A MARINE RISER TO RANDOM WAVE FORCES

#### 4.1 General

A major objective of this thesis is the development of a mathematical model for predicting the random dynamic response of a marine drilling riser to the random forces produced by ocean waves. Parts of this model are derived in the preceding two chapters. A finite difference structural model and a lumped-smeared force model are developed in Chapter 2 and are combined with linear wave theory and Morrison's force equation in Chapter 3 to formulate a model for determining the static response of the riser to random sea waves. Dynamic considerations are purposely avoided in Chapter 3 in order to simplify the overall development and focus attention on how the input sea surface elevation spectrum is modified or filtered by linear wave theory and Morrison's force formula. In this chapter, response spectral density functions are derived with dynamic effects considered.

Some of the relationships derived in Chapters 2 and 3 for the static riser problem remain valid for the dynamic problem. The power transfer functions relating fluid kinematic spectra to sea surface elevation spectra are equally applicable whether the problem is static or dynamic. As shown in Section 2.4.2, the natural frequencies and mode shapes of the riser, which are needed in the dynamic analysis, may be obtained by using the finite difference model. The lumped-smeared system of representing wave force intensity is independent of time effects and thus is also applicable to the dynamic problem.



A unique feature of the dynamic riser problem is that the random wave force intensity is dependent upon the random riser response. The hydrodynamic force intensity is a function not of the absolute water particle velocity and acceleration, but of the relative velocity and acceleration of the water particles with respect to the structure. In addition to modifying the wave force, wave structure interaction also produces a hydraulic damping effect on the structural response.

The method used here for determining the dynamic response of the riser to water waves is adapted from recently published works of Foster<sup>19</sup> and Malhotra and Penzien,<sup>20,21</sup> who developed methods for calculating the random response of offshore towers to ocean waves. The method is modified as necessary to meet the requirements of the riser problem.

## 4.2 Equation of Motion for Dynamic Riser Problem

The governing differential equation of the marine riser is Eq. 1.3, which is repeated here for convenience.

$$EI \frac{d^4 y}{dx^4} - T(x) \frac{d^2 y}{dx^2} - w \frac{dy}{dx} = p(x) \quad (1.3)$$

When dynamic effects are significant, the riser deflection,  $y$ , is a function not only of position,  $x$ , but also of time,  $t$ , and the derivatives in Eq. 1.3 are properly written as partial derivatives.

$$EI \frac{\partial^4 y(x,t)}{\partial x^4} - T(x) \frac{\partial^2 y(x,t)}{\partial x^2} - w \frac{\partial y(x,t)}{\partial x} = p(x,t) \quad (4.1)$$

The lateral force on the riser,  $p(x,t)$ , may consist of several components--a random hydrodynamic force, a force whose effect is equivalent to that of a random top offset, a d'Alembert force caused by opposition of



the riser mass to acceleration, and a damping force which is also opposed to the motion of the riser.

$$p(x,t) = P(x,t) + \hat{P}(x,t) - m \frac{\partial^2 y}{\partial t^2} - P_D(x,t) \quad (4.2)$$

where

$P(x,t)$  = the random hydrodynamic force

$\hat{P}(x,t)$  = the force intensity equivalent to a random top offset

$m$  = riser system mass per unit length

$P_D(x,t)$  = the damping force

#### 4.2.1 Equation of Motion in Matrix Form

When the method of finite differences is applied to Eq. 4.1, the riser is replaced by a system having  $n$  equally spaced nodes and  $n$  degrees of freedom. The terms on the left side of Eq. 4.1 are gathered into the stiffness matrix defined by Eqs. 2.12, and Eq. 4.1 assumes the form

$$[K]_{n \times n} \{Y(t)\}_{n \times 1} = \{p(t)\}_{n \times 1} \quad (4.3)$$

In Eq. 4.3, the force vector  $\{p(t)\}$  may be replaced by its constituent forces as given in Eq. 4.2.

$$\{p(t)\} = \{P(t)\} + \{\hat{P}(t)\} - [m] \{\ddot{Y}\} - [c] \{\dot{Y}\} \quad (4.4)$$

where

$\{P(t)\}$  = a vector of random hydrodynamic force intensities

$\{\hat{P}(t)\}$  = a vector of force intensities which are equivalent to the top offset





- $[m]$  = an nxn diagonal mass matrix  
 $[c]$  = an nxn matrix of damping coefficients  
 $\{\ddot{Y}\}$  = a vector of random riser accelerations at the nodes  
 $\{\dot{Y}\}$  = a vector of random riser velocities at the nodes  
 $[c]\{\dot{Y}\}$  = a vector of damping force intensities

Consideration of the effect of random top offset is deferred until Chapter 5. For the present,  $\{P(t)\}$  is taken as zero.

The applied random hydrodynamic force intensity is a function of the fluid velocity and fluid acceleration, as indicated by Eq. 2.23. The fluid velocity may consist of a steady current and an unsteady component caused by surface waves. The effect of a steady current is studied in Chapter 5. For the present discussion, the steady current is taken as zero, and the fluid velocity is solely that caused by waves. If the structure responds to the applied force in such a way that the structural velocities and accelerations are significant with respect to the fluid velocities and accelerations, then the wave forces of Eq. 2.23 should be written as functions of the relative fluid velocity and acceleration with respect to the structure.

Let  $\dot{V}$  be the relative velocity of the water with respect to the structure and  $\ddot{V}$  be the relative acceleration of the water with respect to the structure.

$$\dot{V} = \dot{U} - \dot{Y} \quad (4.5a)$$

$$\ddot{V} = \ddot{U} - \ddot{Y} \quad (4.5b)$$

The variables  $\dot{V}$  and  $\ddot{V}$  are both linear functions of zero-mean Gaussian random variables and are therefore also zero-mean Gaussian random variables.



When wave structure interaction is considered, Morrison's formula, Eq. 2.23, assumes the form

$$P(x,t) = C_D \frac{1}{2} \rho D \dot{V} |\dot{V}| + C_I \rho \frac{\pi D^2}{4} \ddot{V} \quad (4.6)$$

or in matrix form

$$\{P(t)\} = C_u \{\dot{V}|\dot{V}|\} + C_a \{\ddot{V}\} \quad (4.7)$$

where

$$\dot{V}_{nk} |\dot{V}_{nk}| = (\dot{U}_{nk} - \dot{Y}_{nk}) |\dot{U}_{nk} - \dot{Y}_{nk}|$$

and

$$\ddot{V}_{nk} = \ddot{U}_{nk} - \ddot{Y}_{nk}$$

Equations 4.3, 4.4, and 4.7 combine to yield the following

$$[m]\{\ddot{Y}\} + [c]\{\dot{Y}\} + [K]\{Y\} = C_u \{\dot{V}|\dot{V}|\} + C_a \{\ddot{V}\} \quad (4.8)$$

Equation 4.8 represents, in matrix form, the  $n$  simultaneous differential equations of motion for an  $n$  degree-of-freedom finite difference model of a marine riser subjected to random wave forces. The drag force term is a nonlinear function of the relative velocity. This nonlinearity will be removed by the method of equivalent linearization which was introduced in Section 3.4.1.

#### 4.2.2 Linearization of the Equation of Motion

The technique of linearization used here is essentially the same as that used by Malhotra and Penzien.<sup>20</sup> First the structural displacement, velocity, and acceleration terms of Eq. 4.8 are removed by the transformations



$$\{Y\} = \{U\} - \{V\} \quad (4.9a)$$

$$\{\dot{Y}\} = \{\dot{U}\} - \{\dot{V}\} \quad (4.9b)$$

$$\{\ddot{Y}\} = \{\ddot{U}\} - \{\ddot{V}\} \quad (4.9c)$$

In Eq. 4.9a,  $\{U\}$  and  $\{V\}$  are vectors of the absolute and relative fluid displacements at the nodes. Equations 4.9 follow from Eqs. 4.5. When Eqs. 4.9 are substituted into Eq. 4.8 and the resulting terms are rearranged, the  $n$  simultaneous differential equations are expressed in a relative coordinate system with respect to the riser structure.

$$\begin{aligned} [m_e]\{\ddot{V}\} + [c]\{\dot{V}\} + [K]\{V\} + C_U\{\dot{V}|\dot{V}|\} &= [m]\{\ddot{U}\} \\ &+ [c]\{\dot{U}\} + [K]\{U\} \end{aligned} \quad (4.10)$$

where

$$[m_e] = [m] + C_a[I]$$

and  $[I]$  is the unit diagonal matrix.

In Eq. 4.10, there is one nonlinear term involving the relative fluid velocity with respect to the structure. This nonlinearity will be removed by the method of equivalent linearization. Let

$$[c]\{\dot{V}\} + C_U\{\dot{V}|\dot{V}|\} = [\tilde{c}]\{\dot{V}\} + \{E\} \quad (4.11)$$

where  $[\tilde{c}]$  is a matrix of modified damping coefficients and  $\{E\}$  is a vector of the errors which result when  $[\tilde{c}]\{\dot{V}\}$  is used to replace the two terms on the left side of Eq. 4.11.

$$\{E\} = ([c] - [\tilde{c}])\{\dot{V}\} + C_U\{\dot{V}|\dot{V}|\} \quad (4.12)$$



Elements of the error vector are functions of the random variable  $\dot{V}$ , and hence are random variables themselves. It is convenient to let

$$c_{n_i, n_j} = c_{n_i, n_j} \quad \text{for } n_i \neq n_j \quad (4.13)$$

that is, the off-diagonal terms of  $[\hat{c}]$  are assumed to be identical to the off-diagonal terms of  $[c]$ . This is a reasonable assumption because it simply implies that the hydraulic damping force at a given node is independent of the relative velocity at other nodes. This assumption permits an uncoupling of Eq. 4.12, which may now be written

$$E_{nj} = (c_{nj, nj} - \hat{c}_{nj, nj}) \dot{V}_{nj} + c_u \dot{V}_{nj} |\dot{V}_{nj}| \quad (4.14)$$

To linearize Eq. 4.10, elements of the modified damping matrix  $[\hat{c}]$  are selected such that the mean square values of the elements of the random error vector,  $\{E\}$ , are minimized. The mean square error is the second moment of the error or the expected value of the square of the error.

$$E[E_{nj}^2] = E[(c_{nj, nj} - \hat{c}_{nj, nj}) \dot{V}_{nj} + c_u \dot{V}_{nj} |\dot{V}_{nj}|]^2 \quad (4.15)$$

The mean square error is minimum with respect to  $\hat{c}_{nj, nj}$  when

$$\frac{\partial}{\partial \hat{c}_{nj, nj}} \{E[E_{nj}^2]\} = 0 \quad (4.16)$$

In Eq. 4.16, the partial derivative and the expectation, both being linear operations, may be interchanged.

$$2E\{E_{nj} \frac{\partial E_{nj}}{\partial \hat{c}_{nj, nj}}\} = 0 \quad (4.17)$$





From Eq. 4.14,

$$\frac{\partial E_{nj}}{\partial c_{nj,nj}} = -\dot{V}_{nj} \quad (4.18)$$

Substitution of Eqs. 4.14 and 4.18 into Eq. 4.17 results in

$$2E\{(c_{nj,nj} - c_{nj,nj}) \dot{V}_{nj} + C_u \dot{V}_{nj} |\dot{V}_{nj}| \cdot [-\dot{V}_{nj}]\} = 0 \quad (4.19)$$

Equation 4.19 may be rearranged by combining terms and taking constants outside the expectation operator.

$$-(c_{nj,nj} - c_{nj,nj}) E[\dot{V}_{nj}^2] - C_u E[\dot{V}_{nj}^2 |\dot{V}_{nj}|] = 0 \quad (4.20)$$

Solution of Eq. 4.20 for  $c_{nj,nj}$  results in

$$c_{nj,nj} = c_{nj,nj} + C_u \frac{E[\dot{V}_{nj}^2 |\dot{V}_{nj}|]}{E[\dot{V}_{nj}^2]} \quad (4.21)$$

Because the relative fluid velocity at node  $nj$ ,  $\dot{V}_{nj}$ , is a zero-mean Gaussian random variable,

$$E[\dot{V}_{nj}^2] = \sigma_{V_{nj}}^2 \quad (4.22)$$

From Eq. 3.69, it follows that

$$E[\dot{V}_{nj}^2 |\dot{V}_{nj}|] = \sqrt{\frac{8}{\pi}} \sigma_{V_{nj}}^3 \quad (4.23)$$

Substitution of Eqs. 4.22 and 4.23 into Eq. 4.21 leaves

$$c_{nj,nj} = c_{nj,nj} + C_u \sqrt{\frac{8}{\pi}} \sigma_{V_{nj}} \quad (4.24)$$



Equations 4.13 and 4.24 are conveniently expressed in matrix form.

$$[\tilde{c}] = [c] + C_{\dot{U}} \sqrt{\frac{8}{\pi}} [\sigma_{\dot{V}}] \quad (4.25)$$

where  $[\sigma_{\dot{V}}]$  is an  $n \times n$  diagonal matrix of standard deviations of the relative fluid structure velocity at the riser nodes.

The modified damping matrix,  $[\tilde{c}]$ , given by Eq. 4.25, minimizes the mean square error because

$$\frac{\partial^2}{\partial c_{nj,nj}^2} E[E_{nj}^2] = E \left[ \frac{\partial^2 E_{nj}^2}{\partial c_{nj,nj}^2} \right] = E[\dot{V}_{nj}^2] = \sigma_{\dot{V}_{nj}}^2 \quad (4.26)$$

and the variance is always non-negative. With the mean square error minimized, an approximation to Eq. 4.11 may be made by dropping the error vector.

$$[c]\{\dot{V}\} + C_{\dot{U}}\{\dot{V}|\dot{V}\} \approx [\tilde{c}]\{\dot{V}\} \quad (4.27)$$

Equation 4.27 is suitable for substitution into the matrix form of the equations of motion, Eq. 4.10.

$$[m_e]\{\ddot{V}\} + [\tilde{c}]\{\dot{V}\} + [K]\{V\} = [m]\{\ddot{U}\} + [c]\{\dot{U}\} + [K]\{U\} \quad (4.28)$$

Equation 4.28 may be transformed from the relative coordinate system back into the absolute system by utilizing Eqs. 4.5 and the relationship

$$\{V\} = \{U\} - \{Y\} \quad (4.29)$$

which follows from Eq. 4.9a. This transformation leads to



$$\begin{aligned}
[m_e]\{\ddot{Y}\} + [c]\{\dot{Y}\} + [K]\{Y\} &= ([m_e] - [m])\{\ddot{U}\} \\
&+ ([c] - [c])\{\dot{U}\}
\end{aligned}
\quad (4.30)$$

But

$$[m_e] - [m] = c_a [I]$$

and

$$[c] - [c] = c_u \sqrt{\frac{8}{\pi}} [\sigma \dot{V}]$$

Therefore,

$$[m_e]\{\ddot{Y}\} + [c]\{\dot{Y}\} + [K]\{Y\} = c_a \{\ddot{U}\} + c_u \sqrt{\frac{8}{\pi}} [\sigma \dot{V}]\{\dot{U}\} \quad (4.31)$$

Equation 4.31 is the linearized version of the nonlinear equation of motion, Eq. 4.8, relating random riser node displacements,  $\{Y(t)\}$  to random water particle velocities and accelerations,  $\{\dot{U}(t)\}$  and  $\{\ddot{U}(t)\}$ .

In Eq. 4.31, the drag force and the modified damping matrix are functions of the matrix of standard deviations of the relative fluid velocity, which is itself a function of the response. Therefore, an iterative procedure is required for the solution of Eq. 4.31.

#### 4.2.3 Technique of Solution of Linearized Equations of Motion.

The equation of motion in matrix form, Eq. 4.31, actually represents  $n$  simultaneous differential equations. To obtain a solution relating  $\{Y\}$  to the random water particle kinematics, a choice of techniques is available. Solving a similar problem for an offshore platform model with five degrees of freedom, Foster<sup>19</sup> employs the method of nonclassical,



complex-valued mode superposition as outlined by Hurty and Rubinstein.<sup>19</sup> A more convenient and efficient method for the riser, which has many more degrees of freedom, is classical mode superposition. With a technique similar to that of Malhotra and Penzien,<sup>20</sup> the  $n$  equations of motion, Eq. 4.31, may be uncoupled by using the orthogonal properties of the classical normal modes. Uncoupling the damping terms requires some additional approximations to the damping matrix.

Use of the normal mode superposition technique requires knowledge of the structure's natural frequencies of vibration (eigenvalues) and corresponding mode shapes (eigenvectors). In Section 4.3, solution of the eigenvalue problem is discussed. The following section (Section 4.4) then deals with the application of the eigenvectors and eigenvalues to the problem of uncoupling and solving the equations of motion.

#### 4.3 The Riser Eigenvalue Problem - Natural Frequencies and Mode Shapes

To determine the natural frequencies and mode shapes of the marine riser, it is necessary to solve the undamped free vibration problem, which is stated mathematically by writing Eq. 4.31 without the damping term and with no applied force.

$$[m_e]\{\ddot{Y}\} + [K]\{Y\} = \{0\} \quad (4.32)$$

It is assumed that Eq. 4.32 possesses solutions of the form

$$Y_{nj}(t) = A \cos(\omega t + \psi) \quad (4.33)$$

The double differentiation of Eq. 4.33 with respect to time produces the useful relationship





$$\ddot{Y}_{nj}(t) = -\omega^2 Y_{nj}(t) \quad (4.34)$$

Upon the introduction of Eq. 4.34, Eq. 4.32 becomes

$$-[\underline{m}_e] \omega^2 \{Y\} + [K] \{Y\} = \{0\} \quad (4.35)$$

When Eq. 4.35 is premultiplied by  $\frac{1}{\omega^2} [K]^{-1}$ , there results

$$-[K]^{-1} [\underline{m}_e] \{Y\} + \frac{1}{\omega^2} \{Y\} = \{0\} \quad (4.36)$$

Let  $[\tilde{D}] = [K]^{-1} [\underline{m}_e]$  be the dynamical matrix. Then, Eq. 4.36 simplifies to the characteristic equation

$$[\tilde{D}] \{Y\} = \frac{1}{\omega^2} \{Y\} \quad (4.37)$$

Solutions to Eq. 4.37 are the natural frequencies,  $\omega_r$ , and corresponding mode shapes,  $\{\phi^{(r)}\}_{n \times 1}$ , of the marine riser.

Eigenvalues and eigenvectors of the marine riser were calculated with the University of Illinois subroutine EIGENP, described in Chapter 2. The favorable agreement of the eigenvalues for the first three modes with other published solutions is also discussed in Chapter 2.

The solution for the  $r^{\text{th}}$  mode satisfies Eq. 4.37

$$[\tilde{D}] \{\phi^{(r)}\} = \frac{1}{\omega_r^2} \{\phi^{(r)}\}$$

$$[K]^{-1} [\underline{m}_e] \{\phi^{(r)}\} = \frac{1}{\omega_r^2} \{\phi^{(r)}\} \quad (4.38)$$

Premultiplication of Eq. 4.38 by  $\omega_r^2 [K]$  leaves



$$\omega_r^2 [m_e]_{\{\phi\}}^{(r)} = [K]_{\{\phi\}}^{(r)} \quad (4.39)$$

Equation 4.39 will prove useful in uncoupling the equations of motion for forced vibration in Section 4.4.

### 4.3.1 Behavior of Riser Frequencies

It is instructive to compare the fundamental frequencies of marine risers to the fundamental frequencies of other structures which belong to the same family. Such other structures include the constant tension beam, the two limiting cases of which are the simple beam and the unstiffened (constant tension) string, and the hanging chain (or string with variable tension), which is the limiting case of the riser when the flexural stiffness approaches zero. Figures 4.1 and 4.2 show the variation of the fundamental frequencies of these structures with the cube root of the length ratio,  $G_L$ , for top tension ratios of 1.0 and 1.2 respectively. For the constant tension beam and the unstiffened string, corresponding average tension ratios of 0.5 and 0.7 were used to compute the natural frequencies.

From Figs. 4.1 and 4.2, it is possible to make several observations regarding the behavior of the fundamental riser frequency. The constant tension beam frequency constitutes an upper bound on the fundamental riser frequency. A lower bound is given by the larger of the hanging chain frequency or the simple beam frequency. As the tension ratio increases, the difference between upper and lower bounds decreases. As  $G_L$  decreases, the fundamental riser frequency approaches that of the constant tension beam; as  $G_L$  increases, the fundamental riser frequency approaches that of the hanging chain (A conclusion similar to this latter observation was reached by Frohrib and Plunkett<sup>6</sup> who found that bending stiffness has a



small effect on the natural frequencies of long drill strings.) These observations are useful in estimating the fundamental riser frequency if that frequency is unknown.

It is also of interest to study the variation of the first few riser frequencies with water depth for a given riser section. Figures 4.3 and 4.4 show this variation for the first five frequencies of a typical riser section and for top tension ratios of 1.0 and 1.2 respectively. In general, the frequency for a given mode decreases as water depth increases and as top tension ratio decreases. As water depth increases, the difference between the natural frequencies of various modes decreases, that is, the natural frequencies become more closely grouped along the frequency axis. The significance of this latter observation is that for a given riser section and a given sea surface elevation spectrum, the number of modes which make an appreciable contribution to the dynamic response tends to increase as water depth increases.

#### 4.3.2 Natural Frequencies of the Riser With Static Curvature

The preceding discussion regarding riser frequencies applies to risers with no static curvature. In practice, real risers almost always have some static curvature because of the top offset which results from lateral motion of the floating surface support platform. Frohrib and Plunkett<sup>6</sup> have shown that a drill string suspended in such a way that it deforms under its own weight has natural frequencies which differ from those of a vertical drill string. It will be shown here, however, that for top offsets which are consistent with small allowable bottom rotations, the natural frequencies of the riser may be taken as those for the case of no static curvature.



According to Frohrib and Plunkett,<sup>6</sup> the characteristic equation for the drill string with static curvature and with vibration limited to the plane of that static curvature is given by

$$EI \frac{d^4 y}{dx^4} - T \frac{d^2 y}{dx^2} - \frac{dT}{dx} \frac{dy}{dx} - \omega^2 m y - 2T \left( \frac{d^2 y_s}{dx^2} \right) y = 0 \quad (4.40)$$

where  $y(x)$  is the dynamic component of motion and  $y_s$  is the static deflection. Because the axial tension,  $T$ , is not necessarily vertical,  $dT/dx$  is not exactly equal to  $w$ , the submerged weight of the string per unit length.

Consider the axial tension in a marine riser. The maximum slope in a riser with top offset occurs at the lower end and is limited to a few degrees by the nature of the bottom joint. Even if the bottom rotation is as much as five degrees, the vertical component of the tension,  $T_x$ , is nearly equal to the total tension,  $T$ .

$$T_x = T \cos (5^\circ) = 0.996 T \approx T \quad (4.41a)$$

Furthermore,

$$\frac{dT}{dx} = \frac{1}{0.996} \frac{dT_x}{dx} = 1.004 w \approx w \quad (4.41b)$$

Thus, if the bottom rotation is limited to a small angle, the axial tension may be considered as being essentially vertical in direction and the derivative of axial tension with respect to the vertical coordinate may be taken as the riser submerged weight per unit length.

The last term in Eq. 4.40 is a function of the static curvature,  $d^2 y_s / dx^2$ . The magnitude of the static curvature for a given top offset depends, to a great extent, upon the length ratio,  $G_L = wL^3 / EI$ . If the





riser is infinitely stiff, then  $G_L$  is zero, and a top offset results in a rigid body rotation with constant slope along the riser and no curvature. As stiffness decreases and  $G_L$  increases, a given top offset results in an increasingly large static curvature, and the last term of Eq. 4.40 assumes greater importance. There must be some range of values of  $G_L$  commencing at zero and extending to some upper limit, in which the curvature term has a negligible effect on the natural frequencies. If the riser length ratios are within this range, then the solution to the eigenvalue problem for the vertical riser is a very good approximation to the solution for the riser with static curvature.

Another approach may be used to demonstrate the applicability of the vertical riser solution to the static curvature case. In their investigations, Frohrib and Plunkett<sup>6</sup> found that even for unstiffened strings, if the ratio of the horizontal reaction to the weight of the string is small enough, then static curvature has little influence on the natural frequencies. Figure 4.5 shows the variation of this horizontal reaction ratio with bottom rotation for some typical risers with static curvature caused by a top offset. For a given rotation, the horizontal reaction ratio decreases as stiffness decreases (that is, as  $G_L$  increases). The horizontal reactions corresponding to riser rotations of a few degrees are in the range where Frohrib and Plunkett found that static curvature has little effect on the natural frequencies.

It may be concluded therefore, that if the riser bottom rotation is limited to a few degrees, then the eigenvalues and eigenvectors for the vertical riser are close approximations to the eigenvalues and eigenvectors of the riser with top offset. The analysis of the riser with random top



offset is greatly simplified by this situation. It should be remembered, however, that for a riser installation in which large bottom rotations are permitted and do occur, the use of the vertical riser eigenvalues and eigenvectors for analysis may result in unacceptable errors.

#### 4.4 Solution of the Equations of Motion

The solution of the linearized equations of motion, which are represented in matrix form by Eq. 4.31, is accomplished in two steps. First, because the  $n$  equations are simultaneous, it is necessary to perform a transformation which uncouples them. The  $n$  independent equations which result from the transformation may then be solved using conventional methods of vibration analysis.

##### 4.4.1 Uncoupling the Equations of Motion

It is convenient to replace the hydrodynamic force terms in Eq. 4.31 with a single random force intensity vector,  $\{P(t)\}$ .

$$\{P(t)\} = C_a \{\ddot{U}(t)\} + C_u \sqrt{\frac{g}{\pi}} [\sigma_V] \{\dot{U}(t)\} \quad (4.42)$$

Let

$$[\phi]_{n \times nm} = [\{\phi^{(1)}\} \{\phi^{(2)}\} \dots \{\phi^{(nm)}\}] \quad (4.43)$$

be a matrix of node deflections for all modes beginning with the fundamental mode and including the mode  $nm$ , where  $nm$  is the number of modes considered in the problem. The total number of modes for the finite difference model of the riser structure is  $n$ , so that  $nm$  can take any value from 1 to  $n$ . In many problems, only the lower modes make a significant contribution to the



structural response, and for that reason  $nm$  is chosen to be something less than  $n$ .

A useful property of  $[\phi]$  is its orthogonality with respect to the effective mass matrix.

$$[\phi]^T [m_e] [\phi] = [M^*] \quad (4.44)$$

where  $[\phi]^T$  is the transpose of matrix  $[\phi]$ . For the risers studied herein, the effective mass per unit length is a constant over the length of the riser. Furthermore, the EIGENP routine used to determine the riser eigenvectors produces an eigenvector matrix which is scaled in such a way that

$$[\phi]^T [\phi] = [I] \quad (4.45)$$

These two conditions permit a simplification of Eq. 4.44.

$$\begin{aligned} [\phi]^T [m_e] [\phi] &= m_e [\phi]^T [I] [\phi] \\ &= m_e [\phi]^T [\phi] \\ &= m_e [I] \end{aligned} \quad (4.46)$$

Equation 4.46 will be employed later in this section.

In the normal mode superposition method, the node deflections are expressed as a combination of contributions from  $nm$  normal modes.

$$\{Y(t)\}_{n \times 1} = [\phi]_{n \times nm} \{Z(t)\}_{nm \times 1} \quad (4.47)$$

where  $Z_r(t)$  is the normal coordinate for the  $r^{th}$  mode of vibration. The variable  $Z_r(t)$  is a random variable; the normal mode matrix,  $[\phi]$ , is not random. Equation 4.31 may be transformed into the normal coordinate system



by means of Eq. 4.47.

$$[m_e][\phi]\{\ddot{Z}\} + [c][\phi]\{\dot{Z}\} + [K][\phi]\{Z\} = \{P\} \quad (4.48)$$

The useful relationship expressed by Eq. 4.39, which is true for all modes,  $r$ , ranging from 1 to  $n$ , may be written in matrix form as

$$[K][\phi] = [m_e][\phi][\omega^2] \quad (4.49)$$

where  $[\omega^2]$  is a diagonal matrix of the squares of the natural circular frequencies and  $\omega_r^2$  is the square of the  $r^{\text{th}}$  natural frequency. The position of  $[\omega^2]$  in Eq. 4.49 is critical. Column  $r$  of  $[\phi]$  represents the  $r^{\text{th}}$  eigenvector  $\{\phi^{(r)}\}$ . For each element of  $\{\phi^{(r)}\}$  to be multiplied by  $\omega_r^2$ , it is necessary that  $[\omega^2]$  follow  $[\phi]$  on the right hand side of Eq. 4.49. Substitution of Eq. 4.49 into Eq. 4.48 eliminates the stiffness matrix.

$$[m_e][\phi]\{\ddot{Z}\} + [c][\phi]\{\dot{Z}\} + [m_e][\phi][\omega^2]\{Z\} = \{P\} \quad (4.50)$$

The key to uncoupling Eq. 4.50 is to premultiply each term of the equation by  $[\phi]^T$ .

$$\begin{aligned} [\phi]^T [m_e][\phi]\{\ddot{Z}\} + [\phi]^T [c][\phi]\{\dot{Z}\} \\ + [\phi]^T [m_e][\phi][\omega^2]\{Z\} = [\phi]^T \{P\} \end{aligned} \quad (4.51)$$

By means of Eq. 4.46, Eq. 4.51 may be simplified to

$$m_e\{\ddot{Z}\} + [C_0]\{\dot{Z}\} + m_e[\omega^2]\{Z\} = [\phi]^T \{P\} \quad (4.52)$$

where

$$[C_0] = [\phi]^T [c][\phi] \quad (4.53)$$





is the modal damping matrix. All of the terms of Eq. 4.52 are uncoupled except the damping term. Unless  $[C_0]$  is a diagonal matrix, Eq. 4.52 remains a system of  $nm$  simultaneous differential equations and all that has been achieved so far is to reduce the number of unknowns from  $n$  to  $nm$ . The modal damping matrix,  $[C_0]$ , is not, in general, a diagonal matrix, although, as it is shown in Section 4.6, the diagonal terms will predominate over the off-diagonal elements when damping is treated in a suitable manner.

Malhotra and Penzien<sup>20</sup> present a useful technique by which the modal damping matrix may be diagonalized to complete the uncoupling process. Let

$$[C_0]\{\dot{Z}\} = [C^*]\{\dot{Z}\} + \{E\} \quad (4.54)$$

where  $[C^*]$  is a diagonal matrix of equivalent damping coefficients and  $\{E\}$  is an error vector resulting from the substitution of  $[C^*]\{\dot{Z}\}$  for  $[C_0]\{\dot{Z}\}$ . Because the vector  $\{\dot{Z}\}$  is random, elements of the error vector  $\{E\}$  are also random. In Eq. 4.54, there are two unknown matrices,  $[C^*]$  and  $\{E\}$ . It is therefore possible to choose  $[C^*]$  in such a way as to minimize the errors  $\{E\}$ . Because the errors are random, they will be minimized in a mean square sense.

Equation 4.54 represents  $nm$  equations of the form

$$\sum_{s=1}^{nm} C_{0,r,s} \dot{Z}_s = C_{r,r}^* \dot{Z}_r + E_r \quad (4.55)$$

The value of  $C_{r,r}^*$  is determined from the requirement that the mean square error,  $E[E_r^2]$ , be minimized. Thus,



$$\frac{\partial}{\partial C_{r,r}^*} E[E_r^2] = 0 \quad (4.56)$$

The expectation and differentiation operators in Eq. 4.56 are linear and thus may be interchanged.

$$2E\left[E_r \frac{\partial E_r}{\partial C_{r,r}^*}\right] = 0 \quad (4.57)$$

From Eq. 4.55, the random error and its partial derivative are expressed as

$$E_r = \sum_{s=1}^{nm} C_{0,r,s} \dot{Z}_s - C_{r,r}^* \dot{Z}_r \quad (4.58)$$

$$\frac{\partial E_r}{\partial C_{r,r}^*} = -\dot{Z}_r \quad (4.59)$$

Substitution of Eqs. 4.58 and 4.59 into Eq. 4.57 leaves

$$E\left[-\sum_{s=1}^{nm} C_{0,r,s} \dot{Z}_r \dot{Z}_s + C_{r,r}^* \dot{Z}_r^2\right] = 0 \quad (4.60)$$

Interchanging the order of the expectation and addition operations yields

$$-\sum_{s=1}^{nm} C_{0,r,s} E[\dot{Z}_r \dot{Z}_s] + C_{r,r}^* E[\dot{Z}_r^2] = 0 \quad (4.61)$$

Because  $\dot{Z}_r$  is a zero-mean random variable for all  $r$ ,

$$E[\dot{Z}_r \dot{Z}_s] = c_{\dot{Z}_r \dot{Z}_s}^2$$



which is the covariance of the time derivatives of the normal coordinates for modes  $r$  and  $s$ . Furthermore,

$$E[\dot{z}_r^2] = \sigma_{\dot{z}_r \dot{z}_r}^2$$

which is the variance of the time derivative of the normal coordinate for mode  $r$ .

The solution of Eq. 4.67 for  $C_{r,r}^*$  is

$$C_{r,r}^* = \frac{\sum_{s=1}^{nm} C_{0r,s} \sigma_{\dot{z}_r \dot{z}_s}^2}{\sigma_{\dot{z}_r \dot{z}_r}^2} \quad (4.62)$$

The selection of  $C_{r,r}^*$  for all  $r$  using Eq. 4.62 minimizes the mean square value of elements of the error vector  $E$  because

$$\begin{aligned} \frac{\partial^2 E(E_r^2)}{\partial C_{r,r}^{*2}} &= E \left[ \frac{\partial^2 (E_r^2)}{\partial C_{r,r}^{*2}} \right] \\ &= E [\dot{z}_r^2] \\ &= \sigma_{\dot{z}_r \dot{z}_r}^2 \end{aligned} \quad (4.63)$$

and the variance is always non-negative. When the error is minimized, it is approximately true that

$$[C_0] \{\dot{z}\} = [C^*] \{\dot{z}\} \quad (4.64)$$



Substitution of Eq. 4.64 into Eq. 4.52 completes the uncoupling of the equations of motion.

$$m_e \ddot{\{Z\}} + [-C^*] \{\dot{Z}\} + m_e [-\omega^2] \{Z\} = [\phi]^T \{P\} \quad (4.65)$$

Equation 4.65 represents  $nm$  independent differential equations of the form

$$m_e \ddot{Z}_r + C_{r,r}^* \dot{Z}_r + m_e \omega_r^2 Z_r = \{\phi^{(r)}\}^T \{P\} \quad (4.66)$$

#### 4.4.2 Solution of the Uncoupled Equations of Motion

The solution to Eq. 4.66 is obtained by using the convolution integral (also referred to as Duhamel's integral) to obtain an expression for the random normal coordinate of the  $r^{\text{th}}$  mode. First each term of Eq. 4.66 is divided by  $m_e$ .

$$\ddot{Z}_r + \frac{C_{r,r}^*}{m_e} \dot{Z}_r + \omega_r^2 Z_r = \frac{1}{m_e} \{\phi^{(r)}\}^T \{P\} \quad (4.67)$$

Next, two new variables are introduced. Let  $\zeta_r$  be the damping ratio for mode  $r$ , defined by

$$\zeta_r = \frac{C_{r,r}^*}{2\omega_r m_e} \quad (4.68)$$

and let  $P_r^*(t)$  be the random modal force for mode  $r$  defined by

$$P_r^*(t) = \frac{1}{m_e} \{\phi^{(r)}\}^T \{P\} = \frac{1}{m_e} \sum_{nk=1}^n \phi_{nk}^{(r)} P_{nk}(t) \quad (4.69)$$

The substitution of Eqs. 4.68 and 4.69 into Eq. 4.67 leads to





$$\ddot{Z}_r + 2\zeta_r \omega_r \dot{Z}_r + \omega_r^2 Z_r = P_r^*(t) \quad (4.70)$$

Equation 4.70 is of a form commonly encountered in structural dynamics problems. The solution for  $Z_r(t)$  may be written using the convolution integral.<sup>32</sup>

$$Z_r(t) = \int_{\xi_1=-\infty}^t P_r^*(\xi_1) h_r(t-\xi_1) d\xi_1 \quad (4.71)$$

The function,  $h_r(\tau)$ , which is commonly known as the impulse response function, is defined by

$$\begin{aligned} h_r(\tau) &= 0, & \tau < 0 \\ &= \frac{e^{-\zeta_r \omega_r \tau} \sin(\sqrt{1 - \zeta_r^2} \omega_r \tau)}{\omega_r \sqrt{1 - \zeta_r^2}}, & \tau \geq 0 \end{aligned} \quad (4.72)$$

The variable  $\xi_1$  is simply a dummy time variable used in the integration process. The lower limit of integration,  $-\infty$ , implies that the random process has been going on so long that all transient starting effects have been damped out.

#### 4.5 Derivation of Response Spectral Density Functions

At this point, it is worthwhile to back away from the details of the problem and look again at the overall picture. The goal is a mathematical model relating the riser response spectra,  $S_{Y_{ni} Y_{nj}}(\Omega)$ ,  $S_{\theta_{oi} \theta_{oj}}(\Omega)$ , and  $S_{M_{ni} M_{nj}}(\Omega)$ , to the sea surface elevation spectrum,  $S_{\eta\eta}(\Omega)$ . So far, a relationship between the sea surface elevation spectrum and the water particle kinematic spectra has been developed with the use of linear wave theory.



This link, which is given by Eqs. 3.48, 3.54, and 3.56, is valid for both static and dynamic problems.

In this section, expressions relating the kinematic spectra to the response spectra are derived in four steps. Equation 4.42 gives the random force intensities,  $\{P(t)\}$ , in terms of the random fluid kinematics,  $\{\dot{U}(t)\}$  and  $\{\ddot{U}(t)\}$ . The random modal forces,  $\{P^*(t)\}$ , are expressed as functions of the random force intensities by Eq. 4.69. The random normal coordinates,  $\{Z(t)\}$ , are determined from the modal forces by Eq. 4.71. And the random node deflections,  $\{Y(t)\}$ , may be calculated from the normal coordinates by means of Eq. 4.47. With these four relationships, it is possible to develop formulas relating the corresponding spectral densities in a manner similar to that used in Chapter 3.

#### 4.5.1 Spectral Density of Random Wave Force Intensities

The expression for random wave force intensity for the linearized dynamic problem, Eq. 4.42, is very similar to the equation for random wave force intensity for the linearized static problem, Eq. 3.72.

$$P(x,t) = C_{\dot{U}} \sqrt{\frac{8}{\pi}} \sigma_{\dot{U}} \dot{U}(x,t) + C_{\ddot{U}} \ddot{U}(x,t) \quad (4.42)$$

$$P(x,t) = C_{\dot{U}} \sqrt{\frac{8}{\pi}} \sigma_{\dot{U}} \dot{U}(x,t) + C_{\ddot{U}} \ddot{U}(x,t) \quad (3.72)$$

The only difference between the two force equations is that the drag term of the static equation is a function of the standard deviation of the absolute water particle velocity,  $\sigma_{\dot{U}}$ , while the drag term of the dynamic equation is a function of the standard deviation of the water particle velocity relative to the structure,  $\sigma_{\dot{U}}$ . The force intensity spectral density



function for the dynamic problem could be derived in the same fashion as was used to derive Eq. 3.78 for the static problem. However, an easier derivation is possible by using Eq. 3.78 as a guide and replacing  $\sigma_{ij}^*$  by  $\sigma_{ij}^{\dot{v}}$  wherever it occurs in that equation. When this is done, the spectral density of the random wave force intensity for the dynamic problem is given by

$$S_{P_{nk}P_{n\ell}}(\Omega) = [C_u^2 \frac{8}{\pi} \sigma_{nk}^{\dot{v}} \sigma_{n\ell}^{\dot{v}} + i\Omega C_u C_a \sqrt{\frac{8}{\pi}} (\sigma_{nk}^{\dot{v}} - \sigma_{n\ell}^{\dot{v}}) + \Omega^2 C_a^2] S_{\dot{u}_{nk}\dot{u}_{n\ell}}(\Omega) \quad (4.73)$$

#### 4.5.2 Spectral Density of Random Modal Force

The random modal force for the  $r^{\text{th}}$  mode is given by Eq. 4.69. By means of Eq. 4.69, the correlation function of the modal forces for modes  $r$  and  $s$  may be written

$$R_{P_r^* P_s^*}(\tau) = E[P_r^*(t)P_s^*(t + \tau)] + E[\frac{1}{m_e} \sum_{nk=1}^n \phi_{nk}^{(r)} P_{nk}(t) \frac{1}{m_e} \sum_{n\ell=1}^n \phi_{n\ell}^{(s)} P_{n\ell}(t + \tau)] \quad (4.74)$$

In Eq. 4.74, the summations may be written as a double sum and the order of summation and expectation may be interchanged to give

$$R_{P_r^* P_s^*}(\tau) = \frac{1}{2} \sum_{nk=1}^n \sum_{n\ell=1}^n \phi_{nk}^{(r)} \phi_{n\ell}^{(s)} E[P_{nk}(t)P_{n\ell}(t + \tau)] \quad (4.75)$$

But the expectation term in Eq. 4.75 is simply the correlation function of the random wave force intensities at nodes  $nk$  and  $n\ell$ .



Therefore,

$$R_{P_r P_s}^{*}(\tau) = \frac{1}{m_e} \sum_{nk=1}^n \sum_{n\ell=1}^n \phi_{nk}^{(r)} \phi_{n\ell}^{(s)} R_{P_{nk} P_{n\ell}}(\tau) \quad (4.76)$$

The spectral density function of the modal forces is the Fourier transform of the correlation function, Eq. 4.76,

$$\begin{aligned} \tilde{S}_{P_r P_s}^{*}(\Omega) &= \frac{1}{2\pi} \int_{-\infty}^{\infty} \frac{1}{m_e} \sum_{nk=1}^n \sum_{n\ell=1}^n \phi_{nk}^{(r)} \phi_{n\ell}^{(s)} \\ &\cdot R_{P_{nk} P_{n\ell}}(\tau) e^{-i\Omega\tau} d\tau \end{aligned} \quad (4.77)$$

In Eq. 4.77, the order of integration and summation may be interchanged.

$$\begin{aligned} \tilde{S}_{P_r P_s}^{*}(\Omega) &= \frac{1}{m_e} \sum_{nk=1}^n \sum_{n\ell=1}^n \phi_{nk}^{(r)} \phi_{n\ell}^{(s)} \\ &\cdot \left[ \frac{1}{2\pi} \int_{-\infty}^{\infty} R_{P_{nk} P_{n\ell}}(\tau) e^{-i\Omega\tau} d\tau \right] \end{aligned} \quad (4.78)$$

The term in brackets in Eq. 4.78 is the spectral density function of the random wave force intensities,  $\tilde{S}_{P_{nk} P_{n\ell}}(\Omega)$ . Therefore, the one-sided spectral density of the modal forces is

$$S_{P_r P_s}^{*}(\Omega) = \frac{1}{m_e} \sum_{nk=1}^n \sum_{n\ell=1}^n \phi_{nk}^{(r)} \phi_{n\ell}^{(s)} S_{P_{nk} P_{n\ell}}(\Omega) \quad (4.79)$$

#### 4.5.3 Spectral Density of Random Normal Coordinates

Equation 4.71 expresses the random normal coordinate of the  $r^{\text{th}}$





classical normal mode as a function of the random modal force for that mode. In this section an expression relating the corresponding spectral densities is derived.

In the usual fashion, the correlation function of the normal coordinates for modes  $r$  and  $s$  is written

$$R_{Z_r Z_s}(\tau) = E[Z_r(t) Z_s(t + \tau)] \quad (4.80)$$

From Eq. 4.71,  $Z_s(t + \tau)$  is given by

$$Z_s(t + \tau) = \int_{\xi_2=-\infty}^{t+\tau} P_s^*(\xi_2) \hat{h}_s(t + \tau - \xi_2) d\xi_2 \quad (4.81)$$

where  $\xi_2$ , like  $\xi_1$ , is a dummy time variable used in the integration process. When Eqs. 4.71 and 4.81 are substituted into Eq. 4.80, there results an expanded formula for the correlation function.

$$R_{Z_r Z_s}(\tau) = E \left[ \int_{-\infty}^t P_r^*(\xi_1) \hat{h}_r(t - \xi_1) d\xi_1 \cdot \int_{-\infty}^{t+\tau} P_s^*(\xi_2) \hat{h}_s(t + \tau - \xi_2) d\xi_2 \right] \quad (4.82)$$

The spectral density function of the random normal coordinates is the Fourier transform of the correlation function.



$$\begin{aligned}
\tilde{S}_{Z_r Z_s}(\Omega) &= \frac{1}{2\pi} \int_{\tau=-\infty}^{\infty} E \left[ \int_{\xi_1=-\infty}^t P_r^*(\xi_1) h_r(t - \xi_1) d\xi_1 \right. \\
&\quad \cdot \left. \int_{\xi_2=-\infty}^{t+\tau} P_s^*(\xi_2) h_s(t + \tau - \xi_2) d\xi_2 \right] e^{-i\Omega\tau} d\tau \quad (4.83)
\end{aligned}$$

Evaluation of Eq. 4.83 is simplified by a convenient transformation of coordinates. Let

$$\xi_3 = t - \xi_1 \quad (4.84a)$$

$$\xi_4 = t + \tau - \xi_2 \quad (4.84b)$$

where  $\xi_3$  and  $\xi_4$ , like  $\xi_1$  and  $\xi_2$ , are simply dummy time variables. The use of Eqs. 4.84 transforms Eq. 4.83 to

$$\begin{aligned}
\tilde{S}_{Z_r Z_s}(\Omega) &= \frac{1}{2\pi} \int_{\tau=-\infty}^{\infty} E \left[ \left( - \int_{\xi_3=\infty}^0 P_r^*(t - \xi_3) h_r(\xi_3) d\xi_3 \right) \right. \\
&\quad \cdot \left. \left( - \int_{\xi_4=\infty}^0 P_s^*(t + \tau - \xi_4) h_s(\xi_4) d\xi_4 \right) \right] e^{-i\Omega\tau} d\tau \quad (4.85)
\end{aligned}$$

The terms in Eq. 4.85 may be more conveniently arranged by moving the expectation operator inside of the second and third integrals and reversing the integration limits of those integrals.



$$\begin{aligned} \tilde{S}_{Z_r Z_s}(\Omega) &= \frac{1}{2\pi} \int_{\tau=-\infty}^{\infty} \int_{\xi_3=0}^{\infty} \int_{\xi_4=0}^{\infty} E[P_r^*(t - \xi_3) P_s^*(t + \tau - \xi_4)] \\ &\cdot \hat{h}_r(\xi_3) \hat{h}_s(\xi_4) e^{-i\Omega\tau} d\xi_4 d\xi_3 d\tau \end{aligned} \quad (4.86)$$

In Eq. 4.86, the expectation term is a correlation function,

$$E[P_r^*(t - \xi_3) P_s^*(t + \tau - \xi_4)] = R_{P_r P_s}^*(\tau - \xi_4 + \xi_3) \quad (4.87)$$

and the exponential term may be decomposed into three components.

$$e^{-i\Omega\tau} = e^{-i\Omega(t + \xi_3 - \xi_4)} \cdot e^{i\Omega\xi_3} \cdot e^{-i\Omega\xi_4} \quad (4.88)$$

The introduction of Eqs. 4.87 and 4.88 into Eq. 4.86 results in

$$\begin{aligned} \tilde{S}_{Z_r Z_s}(\Omega) &= \frac{1}{2\pi} \int_{\tau=-\infty}^{\infty} \int_{\xi_3=0}^{\infty} \int_{\xi_4=0}^{\infty} [R_{P_r P_s}^*(t + \xi_3 - \xi_4) \\ &\cdot e^{-i\Omega(t + \xi_3 - \xi_4)}] [\hat{h}_r(\xi_3) e^{i\Omega\xi_3}] \\ &\cdot [\hat{h}_s(\xi_4) e^{-i\Omega\xi_4}] d\tau d\xi_3 d\xi_4 \end{aligned} \quad (4.89)$$

Because  $\hat{h}(t) = 0$  for  $t < 0$ , the lower limits of integration with respect to  $\xi_3$  and  $\xi_4$  may be changed to  $-\infty$  without changing the value of Eq. 4.88. When this is done, the two integrals with respect to  $\xi_3$  and  $\xi_4$  may be recognized as the Fourier transforms of the impulse response functions. From the theory of random vibrations,<sup>27</sup> the Fourier transform of  $\hat{h}_s(\xi_4)$  is



$$\int_{-\infty}^{\infty} h_s(\xi_4) e^{-i\Omega \xi_4} d\xi_4 = H_s(\Omega) \quad (4.90)$$

where

$$H_s(\Omega) = \frac{1}{\omega_s^2 - \Omega^2 + i2\zeta_s \omega_s \Omega} \quad (4.91)$$

The function,  $H_s(\Omega)$ , given by Eq. 4.91, is commonly referred to as the frequency response function or transfer function of the system. The integral with respect to  $\xi_3$  is

$$\int_{-\infty}^{\infty} h_r(\xi_3) e^{i\Omega \xi_3} d\xi_3 = \overline{H_r(\Omega)} \quad (4.92)$$

where the bar in  $\overline{H_r(\Omega)}$  denotes the complex conjugate of  $H_r(\Omega)$ . Substitution of Eqs. 4.90 and 4.92 into Eq. 4.89 leaves

$$\begin{aligned} \tilde{S}_{Z_r Z_s}(\Omega) &= \frac{1}{2\pi} \int_{\tau=-\infty}^{\infty} R_{P_r P_s}^*(\tau + \xi_3 - \xi_4) e^{-i\Omega(\tau + \xi_3 - \xi_4)} d\tau \\ &\cdot \overline{H_r(\Omega)} H_s(\Omega) \end{aligned} \quad (4.93)$$

The integral in Eq. 4.93 is the Fourier transform of a correlation function, which, by definition, is a spectral density function. Therefore,

$$\tilde{S}_{Z_r Z_s}(\Omega) = \tilde{S}_{P_r P_s}^*(\Omega) \overline{H_r(\Omega)} H_s(\Omega) \quad (4.94)$$

and the one-sided spectral density function of the normal coordinates is given by

$$S_{Z_r Z_s}(\Omega) = S_{P_r P_s}^*(\Omega) \overline{H_r(\Omega)} H_s(\Omega) \quad (4.95)$$





#### 4.5.4 Spectral Density of Response

##### Spectral Density of Node Deflections

Equation 4.47 expresses the random node deflections,  $\{Y(t)\}$ , in terms of the random normal coordinates,  $\{Z(t)\}$ , and the eigenvector matrix,  $[\phi]$ . For a single random node deflection, this relationship is

$$Y_{ni}(t) = \sum_{r=1}^{nm} \phi_{ni}^{(r)} Z_r(t) \quad (4.96)$$

Equation 4.96 states that the random deflection of node  $ni$  is the sum over all modes of the products of the node  $ni$  deflection in each mode shape multiplied by the random normal coordinate of that mode. In effect, the normal coordinates are weighting factors which assign the relative importance of the natural modes of vibration in the riser's response.

Equation 4.96 is in a form convenient to use in deriving an expression for the spectral density of the node deflections. As usual, this derivation starts with the correlation function of the random deflections at nodes  $ni$  and  $nj$ .

$$R_{Y_{ni}Y_{nj}}(\tau) = E[Y_{ni}(t)Y_{nj}(t + \tau)] \quad (4.97)$$

Equation 4.97 may be written in terms of the normal coordinates by substituting Eq. 4.96.

$$R_{Y_{ni}Y_{nj}}(\tau) = E\left[\sum_{r=1}^{nm} \phi_{ni}^{(r)} Z_r(t) \sum_{s=1}^{nm} \phi_{nj}^{(s)} Z_s(t + \tau)\right] \quad (4.98)$$



In Eq. 4.98, the order of summation and expectation may be interchanged, the two sums nested, and all deterministic variables removed from the expectation operation. When this is done, the result is

$$R_{Y_{ni}Y_{nj}}(\tau) = \sum_{r=1}^{nm} \sum_{s=1}^{nm} \phi_{ni}^{(r)} \phi_{nj}^{(s)} E[Z_r(t)Z_s(t + \tau)] \quad (4.99)$$

Substitution of Eq. 4.80 into Eq. 4.99 produces

$$R_{Y_{ni}Y_{nj}}(\tau) = \sum_{r=1}^{nm} \sum_{s=1}^{nm} \phi_{ni}^{(r)} \phi_{nj}^{(s)} R_{Z_rZ_s}(\tau) \quad (4.100)$$

The spectral density function of the random deflections at node  $ni$  and node  $nj$  is the Fourier transform of the correlation function, Eq. 4.100.

$$\tilde{S}_{Y_{ni}Y_{nj}}(\Omega) = \frac{1}{2\pi} \int_{-\infty}^{\infty} \sum_{r=1}^{nm} \sum_{s=1}^{nm} \phi_{ni}^{(r)} \phi_{nj}^{(s)} R_{Z_rZ_s}(\tau) e^{-i\Omega\tau} d\tau \quad (4.101)$$

The order of integration and summation in Eq. 4.101 may be interchanged to give

$$\tilde{S}_{Y_{ni}Y_{nj}}(\Omega) = \sum_{r=1}^{nm} \sum_{s=1}^{nm} \phi_{ni}^{(r)} \phi_{nj}^{(s)} \frac{1}{2\pi} \int_{-\infty}^{\infty} R_{Z_rZ_s}(\tau) e^{-i\Omega\tau} d\tau \quad (4.102)$$

Finally, the integral term in Eq. 4.102, being the Fourier transform of the correlation function, is the spectral density function of the random normal coordinates  $r$  and  $s$ . Therefore, the one-sided spectral density function for the node deflections is



$$S_{Y_{ni}Y_{nj}}(\Omega) = \sum_{r=1}^{nm} \sum_{s=1}^{nm} \phi_{ni}^{(r)} \phi_{nj}^{(s)} S_{Z_r Z_s}(\Omega) \quad (4.103)$$

Equations 3.48, 4.95, 4.73, 4.79, and 4.103 provide a mathematical link between the input surface elevation spectral density function and the output node deflection spectral density function. These five equations may be combined into a single expression.

$$\begin{aligned} S_{Y_{ni}Y_{nj}}(\Omega) = & \left\{ \left( \frac{kg}{\Omega m_e} \right)^2 \sum_{r=1}^{nm} \sum_{s=1}^{nm} \phi_{ni}^{(r)} \phi_{nj}^{(s)} \overline{H_r(\Omega)} H_s(\Omega) \right. \\ & \sum_{nk=1}^n \sum_{n\ell=1}^n \phi_{nk}^{(r)} \phi_{n\ell}^{(s)} [C_u^2 \frac{8}{\pi} \sigma_{\dot{V}_{nk}} \sigma_{\dot{V}_{n\ell}} \\ & + i \Omega C_u C_a \sqrt{\frac{8}{\pi}} (\sigma_{\dot{V}_{nk}} - \sigma_{\dot{V}_{n\ell}}) + \Omega^2 C_a^2] \\ & \left. \tilde{q}_{nk}(\Omega) \tilde{q}_{n\ell}(\Omega) \right\} S_{\eta\eta}(\Omega) \end{aligned} \quad (4.104)$$

The power transfer function of the mathematical model is the entire term within the braces in Eq. 4.104.

Before deriving the bottom rotation and bending moment spectral density functions, it is worthwhile to consider the nature of the solution indicated by Eq. 4.104. There are two types of variables that make the solution a trial and error process, because they cannot be immediately determined. One of these variables is the standard deviation of the relative water particle velocity,  $\sigma_{\dot{V}_{nk}}$ , at the nodes. Because the relative water particle velocity is a function of the unknown random structural velocity,  $\dot{Y}_{nk}$ , values must be assumed for  $[\sigma_{\dot{V}}]$  and updated on each iteration



until convergence occurs. The second variable which changes in each iteration is the damping ratio,  $\zeta_r$ , which is used to calculate the frequency response function,  $H_r(\Omega)$ . Equations 4.68 and 4.62 show that  $\zeta_r$  is a function of the covariances of the first time derivatives of the random normal coordinates,  $\sigma_{\dot{z}_r \dot{z}_s}^2$  which are also unknowns. Equations 4.68, 4.62, 4.53, and 4.25 show that  $\zeta_r$  also depends upon  $[\sigma_{\dot{y}}]$ .

Thus, in the calculation of the random response, it is necessary to assume values for  $[\sigma_{\dot{y}}]$  and  $[\sigma_{\dot{z}\dot{z}}^2]$  and use a trial and error process in which  $[\sigma_{\dot{y}}]$  and  $[\sigma_{\dot{z}\dot{z}}^2]$  are calculated in each cycle of iteration. The iterations are continued until the calculated values of the two matrices agree satisfactorily with the assumed values.

### Spectral Density of Bottom Rotation

For the dynamic problem, the bottom rotation bears the same relationship to the deflection of the first node as it does for the static problem. Therefore, Eq. 3.93, which was derived for the static problem, is also applicable to the dynamic problem.

### Spectral Density of Random Dynamic Bending Moments

In Chapter 3, the following expression was derived relating the random bending moment at node  $n_i$ ,  $M_{n_i}(t)$ , to the random node displacements.

$$M_{n_i}(t) = \sum_{nk=n_i-1}^{n_i+1} J_{n_i,nk} Y_{nk}(t) \quad (3.98)$$

where  $[J]$  is a transformation matrix defined by Eqs. 3.97. As indicated by Eq. 4.96, the random node deflections are a function of the classical normal





mode shapes and random normal coordinates. The substitution of Eq. 4.96 into Eq. 3.98 yields

$$M_{ni}(t) = \sum_{nk=ni-1}^{ni+1} J_{ni,nk} \sum_{r=1}^{nm} \phi_{nk}^{(r)} Z_r(t) \quad (4.105)$$

or, in matrix form,

$$\{M(t)\}_{n \times 1} = [J]_{n \times n} [\phi]_{n \times nm} \{Z(t)\}_{nm \times 1} \quad (4.106)$$

Let  $[B] = [J][\phi]$  be an  $n$  by  $nm$  transformation matrix relating random nodal moments to the random normal coordinates. Then

$$\{M(t)\} = [B]\{Z(t)\} \quad (4.107)$$

or for a given nodal moment,

$$M_{ni}(t) = \sum_{r=1}^{nm} B_{ni,r} Z_r(t) \quad (4.108)$$

Equation 4.108 may be used to write the correlation function of the random moment at node  $ni$  with the random moment at node  $nj$ .

$$\begin{aligned} R_{M_{ni}M_{nj}}(\tau) &= E[M_{ni}(t)M_{nj}(t + \tau)] \\ &= E\left[\sum_{r=1}^{nm} B_{ni,r} Z_r(t) \sum_{s=1}^{nm} B_{nj,s} Z_s(t + \tau)\right] \end{aligned} \quad (4.109)$$

In Eq. 4.109, the summation operations may be combined and the expectation operation interchanged with the two summations because all three operations are linear. This leads to



$$R_{M_{ni}M_{nj}}(\tau) = \sum_{r=1}^{nm} \sum_{s=1}^{nm} B_{ni,r} B_{nj,s} R_{Z_r Z_s}(\tau) \quad (4.110)$$

The spectral density function of the moments at nodes  $ni$  and  $nj$  is the Fourier transform of the correlation function.

$$\tilde{S}_{M_{ni}M_{nj}}(\Omega) = \frac{1}{2\pi} \int_{-\infty}^{\infty} \sum_{r=1}^{nm} \sum_{s=1}^{nm} B_{ni,r} B_{nj,s} R_{Z_r Z_s}(\tau) e^{-i\Omega\tau} d\tau \quad (4.111)$$

Interchanging the order of summation and integration in Eq. 4.111 yields

$$\tilde{S}_{M_{ni}M_{nj}} = \sum_{r=1}^{nm} \sum_{s=1}^{nm} B_{ni,r} B_{nj,s} \left[ \frac{1}{2\pi} \int_{-\infty}^{\infty} R_{Z_r Z_s}(\tau) e^{-i\Omega\tau} d\tau \right] \quad (4.112)$$

The expression in brackets in Eq. 4.112 is, by definition, the spectral density function of the random normal coordinates for modes  $r$  and  $s$ . It follows that the one-sided spectral density function for bending moments is

$$S_{M_{ni}M_{nj}}(\Omega) = \sum_{r=1}^{nm} \sum_{s=1}^{nm} B_{ni,r} B_{nj,s} S_{Z_r Z_s}(\Omega) \quad (4.113)$$

Equation 4.113, together with Eqs. 4.95, 4.79, 4.73, and 3.48, forms a mathematical chain of relationships linking the input random sea surface elevation spectrum to the random nodal moment spectra. From the similarity between Eqs. 4.113 and 4.103, it follows that a single expression for bending moment spectral density as a function of the sea surface elevation spectral density can be expressed by Eq. 4.104 with  $B_{ni,r}$  substituted for  $\phi_{ni}^{(r)}$  and  $B_{nj,s}$  substituted for  $\phi_{nj}^{(s)}$ .



## 4.6 Damping

Although it may not be obvious, the response spectral density functions of the riser depend upon the damping matrix,  $[c]$ . That this is so may be seen by considering Eqs. 4.104, 4.91, 4.68, 4.62, 4.53, and 4.25. These equations show that the response is a function of the frequency response functions,  $H_r(\Omega)$ , which depend upon the damping ratios,  $\zeta_r$ , which in turn are functions of the diagonalized modal damping coefficients,  $C_{r,r}^*$ . The diagonalized modal damping coefficients are calculated from the modal damping matrix,  $[C_0]$ , which is a function of the modified damping matrix,  $[\zeta]$ . Because the modified damping matrix is a function of the damping matrix,  $[c]$ , the response spectral density function is also a function of the damping matrix.

The damping matrix was introduced in the damping force term of Eq. 4.4 without any indication as to how the coefficients which constitute the matrix may be determined. In this section, a rational method of formulating the damping matrix is developed.

Consider the modal damping matrix as defined by Eq. 4.53.

$$[C_0] = [\phi]^T [\zeta] [\phi] \quad (4.53)$$

The modal damping matrix results from a coordinate transformation which is used to uncouple the simultaneous differential equations of motion. If  $[C_0]$  is a diagonal matrix, that is, if the normal modes are orthogonal with respect to the modified damping matrix,  $[\zeta]$ , then the equations of motion are indeed uncoupled by the transformation. The modified damping matrix is given by



$$[\underline{c}] = [\underline{c}] + \underline{c}_0 \sqrt{\frac{8}{\pi}} [\underline{\sigma}_V] \quad (4.25)$$

Substitution of Eq. 4.25 into Eq. 4.53 leads to

$$[\underline{C}_0] = [\underline{\phi}]^T [\underline{c}] [\underline{\phi}] + \underline{c}_0 \sqrt{\frac{8}{\pi}} [\underline{\phi}]^T [\underline{\sigma}_V] [\underline{\phi}] \quad (4.114)$$

The second term on the right-hand side of Eq. 4.114 is not, in general, a diagonal matrix, because there is no reason for the normal modes to be orthogonal with respect to the matrix of standard deviations of the relative velocities. Therefore, the modal matrix will not, in general, be a diagonal matrix, and the diagonalization procedure described in Section 4.4.1 must be used to uncouple the equations. The error resulting from this diagonalization may be reduced somewhat, however, if the modal damping matrix is as nearly diagonal as possible, that is, if the diagonal elements of  $[\underline{C}_0]$  are large with respect to the off-diagonal elements. The diagonal elements of the modal damping matrix can be strengthened with respect to the off-diagonal elements if the first term on the right-hand side of Eq. 4.114 is a diagonal matrix.

It may be concluded that a logical criterion governing the formulation of the damping matrix,  $[\underline{c}]$ , is that the normal modes be orthogonal with respect to the damping matrix. In section 4.6.1, the conditions under which this occurs are explored.

#### 4.6.1 Conditions Under Which Normal Modes Are Orthogonal With Respect to the Damping Matrix

The conditions necessary for the normal modes to be orthogonal with respect to the damping matrix have been demonstrated by Caughey<sup>33</sup> and





are repeated here without proof. Caughey shows that simultaneous equations of motion expressed by

$$[I]\{\ddot{p}\} + [A]\{\dot{p}\} + [B]\{p\} = \{f(t)\} \quad (4.115)$$

are uncoupled by the same transformation which diagonalizes the undamped system if

$$[A] = \sum_{j=1}^{\infty} \sum_{\ell=0}^{N-1} a_{j\ell} [B]_1^{\ell/j} \quad (4.116)$$

Equation 4.116 is a sufficient condition, but not a necessary condition.

In Eq. 4.116,  $N$  is the order of the matrix  $[B]$ , the subscript 1 on the matrix  $[B]$  means that only one root of  $[B]$  is taken, and  $a_{j\ell}$  is a linear coefficient.

Caughey's findings may be applied to the riser problem, for which the linearized equation of motion is Eq. 4.31,

$$[m_e]\{\ddot{Y}\} + [c]\{\dot{Y}\} + [K]\{Y\} = \{P(t)\} \quad (4.31)$$

where  $\{P(t)\}$  is defined by Eq. 4.42. A form similar to that of Eq. 4.115 is obtained by premultiplying Eq. 4.31 by  $[m_e]^{-1}$ . When this is done and Eq. 4.25 is substituted for  $[c]$ , the result is

$$\begin{aligned} [I]\{\ddot{Y}\} &= [m_e]^{-1}[c]\{\dot{Y}\} + c_u \sqrt{\frac{8}{\pi}} [m_e]^{-1} [\sigma \dot{Y}] \\ &+ [m_e]^{-1}[K]\{Y\} = [m_e]^{-1}\{P(t)\} \end{aligned} \quad (4.117)$$

From Eqs. 4.116 and 4.117, it follows that  $[\phi]^T [c] [\phi]$  is a diagonal matrix if



$$[\bar{m}_e]^{-1}[c] = \sum_{j=1}^{\infty} \sum_{\ell=0}^{N-1} a_{j\ell} [B]_1^{\ell/j} \quad (4.118)$$

where

$$[B] = [\bar{m}_e]^{-1}[K]$$

Premultiplying Eq. 4.118 by  $[\bar{m}_e]$  yields the desired expression for the damping matrix.

$$[c] = [\bar{m}_e] \sum_{j=1}^{\infty} \sum_{\ell=0}^{N-1} a_{j\ell} [B]_1^{\ell/j} \quad (4.119)$$

For illustration purposes, consider the case where the coefficient  $a_{j\ell}$  is non-zero only when  $j$  is 1 and  $\ell$  is zero or one. From Eq. 4.119, the damping matrix for this case is given by

$$\begin{aligned} [c] &= [\bar{m}_e] (a_{10}[B]_1^{0/1} + a_{11}[B]_1^{1/1}) \\ &= a_{10}[\bar{m}_e] + a_{11}[K] \end{aligned} \quad (4.120)$$

Equation 4.120 describes Rayleigh damping, which is frequently assumed in dynamic analysis in order to insure that the orthogonality transformation will uncouple the equations of motion. Because the index  $j$  in Eq. 4.119 has no finite upper limit, Eq. 4.120 is only one of an infinite number of ways in which the damping matrix may be formulated such that the normal modes are orthogonal with respect to it.

#### 4.6.2 Formulation of the Damping Matrix for the Marine Riser

Consider the schematic representation of a marine riser shown in Fig. 4.6, in which damping is represented by a series of dashpots. The damping forces may be divided into two classifications--environmental damping,



which depends upon the velocity of the structure with respect to the surrounding medium, and internal friction damping, which depends upon the relative velocity of one part of the structure with respect to other parts of the structure. In Fig. 4.6, environmental damping is represented by the dashpots labeled  $c_e$ , and internal friction damping is indicated by the dashpots labeled  $c_f$ , which connect adjacent nodes. Although they have been omitted for the sake of clarity, dashpots representing internal friction damping could be shown connecting each node to every other node.

When the equations of motion of the riser shown in Fig. 4.6 are written in matrix form, the damping matrix is composed of elements which are combinations of the coefficients  $c_e$  and  $c_f$ . The environmental damping coefficients appear only in the diagonal elements of the damping matrix, but internal friction damping coefficients contribute to all elements of the matrix. Thus, environmental damping is similar to the first term of Eq. 4.120 in the sense that both contribute only to the diagonal elements. In like manner, internal friction damping is similar to the second term of Eq. 4.120 in the sense that both contribute to all elements of the damping matrix.

Let  $\beta_r$  be the damping ratio for mode  $r$  defined by

$$\beta_r = \frac{1}{2m_e \omega_r} \{\phi^{(r)}\}^T [c] \{\phi^{(r)}\} \quad (4.121)$$

and suppose that  $[c]$  is formulated according to Eq. 4.120. Then

$$\beta_r = \frac{1}{2m_e \omega_r} (a_{10} \{\phi^{(r)}\}^T [m_e] \{\phi^{(r)}\} + a_{11} \{\phi^{(r)}\}^T [K] \{\phi^{(r)}\}) \quad (4.122)$$



Utilization of Eqs. 4.39 and 4.46 in Eq. 4.122 leads to

$$\beta_r = \frac{1}{2m_e\omega_r} (a_{10}m_e + a_{11}\omega_r^2 m_e) = \frac{a_{10}}{2\omega_r} + \frac{a_{11}\omega_r}{2} \quad (4.123)$$

Equation 4.123 shows that if the damping matrix is proportional to the mass matrix alone, then the damping ratio decreases with increasing natural frequency, and higher modes are damped less than lower modes are. Further, if the damping matrix is proportional to the stiffness matrix alone, then the damping ratio increases as frequency increases, and higher modes are damped more than lower modes are.

It can be shown that the damping matrix,  $[c]$ , can be completely specified by selecting the modal damping ratios. Let  $[\beta]$  be an  $nm$  by  $nm$  diagonal matrix of modal damping ratios and let  $[\omega]$  be an  $nm$  by  $nm$  diagonal matrix of natural frequencies. Then, if  $[c]$  is chosen so that the normal modes are orthogonal with respect to it,  $[\beta]$  is given by

$$\frac{1}{m_e} [\phi]^T [c] [\phi] = 2[\beta][\omega] \quad (4.124)$$

Premultiplication of both sides of Eq. 4.124 by  $[\phi]$ , postmultiplication by  $[\phi]^T$ , and utilization of Eq. 4.45 leads to

$$[c] = 2m_e [\phi] [\beta] [\omega] [\phi]^T \quad (4.125)$$

Equation 4.125 reduces the problem of selecting  $n^2$  damping coefficients to one of selecting  $nm$  damping ratios.

Consider now the selection of the damping ratios,  $\beta_r$ ,  $r = 1, 2, \dots, nm$ . The damping ratios may increase with mode number, they may





decrease with mode number, and they may be constant for all modes.

The case in which the damping ratios increase with mode number occurs if damping is proportional to the stiffness matrix alone, a condition which has been compared to internal friction damping. If the last term of Eq. 4.120 is used to represent internal friction damping, and if internal friction damping predominates over environmental damping, then the damping ratio for higher modes will be greater than it is for lower modes.

The case in which damping ratios decrease as mode numbers increase occurs if damping is proportional to the mass matrix alone, a situation which has been compared to environmental damping. If the first term of Eq. 4.120 is used to represent environmental damping forces and if environmental damping predominates over internal friction damping, then higher modes will be damped less than lower modes are.

A third alternative is for the damping ratio to be constant for all modes. Because Eq. 4.120 contains only two coefficients which may be varied, a constant damping ratio may be specified for only two modes if Rayleigh damping is assumed. However, a constant damping ratio for all modes may be specified by the more general combination of mass and stiffness matrices indicated by Eq. 4.119. A more direct method of specifying constant damping ratios is by substitution in Eq. 4.123.

Based on the foregoing discussion, an argument for the specification of the damping ratios may be made. For the marine riser moving through the water, the environmental damping force is simply the drag force of the water which resists the motion of the riser. In the formulation of the equation of motion for the riser, Eq. 4.8, this drag force is



accounted for by considering wave structure interaction. The drag force caused by wave motion, which is an exciting force, and the drag force caused by the riser's motion through the water, which is a damping force, are both included in the single term  $C_D \{\dot{V}|\dot{V}|\}$ . Because the environmental damping is treated as an applied force in Eq. 4.8, the damping term,  $[c]\{\dot{V}\}$ , represents only the resistance to riser motion caused by internal friction. Both internal friction damping and environmental damping are included in the modified damping matrix,  $[c]$ , which results from the linearization of the equation of motion. This is shown best by Eq. 4.25, the first term of which,  $[c]$ , represents internal friction damping and the last term of which is a modified drag coefficient.

The damping ratios,  $[\beta]$ , which determine the damping matrix,  $[c]$ , may be considered as internal friction damping ratios. Given the argument that internal friction damping is similar to that component of Rayleigh damping which is proportional to the stiffness matrix, it appears unlikely that  $\beta_r$  decreases with mode number. On the contrary, it is logical to assume that  $\beta_r$  increases with mode number. But if the method of analysis permits  $\beta_r$  to increase too much with  $r$ , significant contributions of higher modes may be damped into insignificance. It is reasonable, therefore, to select  $[c]$  such that  $\beta_r$  is constant for all modes, with the expectation that such a procedure will make any errors in higher mode contributions tend to be conservative ones.

There are precedents in the literature for using a constant damping ratio for all modes. Caughey<sup>33</sup> gives an example of this type of damping and refers to it as linear hysteresis damping. Hart<sup>34</sup> uses a damping ratio of .02 for all modes in considering the response of steel building frames.



In this thesis, the damping matrix,  $[c]$ , will be determined in such a way that  $\beta_r$  is constant for all modes. When this assumption is made, Eq. 4.124 simplifies to

$$[\phi]^T [c] [\phi] = 2m_e \beta [\omega] \quad (4.124a)$$

and Eq. 4.114 becomes

$$[C_0] = 2m_e \beta [\omega] + C_u \sqrt{\frac{8}{\pi}} [\phi]^T [\sigma_V] [\phi] \quad (4.114a)$$

The first term of Eq. 4.114a contributes only to the diagonal elements of  $[C_0]$  and represents modal damping due to internal friction in the riser. The second term represents damping due to fluid drag forces resulting from the relative velocity between the riser and the surrounding water.

#### 4.7 Variances and Covariances of Time Derivatives of Random Normal Coordinates

The simultaneous equations of motion are uncoupled by using the orthogonality of the normal modes with respect to the mass matrix and by employing a diagonalization technique to eliminate the off-diagonal elements of the modal damping matrix,  $[C_0]$ . As indicated by Eq. 4.62, elements of the diagonalized modal damping matrix are functions of the variances,  $\sigma_{\dot{Z}_r \dot{Z}_r}^2$ , and covariances,  $\sigma_{\dot{Z}_r \dot{Z}_s}^2$ , of the first time derivatives of the random normal coordinates. The variance or covariance may be calculated by integrating the corresponding spectral density with respect to frequency.

$$\sigma_{\dot{Z}_r \dot{Z}_s}^2 \approx \int_0^\infty S_{\dot{Z}_r \dot{Z}_s}(\omega) d\omega \quad (4.126)$$



In a fashion similar to that used in Section 3.3.4 to derive Eq. 3.56b, it can be shown that

$$S_{\dot{Z}_r \dot{Z}_s}(\Omega) = \Omega^2 S_{Z_r Z_s}(\Omega) \quad (4.127)$$

Combining Eqs. 4.126 and 4.127 leads to

$$\sigma_{\dot{Z}_r \dot{Z}_s}^2 = \int_0^\infty \Omega^2 S_{Z_r Z_s}(\Omega) d\Omega \quad (4.128)$$

Equation 4.128 may be used to calculate the variances and covariances used to diagonalize the modal damping matrix.

#### 4.8 Calculation of Standard Deviations of Relative Velocities

In computations for the random riser response, the standard deviations of the relative water velocities with respect to the structure,  $[\sigma_{\dot{V}}]$ , are needed in two instances. These standard deviations are first used to calculate the modified damping matrix,  $[\bar{c}]$ , according to Eq. 4.25. In this instance, the relative velocity standard deviations are a measure of the environmental damping of the dynamic structural response by the water. Secondly, the relative velocity standard deviations are used in Eq. 4.73 to calculate the spectral density functions of the linearized force intensities at the nodes.

The random relative velocity at node  $nk$ , as defined by Eq. 4.5a, is

$$\dot{V}_{nk}(t) = \dot{U}_{nk}(t) - \dot{V}_{nk}(t) \quad (4.129)$$





The autocorrelation function of the relative velocity is

$$\begin{aligned} R_{\dot{V}_{nk}\dot{V}_{nk}}(\tau) &= E[\dot{V}_{nk}(t)\dot{V}_{nk}(t+\tau)] = E[(\dot{U}_{nk}(t) - \dot{Y}_{nk}(t)) \\ &\quad \cdot (\dot{U}_{nk}(t+\tau) - \dot{Y}_{nk}(t+\tau))] \end{aligned} \quad (4.130)$$

Expansion of Eq. 4.130 and interchanging the order of addition and expectation operators leads to

$$\begin{aligned} R_{\dot{V}_{nk}\dot{V}_{nk}}(\tau) &= E[\dot{U}_{nk}(t)\dot{U}_{nk}(t+\tau)] - E[\dot{Y}_{nk}(t)\dot{U}_{nk}(t+\tau)] \\ &\quad - E[\dot{U}_{nk}(t)\dot{Y}_{nk}(t+\tau)] + E[\dot{Y}_{nk}(t)\dot{Y}_{nk}(t+\tau)] \end{aligned} \quad (4.131)$$

Each of the four terms in Eq. 4.131 is an autocorrelation or cross correlation function. Therefore,

$$\begin{aligned} R_{\dot{V}_{nk}\dot{V}_{nk}}(\tau) &= R_{\dot{U}_{nk}\dot{U}_{nk}}(\tau) - R_{\dot{Y}_{nk}\dot{U}_{nk}}(\tau) - R_{\dot{U}_{nk}\dot{Y}_{nk}}(\tau) \\ &\quad + R_{\dot{Y}_{nk}\dot{Y}_{nk}}(\tau) \end{aligned} \quad (4.132)$$

The spectral density of the random relative velocity at node  $nk$  is obtained by taking the Fourier transform of Eq. 4.132. Because the Fourier transform of each of the four terms on the right-hand side of Eq. 4.132 is a spectral density function, there results

$$\begin{aligned} S_{\dot{V}_{nk}\dot{V}_{nk}}(\Omega) &= S_{\dot{U}_{nk}\dot{U}_{nk}}(\Omega) - S_{\dot{Y}_{nk}\dot{U}_{nk}}(\Omega) - S_{\dot{U}_{nk}\dot{Y}_{nk}}(\Omega) \\ &\quad + S_{\dot{Y}_{nk}\dot{Y}_{nk}}(\Omega) \end{aligned} \quad (4.133)$$



Finally, the variance of the relative velocity at node  $nk$  is the integral of the spectral density with respect to frequency,

$$\sigma_{\dot{V}_{nk}}^2 = \int_0^{\infty} S_{\dot{V}_{nk} \dot{V}_{nk}}(\Omega) d\Omega \quad (4.134)$$

and the standard deviation is the square root of the variance.

$$\sigma_{\dot{V}_{nk}} = \sqrt{\sigma_{\dot{V}_{nk}}^2} \quad (4.135)$$

Consider the four terms of Eq. 4.133 which contribute to the spectral density of the relative velocity. The first term,  $S_{\dot{U}_{nk} \dot{U}_{nk}}(\Omega)$ , is the spectral density of the random water velocity and is given by Eq. 3.48. The last term is readily calculated because

$$S_{\dot{Y}_{nk} \dot{Y}_{nk}}(\Omega) = \Omega^2 S_{Y_{nk} Y_{nk}}(\Omega) \quad (4.136)$$

where  $S_{Y_{nk} Y_{nk}}(\Omega)$ , the spectral density of the random deflection at node  $nk$ , is determined from either Eq. 4.103 or 4.104. The two cross spectral density terms remain to be determined. By analogy to Eqs. 3.54 and 3.56a, it follows that

$$S_{\dot{U}_{nk} \dot{Y}_{nk}}(\Omega) = i\Omega S_{U_{nk} Y_{nk}}(\Omega) \quad (4.137)$$

and

$$S_{\dot{Y}_{nk} \dot{U}_{nk}}(\Omega) = -i\Omega S_{Y_{nk} U_{nk}}(\Omega) \quad (4.138)$$

A general property of cross spectral density functions is that they are hermitian,<sup>27</sup> that is



$$S_{\dot{Y}_{nk} \dot{U}_{nk}}(\Omega) = \overline{S_{\dot{U}_{nk} \dot{Y}_{nk}}(\Omega)} \quad (4.139)$$

where the line over the spectral density function denotes the complex conjugate. Therefore,

$$S_{\dot{Y}_{nk} \dot{U}_{nk}}(\Omega) = -i\Omega \overline{S_{\dot{U}_{nk} Y_{nk}}(\Omega)} \quad (4.140)$$

and it is only necessary to derive an expression for  $S_{\dot{U}_{nk} Y_{nk}}(\Omega)$  to determine the two cross spectral density functions of Eq. 4.133.

#### 4.8.1 Cross Spectral Density of Water Velocity and Node Displacement

The random displacement of node  $nk$  may be written in expanded form by using Eqs. 4.96, 4.71, 4.69, and 4.42.

$$\begin{aligned} Y_{nk}(t) = & \frac{1}{m_e} \sum_{r=1}^{nm} \phi_{nk}^{(r)} \int_{\xi_1=-\infty}^t \left[ \sum_{n\ell=1}^n \phi_{n\ell}^{(r)} (C_{\dot{U}} \sqrt{\frac{8}{\pi}} \sigma_{\dot{V}_{n\ell}} \dot{U}_{n\ell}(\xi_1) \right. \\ & \left. + C_a \ddot{U}_{n\ell}(\xi_1)) \right] h_r(t - \xi_1) d\xi_1 \end{aligned} \quad (4.141)$$

The cross correlation function of the water velocity and deflection at node  $nk$  is

$$R_{\dot{U}_{nk} Y_{nk}}(\tau) = E[\dot{U}_{nk}(t) Y_{nk}(t + \tau)] \quad (4.142)$$

Equation 4.142 may be expanded by the introduction of Eq. 4.141 for the node displacement.

$$\begin{aligned} R_{\dot{U}_{nk} Y_{nk}}(\tau) = & E[\dot{U}_{nk}(t) \frac{1}{m_e} \sum_{r=1}^{nm} \phi_{nk}^{(r)} \int_{\xi_1=-\infty}^{t+\tau} \sum_{n\ell=1}^n \phi_{n\ell}^{(r)} (C_{\dot{U}} \sqrt{\frac{8}{\pi}} \\ & \cdot \sigma_{\dot{V}_{n\ell}} \dot{U}_{n\ell}(\xi_1) + C_a \ddot{U}_{n\ell}(\xi_1)) h_r(t + \tau - \xi_1) d\xi_1] \end{aligned} \quad (4.143)$$



In Eq. 4.143, because the expectation operation, summations, and integration are all linear operations, their order may be interchanged. When this is done and the substitution,  $\xi_2 = t + \tau - \xi_1$  is made, there results

$$\begin{aligned}
 R_{\dot{U}_{nk} \dot{Y}_{nk}}(\tau) &= \frac{1}{m_e} \sum_{r=1}^{nm} \phi_{nk}^{(r)} \sum_{n\ell=1}^n \phi_{n\ell}^{(r)} \{ C_{\dot{U}} \sqrt{\frac{8}{\pi}} \sigma_{\dot{V}_{n\ell}} \\
 &\quad \int_0^{\infty} E[\dot{U}_{nk}(t) \dot{U}_{n\ell}(t + \tau - \xi_2)] h_r(\xi_2) d\xi_2 \\
 &\quad + C_a \int_0^{\infty} E[\dot{U}_{nk}(t) \ddot{U}_{n\ell}(t + \tau - \xi_2)] \\
 &\quad \cdot h_r(\xi_2) d\xi_2 \} \quad (4.144)
 \end{aligned}$$

By definition, the impulse response function,  $h_r(\xi_2)$ , is zero for  $\xi_2 < 0$ . Therefore, the lower limits of the integration in Eq. 4.144 may be changed to  $-\infty$  without changing the value of the equation. The two expectation terms in Eq. 4.144 are recognizable as the correlation functions,  $R_{\dot{U}_{nk} \dot{U}_{n\ell}}(\tau - \xi_2)$  and  $R_{\dot{U}_{nk} \ddot{U}_{n\ell}}(\tau - \xi_2)$  respectively. If  $\xi_3 = \tau - \xi_2$ , Eq. 4.144 may be written

$$\begin{aligned}
 R_{\dot{U}_{nk} \dot{Y}_{nk}}(\tau) &= \frac{1}{m_e} \sum_{r=1}^{nm} \phi_{nk}^{(r)} \sum_{n\ell=1}^n \phi_{n\ell}^{(r)} [C_{\dot{U}} \sqrt{\frac{8}{\pi}} \sigma_{\dot{V}_{n\ell}} \int_{-\infty}^{\infty} R_{\dot{U}_{nk} \dot{U}_{n\ell}}(\xi_3) \\
 &\quad \cdot h_r(\xi_2) d\xi_2 + C_a \int_{-\infty}^{\infty} R_{\dot{U}_{nk} \ddot{U}_{n\ell}}(\xi_3) h_r(\xi_2) d\xi_2] \quad (4.145)
 \end{aligned}$$

The cross spectral density function of the water velocity at node  $nk$  and the structural displacement at node  $nk$  is the Fourier transform of the cross correlation function.





$$\dot{\tilde{U}}_{nk}^Y_{nk} = \frac{1}{2\pi} \int_{-\infty}^{\infty} \dot{R}_{nk}^Y_{nk}(\tau) e^{-i\Omega\tau} d\tau \quad (4.146)$$

In Eq. 4.146, the term  $e^{-i\Omega\tau}$  may be written  $e^{-i\Omega\xi_2} \cdot e^{-i\Omega\xi_3}$  by the definition of  $\xi_3$ . Substitution of Eq. 4.145 into Eq. 4.146 produces

$$\begin{aligned} \dot{\tilde{U}}_{nk}^Y_{nk}(\Omega) &= \frac{1}{m_e} \frac{1}{2\pi} \int_{\xi_3=-\infty}^{\infty} \sum_{r=1}^{nm} \phi_{nk}^{(r)} \sum_{n\ell=1}^n \phi_{n\ell}^{(r)} \\ &\quad \cdot \{ C_{\dot{U}} \sqrt{\frac{8}{\pi}} \sigma_{\dot{V}_{n\ell}} \int_{\xi_2=-\infty}^{\infty} \dot{R}_{nk} \dot{U}_{n\ell}(\xi_3) \hat{h}_r(\xi_2) e^{-i\Omega\xi_2} d\xi_2 \\ &\quad + C_a \int_{\xi_2=-\infty}^{\infty} \dot{R}_{nk} \ddot{U}_{n\ell}(\xi_3) \hat{h}_r(\xi_2) e^{-i\Omega\xi_2} d\xi_2 \} \\ &\quad e^{-i\Omega\xi_3} d\xi_3 \end{aligned} \quad (4.147)$$

Integration of Eq. 4.147 with respect to  $\xi_2$  yields

$$\begin{aligned} \dot{\tilde{U}}_{nk}^Y_{nk}(\Omega) &= \frac{1}{m_e} \frac{1}{2\pi} \int_{\xi_3=-\infty}^{\infty} \sum_{r=1}^{nm} \phi_{nk}^{(r)} \sum_{n\ell=1}^n \phi_{n\ell}^{(r)} \\ &\quad \cdot \{ C_{\dot{U}} \sqrt{\frac{8}{\pi}} \sigma_{\dot{V}_{n\ell}} \dot{R}_{nk} \dot{U}_{n\ell}(\xi_3) H_r(\Omega) \\ &\quad + C_a \dot{R}_{nk} \ddot{U}_{n\ell}(\xi_3) H_r(\Omega) \} e^{-i\Omega\xi_3} d\xi_3 \end{aligned} \quad (4.148)$$



Finally, integration of Eq. 4.148 and substitution of Eq. 3.54 results in the following expression for the one-sided spectral density.

$$S_{\dot{U}_{nk} \dot{Y}_{nk}}(\Omega) = \frac{1}{m_e} \sum_{r=1}^{nm} H_r(\Omega) \phi_{nk}^{(r)} \sum_{n\ell=1}^n \phi_{n\ell}^{(r)} \cdot [C_{\dot{U}} \sqrt{\frac{8}{\pi}} \sigma_{\dot{V}_{n\ell}} + i\Omega C_a] S_{\dot{U}_{nk} \dot{U}_{n\ell}}(\Omega) \quad (4.149)$$

#### 4.8.2 Spectral Density Function of Relative Water Velocity

The spectral density function of the relative water velocity may be written by substituting Eqs. 4.136, 4.137, and 4.140 into Eq. 4.133.

$$S_{\dot{V}_{nk} \dot{V}_{nk}}(\Omega) = S_{\dot{U}_{nk} \dot{U}_{nk}}(\Omega) - i\Omega S_{\dot{U}_{nk} \dot{Y}_{nk}}(\Omega) + i\Omega \overline{S_{\dot{U}_{nk} \dot{Y}_{nk}}(\Omega)} + \Omega^2 S_{Y_{nk} Y_{nk}}(\Omega) \quad (4.150)$$

The second and third terms on the right-hand side of Eq. 4.150 are complex conjugates, the sum of which is simply twice the real part of either term.

$$-i\Omega S_{\dot{U}_{nk} \dot{Y}_{nk}}(\Omega) + i\Omega \overline{S_{\dot{U}_{nk} \dot{Y}_{nk}}(\Omega)} = 2 \operatorname{Re}[-i\Omega S_{\dot{U}_{nk} \dot{Y}_{nk}}(\Omega)] \quad (4.151)$$

The real part of these terms may be evaluated from Eq. 4.149.

$$\operatorname{Re}[-i\Omega S_{\dot{U}_{nk} \dot{Y}_{nk}}(\Omega)] = \frac{\Omega}{m_e} \sum_{r=1}^{nm} \phi_{nk}^{(r)} \sum_{n\ell=1}^n \phi_{n\ell}^{(r)} \{ \operatorname{Re}[H_r(\Omega)] \cdot \Omega C_a + \operatorname{Im}[H_r(\Omega)] C_{\dot{U}} \sqrt{\frac{8}{\pi}} \sigma_{\dot{V}_{n\ell}} \} \quad (4.152)$$



In Eqs. 4.151 and 4.152, Re indicates "real part of," and Im indicates "imaginary part of." By using Eqs. 4.151 and 4.152, Eqs. 4.150 may be written in the following form.

$$\begin{aligned}
 S_{\dot{V}_{nk}\dot{V}_{nk}}(\Omega) &= S_{\dot{U}_{nk}\dot{U}_{nk}}(\Omega) + \Omega^2 S_{Y_{nk}Y_{nk}}(\Omega) \\
 &+ \frac{2\Omega}{m_e} \sum_{r=1}^{nm} \phi_{nk}^{(r)} \sum_{n\ell=1}^n \phi_{n\ell}^{(r)} \{C_a^{\Omega} \cdot \text{Re}[H_r(\Omega)] \\
 &+ C_{\dot{U}} \sqrt{\frac{8}{\pi}} \sigma_{\dot{V}_{n\ell}} \cdot \text{Im}[H_r(\Omega)]\} \cdot S_{\dot{U}_{nk}\dot{U}_{n\ell}}(\Omega)
 \end{aligned} \quad (4.153)$$

Because each of the variables in Eq. 4.153 has been previously derived, Eqs. 4.153, 4.134, and 4.135 may be used to calculate the standard deviation of the relative velocity. The appearance of this standard deviation on the right-hand side of Eq. 4.153 necessitates the use of an iterative procedure in response calculations.



## Chapter 5

### THE DYNAMIC RESPONSE OF A MARINE RISER TO COMBINATIONS OF RANDOM WAVE FORCES, RANDOM TOP OFFSET, AND DETERMINISTIC CURRENT FORCES

#### 5.1 General

So far, the only forces which have been included in the riser analysis are those caused by random waves. It is not uncommon that a marine riser installation be subjected to a steady current force as well as random wave forces. Furthermore, unless the surface support platform is fixed, there is almost always some offset of the riser top, which results from lateral motion of the surface support platform. The introduction of current and top offset produces additional forces on the riser which, when combined with the random wave forces, lead to a response which is different from that caused by random waves alone. In this chapter, a method is developed for determining the total response to random waves, steady current, and random top offset.

#### 5.2 Response to Random Wave Forces and Steady Current Forces

##### 5.2.1 Equation of Motion

Consider a marine riser which is subjected to random wave forces and a deterministic steady current which varies in some known manner along the riser axis. For the present discussion the top offset is assumed to be zero. Let  $\dot{u}_c(x)$  be the steady current velocity and  $\{\dot{u}_c\}$  be an  $n$  by 1 vector of current velocities at the riser model nodes. The total relative water velocity due to current, waves, and structural response is given by





$$\begin{aligned}
 \dot{\tilde{V}}(x,t) &= \dot{u}_c(x) + \dot{U}(x,t) - \dot{V}(x,t) \\
 &= \dot{u}_c(x) + \dot{V}(x,t)
 \end{aligned}
 \quad (5.1)$$

and the equation of motion of the riser model (Eq. 4.8) becomes

$$\begin{aligned}
 [m] \{\ddot{Y}\} + [c] \{\dot{Y}\} + [K] \{Y\} \\
 = C_u \{\dot{\tilde{V}}|\dot{\tilde{V}}|\} + C_a \{\ddot{V}\}
 \end{aligned}
 \quad (5.2)$$

While this equation of motion is somewhat similar to Eq. 4.8, there is one highly significant difference. The velocity parameter,  $\dot{\tilde{V}}(x,t)$ , is a random variable whose mean is nonzero. In fact the mean value of the random velocity is exactly equal to the current velocity,  $\dot{u}_c(x)$ .

$$\begin{aligned}
 E[\dot{\tilde{V}}(x,t)] &= E[\dot{u}_c(x)] + E[\dot{V}(x,t)] \\
 &= \dot{u}_c(x)
 \end{aligned}
 \quad (5.3)$$

Because this input parameter has a nonzero mean value, the response of the structure will also have a nonzero mean value. Therefore the complete solution for the response must include a determination of the mean response as well as the response variance.

Because the drag force on the riser is a nonlinear function of the relative water velocity with respect to the structure, the total riser response cannot be obtained by superimposing the separate responses to the steady current acting alone and the random waves acting alone. Removal of the nonlinearity by the equivalent linearization technique leads to coefficients which are functions of both the steady current velocity,  $\{\dot{u}_c\}$ , and the standard deviation of the relative water velocity due to random waves,



$[\sigma_V]$ . Therefore, the current and wave effects remain coupled in the solution of the problem, and the response is expressed in terms of the mean and variance instead of in terms of a component due to current and a component caused by waves.

### 5.2.2 Linearization of the Equation of Motion

The linearization of Eq. 5.2 begins with a transformation of coordinates which is achieved by substituting Eqs. 4.9 in Eq. 5.2. The result is

$$[m][\ddot{U}] + [c]\{\dot{U}\} + [K]\{U\} = [m_e][\ddot{V}] + C_U\{\dot{\tilde{V}}|\dot{\tilde{V}}|\} + [c]\{\dot{V}\} + [K]\{V\} \quad (5.4)$$

To both sides of Eq. 5.4, the term  $[c]\{\dot{U}_c\}$  is next added, leading to

$$[m][\ddot{U}] + [c]\{\dot{U} + \dot{U}_c\} + [K]\{U\} = [m_e][\ddot{V}] + C_U\{\dot{\tilde{V}}|\dot{\tilde{V}}|\} + [c]\{\dot{V}\} + [K]\{V\} \quad (5.5)$$

The goal of the equivalent linearization process is to replace the two velocity terms on the right-hand side of Eq. 5.5 with a linearized version of the two terms. Let

$$C_U\{\dot{\tilde{V}}|\dot{\tilde{V}}|\} + [c]\{\dot{V}\} = \{\tilde{c}\} + [\tilde{c}]\{\dot{\tilde{V}}\} + \{E\} \quad (5.6)$$

where  $\{E\}$  is a vector of random errors which result from the linearization, and  $\{\tilde{c}\}$  and  $[\tilde{c}]$  are matrices of coefficients which are chosen in some optimal



manner. Equation 5.6 is similar to Eq. 4.11 except for the vector of constants,  $\{\tilde{c}\}$ , which is introduced because of the nonzero mean nature of  $\dot{\tilde{V}}(x,t)$ .

By assuming that the off diagonal terms of  $[c]$  and  $[\tilde{c}]$  are identical and letting  $[\tilde{c}] - [c] = [\tilde{c}_{e-}]$ , the error vector in Eq. 5.6 may be written

$$\{E\} = -[\tilde{c}_{e-}]\{\dot{\tilde{V}}\} + C_U \{\dot{\tilde{V}}|\dot{\tilde{V}}|\} - \{\tilde{c}\} \quad (5.7)$$

A typical element of the error vector is

$$E_{nj} = -c_{enj} \dot{\tilde{V}}_{nj} + C_U (\dot{\tilde{V}}_{nj} |\dot{\tilde{V}}_{nj}|) - \tilde{c}_{nj} \quad (5.8)$$

With two unknown coefficients in Eq. 5.8, it is possible to satisfy two conditions concerning the random error,  $E_{nj}$ . The two conditions which will be satisfied here are to choose  $c_{enj}$  and  $\tilde{c}_{nj}$  in such a way that the mean square error is minimized.

$$\frac{\partial}{\partial c_{enj}} E [E_{nj}^2] = 0 \quad (5.9a)$$

$$\frac{\partial}{\partial \tilde{c}_{nj}} E [E_{nj}^2] = 0 \quad (5.9b)$$

Interchanging the order of the differentiation and expectation in Eqs. 5.9 leads to

$$2 E \left[ E_{nj} \frac{\partial E_{nj}}{\partial c_{enj}} \right] = 0 \quad (5.10a)$$

and

$$2 E \left[ E_{nj} \frac{\partial E_{nj}}{\partial \tilde{c}_{nj}} \right] = 0 \quad (5.10b)$$



When Eq. 5.8 is substituted into Eqs. 5.10, the following two simultaneous equations in  $c_{e_{nj}}$  and  $\hat{c}_{nj}$  result.

$$c_{e_{nj}} E [\dot{\hat{V}}_{nj}^2] + \hat{c}_{nj} E [\dot{\hat{V}}_{nj}] = C_{\dot{u}} E [\dot{\hat{V}}_{nj}^2 | \dot{\hat{V}}_{nj}|] \quad (5.11a)$$

$$c_{e_{nj}} E [\dot{\hat{V}}_{nj}] + \hat{c}_{nj} = C_{\dot{u}} E [\dot{\hat{V}}_{nj} | \dot{\hat{V}}_{nj}|] \quad (5.11b)$$

Consider the expectation terms on the left hand sides of Eqs. 5.11. It has already been shown in Eq. 5.3 that the expected value of  $\dot{\hat{V}}_{nj}$  is the current velocity at node  $nj$ ,  $\dot{u}_{c_{nj}}$ . Furthermore, the second moment of  $\dot{\hat{V}}_{nj}$  is equal to the sum of the square of the mean value and the variance as shown by

$$\begin{aligned} E [\dot{\hat{V}}_{nj}^2] &= E [(\dot{u}_{c_{nj}} + \dot{\hat{V}}_{nj})^2] \\ &= E [\dot{u}_{c_{nj}}^2] + E [2\dot{u}_{c_{nj}} \dot{\hat{V}}_{nj}] + E [\dot{\hat{V}}_{nj}^2] \\ &= \dot{u}_{c_{nj}}^2 + \sigma_{\dot{\hat{V}}_{nj}}^2 \end{aligned} \quad (5.12)$$

The introduction of Eqs. 5.3 and 5.12 into Eqs. 5.11 results in

$$c_{e_{nj}} [\dot{u}_{c_{nj}}^2 + \sigma_{\dot{\hat{V}}_{nj}}^2] + \hat{c}_{nj} \dot{u}_{c_{nj}} = C_{\dot{u}} E [\dot{\hat{V}}_{nj}^2 | \dot{\hat{V}}_{nj}|] \quad (5.13a)$$

and

$$c_{e_{nj}} \dot{u}_{c_{nj}} + \hat{c}_{nj} = C_{\dot{u}} E [\dot{\hat{V}}_{nj} | \dot{\hat{V}}_{nj}|] \quad (5.13b)$$

The evaluation of the two expectations found on the right hand sides of Eqs. 5.13 is simplified by the introduction of a new random variable,





$\dot{V}_{nj}^*$ , defined as

$$\dot{V}_{nj}^* = \frac{\dot{V}_{nj} - \dot{u}_{cnj}}{\sigma_{\dot{V}_{nj}}} = \frac{\dot{V}_{nj}}{\sigma_{\dot{V}_{nj}}} \quad (5.14)$$

Because  $\dot{V}_{nj}$  is zero mean and Gaussian, it is readily seen that  $\dot{V}_{nj}^*$  is a standard Gaussian random variable with a mean of zero and a variance of one. From Eq. 5.14, it follows that

$$\dot{V}_{nj} = \dot{u}_{cnj} + \sigma_{\dot{V}_{nj}} \dot{V}_{nj}^* \quad (5.15)$$

Another useful parameter,  $\alpha_{nj}$ , is defined as the ratio of the current velocity to the standard deviation of the relative velocity caused by waves at node  $nj$ .

$$\alpha_{nj} = \frac{\dot{u}_{cnj}}{\sigma_{\dot{V}_{nj}}} \quad (5.16)$$

From Eq. 5.15 it is apparent that  $\dot{V}_{nj}$  is negative for all values of  $\dot{V}_{nj}^*$  less than  $-\alpha_{nj}$  and  $\dot{V}_{nj}$  is positive whenever  $\dot{V}_{nj}^*$  is greater than  $-\alpha_{nj}$ .

$$\begin{aligned} \dot{V}_{nj} = \dot{u}_{cnj} + \sigma_{\dot{V}_{nj}} \dot{V}_{nj}^* < 0, \quad \dot{V}_{nj}^* < -\alpha_{nj} \\ > 0, \quad \dot{V}_{nj}^* > -\alpha_{nj} \end{aligned} \quad (5.17)$$

Equations 5.17 are useful in evaluating the expectations on the right-hand side of Eqs. 5.13.

Consider the term on the right-hand side of Eq. 5.13a. By the definition of an expectation and with the use of Eqs. 5.15 and 5.17, the



expected value may be written

$$E [\dot{V}_{nj}^2 | \dot{V}_{nj}|] = - \int_{-\infty}^{-\alpha_{nj}} (\dot{u}_{cnj} + \sigma_{\dot{V}_{nj}} \dot{v}^*)^3 \cdot f_1(\dot{v}^*) d\dot{v}^* \\ + \int_{-\alpha_{nj}}^{\infty} (\dot{u}_{cnj} + \sigma_{\dot{V}_{nj}} \dot{v}^*)^3 \cdot f_1(\dot{v}^*) d\dot{v}^* \quad (5.18)$$

where

$$f_1(\dot{v}^*) = \frac{1}{\sqrt{2\pi}} e^{-\frac{\dot{v}^{*2}}{2}} \quad (5.19)$$

is the probability density function for a zero mean Gaussian random variable with unit variance. Expansion of Eq. 5.18 leads to an expression for the expectation in terms of eight integrals.

$$E [\dot{V}_{nj}^2 | \dot{V}_{nj}|] = - \int_{-\infty}^{-\alpha_{nj}} \dot{u}_{cnj}^3 \cdot f_1(\dot{v}^*) d\dot{v}^* \\ - 3 \int_{-\infty}^{-\alpha_{nj}} \dot{u}_{cnj}^2 \sigma_{\dot{V}_{nj}} \dot{v}^* \cdot f_1(\dot{v}^*) d\dot{v}^* \\ - 3 \int_{-\infty}^{-\alpha_{nj}} \dot{u}_{cnj} \sigma_{\dot{V}_{nj}}^2 \dot{v}^{*2} \cdot f_1(\dot{v}^*) d\dot{v}^* \\ - \int_{-\infty}^{-\alpha_{nj}} \sigma_{\dot{V}_{nj}}^3 \dot{v}^{*3} \cdot f_1(\dot{v}^*) d\dot{v}^* \\ + \int_{-\alpha_{nj}}^{\infty} \dot{u}_{cnj}^3 \cdot f_1(\dot{v}^*) d\dot{v}^* \\ + 3 \int_{-\alpha_{nj}}^{\infty} \dot{u}_{cnj}^2 \sigma_{\dot{V}_{nj}} \dot{v}^* \cdot f_1(\dot{v}^*) d\dot{v}^* \\ + 3 \int_{-\alpha_{nj}}^{\infty} \dot{u}_{cnj} \sigma_{\dot{V}_{nj}}^2 \dot{v}^{*2} \cdot f_1(\dot{v}^*) d\dot{v}^* \\ + \int_{-\alpha_{nj}}^{\infty} \sigma_{\dot{V}_{nj}}^3 \dot{v}^{*3} \cdot f_1(\dot{v}^*) d\dot{v}^*$$



$$\begin{aligned}
& + 3 \int_{-\alpha_{nj}}^{\infty} \dot{u}_{c_{nj}}^2 \sigma_{\dot{v}_{nj}} \dot{v}^* \cdot f_1(\dot{v}^*) d\dot{v}^* \\
& + 3 \int_{-\alpha_{nj}}^{\infty} \dot{u}_{c_{nj}} \sigma_{\dot{v}_{nj}}^2 \dot{v}^{*2} \cdot f_1(\dot{v}^*) d\dot{v}^* \\
& + \int_{-\alpha_{nj}}^{\infty} \sigma_{\dot{v}_{nj}}^3 \dot{v}^{*3} \cdot f_1(\dot{v}^*) d\dot{v}^* \quad (5.20)
\end{aligned}$$

Let

$$F_1(\alpha_{nj}) = \int_{-\infty}^{\alpha_{nj}} f_1(\xi) d\xi \quad (5.21)$$

where  $f_1(\xi)$  is defined by Eq. 5.19. The function  $F_1$  is simply the probability distribution function for a Gaussian random variable with zero mean and unit variance. Because of the symmetry of the Gaussian probability density function about the mean value,

$$F_1(-\alpha_{nj}) = 1 - F_1(\alpha_{nj}) \quad (5.22)$$

Equations 5.21 and 5.22 are helpful in evaluating the integrals on the right hand side of Eqs. 5.20.

The first and fifth integrals in Eq. 5.20 follow directly from Eqs. 5.21 and 5.22.

$$- \int_{-\infty}^{-\alpha_{nj}} \dot{u}_{c_{nj}}^3 \cdot f_1(\dot{v}^*) d\dot{v}^* = - \dot{u}_{c_{nj}}^3 [1 - F_1(\alpha_{nj})] \quad (5.23a)$$



$$\int_{-\alpha_{nj}}^{\infty} \dot{u}_{cnj}^3 \cdot f_1(\dot{v}^*) d\dot{v}^* = \dot{u}_{cnj}^3 F_1(\alpha_{nj}) \quad (5.23b)$$

The second and sixth integrals in Eq. 5.20 are determined by direct integration and by the use of Eq. 5.19.

$$\begin{aligned} -3 \int_{-\infty}^{-\alpha_{nj}} \dot{u}_{cnj}^2 \sigma_{\dot{v}_{nj}} \dot{v}^* \cdot f_1(\dot{v}^*) d\dot{v}^* \\ = 3 \dot{u}_{cnj}^2 \sigma_{\dot{v}_{nj}} f_1(\alpha_{nj}) \end{aligned} \quad (5.24a)$$

$$\begin{aligned} 3 \int_{-\alpha_{nj}}^{\infty} \dot{u}_{cnj}^2 \sigma_{\dot{v}_{nj}} \dot{v}^* \cdot f_1(\dot{v}^*) d\dot{v}^* \\ = 3 \dot{u}_{cnj}^2 \sigma_{\dot{v}_{nj}} f_1(\alpha_{nj}) \end{aligned} \quad (5.24b)$$

By employing the method of integration by parts, the third and seventh integrals in Eq. 5.20 are evaluated as

$$\begin{aligned} -3 \int_{-\infty}^{-\alpha_{nj}} \dot{u}_{cnj} \sigma_{\dot{v}_{nj}}^2 \dot{v}^{*2} \cdot f_1(\dot{v}^*) d\dot{v}^* \\ = -3 \dot{u}_{cnj} \sigma_{\dot{v}_{nj}}^2 [\alpha_{nj} f_1(\alpha_{nj}) + 1 - F_1(\alpha_{nj})] \end{aligned} \quad (5.25a)$$

$$\begin{aligned} 3 \int_{-\alpha_{nj}}^{\infty} \dot{u}_{cnj} \sigma_{\dot{v}_{nj}}^2 \dot{v}^{*2} \cdot f_1(\dot{v}^*) d\dot{v}^* \\ = 3 \dot{u}_{cnj} \sigma_{\dot{v}_{nj}}^2 [F_1(\alpha_{nj}) - \alpha_{nj} f_1(\alpha_{nj})] \end{aligned} \quad (5.25b)$$





Finally, the fourth and eighth integrals are given by

$$\begin{aligned}
 - \int_{-\infty}^{-\alpha_{nj}} \sigma_{\dot{V}_{nj}}^3 \dot{V}^{*3} \cdot f_1(\dot{V}^*) d\dot{V}^* \\
 = \sigma_{\dot{V}_{nj}}^3 f_1(\alpha_{nj}) [\alpha_{nj}^2 + 2]
 \end{aligned} \quad (5.26a)$$

and

$$\begin{aligned}
 \int_{-\alpha_{nj}}^{\infty} \sigma_{\dot{V}_{nj}}^3 \dot{V}^{*3} \cdot f_1(\dot{V}^*) d\dot{V}^* \\
 = \sigma_{\dot{V}_{nj}}^3 f_1(\alpha_{nj}) [\alpha_{nj}^2 + 2]
 \end{aligned} \quad (5.26b)$$

Substitution of Eqs. 5.23 through 5.26 into Eq. 5.20 and rearranging terms leads to

$$\begin{aligned}
 E[\dot{V}_{nj}^2 | \dot{V}_{nj}] &= 2 \dot{u}_{c_{nj}} [\dot{u}_{c_{nj}}^2 + 3 \sigma_{\dot{V}_{nj}}^2] \cdot F_1(\alpha_{nj}) \\
 &+ 2 \sigma_{\dot{V}_{nj}} [\dot{u}_{c_{nj}}^2 + 2 \sigma_{\dot{V}_{nj}}^2] \cdot f_1(\alpha_{nj}) \\
 &- \dot{u}_{c_{nj}} [\dot{u}_{c_{nj}}^2 + 3 \sigma_{\dot{V}_{nj}}^2]
 \end{aligned} \quad (5.27)$$

The expectation term on the right hand side of Eq. 5.13b remains to be evaluated. Because of Eqs. 5.15 and 5.17, this expected value may be written as



$$\begin{aligned}
E [\dot{\tilde{v}}_{nj} | \dot{\tilde{v}}_{nj}] &= - \int_{-\infty}^{-\alpha_{nj}} (\dot{u}_{c_{nj}} + \sigma_{\tilde{v}_{nj}} \dot{v}^*)^2 f_1(\dot{v}^*) d\dot{v}^* \\
&+ \int_{-\alpha_{nj}}^{\infty} (\dot{u}_{c_{nj}} + \sigma_{\tilde{v}_{nj}} \dot{v}^*)^2 f_1(\dot{v}^*) d\dot{v}^* \quad (5.28)
\end{aligned}$$

Expansion of Eq. 5.28 leads to six integrals of the same form as those evaluated in Eqs. 5.23 through 5.25. Substitution of these integrals into Eq. 5.28 yields

$$\begin{aligned}
E [\dot{\tilde{v}}_{nj} | \dot{\tilde{v}}_{nj}] &= 2 \dot{u}_{c_{nj}}^2 F_1(\alpha_{nj}) - \dot{u}_{c_{nj}}^2 \\
&+ 4 \dot{u}_{c_{nj}} \sigma_{\tilde{v}_{nj}} f_1(\alpha_{nj}) \\
&+ \sigma_{\tilde{v}_{nj}}^2 [2 F_1(\alpha_{nj}) - 2 \alpha_{nj} f_1(\alpha_{nj}) - 1] \quad (5.29)
\end{aligned}$$

When coefficients of  $F_1$  and  $f_1$  are combined, there results

$$\begin{aligned}
E [\dot{\tilde{v}}_{nj} | \dot{\tilde{v}}_{nj}] &= 2 [\dot{u}_{c_{nj}}^2 + \sigma_{\tilde{v}_{nj}}^2] F_1(\alpha_{nj}) \\
&+ 2 \dot{u}_{c_{nj}} \sigma_{\tilde{v}_{nj}} f_1(\alpha_{nj}) \\
&- [\dot{u}_{c_{nj}}^2 + \sigma_{\tilde{v}_{nj}}^2] \quad (5.30)
\end{aligned}$$

Substitution of Eqs. 5.27 and 5.30 into Eqs. 5.13 leads to two simultaneous equations for the two coefficients  $c_{e_{nj}}$  and  $\tilde{c}_{nj}$ . Solution of these equations results in the following expressions for the optimized coefficients,  $c_{e_{nj}}$  and  $\tilde{c}_{nj}$ .



$$c_{e_{nj}} = c_{nj,nj} - c_{nj,nj} = \dot{c}_{nj} \{ 4 \dot{u}_{c_{nj}} F_1(\alpha_{nj}) + 4 \sigma_{\dot{v}_{nj}} f_1(\alpha_{nj}) - 2 \dot{u}_{c_{nj}} \} \quad (5.31a)$$

$$\tilde{c}_{nj} = \dot{c}_{nj} \{ [\sigma_{\dot{v}_{nj}}^2 - \dot{u}_{c_{nj}}^2] [2 F_1(\alpha_{nj}) - 1] - 2 \dot{u}_{c_{nj}} \sigma_{\dot{v}_{nj}} f_1(\alpha_{nj}) \} \quad (5.31b)$$

It is readily shown that Eqs. 5.31 do, in fact, minimize the mean square error because the second derivatives of the mean square error are all positive.

$$\frac{\partial^2}{\partial \dot{c}_{e_{nj}}^2} E [E_{nj}^2] = 2 E [\dot{v}_{nj}^2] \geq 0 \quad (5.32a)$$

$$\frac{\partial^2}{\partial \dot{c}_{nj}^2} E [E_{nj}^2] = 2 \quad (5.32b)$$

and

$$\begin{aligned} \frac{\partial^2}{\partial \dot{c}_{nj} \partial \dot{c}_{e_{nj}}} E [E_{nj}^2] &= 2 E [\dot{v}_{nj}] \\ &= 2 \dot{u}_{c_{nj}} \geq 0 \end{aligned} \quad (5.32c)$$

It is interesting to note the behavior of the coefficients  $c_{e_{nj}}$  and  $\tilde{c}_{nj}$  as the current approaches zero velocity. As  $\dot{u}_{c_{nj}} \rightarrow 0$ ,

$$\alpha_{nj} = \frac{\dot{u}_{c_{nj}}}{\sigma_{\dot{v}_{nj}}} \rightarrow 0$$

$$F_1(\alpha_{nj}) \rightarrow \frac{1}{2}$$



and

$$f_1(\alpha_{nj}) \rightarrow \frac{1}{\sqrt{2\pi}}$$

Therefore, as  $\dot{u}_{c_{nj}} \rightarrow 0$ ,

$$c_{e_{nj}} \rightarrow c_{\dot{u}} \cdot 4 \sigma_{\dot{V}_{nj}} \frac{1}{\sqrt{2\pi}} = c_{\dot{u}} \sqrt{\frac{8}{\pi}} \sigma_{\dot{V}_{nj}} \quad (5.33a)$$

and

$$\hat{c}_{nj} \rightarrow 0 \quad (5.33b)$$

Equations 5.33 are identical to the optimized coefficients for the case of no current given by Eq. 4.24.

With the mean square error minimized, the random error vector is now dropped from Eq. 5.6 leaving the approximate relationship,

$$C_{\dot{u}} \{ \dot{V} | \dot{V} \} + [c] \{ \dot{V} \} \cong \{ \tilde{c} \} + [c_{\tilde{c}}] \{ \dot{V} \} \quad (5.34)$$

Substitution of Eq. 5.34 into Eq. 5.5 yields

$$\begin{aligned} [m_{\sim}] \{ \ddot{U} \} + [c] \{ \dot{U} + \dot{u}_c \} + [K] \{ U \} \\ = [m_{e\sim}] \{ \ddot{V} \} + [c_{\tilde{c}}] \{ \dot{V} \} + [K] \{ V \} + \{ \tilde{c} \} \end{aligned} \quad (5.35)$$

Subtraction of  $[c] \{ \dot{u}_c \}$  from both sides of Eq. 5.35 and utilization of the relationships

$$\{ V \} = \{ U \} - \{ Y \}$$

$$\{ \dot{V} \} = \{ \dot{U} \} - \{ \dot{Y} \}$$

and





$$\{\ddot{V}\} = \{\ddot{U}\} - \{\ddot{Y}\}$$

transforms Eq. 5.35 into the following.

$$\begin{aligned} [m_e] \{\ddot{Y}\} + [c] \{\dot{Y}\} + [K] \{Y\} \\ = c_a \{\ddot{U}\} + [c_e] \{\dot{U}\} + [c_e] \{\dot{u}_c\} + \{\tilde{c}\} \end{aligned} \quad (5.36)$$

Equation 5.36 is the linearized version of the equation of motion, Eq. 5.2.

### 5.2.3 Calculation of Response Statistics

By definition, the random riser deflection,  $Y(x,t)$ , is measured from the undeflected position of the riser, which is the  $x$  axis. The solution of Eq. 5.36 is simplified somewhat if a transformation of coordinates is used. Let

$$Y^*(x,t) = Y(x,t) - \mu_Y(x) \quad (5.37)$$

where  $\mu_Y(x)$ , the mean deflection of the riser, is constant for all time because the response is a stationary random process. It follows that

$$\dot{Y}(x,t) = \dot{Y}^*(x,t) \quad (5.38a)$$

and

$$\ddot{Y}(x,t) = \ddot{Y}^*(x,t) \quad (5.38b)$$

By using Eqs. 5.37 and 5.38, Eq. 5.36 may be rewritten as



$$\begin{aligned}
[m_e] \{\ddot{Y}^*\} + [c] \{\dot{Y}^*\} + [K] \{Y^*\} + [K] \{\mu_Y\} \\
= c_a \{\ddot{U}\} + [c_e] \{\dot{U}\} + [c_e] \{\dot{U}_C\} + \{\dot{c}\}
\end{aligned} \quad (5.39)$$

Equation 5.39 contains both time dependent and steady terms. For the equation to be valid for all time, the steady terms on each side of Eq. 5.39 must be equal. Thus

$$[K] \{\mu_Y\} = [c_e] \{\dot{U}_C\} + \{\dot{c}\} \quad (5.40)$$

Premultiplication of both sides of Eq. 5.40 by  $[K]^{-1}$  leads to a solution for the mean deflections at the nodes.

$$\{\mu_Y\} = [K]^{-1} ([c_e] \{\dot{U}_C\} + \{\dot{c}\}) \quad (5.41)$$

Because of Eq. 5.40, the time dependent terms of Eq. 5.39 are related by

$$\begin{aligned}
[m_e] \{\ddot{Y}^*\} + [c] \{\dot{Y}^*\} + [K] \{Y^*\} \\
= c_a \{\ddot{U}\} + [c_e] \{\dot{U}\}
\end{aligned} \quad (5.42)$$

The solution to Eq. 5.42 may be obtained by analogy to the solution of Eq. 4.31 which is derived in Chapter 4. From Eq. 4.104, it follows that



$$\begin{aligned}
S_{Y_{ni}^* Y_{nj}^*}(\Omega) &= \left[ \left( \frac{kq}{\Omega m_e} \right)^2 \sum_{r=1}^{nm} \sum_{s=1}^{nm} \phi_{ni}^{(r)} \phi_{nj}^{(s)} \right. \\
&\quad \overline{H_r(\Omega)} H_s(\Omega) \sum_{nk=1}^n \sum_{n\ell=1}^n \phi_{nk}^{(r)} \phi_{n\ell}^{(s)} \\
&\quad [c_{e_{nk}} c_{e_{n\ell}} + i\Omega c_a (c_{e_{nk}} - c_{e_{n\ell}}) + \Omega^2 c_a^2] \\
&\quad \left. \cdot \tilde{q}_{nk}(\Omega) \cdot \tilde{q}_{n\ell}(\Omega) \right] S_{nn}(\Omega) \quad (5.43)
\end{aligned}$$

Because  $Y^*(x, t)$  is, by definition, a zero mean random variable, the variance is given by

$$\sigma_{Y_{ni}^*}^2 = \int_0^\infty S_{Y_{ni}^* Y_{ni}^*}(\Omega) d\Omega \quad (5.44)$$

The variance of  $Y_{ni}(t)$  is

$$\begin{aligned}
\sigma_{Y_{ni}}^2 &= E[(Y_{ni}(t) - \mu_{Y_{ni}})^2] \\
&= E[Y_{ni}^{*2}] \\
&= \sigma_{Y_{ni}^*}^2 \quad (5.45)
\end{aligned}$$

From Eqs. 5.44 and 5.45, it follows that

$$\sigma_{Y_{ni}}^2 = \int_0^\infty S_{Y_{ni}^* Y_{ni}^*}(\Omega) d\Omega \quad (5.46)$$

Equations 5.41 and 5.46 may be used to calculate the mean and variance of the response. Because the input is assumed to be Gaussian and the problem



has been linearized, the response is also Gaussian. Therefore, the probability density function of the response is uniquely determined by the response mean and variance, and the solution is complete.

### 5.3 Riser Response to Random Top Offset

Even in the absence of external forces, a marine riser will undergo a deflection caused by its own weight whenever the top is offset from a point vertically above the bottom. Unless the surface support platform is fixed, there is almost always some top offset produced by the lateral motion of the platform in response to the exciting forces of wind, wave, and current and the restoring forces of a mooring system or a dynamic positioning system. While a complete study of the motion of surface support platforms is beyond the scope of this thesis, an elementary model for top offset may be used to calculate the riser response to the combination of wave and current forces and top offset. It will be assumed that the top offset is a random process,  $Y_{\text{top}}(t)$ , which changes so slowly that the associated riser response is essentially static. This assumption limits the study to platforms and sea conditions for which the wave-induced platform motion has a negligible effect on the riser behavior.

The random static deflection produced by a random top offset may be expressed simply as

$$\{\hat{Y}(t)\} = \{\hat{b}\} Y_{\text{top}}(t) \quad (5.47)$$

where elements of  $\{\hat{b}\}$ , the vector of influence coefficients, may be determined from Eqs. 2.11 and 2.13 as

$$b_{ni} = \frac{1}{L^*} [-K_{ni,n-1}^{-1} + (2 + T_n^* + W_n^*) K_{ni,n}^{-1}] \quad (5.48)$$





The random bottom rotation  $\varphi_0(t)$  caused by top offset is given by

$$\varphi_0(t) = \frac{n+1}{L} \gamma_1(t) = \frac{n+1}{L} b_1 \gamma_{\text{top}}(t) \quad (5.49)$$

and the random bending moments  $\{M(t)\}$  caused by top offset are determined after the manner of Eq. 3.96.

$$\{M(t)\} = [J] \{\gamma(t)\} \quad (5.50)$$

Equation 5.47 may be used to express the correlation function of the deflections at two nodes in terms of the autocorrelation function of the top offset.

$$R_{\gamma_{n1}\gamma_{nj}}(\tau) = b_{n1} b_{nj} R_{\gamma_{\text{top}}}(\tau) \quad (5.51)$$

A Fourier transformation of both sides of Eq. 5.51 leads to

$$S_{\gamma_{n1}\gamma_{nj}}(\Omega) = b_{n1} b_{nj} S_{\gamma_{\text{top}}}(\Omega) \quad (5.52)$$

If the top offset has a zero mean value, then integration of Eq. 5.52 gives the variance of the node deflections in terms of the variance of the top offset.

$$\sigma_{\gamma_{n1}}^2 = b_{n1}^2 \sigma_{\gamma_{\text{top}}}^2 \quad (5.53)$$

In a similar manner, it can be shown that

$$\sigma_{\varphi_0}^2 = \left( \frac{n+1}{L} \right)^2 b_1^2 \sigma_{\gamma_{\text{top}}}^2 \quad (5.54)$$

and



$$\sigma_{ni}^2 = \sum_{nk=1}^n \sum_{nl=1}^n J_{ni,nk} b_{nk} b_{nl} \sigma_{Y_{top}}^2 \quad (5.55)$$

If the top offset has a nonzero mean value,  $\mu_{Y_{top}}$ , then the mean responses may be calculated by adapting Eqs. 5.47, 5.49 and 5.50.

$$\{\mu_Y\} = \{b\} \mu_{Y_{top}} \quad (5.56)$$

$$\mu_{\theta_0} = \frac{n+1}{L} b_1 \mu_{Y_{top}} \quad (5.57)$$

$$\{\mu_M\} = [J] \{b\} \mu_{Y_{top}} \quad (5.58)$$

Figures 5.1 and 5.2, which were derived from the results of Fischer and Ludwig,<sup>4</sup> summarize the behavior of the mean and variance of the bottom rotation caused by top offset. In order to maintain a given bottom rotation, the ratio of top offset to riser length must decrease as length ratio increases.

#### 5.4 Total Response to Current, Waves, and Top Offset

Let  $\hat{Y}(x,t)$  be the total response of the riser to current, waves, and top offset.

$$\hat{Y}(x,t) = Y(x,t) + \hat{Y}_t(x,t) \quad (5.59)$$

The response to current and waves has been shown to be Gaussian with mean  $\mu_{Y_{ni}}$  and variance  $\sigma_{Y_{ni}}^2$  given by Eqs. 5.41 and 5.46. An elementary model for the total riser response may be formulated by assuming that the top offset is Gaussian (not necessarily zero mean) and that the random response caused by waves and current,  $Y(x,t)$ , and the random response caused by top offset,



$\hat{Y}(x,t)$ , are independent. A Gaussian top offset implies a Gaussian response,  $\hat{Y}(x,t)$ , because the system is linear as shown by Eq. 5.47. If  $Y(x,t)$  and  $\hat{Y}(x,t)$  are Gaussian and independent, then  $\tilde{Y}(x,t)$  is also Gaussian<sup>27</sup> with mean value

$$\mu_{\tilde{Y}_{ni}} = \mu_{Y_{ni}} + \mu_{\hat{Y}_{ni}} \quad (5.60)$$

and variance

$$\sigma_{\tilde{Y}_{ni}}^2 = \sigma_{Y_{ni}}^2 + \sigma_{\hat{Y}_{ni}}^2 \quad (5.61)$$

In this elementary model, the effect of top offset is completely described by the mean and variance of the top offset.



## Chapter 6

## SAMPLE PROBLEMS

## 6.1 General

The theory derived in Chapters 4 and 5 was used to study the behavior of a typical riser system under various random environmental conditions. To make this study, two computer programs were developed and coded in FORTRAN IV. The first program, RISER DYNAMIC III, calculates the response of a riser to random waves only, and the second, RISER DYNAMIC IV, calculates the response to a combination of random waves and a steady, deterministic current. The University of Illinois IBM System 360-75 computer with the FORTRAN IV, Level G compiler was used to obtain solutions.

The following input parameters were held constant.

$$D = 20 \text{ inches}$$

$$I = .0621 \text{ feet}^4$$

$$E = 29 \times 10^6 \text{ pounds per square inch}$$

$$w = 248 \text{ pounds per foot}$$

$$C_D = 1.0$$

$$C_I = 1.5$$

A finite difference model having 31 equally spaced nodes was used to represent the riser. Internal friction damping was taken as two percent of critical damping for all calculations.

Input parameters which were varied include the water depth, top tension ratio, wind velocity, sea surface elevation spectral density function,





and current velocity profile. The natural modes used in each solution included all modes whose frequencies lie in the range where the input sea surface elevation spectral density function is significant.

Both computer programs use an iterative procedure which continues until  $[\sigma_{\dot{v}}]$  and  $[\sigma_{zz}^2]$  converge. Convergence was considered to occur when the assumed value of  $\sigma_{\dot{v}_{nj}}$  was within five percent of the calculated value for every node and the assumed value of  $\sigma_{z_r z_r}^2$  was within ten percent of the calculated value for all modes considered. In most cases, these convergence criteria were satisfied after two to four cycles.

## 6.2 Riser Response to Random Waves Alone

The marine riser response to random waves alone was investigated for water depths of 609 feet, 1015 feet, 1523 feet, and 2030 feet and sea surface elevation spectra given by the Pierson-Moskowitz<sup>16</sup> formula for wind velocities of ten to forty knots. For this series of problems a top tension ratio of 1.2 was used. Two additional studies were made of the 609 foot riser, one with the top tension ratio changed to 1.0, the other with the sea surface elevation spectrum given by the Sverdrup-Munk-Bretschneider<sup>15</sup> formula.

### 6.2.1 Bottom Rotation

Figure 6.1 shows the effect of wind velocity, top tension ratio, water depth, and sea surface elevation spectral density formula on the root mean square bottom rotation.

As expected,  $\sigma_{\theta_0}$  increases with wind velocity. The rate of increase changes rather abruptly at certain wind velocities and remains fairly



constant between these changes. This abrupt change in slope occurs whenever the low frequency face of the sea surface elevation spectrum approaches a natural frequency of the riser. This behavior is best illustrated in the case of the 609 foot riser where pronounced changes in slope occur as the fundamental mode begins to participate in the response. As shown by Fig. 6.2, for an input SMB sea surface elevation spectrum, the fundamental mode is beginning to participate significantly in the response when the wind velocity is thirteen knots. The bottom rotation spectra for the 609 foot riser with input PM spectra for twenty, twenty-five, and thirty knot winds are shown in Figs. 6.3, 6.4 and 6.5. The participation of the fundamental mode in the response is seen to correlate with the increased slope of the corresponding curves in Fig. 6.1. Once the fundamental mode has been picked up, the slope of the 609 foot riser curves remains fairly constant. This slope does not appear in the curves for the longer risers because the first mode does not participate significantly in their response for the wind velocities studied.

Figure 6.1 shows that the bottom rotation decreases as riser length increases, all other parameters remaining constant. In a mathematical sense, this results from the fact that the bottom rotation of the normalized mode shapes decreases as riser length increases. In a physical sense, the reason for this behavior is that the random wave forces become relatively closer to the upper end of the riser as length increases.

The decrease in bottom rotation with increasing water depth is not the result of increased damping. On the contrary, damping ratios decrease somewhat as water depth increases, as shown in Fig. 6.6. This behavior may be understood by recalling that hydraulic damping is a function



of the relative fluid structure velocity. As water depth increases, a decrease in structural response results in smaller relative velocities, as shown in Fig. 6.8.

In Fig. 6.1, the response of the 609 foot riser with top tension ratio of 1.2 to the 20 knot PM spectrum is somewhat larger than a smooth curve through the points for other wind velocities would indicate. The explanation for this perturbation is that the peak frequency of the twenty knot PM spectrum and the second mode frequency of the 609 foot riser nearly coincide, as shown in Fig. 6.3. Similar perturbations might appear in the other curves of Fig. 6.1 if additional data points were generated where natural frequencies of the riser coincide with peak frequencies of the sea surface elevation spectrum.

The effect of top tension ratio on the bottom rotation of the 609 foot riser is shown in Fig. 6.1. The reduction in rotation which results from increased tension may be traced to two factors. First, increasing top tension increases the natural frequency somewhat and therefore reduces the value of the frequency response function. An increase in top tension also decreases the bottom rotation of the normalized mode shapes.

Comparison of the response of the 609 foot riser to SMB and PM spectra illustrates the significant effect which the input spectrum has on the response. Of course, part of this difference can be attributed to the fact that, for a given wind velocity, the SMB spectrum implies a larger energy density than the PM spectrum, as shown by Fig. C.4. To eliminate this source of difference,  $\sigma_{\theta_0}$  is plotted versus energy density in Fig. 6.9. Although the difference between the two response curves is smaller than in Fig. 6.1, it is still significant, particularly for wind velocities of 25



to 30 knots. Thus the response of the riser is dependent not only upon the energy density of the sea but also upon the distribution of that energy with respect to frequency. A good illustration of this distribution difference is given in Fig. 6.10, which shows the SMB and PM spectra for an energy density of 1000 foot pounds per square foot. Although the areas under these spectra are equal, the SMB spectrum is concentrated near the fundamental riser frequency, and the PM spectrum is spread over higher frequencies.

The variation of bottom rotation with energy density shows an interesting trend when plotted with energy density on a natural scale as in Fig. 6.11. The decrease in initial slope with increasing energy density is a result of increased hydraulic damping, as shown in Fig. 6.7. Above an energy density of 1000 foot pounds per square foot, the variation of  $\sigma_{\theta_0}$  with  $E^*$  is nearly linear.

### 6.2.2 Bending Moments

The variation of root mean square maximum bending moment with wind velocity is shown in Fig. 6.12. A comparison of Figs. 6.12 and 6.1 shows that the maximum bending moment behaves very much like the bottom rotation as the problem parameters are varied. However, top tension is somewhat more effective in reducing bending moments than it is in reducing bottom rotations. While the bending moments induced by the SMB spectrum are greater than those caused by the corresponding PM spectrum, the difference is not as great as the difference between bottom rotations produced by these two spectra.

For the riser cross section studied, the relationship between bending moment,  $M$ , and flexural stress,  $f$ , is





$$f \text{ (kips/square inch)} = \frac{M \text{ (foot-kips)}}{10.73} \quad (6.1)$$

### 6.2.3 Number of Modes in Response

It has already been shown, in Figs. 6.2 through 6.5, that two or three natural modes may participate in the response of the 609 foot riser. As riser length increases, the natural frequencies decrease and become more closely grouped with respect to frequency, as shown in Figs. 4.3 and 4.4. Therefore, as water depth increases, more modes and higher modes participate in the response. This behavior is illustrated in Figs. 6.13 and 6.14 for the 2030 foot riser. The response to the twenty knot PM spectrum contains modes three through six, and the second through fifth modes contribute significantly to the response to the thirty knot PM spectrum. Figures 6.15 and 6.16 show the modal contributions to profiles of root mean square deflection and moment produced by the thirty knot PM spectrum.

### 6.3 Riser Response to Random Waves and Steady Deterministic Current

To investigate the effect of steady current on riser response to random waves, a series of studies was made using the 609 foot riser with a top tension ratio of 1.2 and the 30 knot PM wave spectrum. Two current profiles were considered, a uniform current and an exponentially decaying current given by

$$\dot{u}_c(x) = \dot{u}_c(h) \cdot e^{-\frac{\pi}{D_f}(h-x)} \quad (6.2)$$

where  $D_f$  is the depth of frictional influence. Equation 6.2, is Ekman's equation for the magnitude of a pure wind driven current.<sup>35</sup> Although Ekman's



solution indicates that the current direction changes with depth (the Ekman spiral), for the present investigations the current was considered to be unidirectional. The depth of frictional influence was taken as 200 feet.

### 6.3.1 Uniform Current

Figure 6.17 summarizes the behavior of the bottom rotation as uniform current velocity is varied. As expected, both the mean response and static response to current alone increase as current velocity increases. The static response becomes a better predictor of the mean response as current velocity increases.

As current velocity increases, the standard deviation of the bottom rotation decreases somewhat because of rather large increases in the damping ratios, as shown in Fig. 6.18. These increased damping ratios may be traced to increased hydraulic damping coefficients at the nodes of the riser. Fig. 6.19 shows the ratio of hydraulic damping coefficients for a uniform current of one-half knot to the same coefficients for no current. The relative velocity profile of Fig. 6.20 helps explain the behavior of the hydraulic damping coefficients. The uniform current causes the greatest relative change in hydraulic damping near the midpoint and lower end of the riser where the relative velocity is smallest. Where the relative velocity is large with respect to the steady current, the current has little effect on hydraulic damping.

Figures 6.21 and 6.22 show the effect of a one-half knot uniform current on deflection and bending moment statistics of the 609 foot riser with a thirty knot PM spectrum. The mean deflections and moments are somewhat greater than the static response to current alone, and near the top of



the riser the mean moment is considerably greater than the static moment. Increased hydraulic damping results in standard deviations of deflection and moment which are lower with the current than without it.

### 6.3.2 Wind Driven Current

The behavior of the bottom rotation as wind driven current is varied is summarized in Fig. 6.23. The increase in mean and static rotations is small with respect to the standard deviation, and on a relative basis the mean rotation is considerably greater than the static rotation. Unlike the uniform current, the wind driven current produces a slight increase in the standard deviation of bottom rotation and only a small increase in damping ratios for the first two modes, as shown in Fig. 6.24. The reason for this behavior is evident from the velocity profiles of Fig. 6.25. The wind driven current increases the water velocity in the upper half of the riser where it is already large as a result of waves and has a negligible effect in the lower half. Therefore the hydraulic damping coefficients are increased slightly in the upper half of the riser and unaffected in the lower half, as shown by Fig. 6.26.

Figures 6.27 and 6.28 show the effect of a wind driven current with surface velocity of two knots on the deflection and moment statistics. The current causes a slight increase in the standard deviations, and the mean response is nearly twice the static response.



## Chapter 7

### CONCLUSIONS AND RECOMMENDATIONS FOR FURTHER STUDY

#### 7.1 Conclusions

In this thesis a mathematical model has been developed for predicting the nondeterministic response of a marine riser to random wave forces, current forces, and random top offset. In this model the continuous riser structure is represented as a finite degree of freedom system by means of the method of finite differences. The validity of this structural model and the lumped-smeared force model used to represent wave force distributions is demonstrated in Chapter 2. In Chapter 3 a method is derived to calculate the static riser response to random waves, and in Chapter 4 the method is extended to the determination of the dynamic riser response to random waves. Chapter 5 completes the derivation of the mathematical model by introducing procedures for calculating the response to a combination of random waves, a steady deterministic current, and random top offset. In Chapter 6 the model is used to demonstrate the effect of several problem parameters on riser response.

From the derivations and sample problems of the preceding five chapters several conclusions may be drawn.

1. The lumped-smeared force model accurately represents wave force distributions with a relatively small number of nodes, even when the wave force is essentially concentrated at the upper end of the riser.
2. The finite difference structural model, when used with the lumped-smeared force model, is a satisfactory representation





of the marine riser for purposes of analyzing the riser's behavior in its operating environment.

3. The mathematical model derived herein permits an estimation of the random dynamic structural response of marine risers caused by random waves, steady currents, and random top off-sets.
4. The high frequency tail of the input sea surface elevation spectrum contributes little to random water velocity and acceleration.
5. The dynamic response of marine risers to random wave forces is significantly greater than the static response.
6. The response to random wave forces is highly dependent upon the spectral distribution of the wave energy density as well as the total average energy density.
7. The dynamic response of the riser to waves which are described by a given sea surface elevation spectrum decreases as water depth increases.
8. The random dynamic bottom rotation caused by waves is reduced somewhat by increasing the top tension.
9. The dynamic response of the riser to random waves may include significant participation by more than one natural mode, the lowest one of which is not necessarily the fundamental mode. The number of modes which contribute appreciably to the response increases as water depth increases.
10. Wave structure interaction results in modified drag forces and hydraulic damping which increases significantly with increased energy density of the sea.



11. For a current velocity profile which is small with respect to the standard deviation of the relative water velocity, the effect of current on the riser bottom rotation is small and may be neglected without appreciable error.
12. For a current velocity profile which is large with respect to the standard deviation of the relative water velocity, the current increases hydraulic damping significantly and thus reduces the response variance. When this condition exists, the static response to current is a good approximation of the mean response to current and waves, and the response variance for waves alone is a conservative estimate of the response variance for the combination of waves and current.

## 7.2 Recommendations for Further Study

The model derived herein is somewhat limited by the assumptions which were made in its derivation as well as the scope of this thesis. Several areas where further research would improve the model may be cited.

1. The model should be tested by comparing calculated riser behavior with field observations of actual riser behavior in the ocean environment. A monitoring device for the bottom rotation is presently operational<sup>3</sup> and could provide data which, along with synoptic wave, current, and top offset observations, could be used to verify the model.
2. Further studies of the platform motion are recommended. Attention should be given to the effect of wave induced platform motion on riser response. Spectral density functions



and probability distribution functions for platform motion need to be determined to improve the model. The dynamic effect of operational platform motion in deep water, where the fundamental frequency may approach platform motion frequencies, should also be investigated.

3. Because of the cyclic nature of the loads imposed on the riser by its environment, fatigue failure is of concern. It is recommended that the model developed herein be extended to the study of fatigue in marine risers.
4. Better information is needed on the spectral distribution of the energy of a random sea. While existing wave spectra may be satisfactory for wave forecasting, it has been demonstrated herein that different spectra lead to greatly different responses because the riser is very sensitive to the spectral distribution of wave energy. As good directional wave spectra are developed, the riser model should also be extended to three dimensions.
5. The drag and inertia coefficients used in the force formula are based on experiments with relatively rigid piles. More information is needed on drag and inertia coefficients which are appropriate for the rather flexible marine riser.
6. The method of analysis employed in this thesis requires the use of a digital computer. A simple method should be developed for estimating the dynamic response of the riser using hand computations only.



## LIST OF REFERENCES

1. Harris, L. M. and Ilfrey, W. T., "Drilling in 1300 Feet of Water - Santa Barbara Channel, California," Preprints, First Annual Offshore Technology Conference, Vol. I, Paper No. OTC 1018, 1969, pp. I-167 - I-182.
2. "Shell Completing Drillship for Deep-Ocean Drilling," *Oceanology International*, Oct. 1971, pp. 13-14.
3. Childers, M. A., Hazlewood, G. and Ilfrey, W. T., "Marine Riser Monitoring with the Acoustic Ball Joint Angle-Azimuth Indicator," Preprints, Third Annual Offshore Technology Conference, Vol. I, Paper No. OTC 1386, 1971, pp. I-571 - I-584.
4. Fischer, W. and Ludwig, M., "Design of Floating Vessel Drilling Riser," *Journal of Petroleum Technology*, March 1966, pp. 272-280.
5. Huang, T. and Dareing, D. W., "Buckling and Frequencies of Long Vertical Pipes," *Journal of the Engineering Mechanics Division, ASCE*, Vol. 95, No. EM1, Feb. 1969, pp. 167-181.
6. Frohrib, D. A. and Plunkett, R., "The Free Vibrations of Stiffened Drill Strings with Static Curvature," *Journal of Engineering for Industry, Trans. ASME, Series B*, Vol. 89, No. 1, Feb. 1967.
7. Butler, H. L., Delfosse, C., Galef, A. and Thorn, B. J., "Numerical Analysis of a Beam Under Tension," *Journal of the Structural Division, ASCE*, Vol. 93, No. ST5, Oct. 1967, pp. 165-174.
8. St. Denis, M., *On the Dynamic Analysis of the Mohole Riser*, National Engineering Science Company, Pasadena, California, 1964.
9. Gosse, C. G. and Barksdale, G. L., "The Marine Riser - A Procedure for Analysis," Preprints, First Annual Offshore Technology Conference, Vol. II, Paper No. OTC 1080, 1969, pp. II-109 - II-116.
10. Pierson, W. J., Jr., "Wind Generated Gravity Waves," *Advances in Geophysics*, Vol. 2, Academic Press, N. Y., 1955, pp. 93-178.
11. Neumann, G. and Pierson, W. J., Jr., "Known and Unknown Properties of the Frequency Spectrum of a Wind-Generated Sea," *Ocean Wave Spectra, Proceedings of a Conference*, Prentice-Hall, Englewood Cliffs, N. J., 1963.
12. Rice, S. O., "Mathematical Analysis of Random Noise," *Bell System Technical Journal*, Vol. 23, 1944, pp. 282-332; and Vol. 24, 1945, pp. 46-156.





13. Longuet-Higgins, M. S., "On the Statistical Distribution of the Heights of Sea Waves," *Journal of Marine Research*, Vol. 11, No. 3, 1952, pp. 245-266.
14. Neumann, G., "On Ocean Wave Spectra and a New Method of Forecasting Wind-Generated Sea," Technical Memorandum No. 43, Beach Erosion Board, U. S. Army Corps of Engineers, 1952.
15. Bretschneider, C. L., "Wave Generation by Wind, Deep and Shallow Water," *Estuary and Coastline Hydrodynamics*, edited by A. T. Ippen, McGraw-Hill, 1966.
16. Pierson, W. J., Jr. and Moskowitz, L. A., "A Proposed Spectral Form for Fully Developed Wind Seas Based on the Similarity Theory of S. A. Kitagorodskii," *Journal of Geophysical Research*, Vol. 69, No. 24, 1964, pp. 1581-1590.
17. Borgman, L. E., "Spectral Analysis of Ocean Wave Forces on Piling," *Journal of the Waterways and Harbors Division, ASCE*, Vol. 93, No. WW2, May 1967, pp. 129-156.
18. Borgman, L. E., "Ocean Wave Simulation for Engineering Design," *Journal of the Waterways and Harbors Division, ASCE*, Vol. 95, No. WW4, Nov. 1969, pp. 557-583.
19. Foster, E. T., Jr., "Model for Nonlinear Dynamics of Offshore Towers," *Journal of the Engineering Mechanics Division, ASCE*, Vol. 96, No. EM1, Feb. 1970, pp. 41-67.
20. Malhotra, A. K. and Penzien, J., "Nondeterministic Analysis of Off-shore Structures," *Journal of the Engineering Mechanics Division, ASCE*, Vol. 96, No. EM6, Dec. 1970, pp. 985-1003.
21. Malhotra, A. K. and Penzien, J., "Response of Offshore Structures to Random Wave Forces," *Journal of the Structural Division, ASCE*, Vol. 96, No. ST10, Oct. 1970, pp. 2155-2173.
22. Salvadori, M. G., *Numerical Methods in Engineering*, Prentice-Hall, New York, 1952.
23. Timoshenko, S., *Vibration Problems in Engineering*, D. Van Nostrand, New York, 1937.
24. Grad, J. and Brebner, M. A., "Eigenvalues and Eigenvectors of a Real General Matrix," *Communications of the Association for Computing Machinery*, Vol. 11, No. 12, Dec. 1968, pp. 820-826.
25. Morrison, J. R., O'Brien, M. P., Johnson, J. W. and Schaaf, S. A., "The Force Exerted by Surface Waves on Piles," *Petroleum Transactions, American Institute of Mining, Metallurgical and Petroleum Engineers*, Vol. 189, 1950, pp. 149-154.



26. Eagleson, P. S. and Dean, R. G., "Small Amplitude Wave Theory," Estuary and Coastline Hydrodynamics, edited by A. T. Ippen, McGraw-Hill, 1966.
27. Lin, Y. K., Probabilistic Theory of Structural Dynamics, McGraw-Hill, New York, 1967.
28. Hannan, E. J., Time Series Analysis, Metheun and Co., Ltd., 1967.
29. Davenport, W. B., Jr. and Root, W. L., An Introduction to the Theory of Random Signals and Noise, McGraw-Hill, New York, 1958.
30. Blackman, R. B. and Tukey, J. W., The Measurement of Power Spectra, Dover Publications, Inc., New York, 1958.
31. Hurty, W. C. and Rubinstein, M. F., Dynamics of Structures, Prentice-Hall, Englewood Cliffs, N. J., 1965.
32. Crandall, S. H., "Mechanical Vibrations with Deterministic Excitation," Random Vibration, The M.I.T. Press, Cambridge, Mass., 1958.
33. Caughey, T. K., "Classical Normal Modes in Damped Linear Dynamic Systems," Journal of Applied Mechanics, Vol. 27, Series E, No. 2, June 1960, pp. 269-271.
34. Hart, G. C., "Stochastic Frame Response Using Modal Truncation," Journal of the Engineering Mechanics Division, ASCE, Vol. 96, No. EM5, Oct. 1970, pp. 565-575.
35. Neumann, G. and Pierson, W. J., Jr., Principles of Physical Oceanography, Prentice-Hall, Englewood Cliffs, N. J., 1966.
36. Kinsman, B., Wind Waves, Prentice-Hall, Englewood Cliffs, N. J., 1965.



Table 2.1

## COMPARISON OF MARINE RISER NATURAL FREQUENCIES

$G_L = \frac{wL^3}{EI}$	$\lambda_1$		$\lambda_2$		$\lambda_3$	
	Series Solution	Finite Difference Solution	Series Solution	Finite Difference Solution	Series Solution	Finite Difference Solution
0	3.1416	3.1403	6.2832	6.2731	9.4248	9.3908
200	5.4652	5.4638	8.4625	8.4526	11.3031	11.2713
400	6.3076	6.3061	9.5456	9.5347	12.4565	12.4233
600	6.8804	6.8789	10.3113	10.2994	13.3145	13.2796
800	7.3261	7.3245	10.9171	10.9044	14.0089	13.9722
1000	7.6957	7.6942	11.4243	11.4110	14.5980	14.5597

$$G_T = \frac{T_L}{wL} = 1.0$$

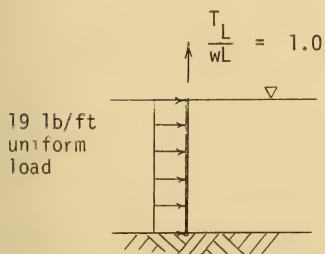
$$\omega = \frac{\lambda^2}{L^2} \sqrt{\frac{EI}{m}}$$

Finite difference solution uses 31 equally spaced nodes.



Table 2.2

## COMPARISON OF SERIES AND FINITE DIFFERENCE SOLUTIONS

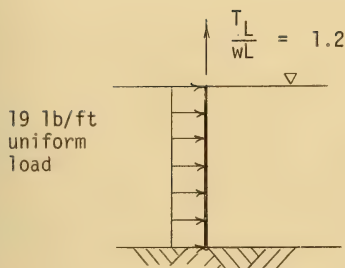


Method of Solution	Number of Nodes	Maximum Moment (ft-k)	Top Rotation (radians)	Bottom Rotation (radians)
Series	--	165.7	-.0498	.1073
Finite Difference (equal node spacing)	5	156.6	-.0484	.09505
	8	153.6	-.0493	.1030
	11	161.3	-.0496	.1058
	17	162.0	-.0499	.1078
Finite Difference (unequal node spacing)	11	173.71	-.051	.1134
	17	167.7	-.0507	.1116





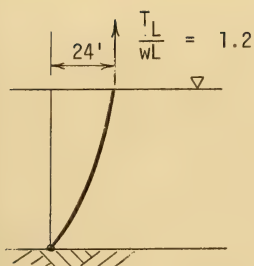
Table 2.2 Continued



Method of Solution	Number of Nodes	Maximum Moment (ft-k)	Top Rotation (radians)	Bottom Rotation (radians)
Series	--	94.7	-.0375	.0682
Finite Difference (equal node spacing)	5	88.9	-.0357	.0595
	11	92.3	-.0370	.0660
	17	93.0	-.0372	.0673
Finite Difference (unequal node spacing)	11	96.7	-.0375	.0690
	17	94.9	-.0376	.0689



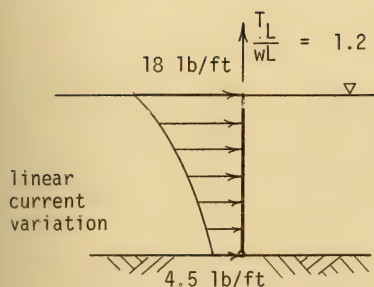
Table 2.2 Continued



Method of Solution	Number of Nodes	Maximum Moment (ft-k)	Top Rotation (radians)	Bottom Rotation (radians)
Series	--	49.6	.0204	.0756
Finite Difference (equal node spacing)	5	46.4	.0214	.0710
	11	48.2	.0207	.0745
	17	48.5	.0206	.0751
Finite Difference (unequal node spacing)	11	50.6	.0204	.0761
	17	49.8	.0204	.0761



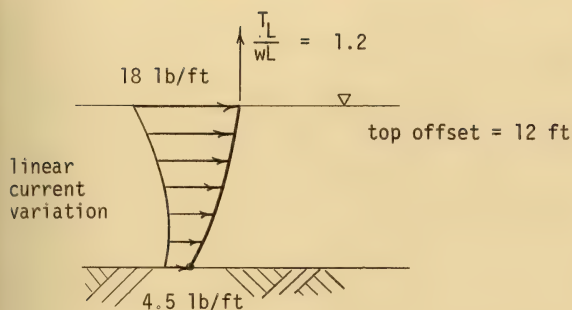
Table 2.2 Continued



Method of Solution	Number of Nodes	Maximum Moment (ft-k)	Top Rotation (radians)	Bottom Rotation (radians)
Series	--	37.5	-.0229	.0312
Finite Difference (equal node spacing)	5	35.1	-.0211	.0276
	11	36.4	-.0223	.0300
	17	36.8	-.0226	.0305
Finite Difference (unequal node spacing)	11	38.4	-.0227	.0312
	17	37.9	-.0228	.0311



Table 2.2 Continued



Method of Solution	Number of Nodes	Maximum Moment (ft-k)	Top Rotation (radians)	Bottom Rotation (radians)
Series	--	62.25	-.0127	.069
Finite Difference (equal node spacing)	5	58.3	-.0104	.0631
	11	60.5	-.0120	.0673
	17	60.9	-.0123	.0681
Finite Difference (unequal node spacing)	11	63.7	-.0125	.0692
	17	62.6	-.0126	.0692





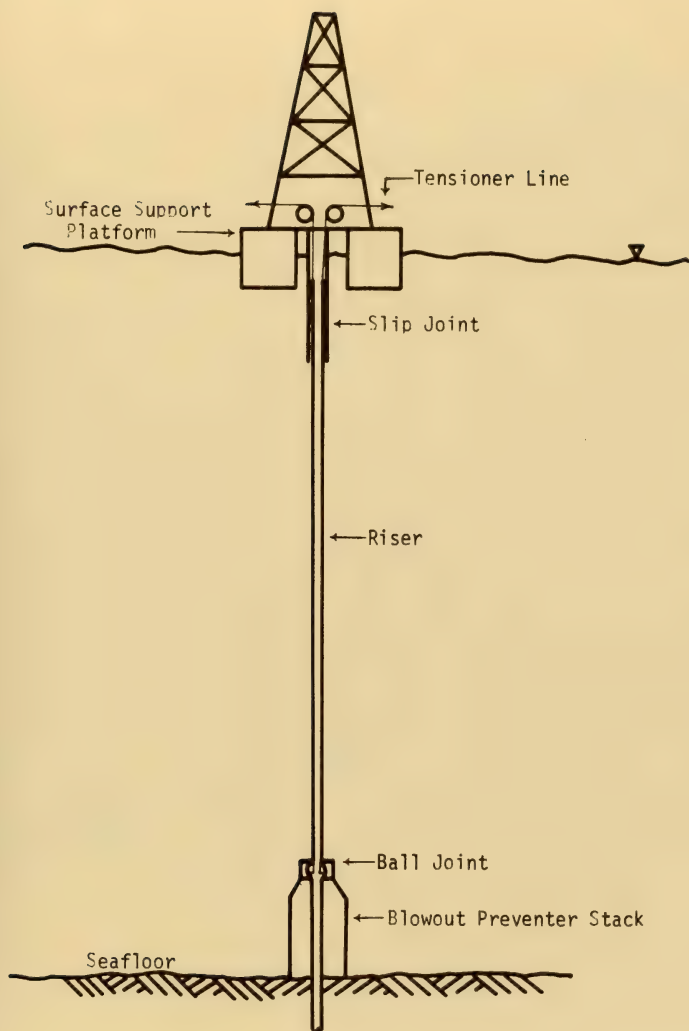


Fig. 1.1 Typical Marine Riser Installation



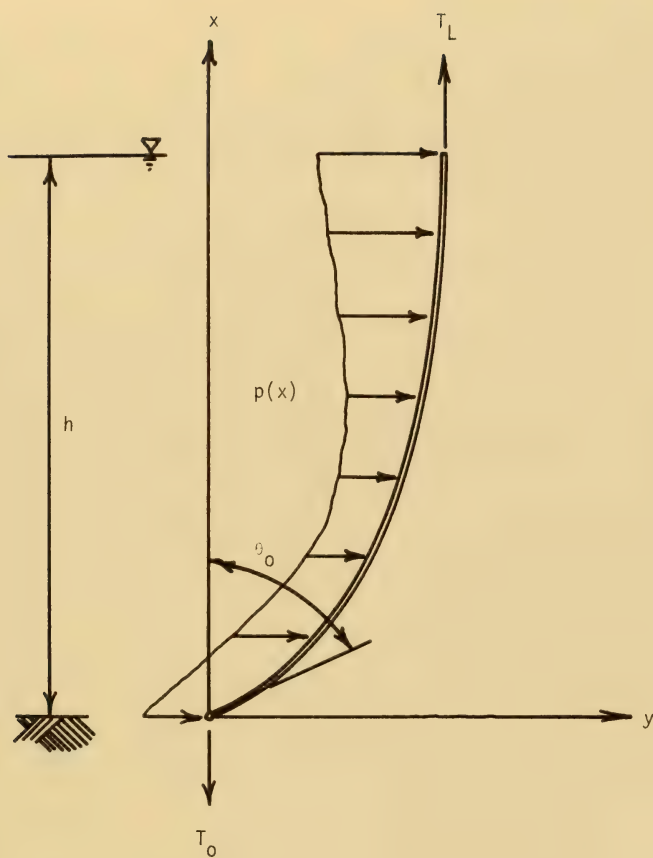


Fig. 1.2 Free Body Diagram of Deflected Riser



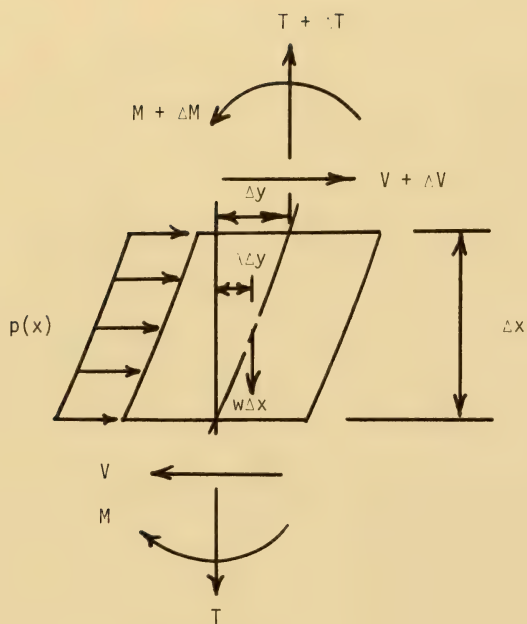


Fig. 1.3 Forces on Element of Riser Length



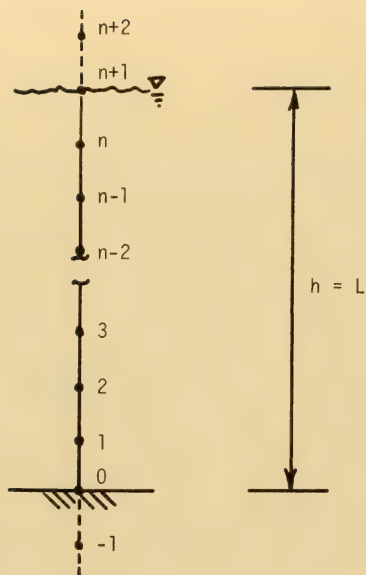


Fig. 2.1 Node Numbering Scheme

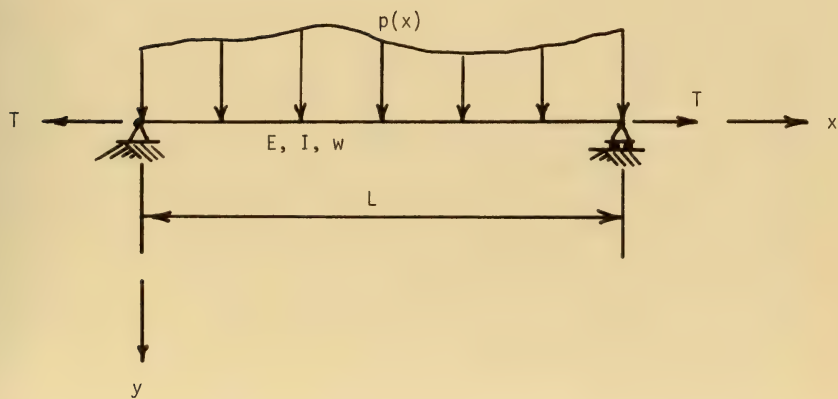


Fig. 2.2 Definition Sketch of Constant Tension Beam





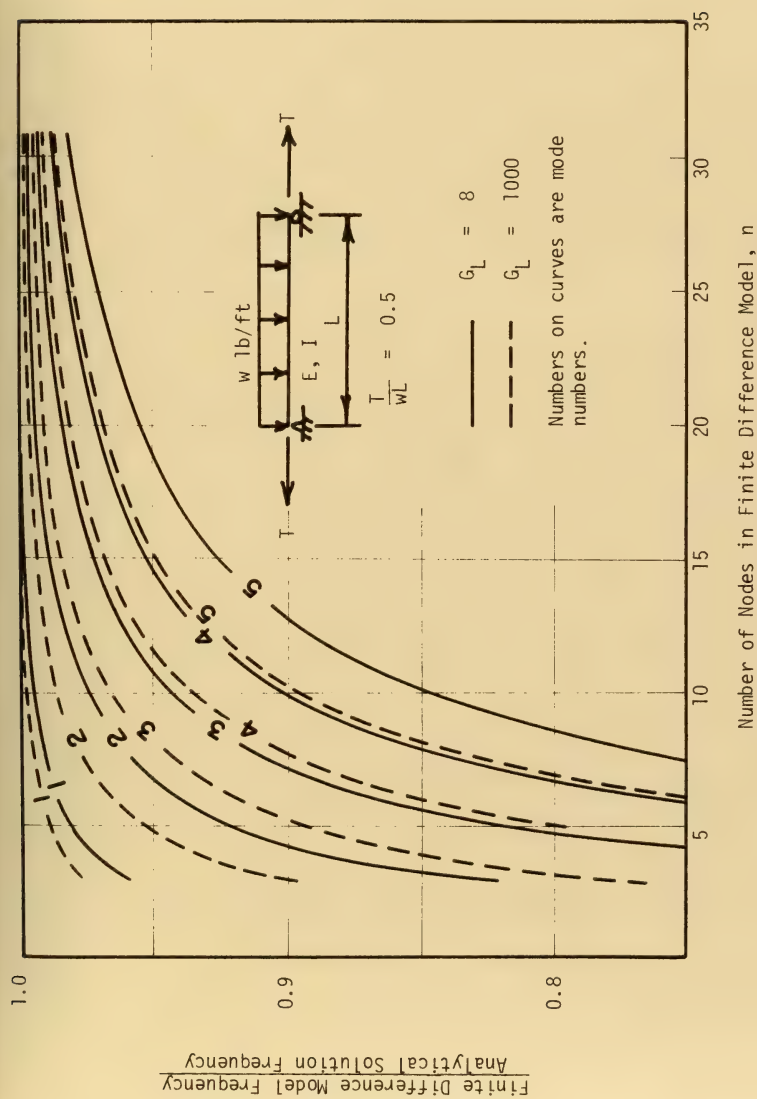


Fig. 2.3 Frequency Ratios for Finite Difference Model of Constant Tension Beam



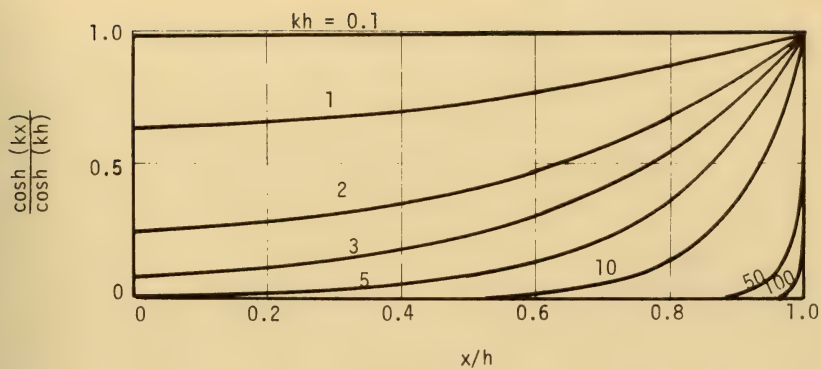


Fig. 2.4 Spatial Variation of Inertia Force

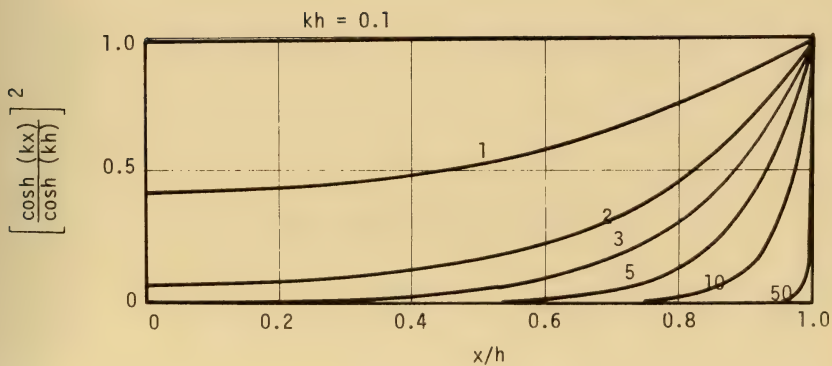


Fig. 2.5 Spatial Variation of Drag Force



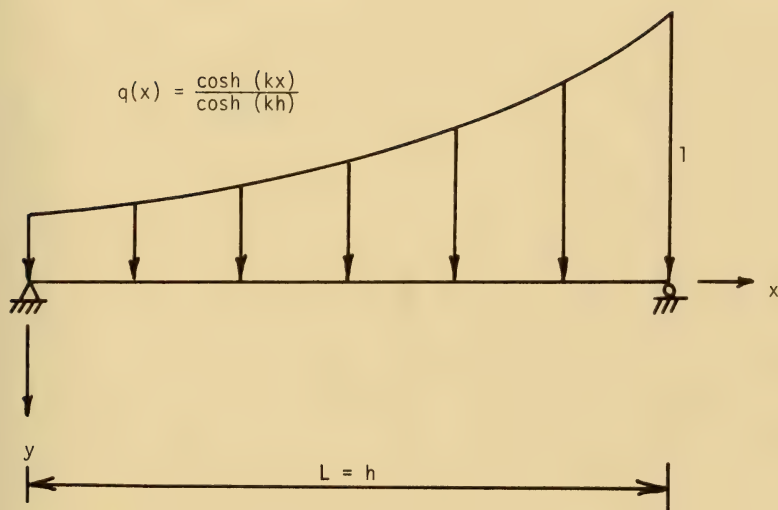


Fig. 2.6 Definition Sketch of Simple Beam Subjected to Inertia Force



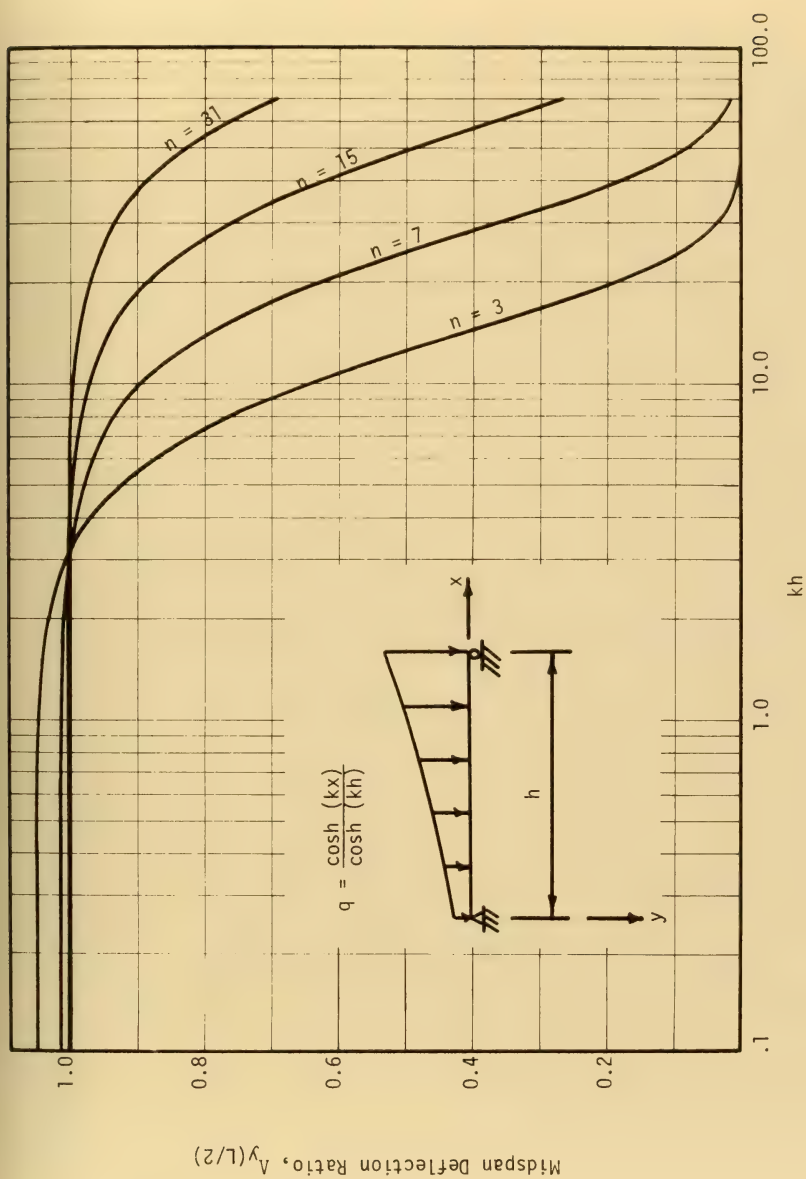


Fig. 2.7 Midspan Deflection Ratios for Simple Beam





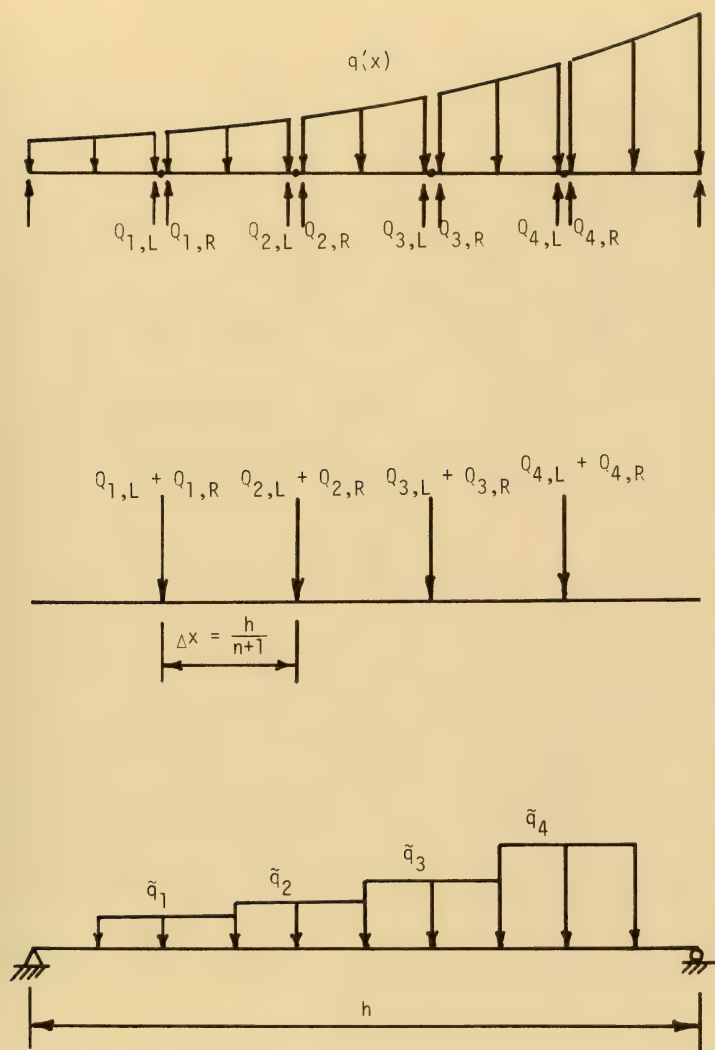


Fig. 2.8 Schematic Representation of Lumped-Smeared Force Model



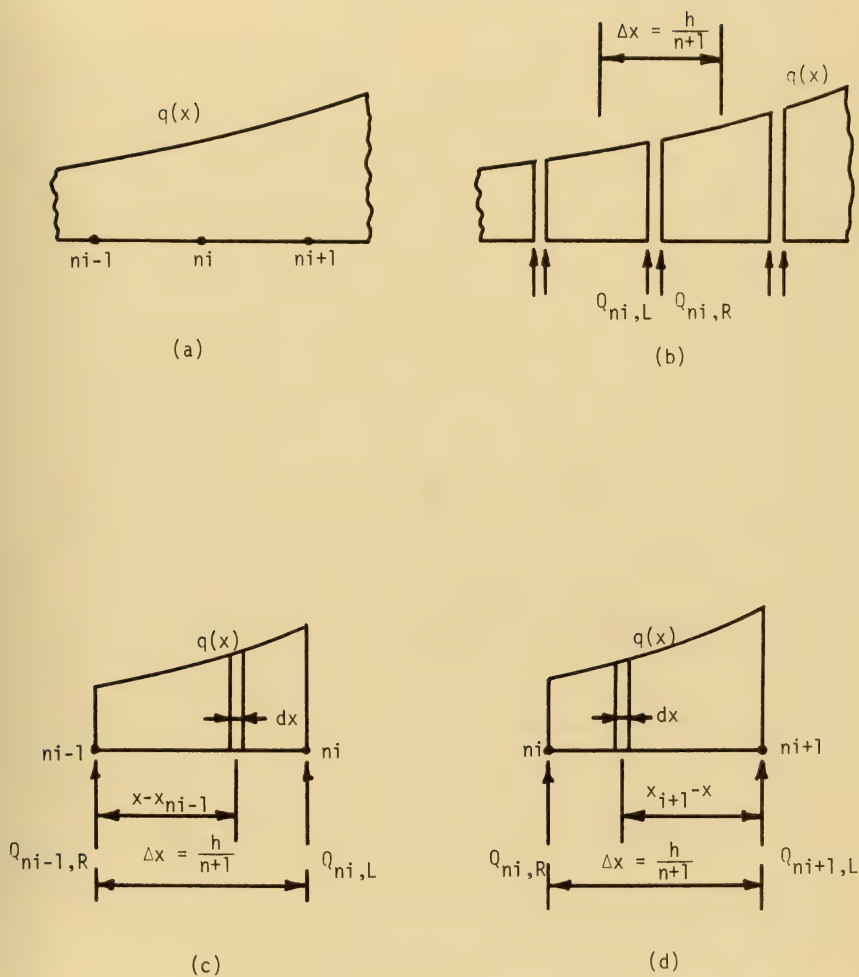


Fig. 2.9 Sketches Used in Derivation of Lumped-Smeared Force Model



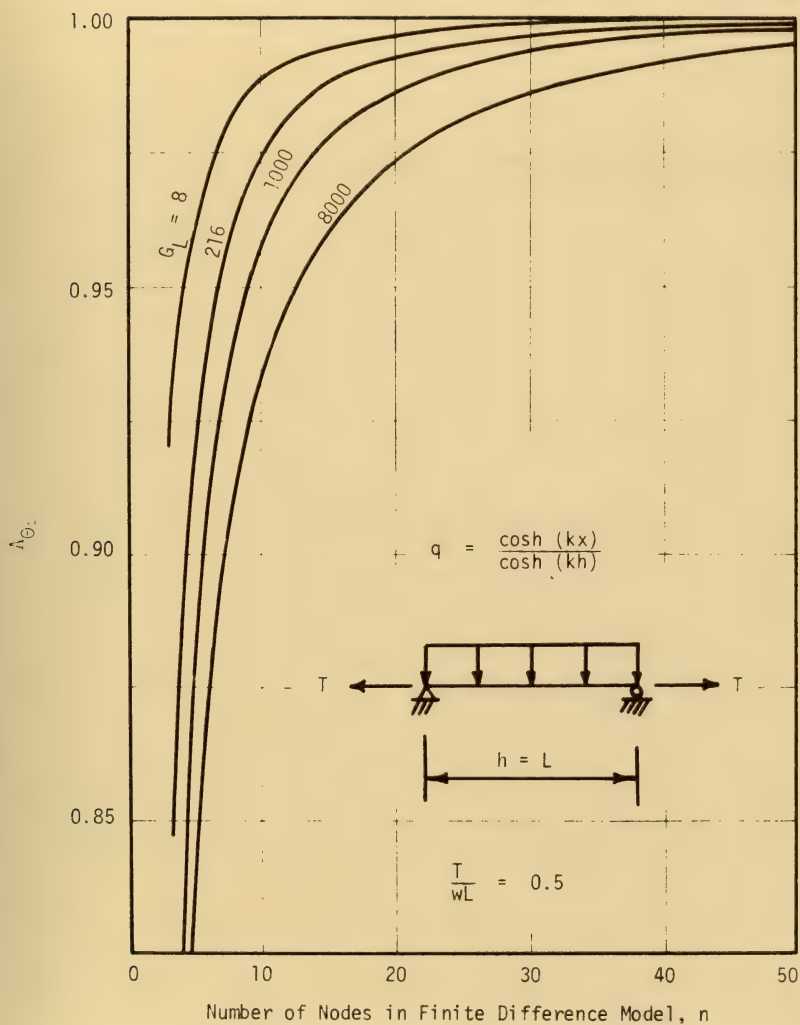


Fig. 2.10a End Rotation Ratios, Inertia Force,  $kh = .01$



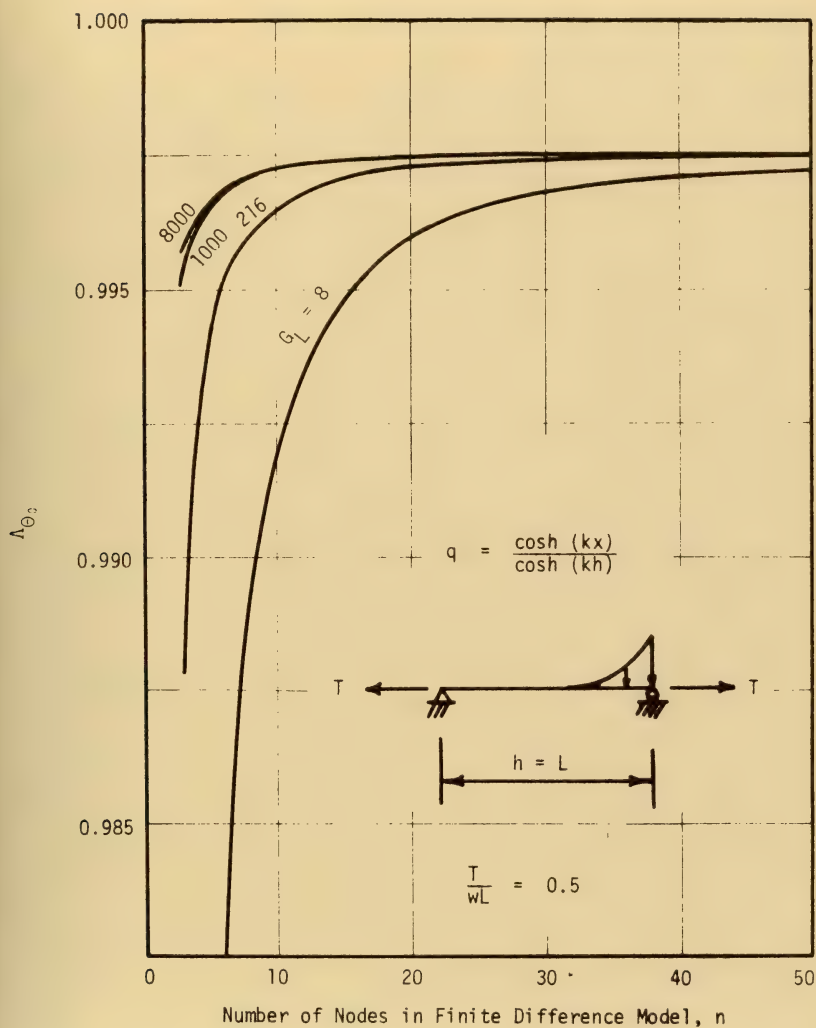
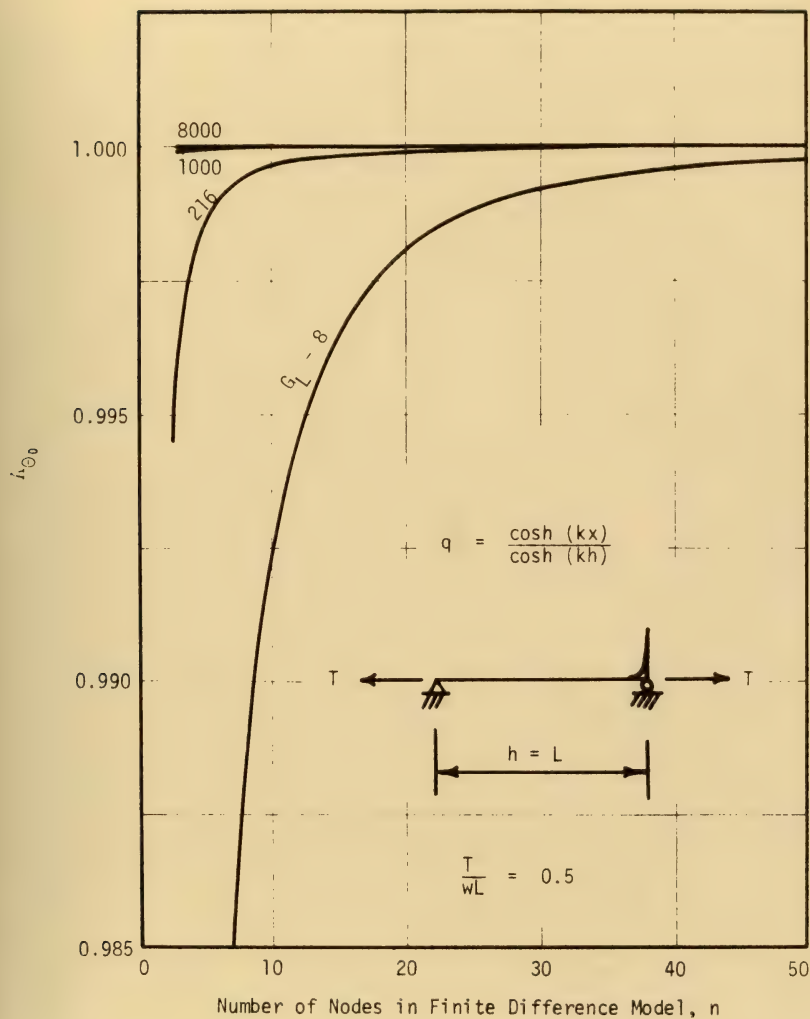


Fig. 2.10b End Rotation Ratios, Inertia Force,  $kh = 10$





Fig. 2.10c End Rotation Ratios, Inertia Force,  $kh = 100$



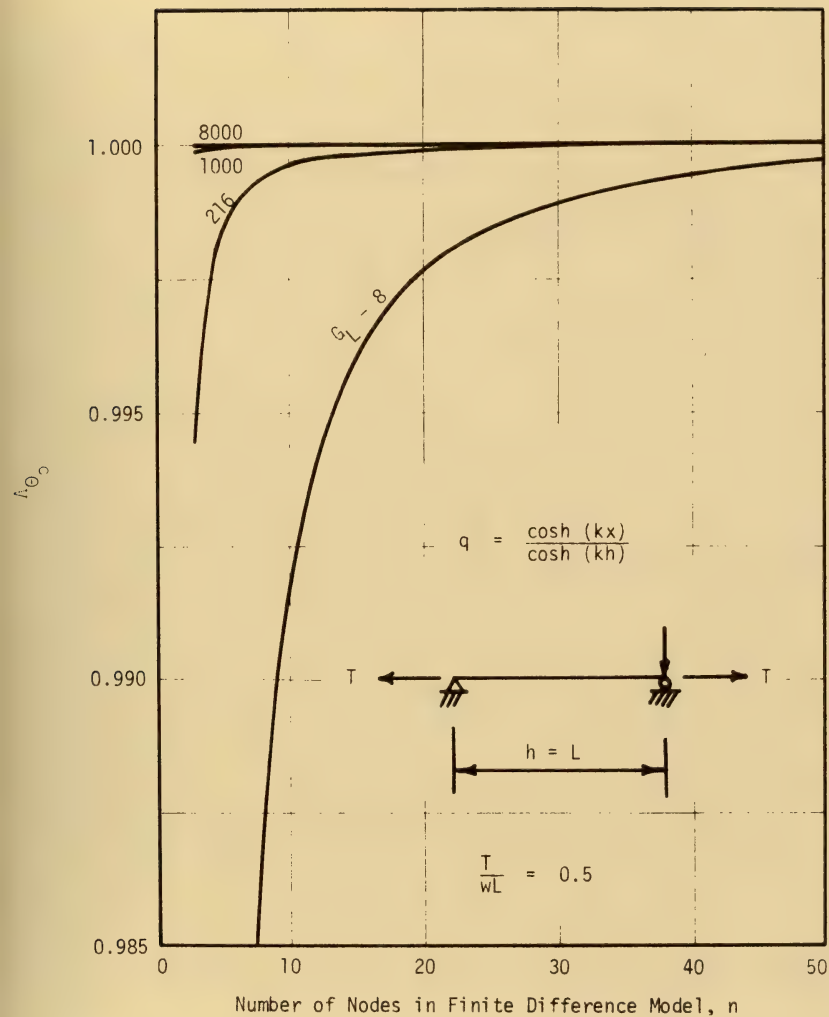


Fig. 2.10d End Rotation Ratios, Inertia Force,  $kh = 10^5$



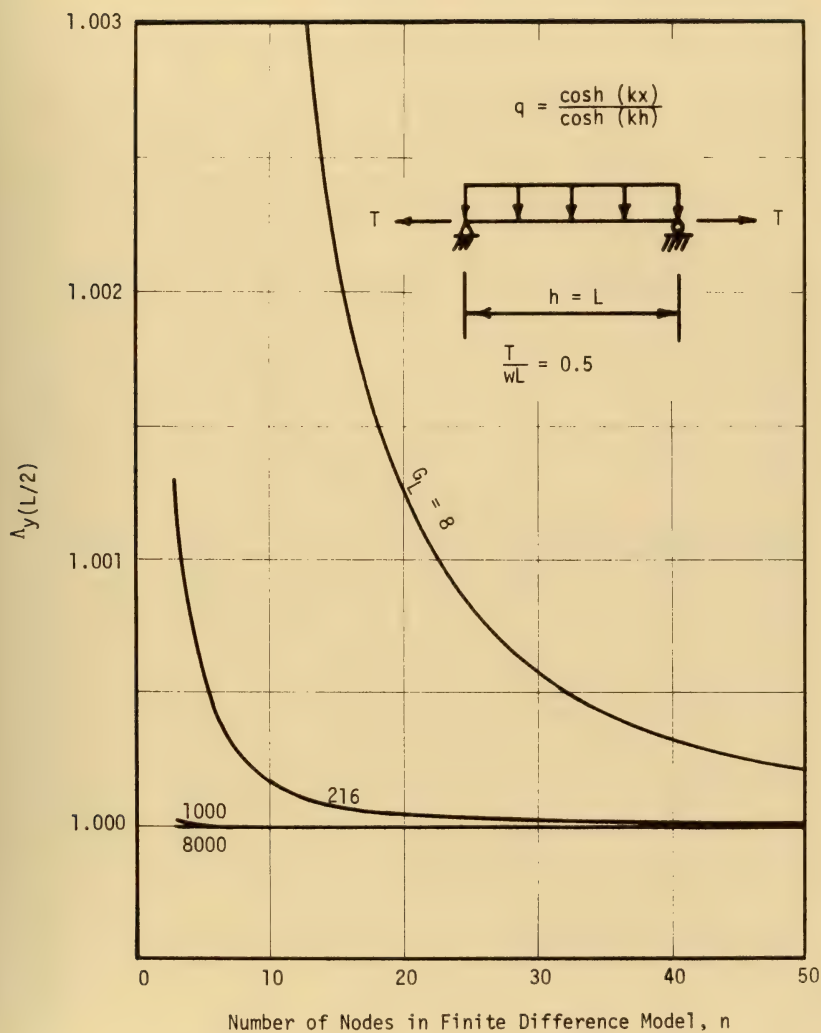


Fig. 2.11a Midspan Deflection Ratios, Inertia Force,  $kh = .01$



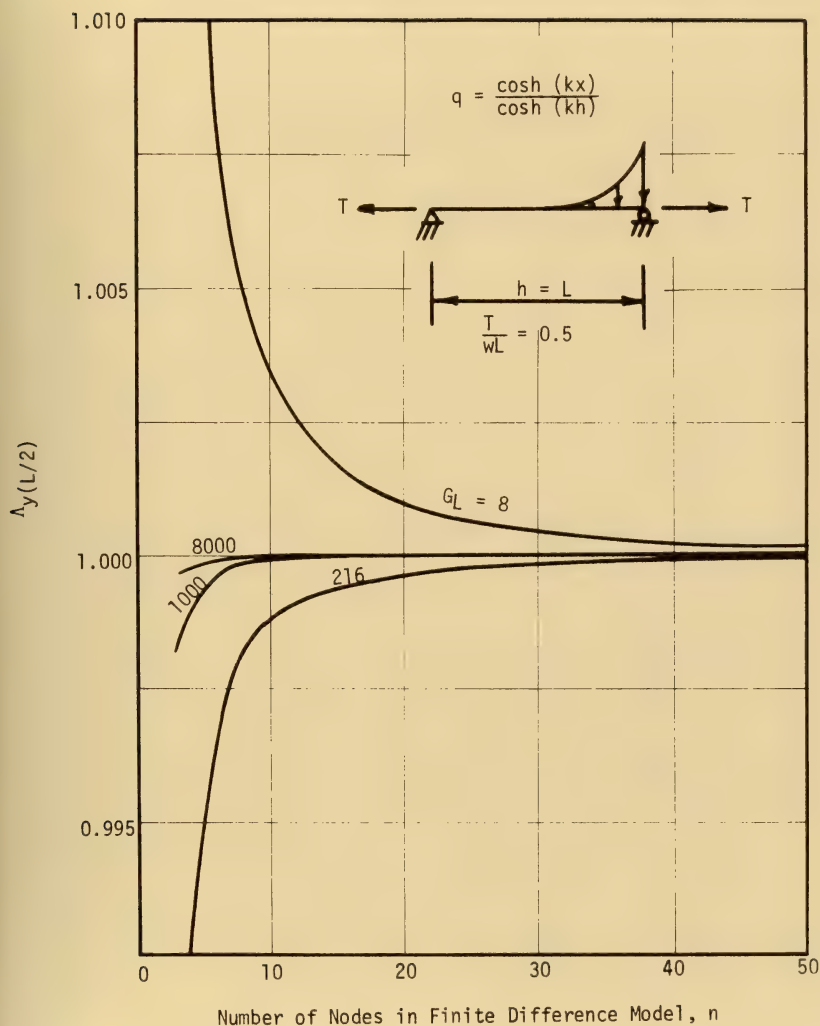


Fig. 2.11b Midspan Deflection Ratios, Inertia Force,  $kh = 10$





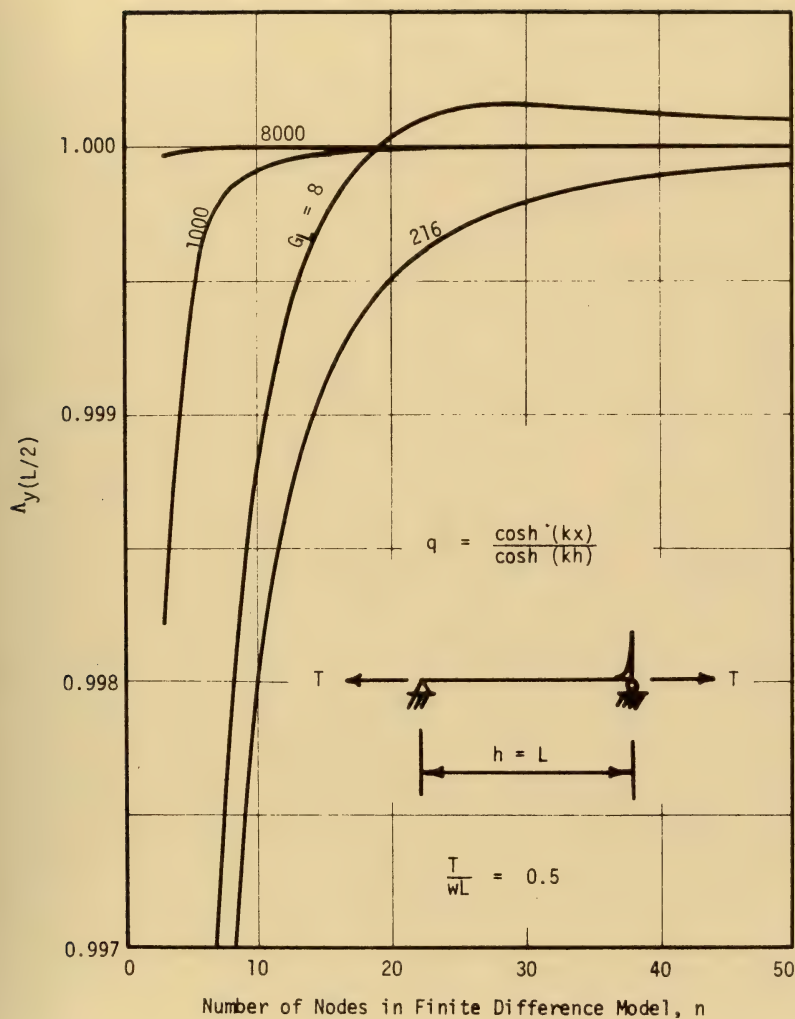


Fig. 2.11c Midspan Deflection Ratios, Inertia Force,  $kh = 100$



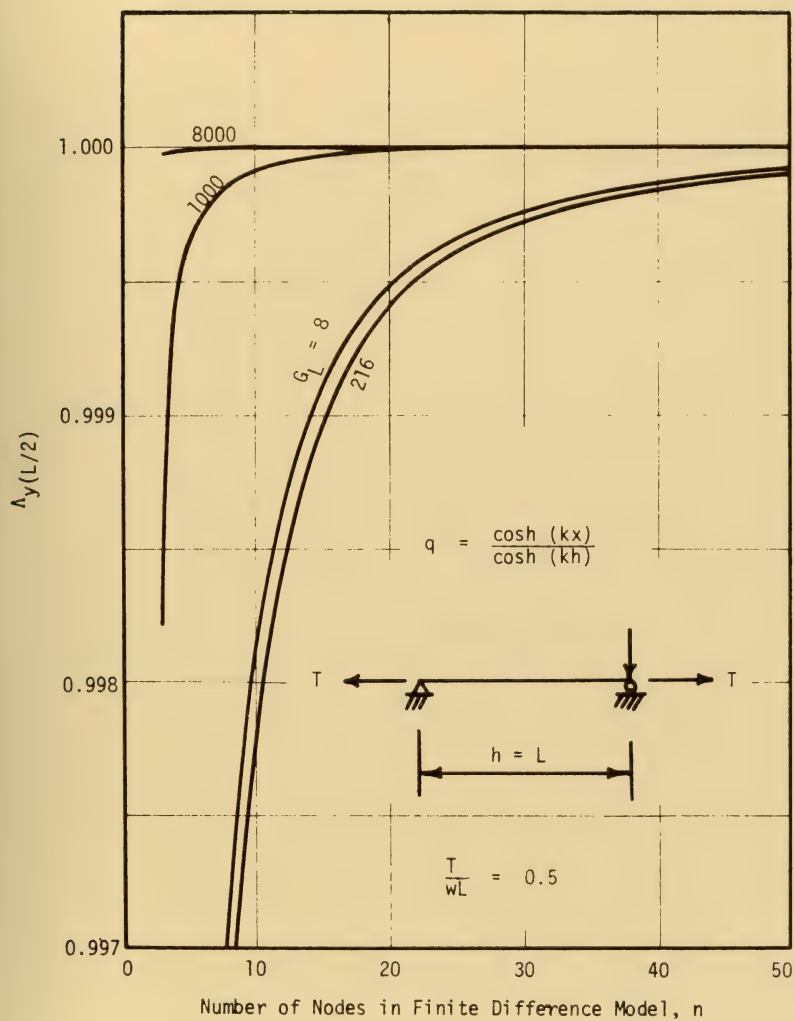


Fig. 2.11d Midspan Deflection Ratios, Inertia Force,  $kh = 10^5$



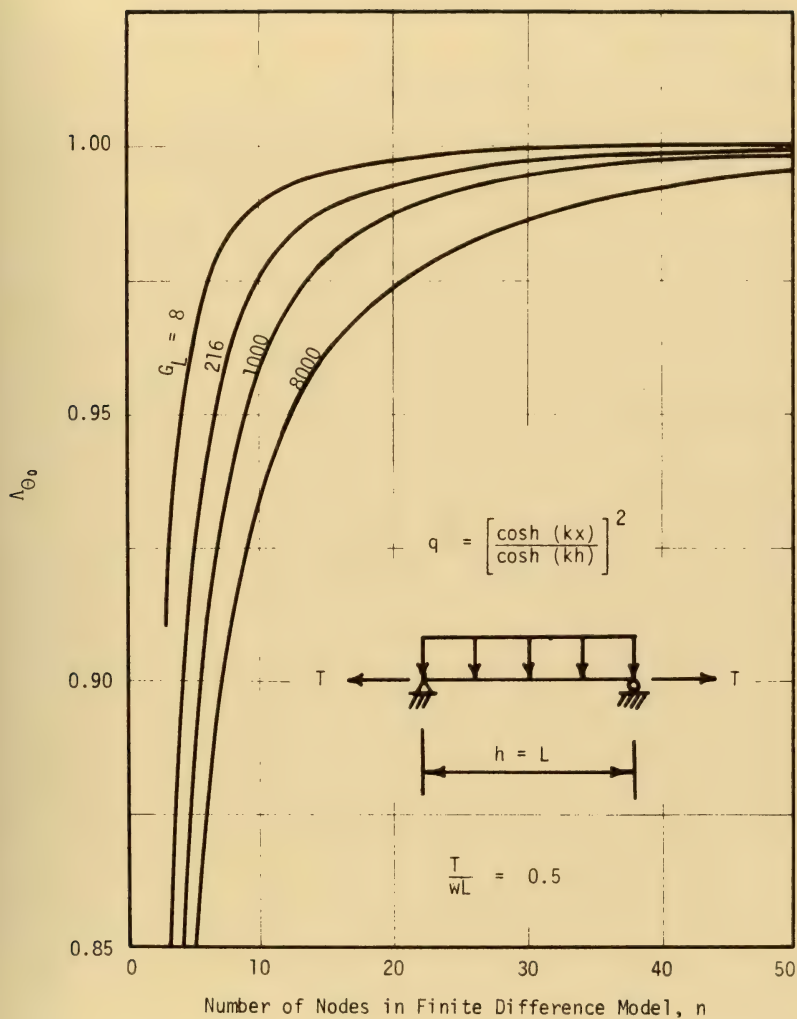


Fig. 2.12a End Rotation Ratios, Drag Force,  $kh = .01$



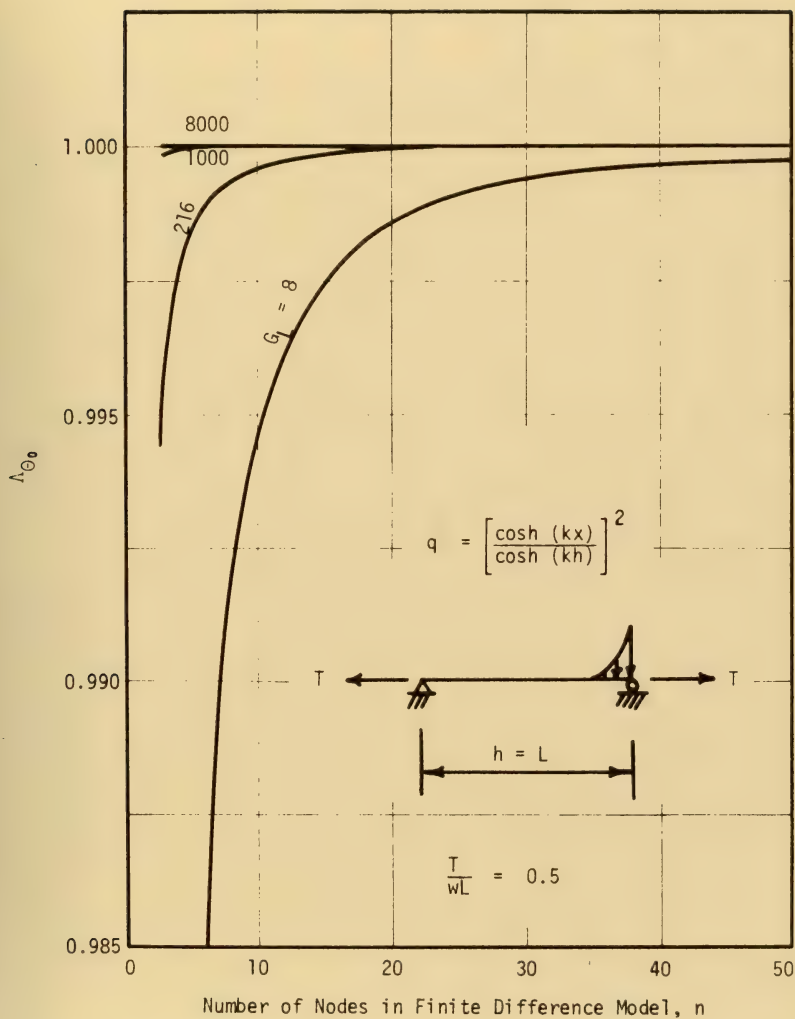
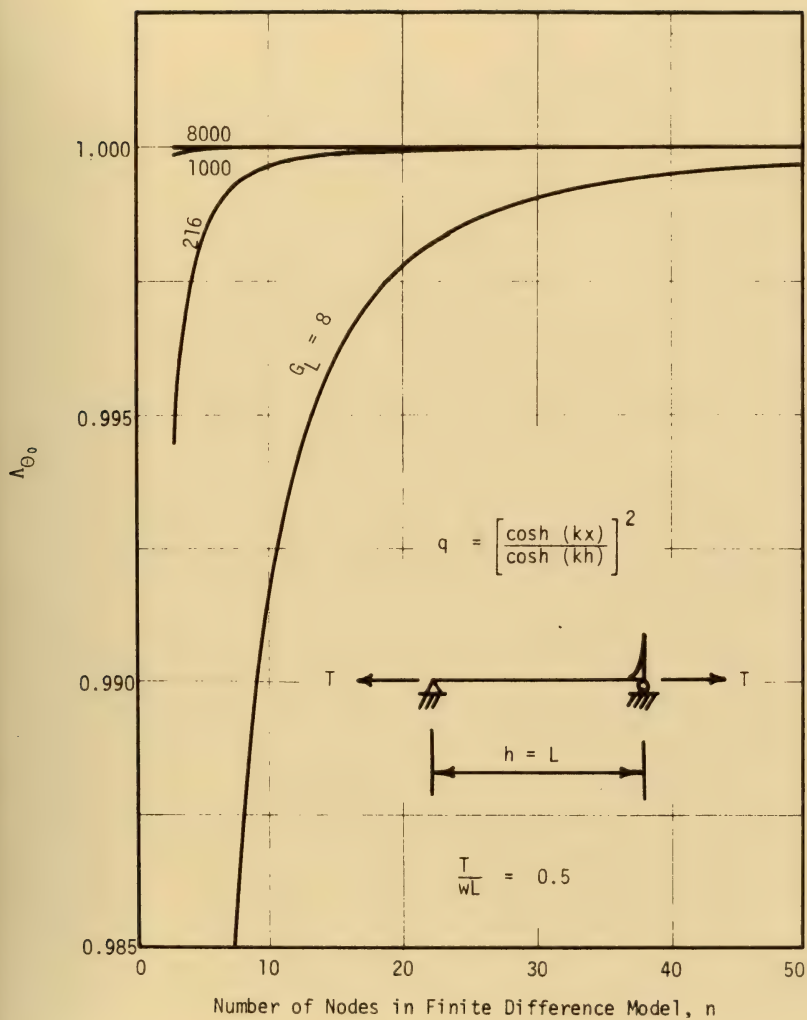


Fig. 2.12b End Rotation Ratios, Drag Force,  $kh = 10$





Fig. 2.12c End Rotation Ratios, Drag Force,  $kh = 100$



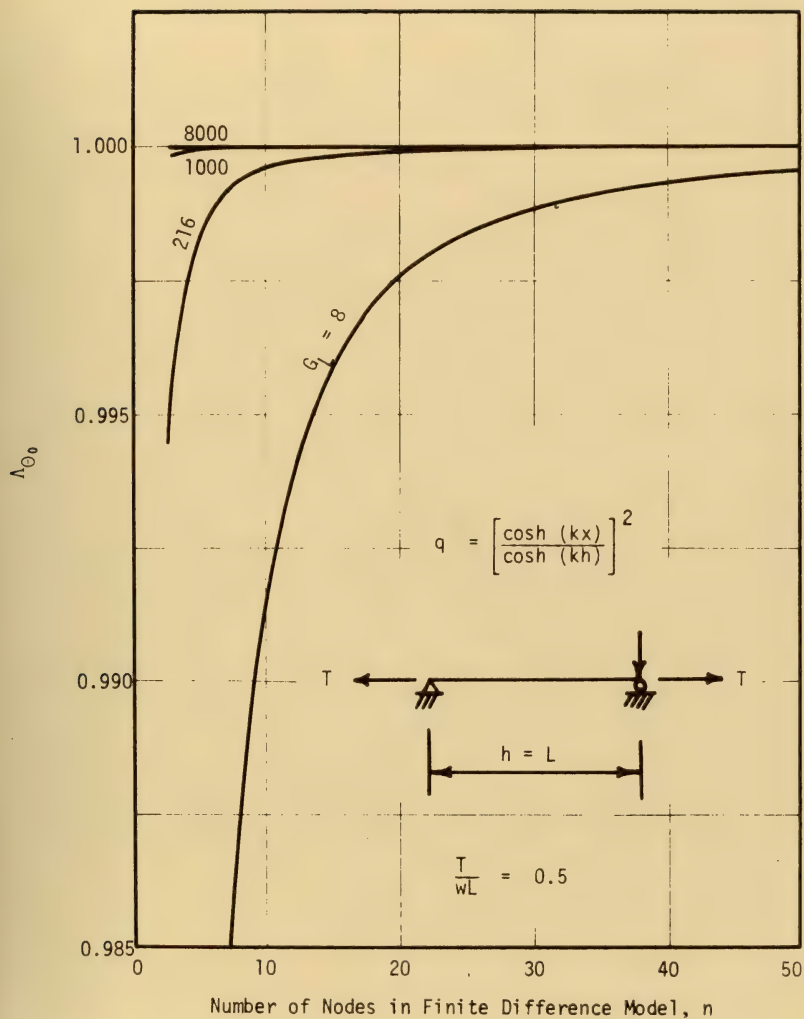


Fig. 2.12d End Rotation Ratios, Drag Force,  $kh = 10^5$



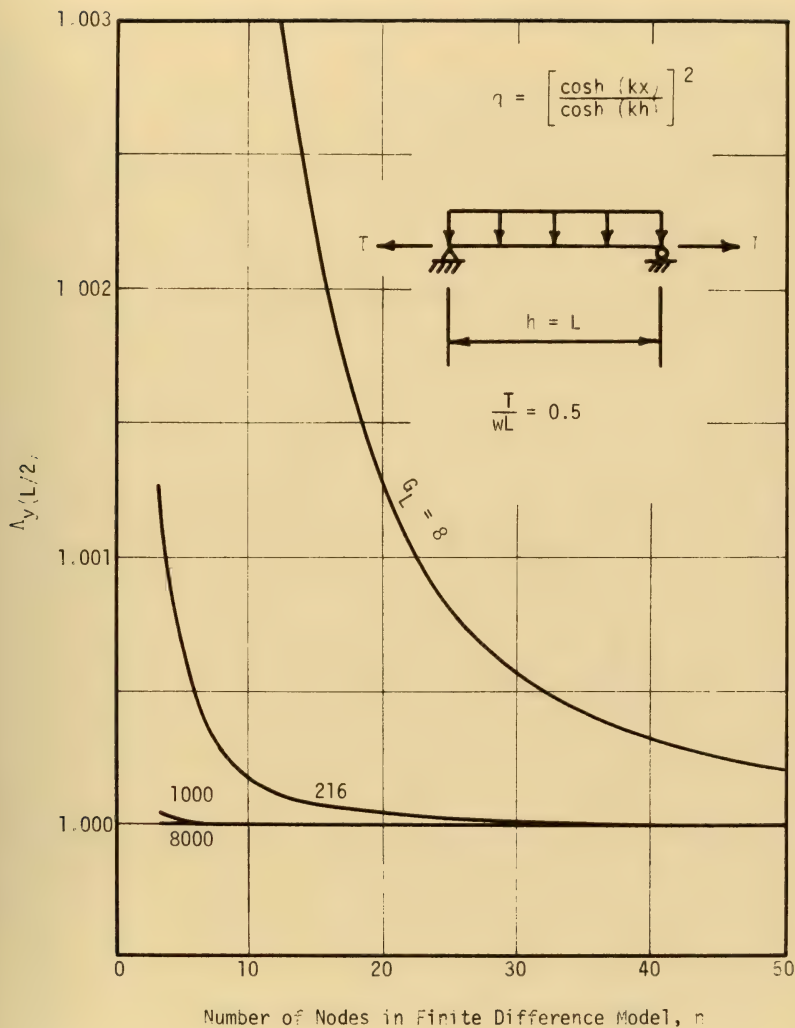


Fig. 2.13a Midspan Deflection Ratios, Drag Force,  $kh = .01$



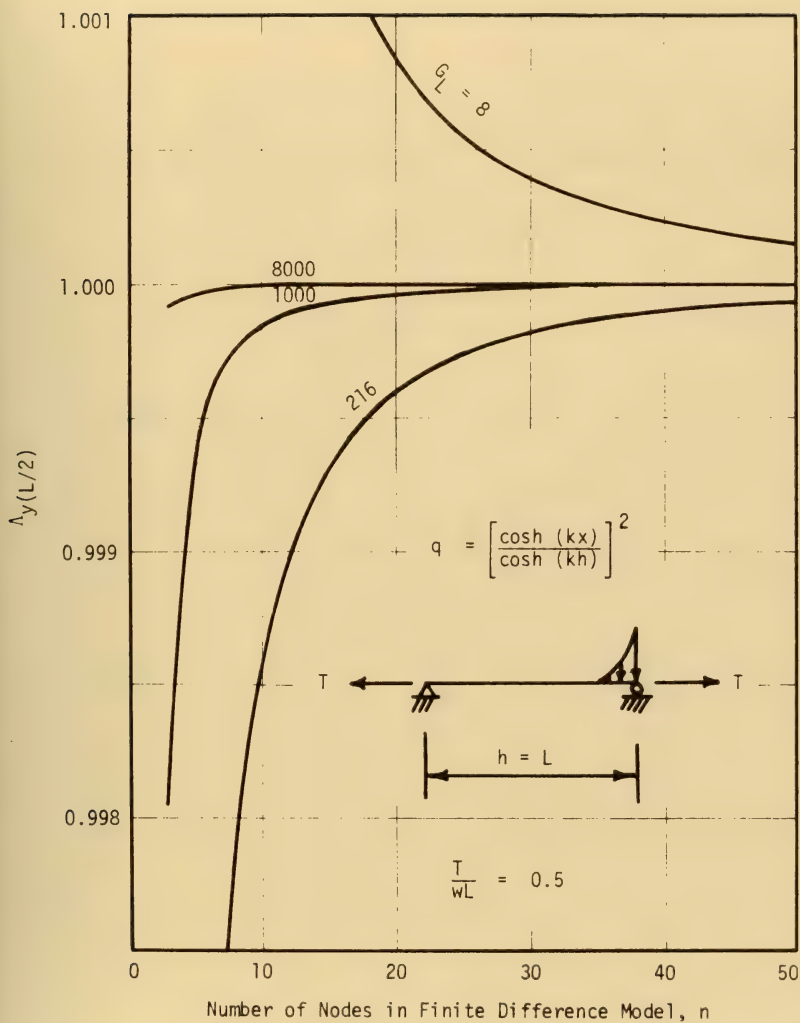


Fig. 2.13b Midspan Deflection Ratios, Drag Force,  $kh = 10$





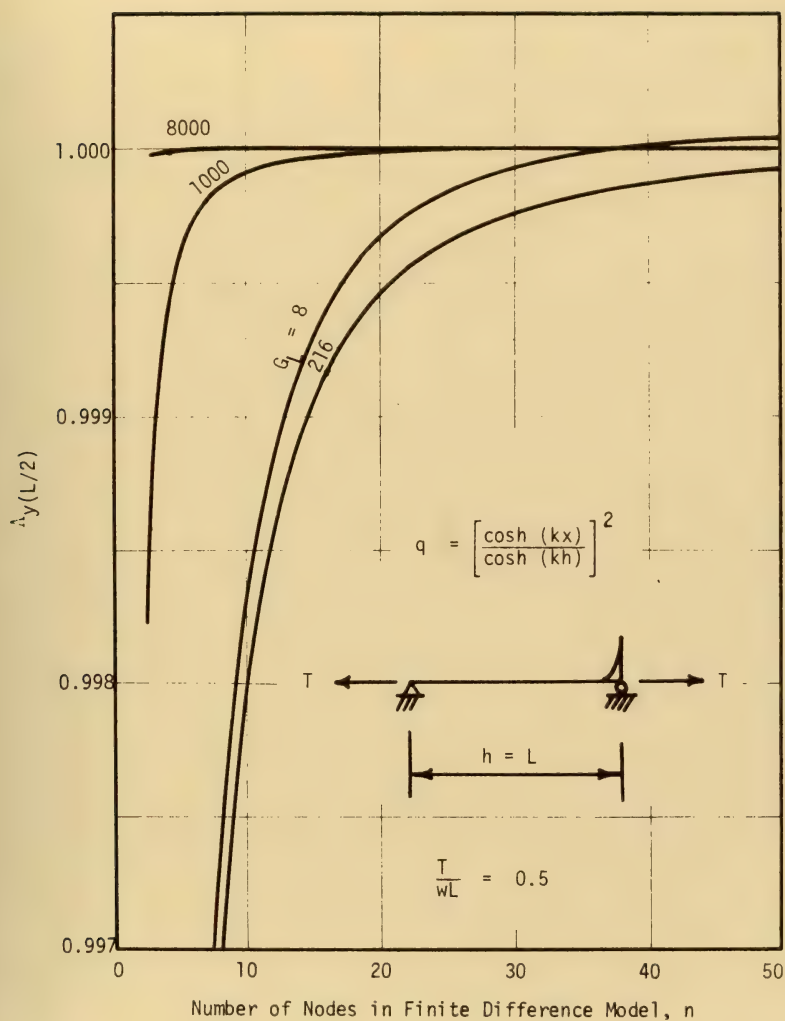


Fig. 2.13c Midspan Deflection Ratios, Drag Force,  $kh = 100$



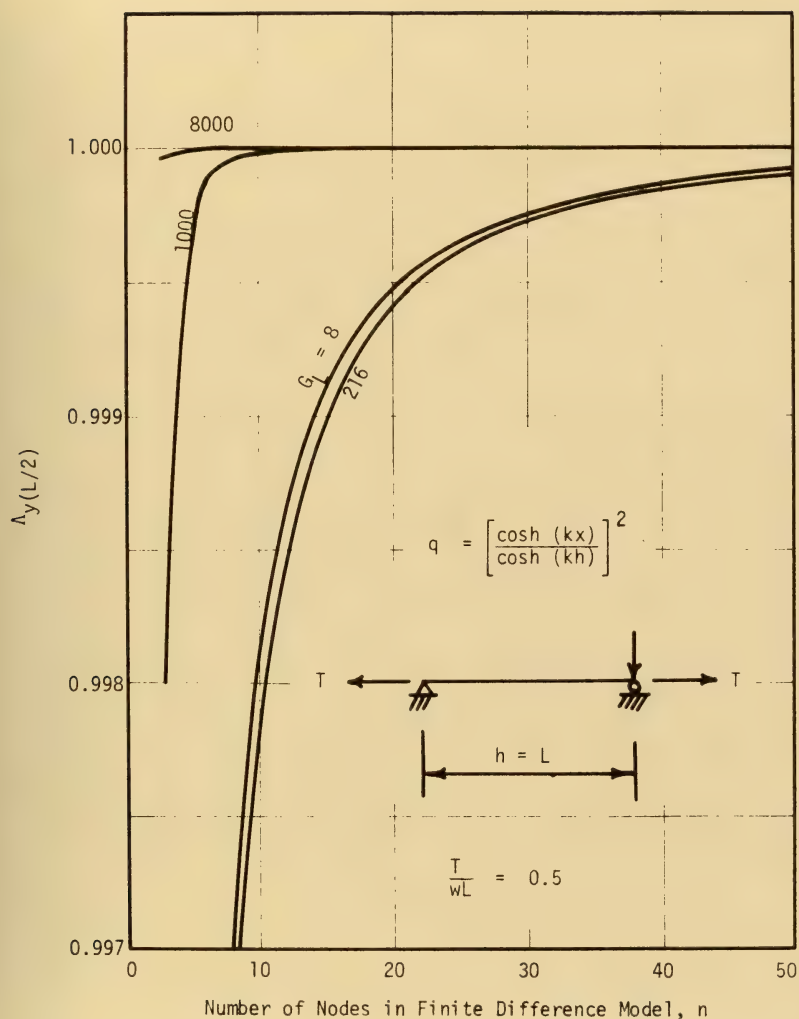


Fig. 2.13d Midspan Deflection Ratios, Drag Force,  $kh = 10^5$



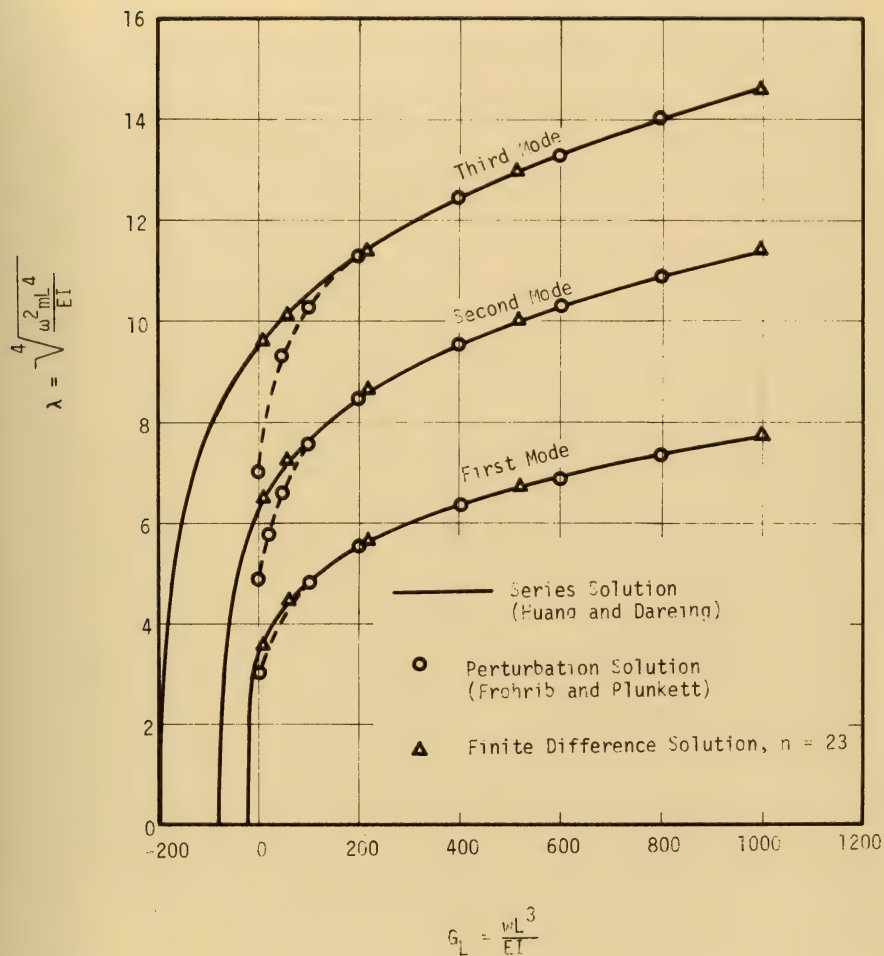


Fig. 2.14 Natural Frequencies of Vertical Marine Riser,  $G_T = 1.0$



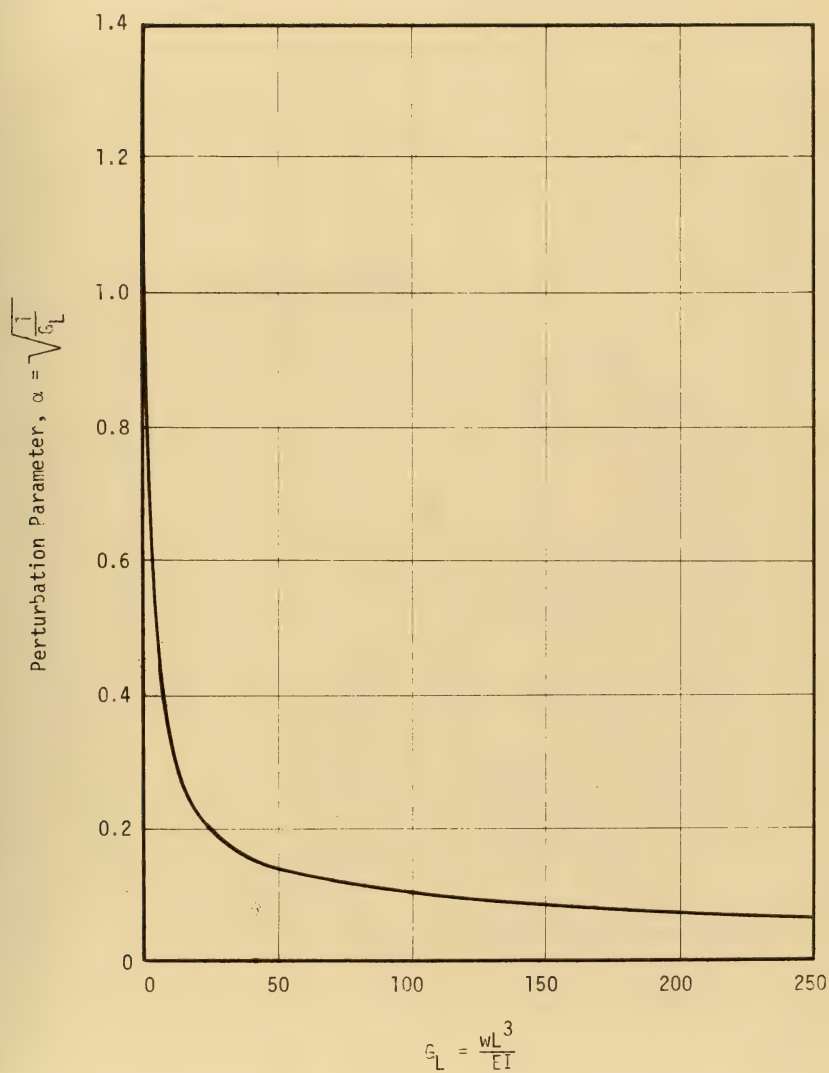


Fig. 2.15 Perturbation Parameter





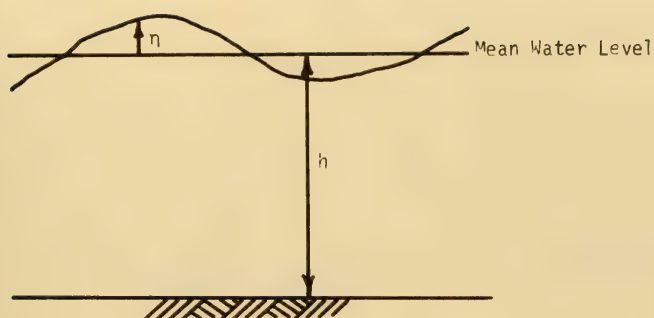


Fig. 3.1 Definition Sketch of Sea Surface Elevation

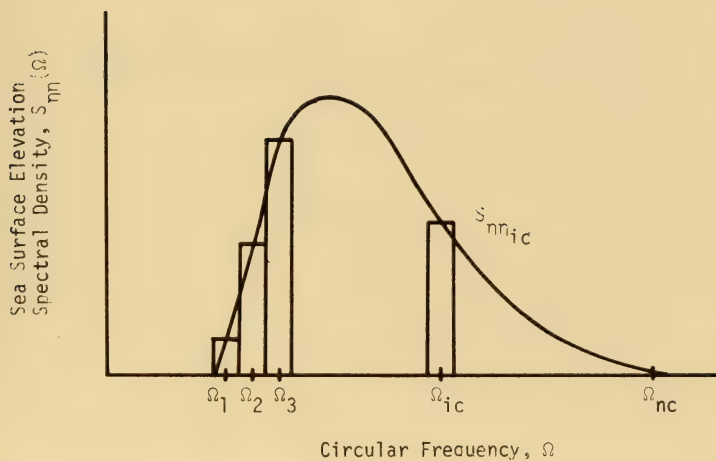


Fig. 3.2 Typical Sea Surface Elevation Spectrum



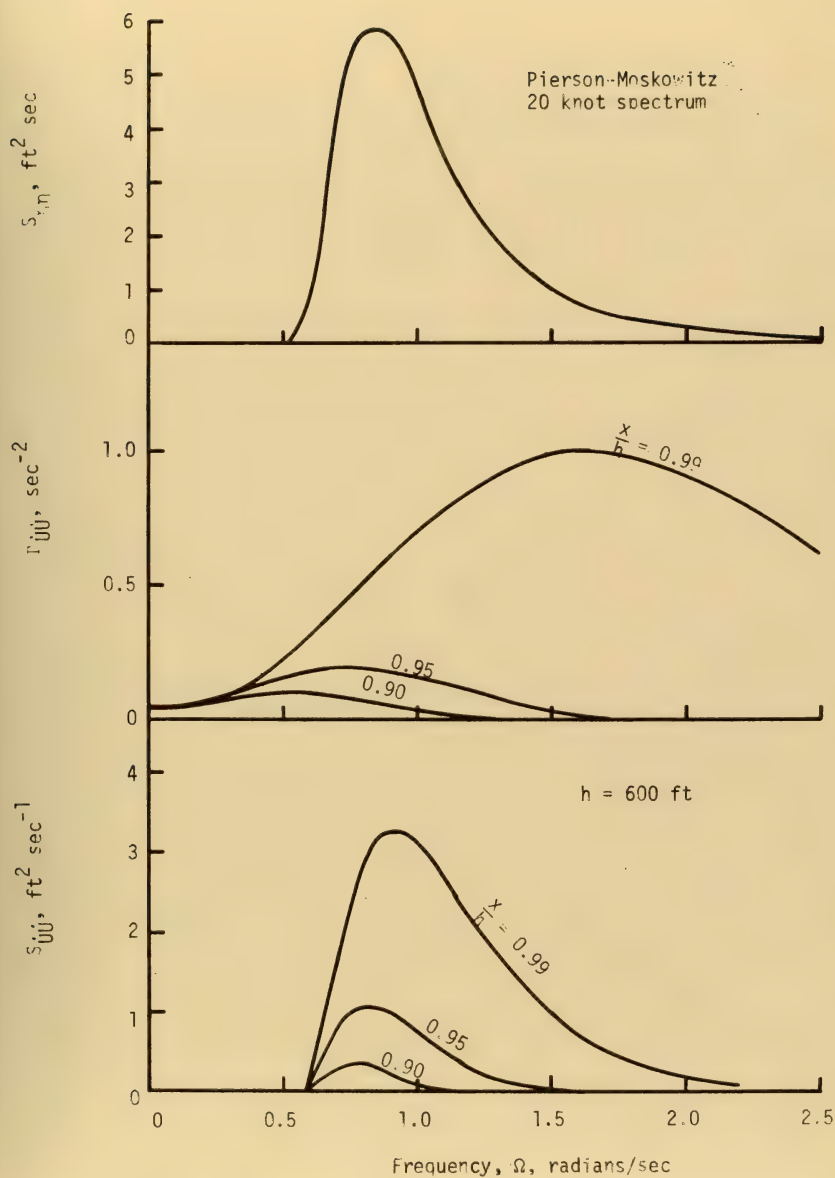


Fig. 3.3 Water Velocity Spectra



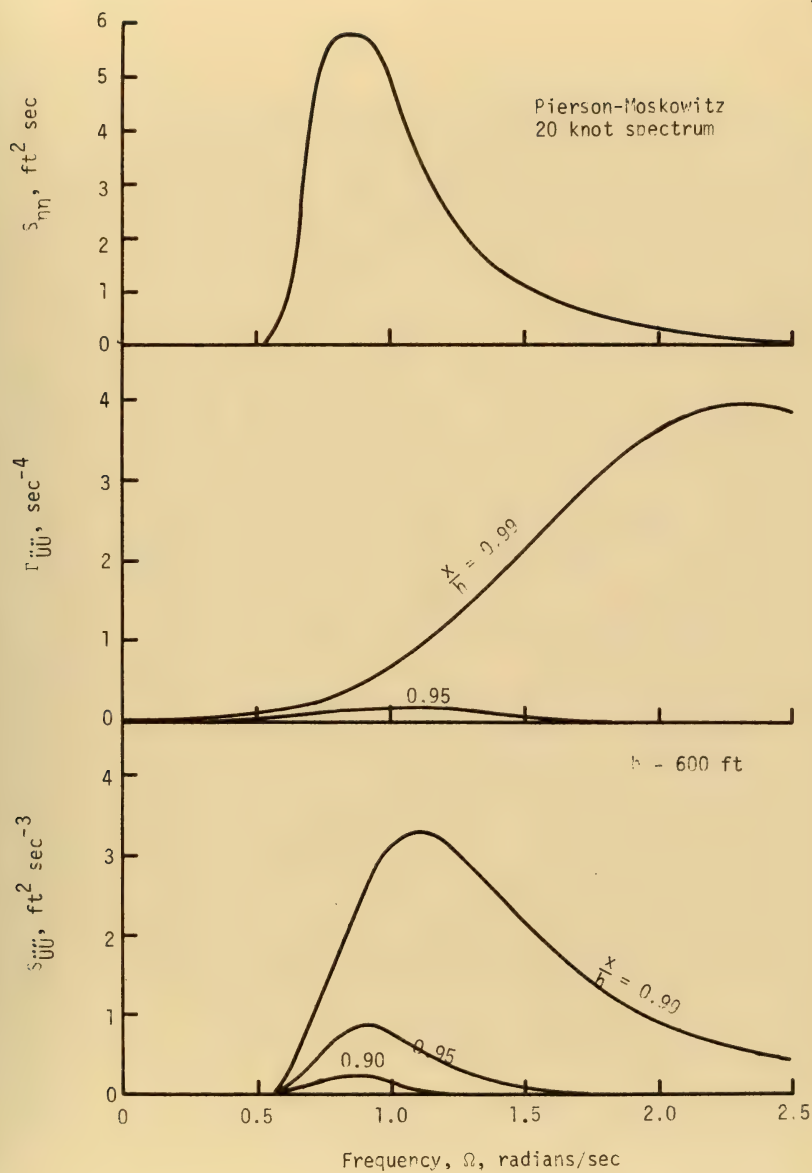


Fig. 3.4 Water Acceleration Spectra



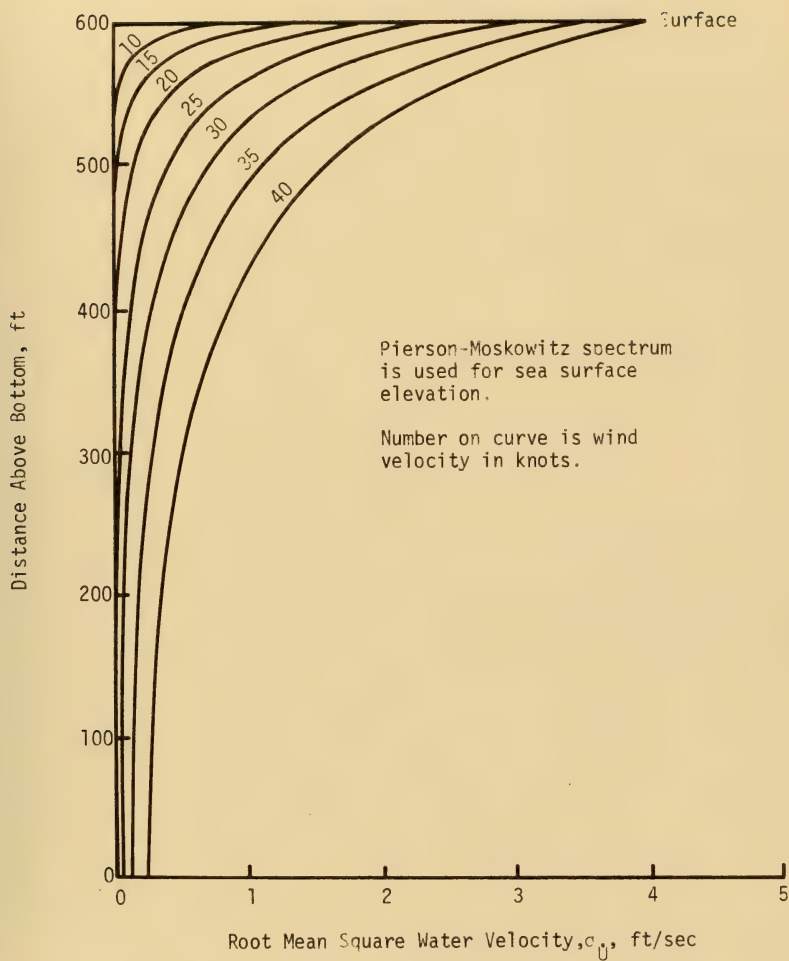


Fig. 3.5 Root Mean Square Water Velocity Profiles





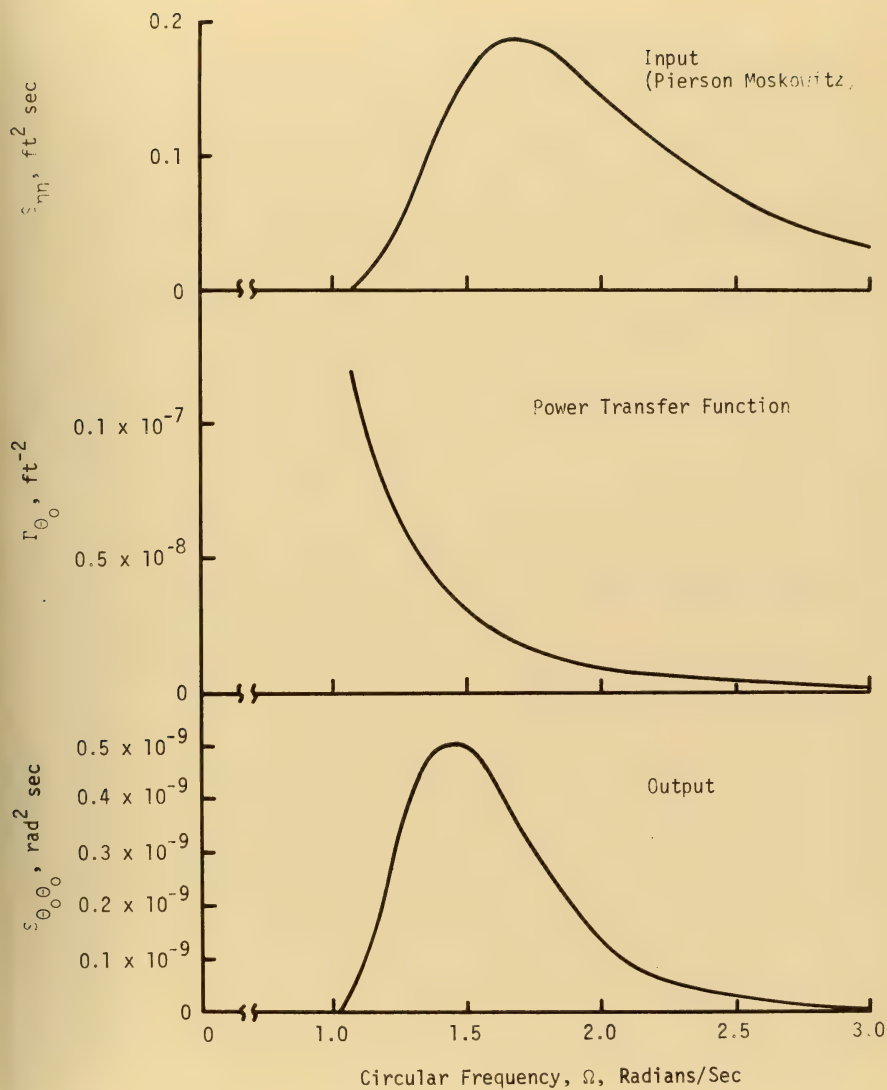


Fig. 3.6a Static Bottom Rotation Spectrum for Ten Knot Wind Velocity



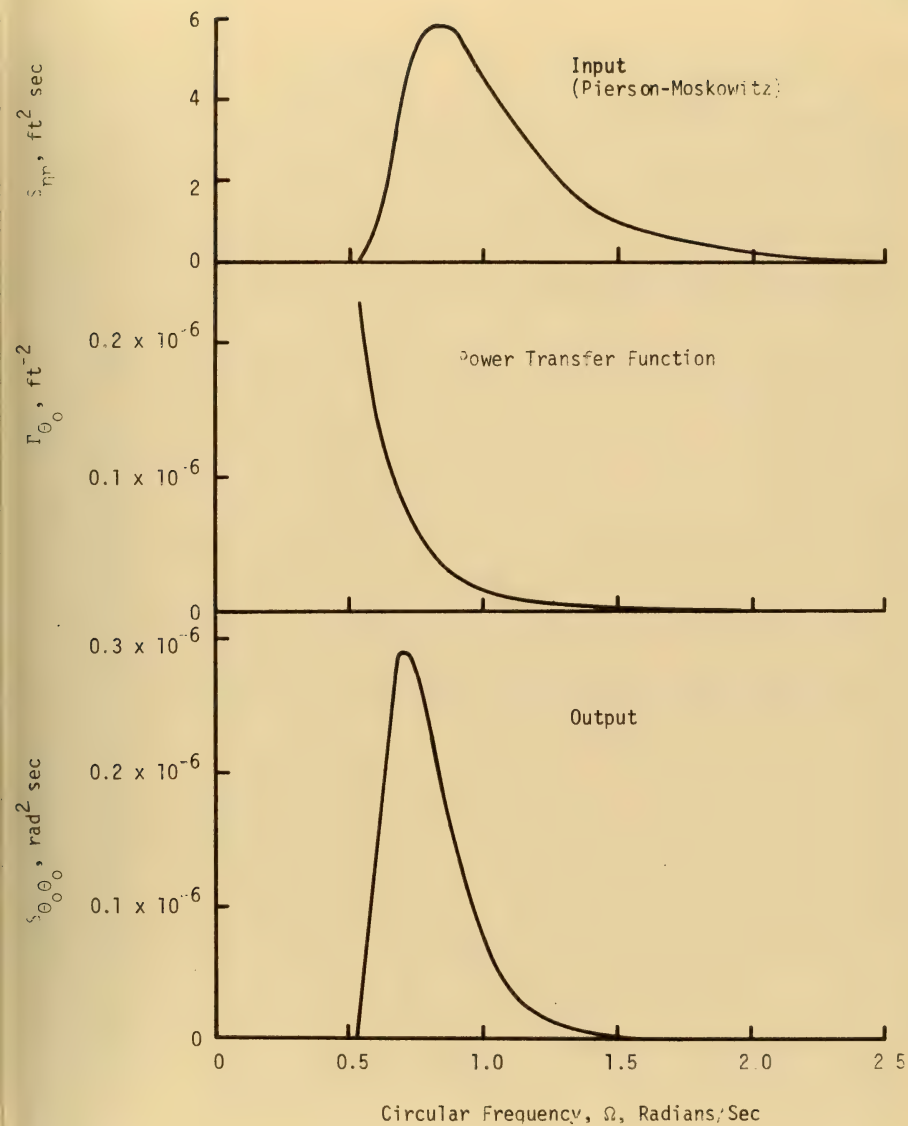


Fig. 3.6b Static Bottom Rotation Spectrum for Twenty Knot Wind Velocity



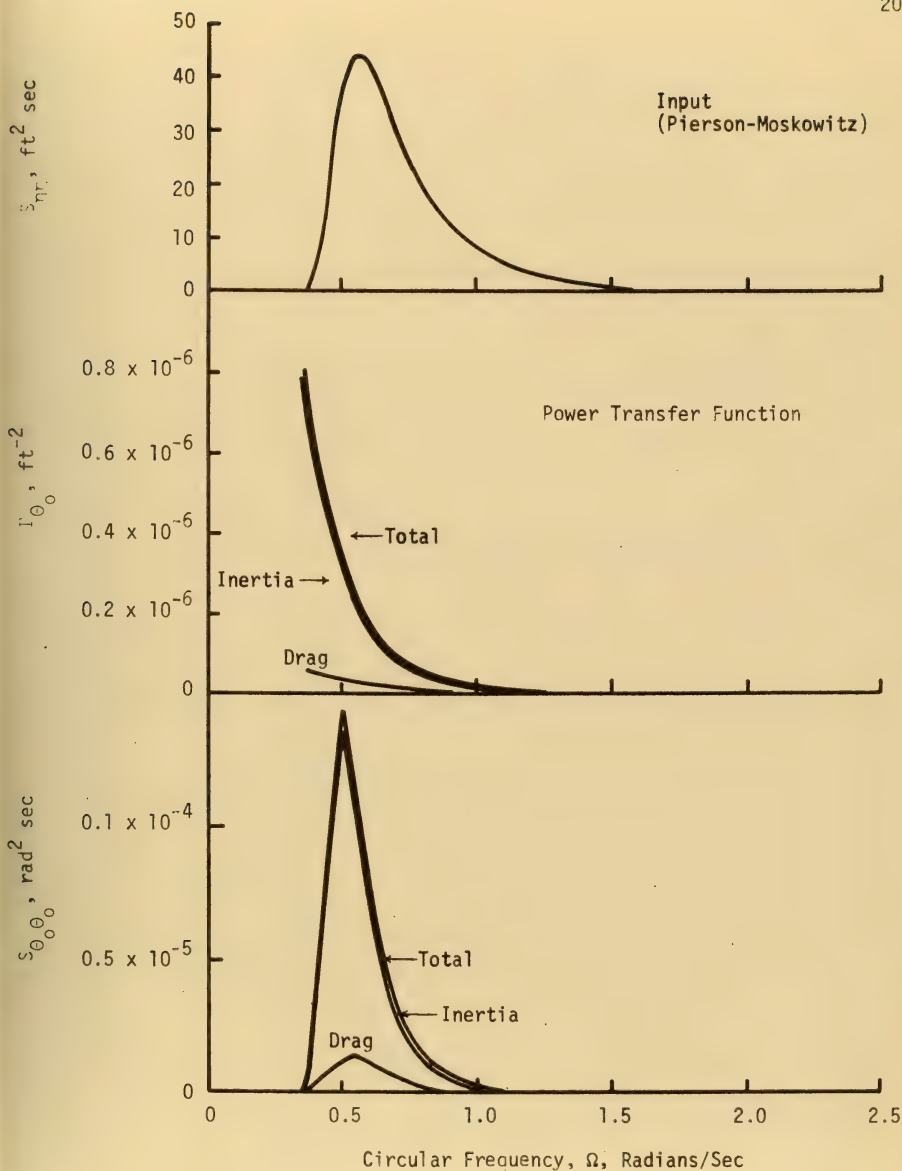


Fig. 3.6c Static Bottom Rotation Spectrum  
for Thirty Knot Wind Velocity



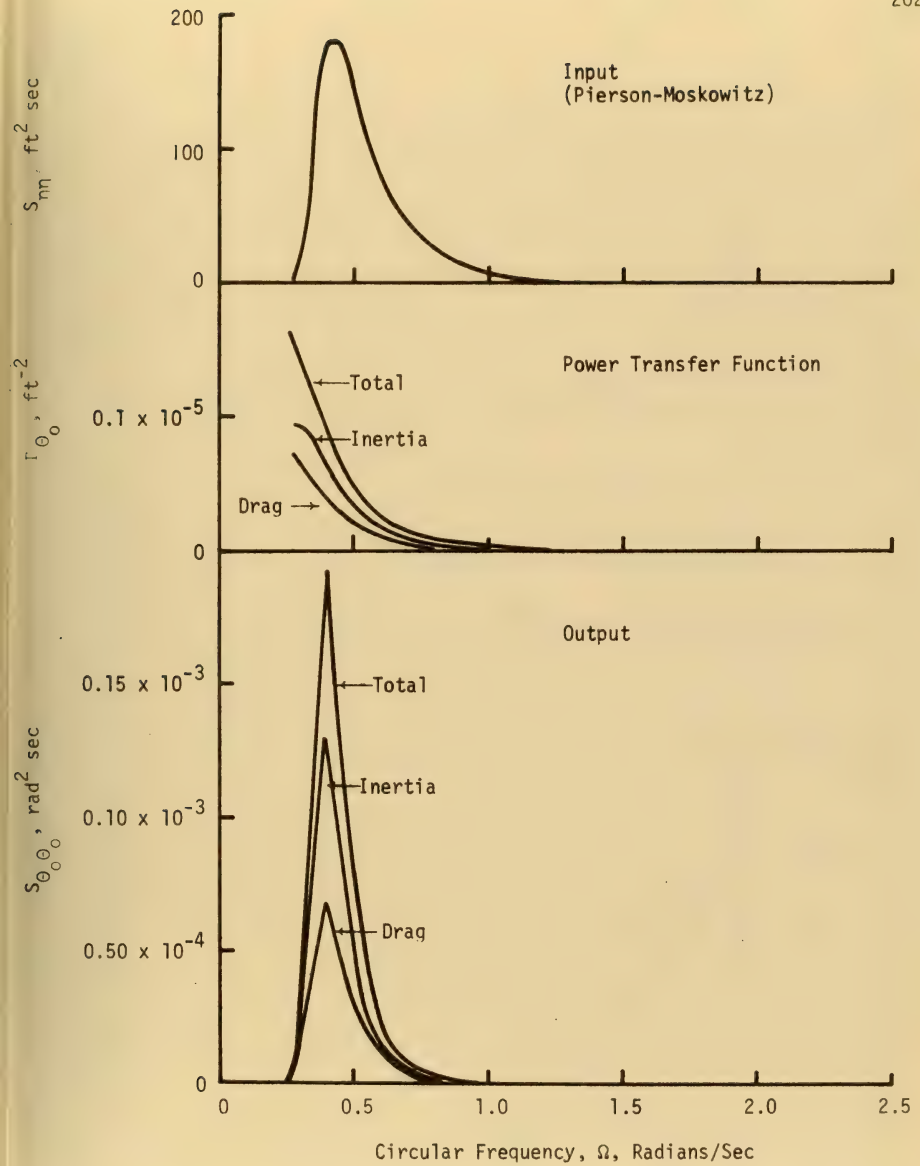


Fig. 3.6d Static Bottom Rotation Spectrum  
for Forty Knot Wind Velocity





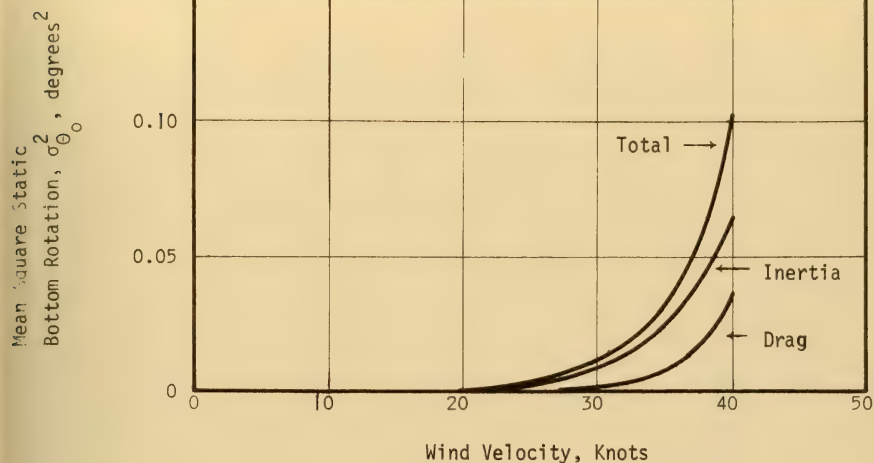


Fig. 3.7a Effect of Wind Velocity on Mean Square Static Bottom Rotation

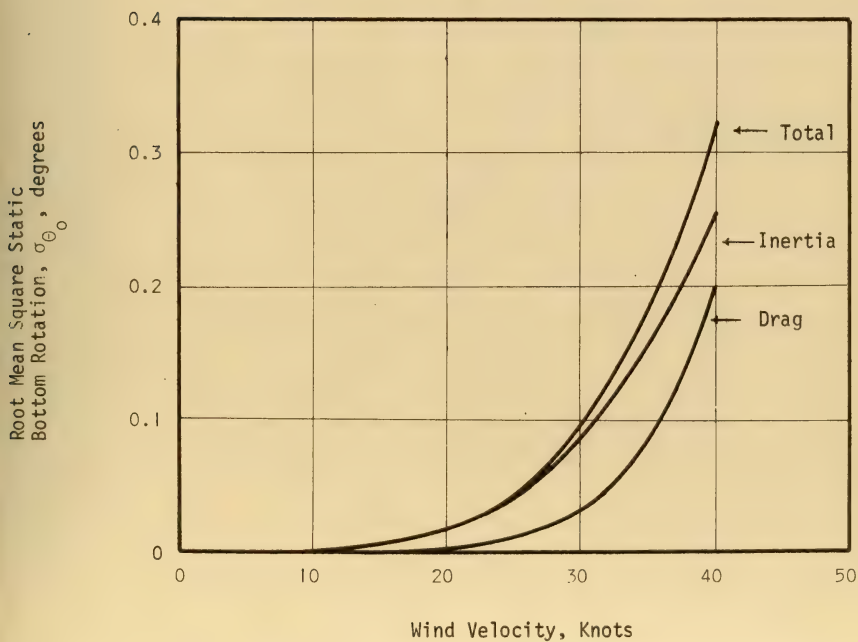


Fig. 3.7b Effect of Wind Velocity on Root Mean Square Static Bottom Rotation



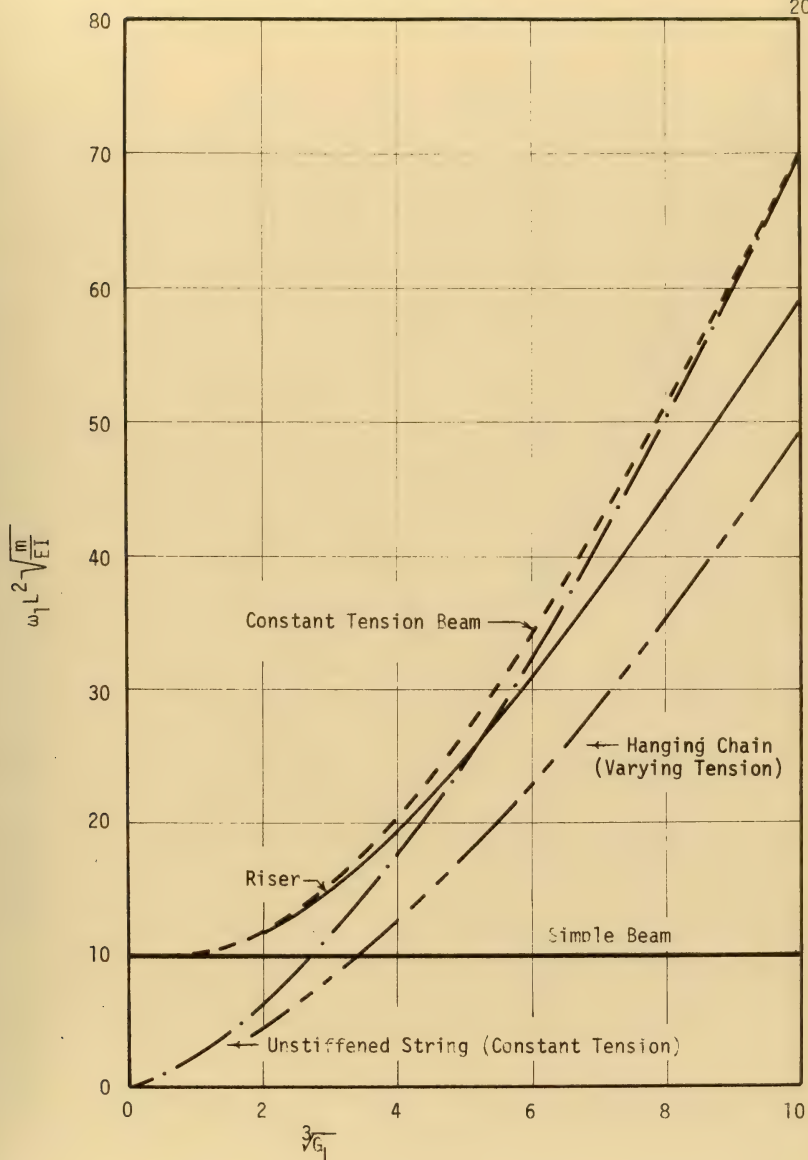


Fig. 4.1 Comparison of Fundamental Frequencies,  $G_T = 1.0$



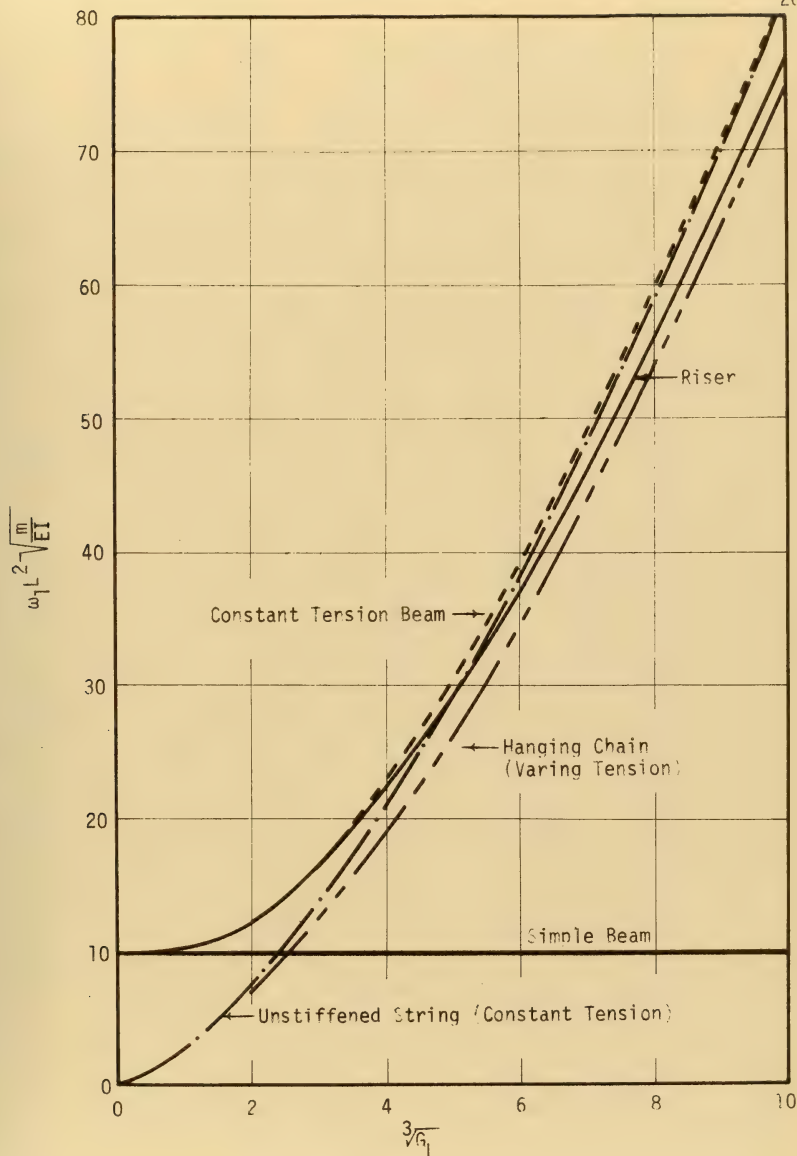


Fig. 4.2 Comparison of Fundamental Frequencies,  $G_T = 1.2$



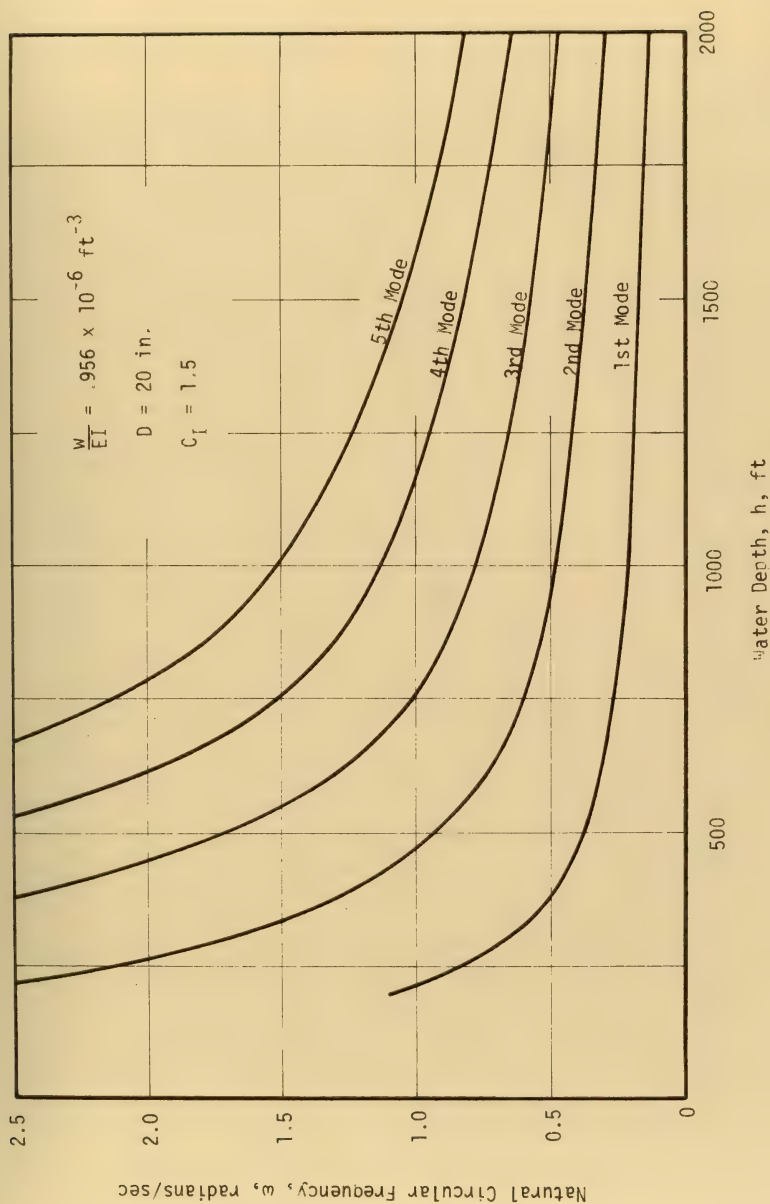


Fig. 4.3 Natural Frequencies of Typical Marine Riser;  $G_T = 1.0$





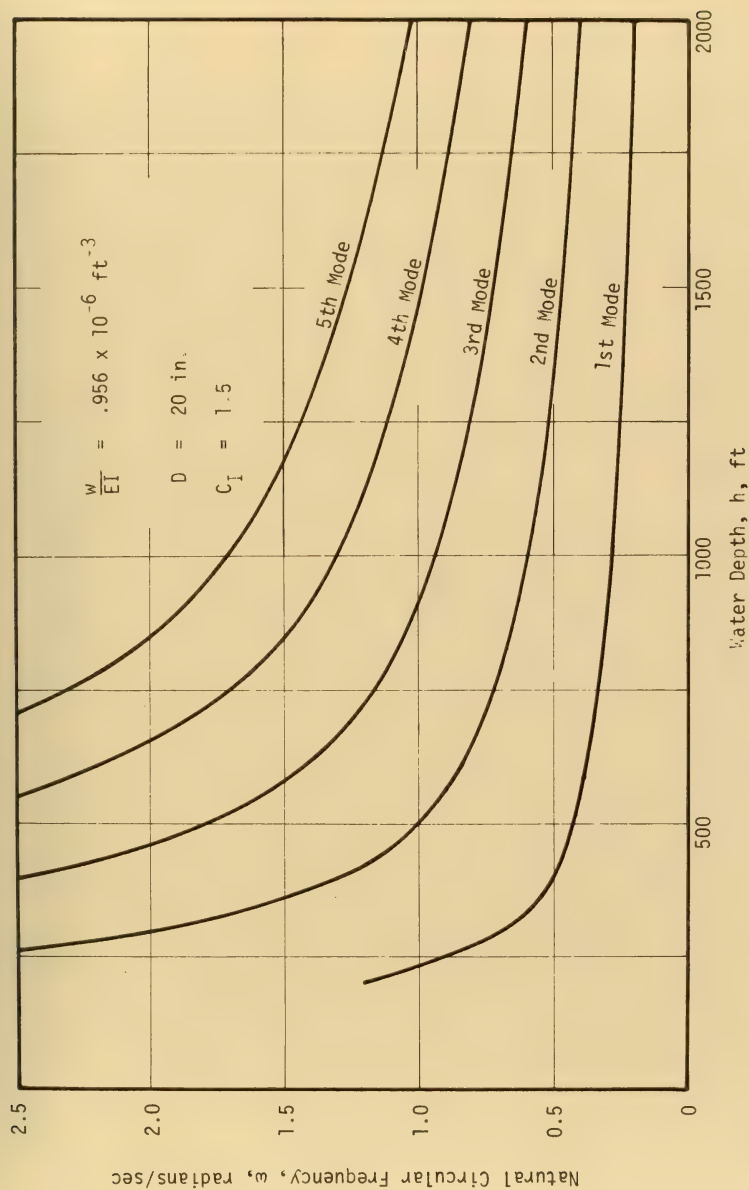


Fig. 4.4 Natural Frequencies of Typical Marine Riser,  $G_T = 1.2$



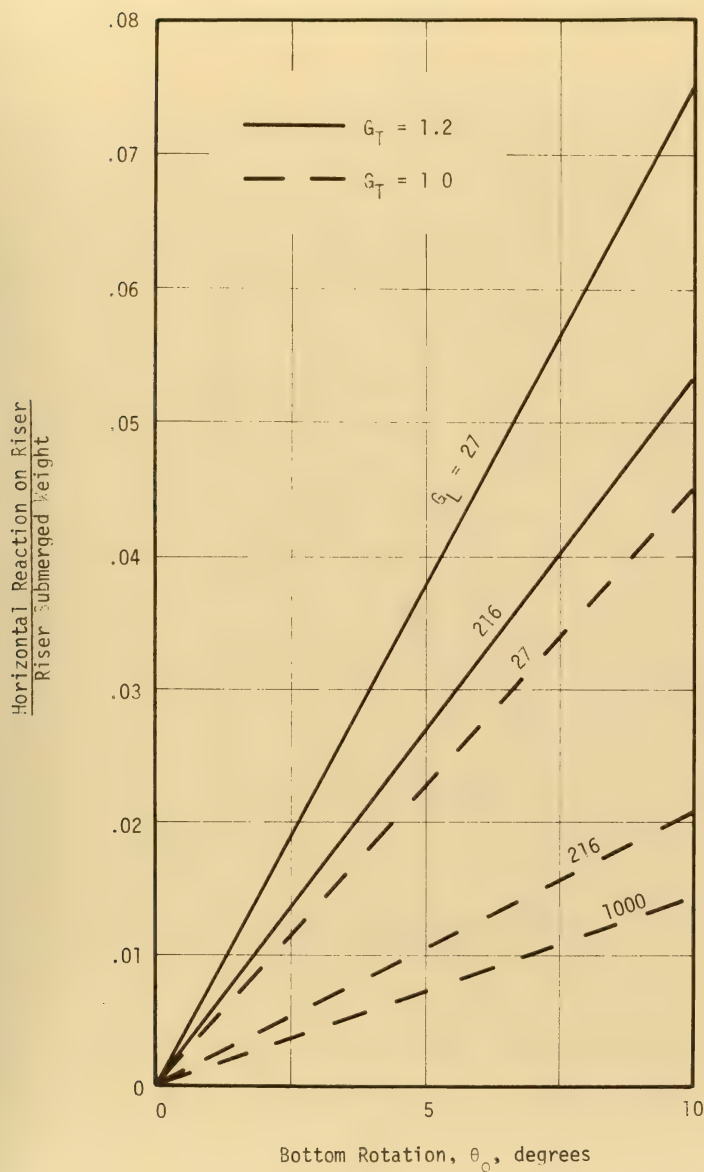


Fig. 4.5 Variation of Horizontal Reaction with Bottom Rotation of Riser



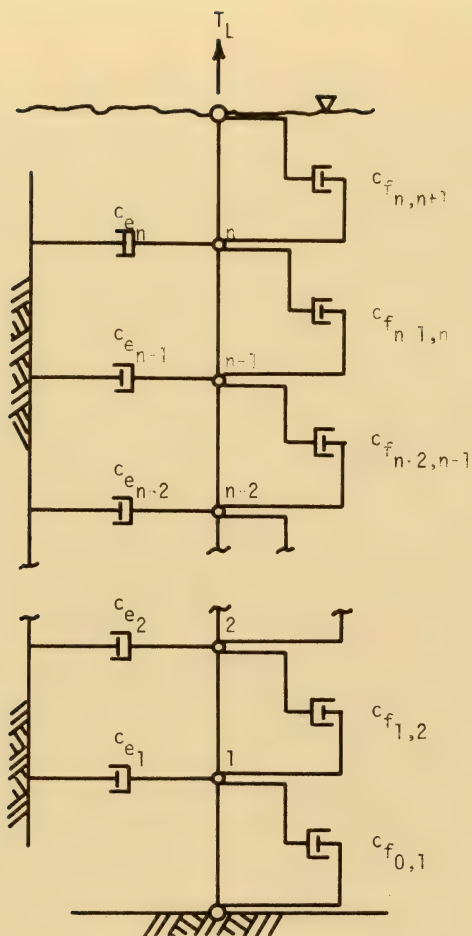


Fig. 4.6 Schematic Representation of Damping in Marine Riser



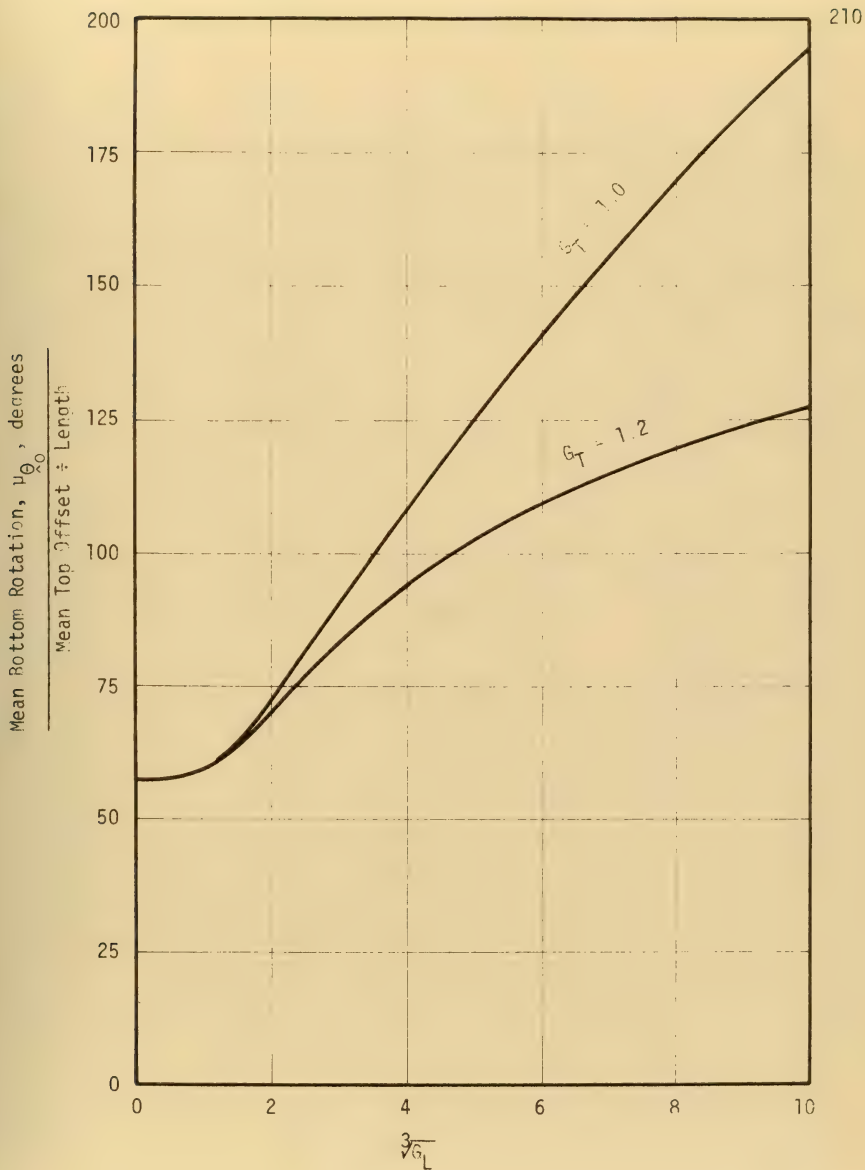


Fig. 5.1 Variation of Mean Bottom Rotation with Mean Top Offset





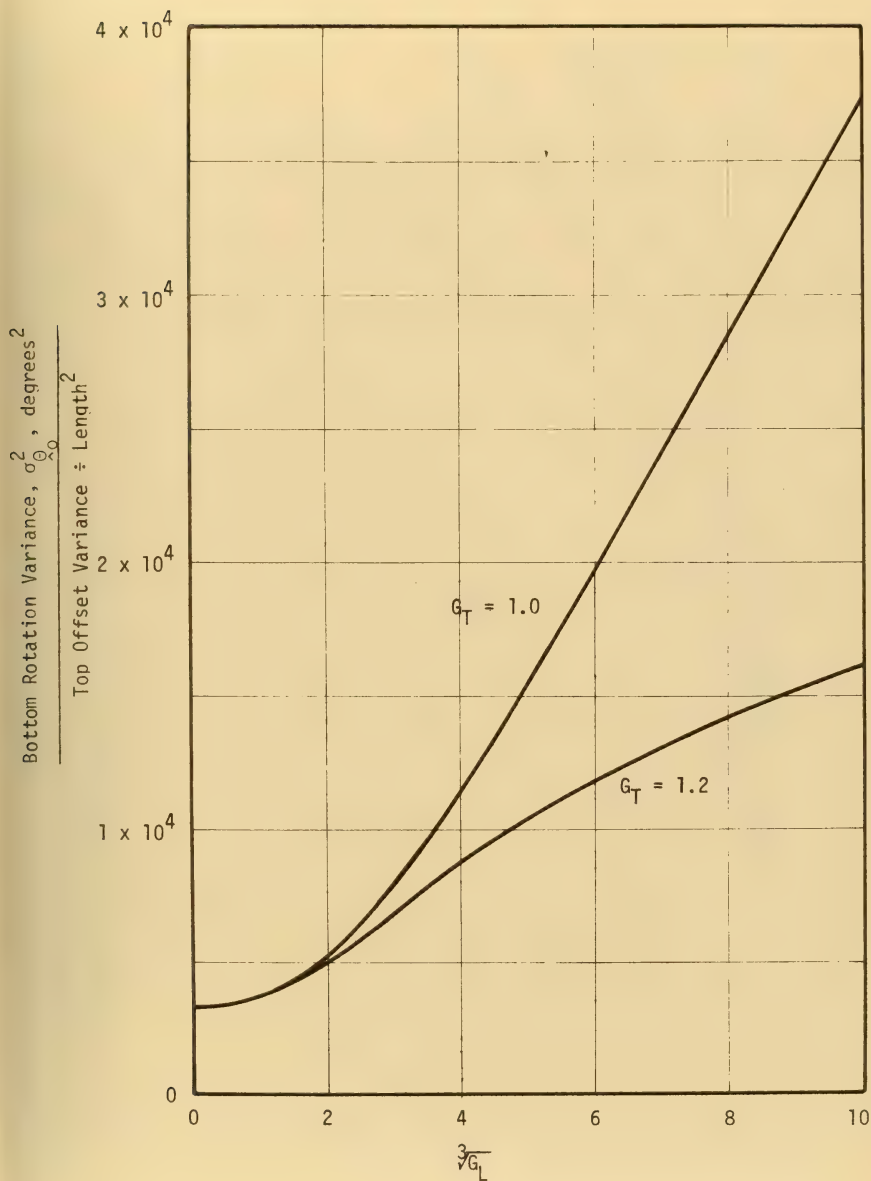


Fig. 5.2 Variation of Bottom Rotation Variance with Top Offset Variance



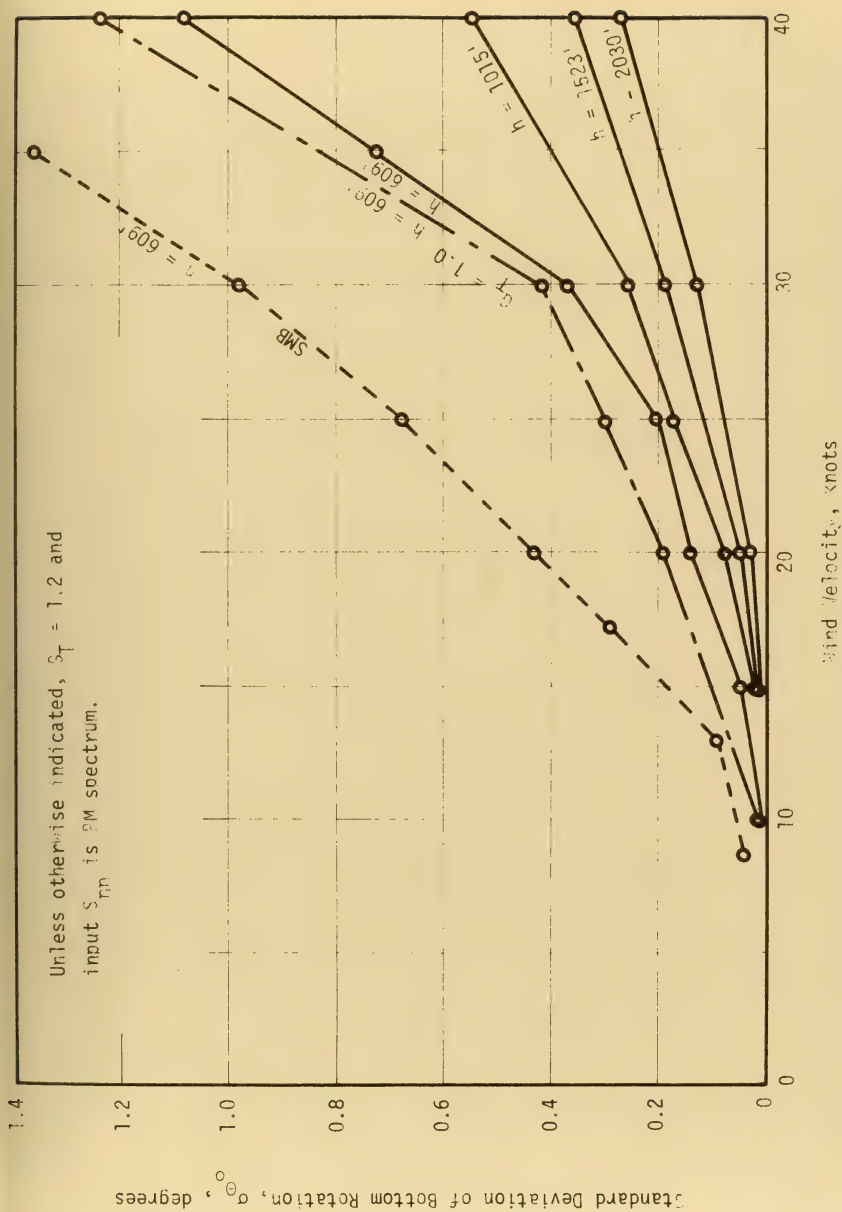


Fig. 6.1 Standard Deviation of Wave-Induced Bottom Rotation Versus Wind Velocity



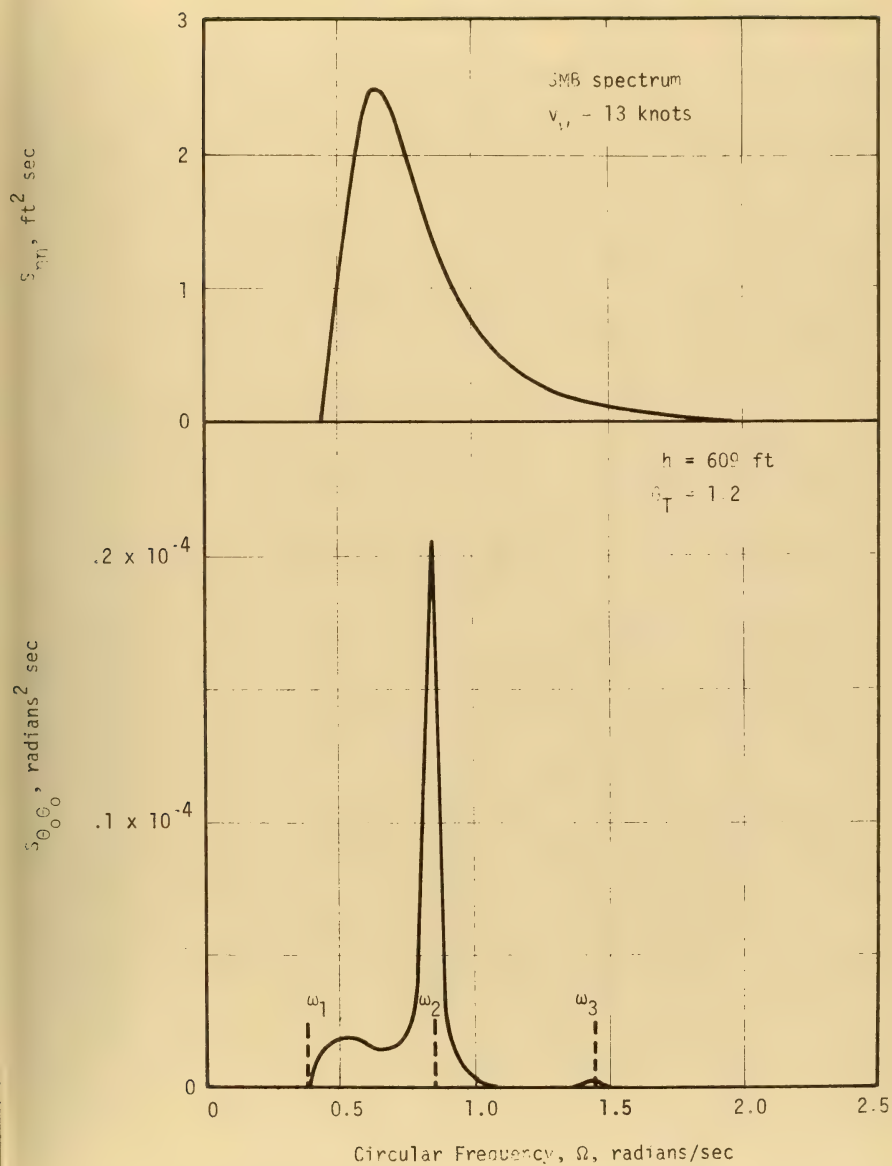


Fig. 6.2 Bottom Rotation Spectrum Induced by 13 Knot SMB Spectrum



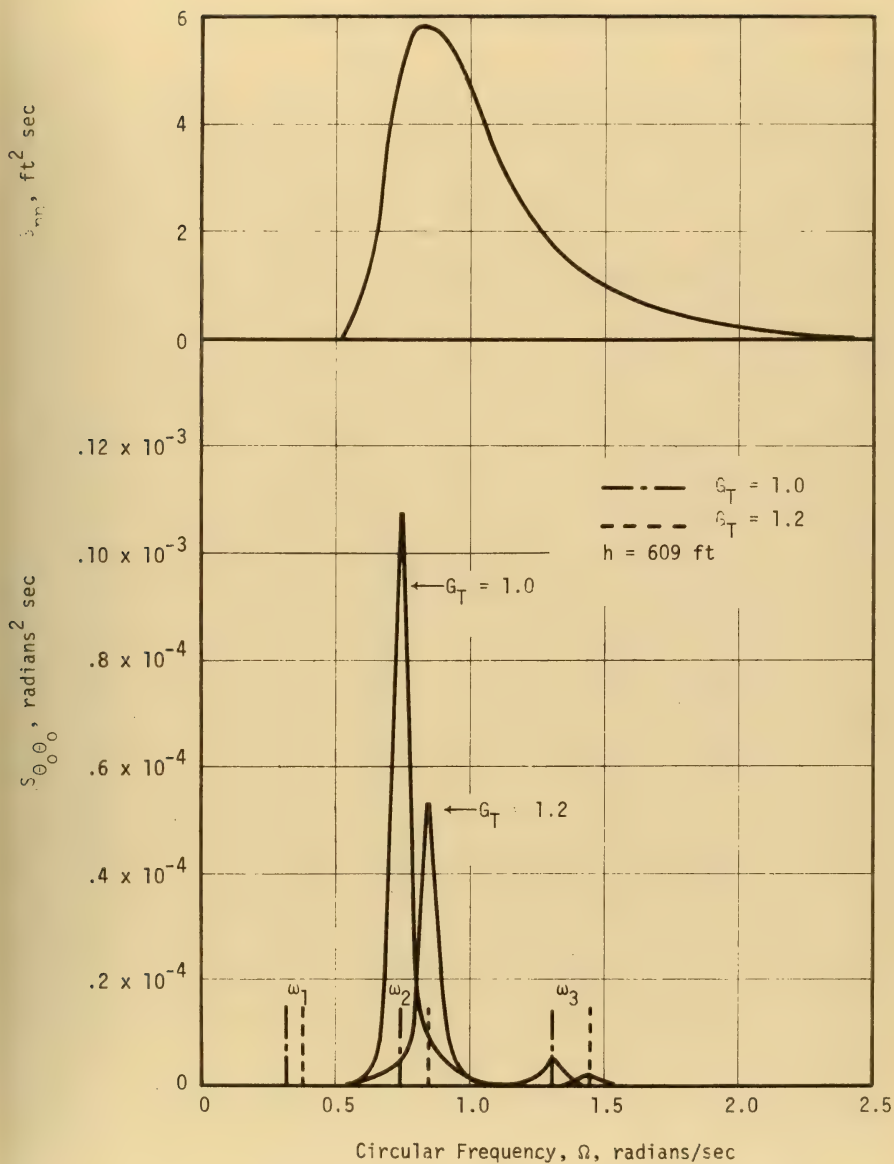


Fig. 6.3 Bottom Rotation Spectra Induced by 20 Knot <sup>PM</sup> Spectrum





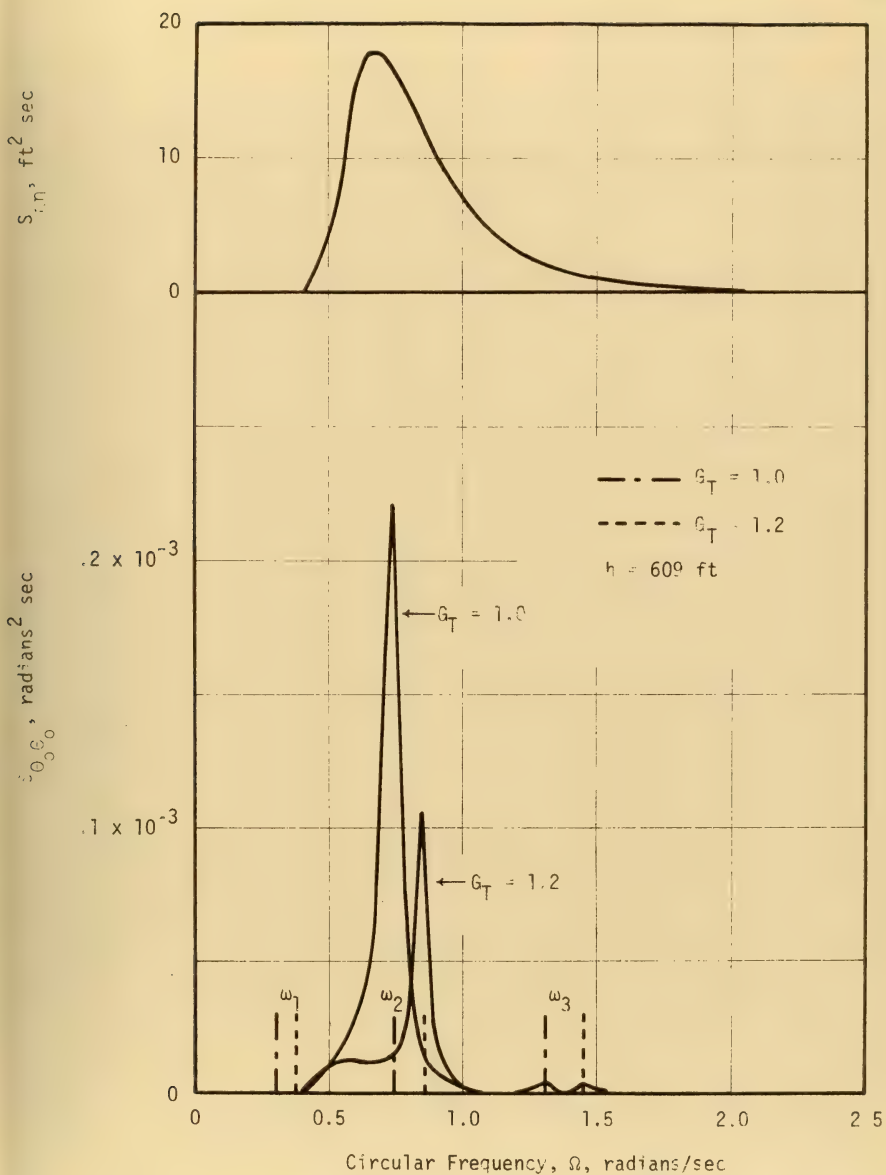


Fig. 6.4 Bottom Rotation Spectra Induced by 25 Knot PM Spectrum



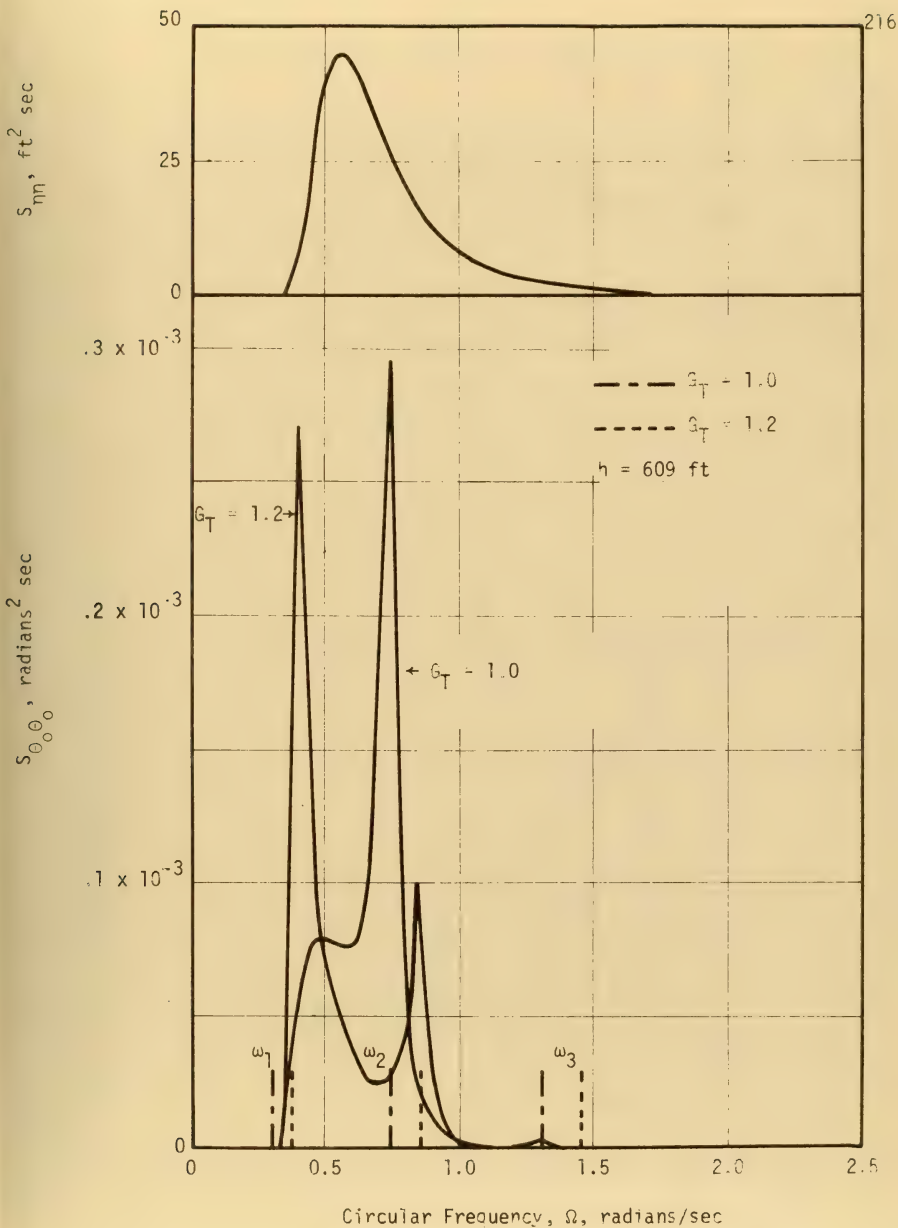


Fig. 6.5 Bottom Rotation Spectra Induced by 30 Knot PM Spectrum



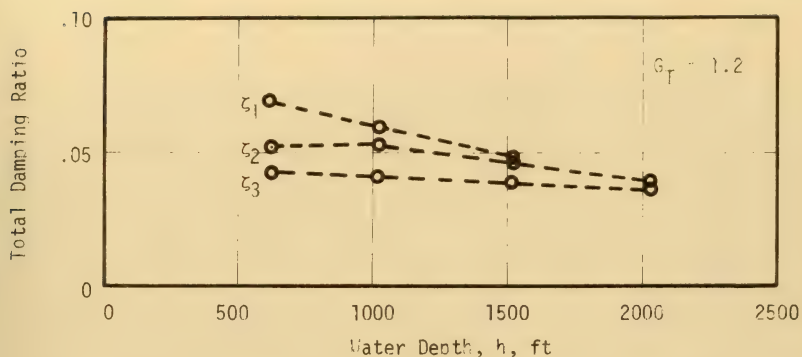


Fig. 6.6 Variation of Damping Ratio with Depth, 30 Knot PM Spectrum.

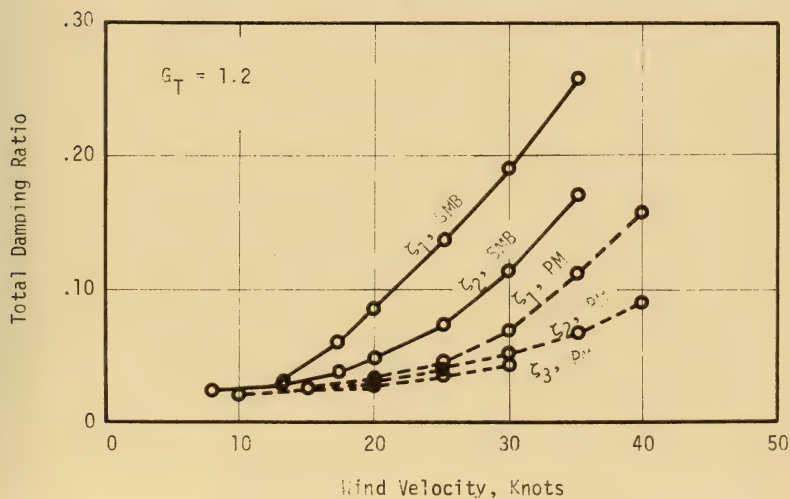


Fig. 6.7 Variation of Damping Ratio with Wind Velocity, 609 Ft Riser



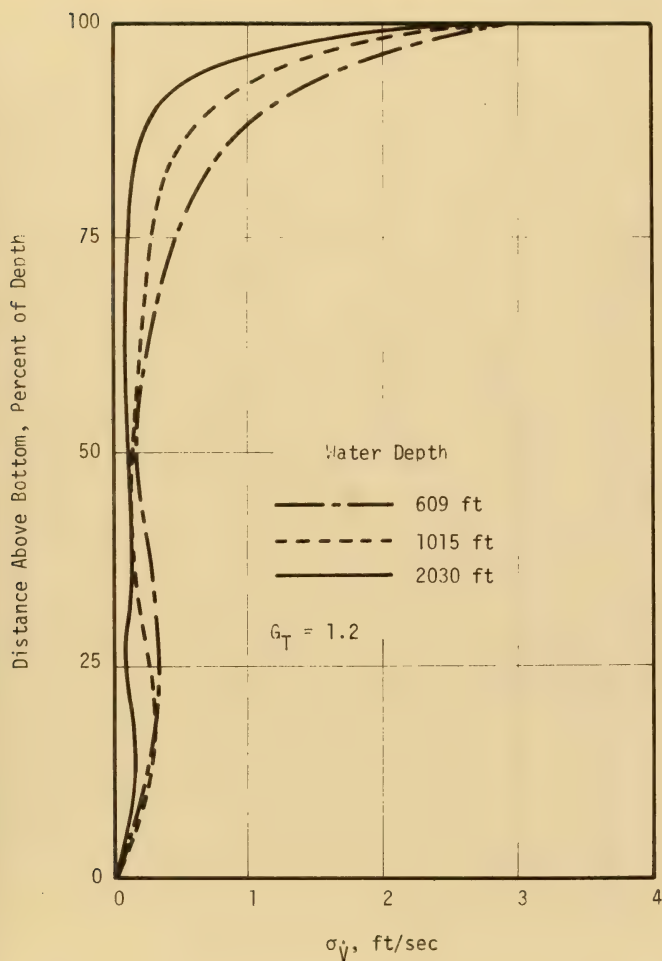


Fig. 6.8 Profiles of Standard Deviation of Relative Water Velocity for 30 Knot PM Spectrum





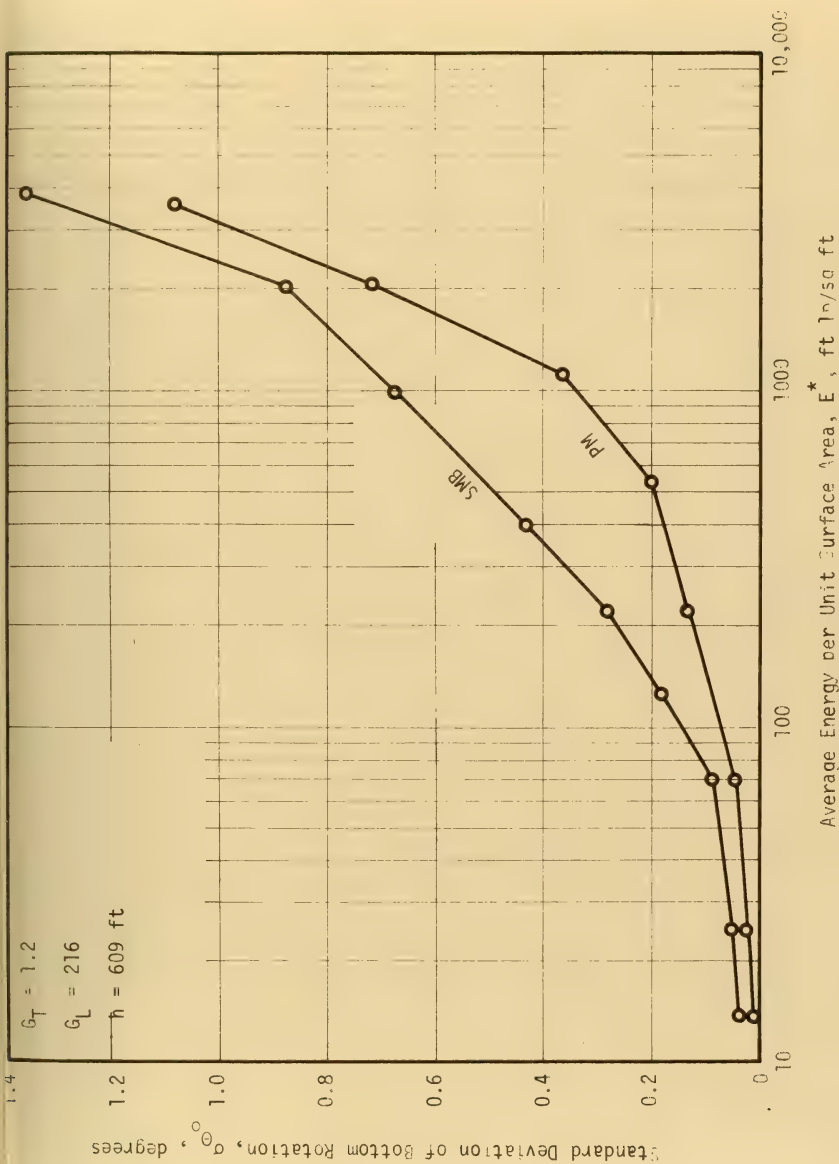


Fig. 6.9 Standard Deviation of Wave-Induced Bottom Rotation Versus Energy Density



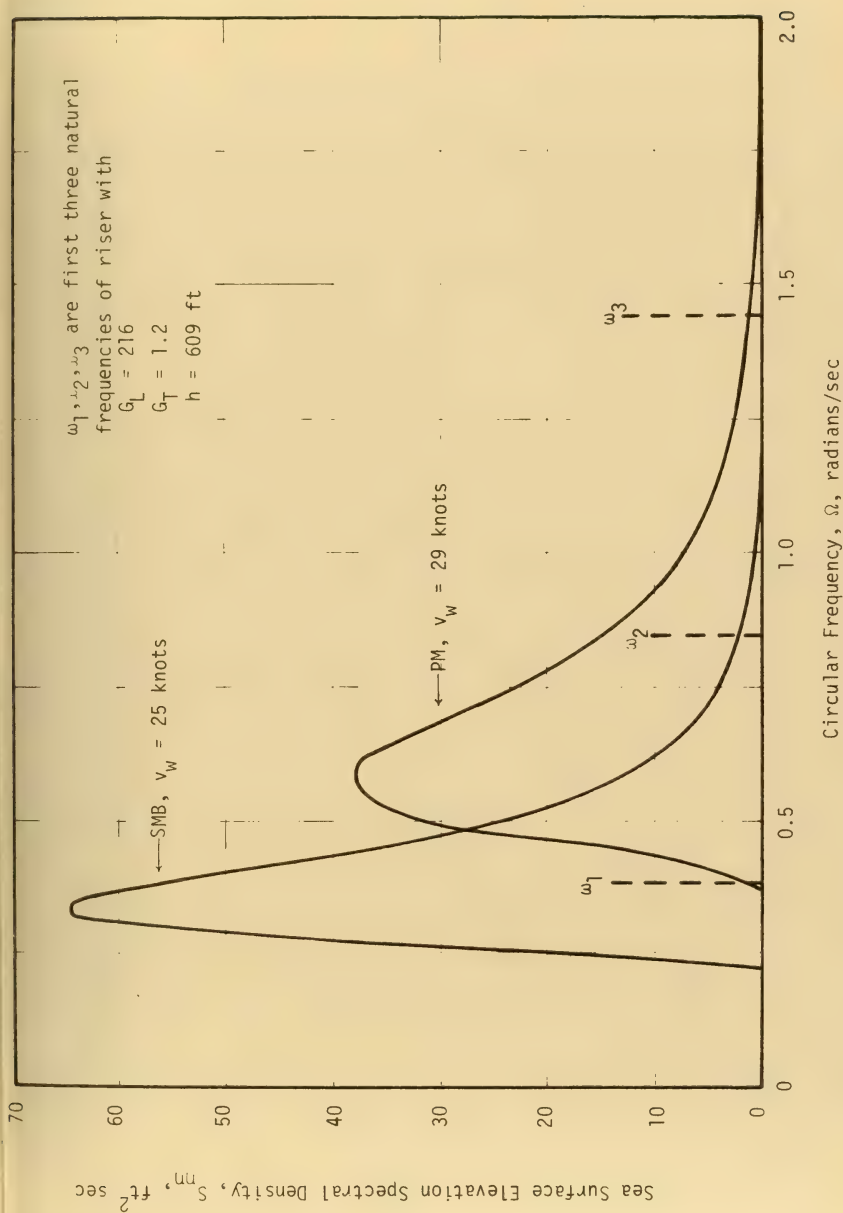


Fig. 6.10 Comparison of SMB and PM Spectra



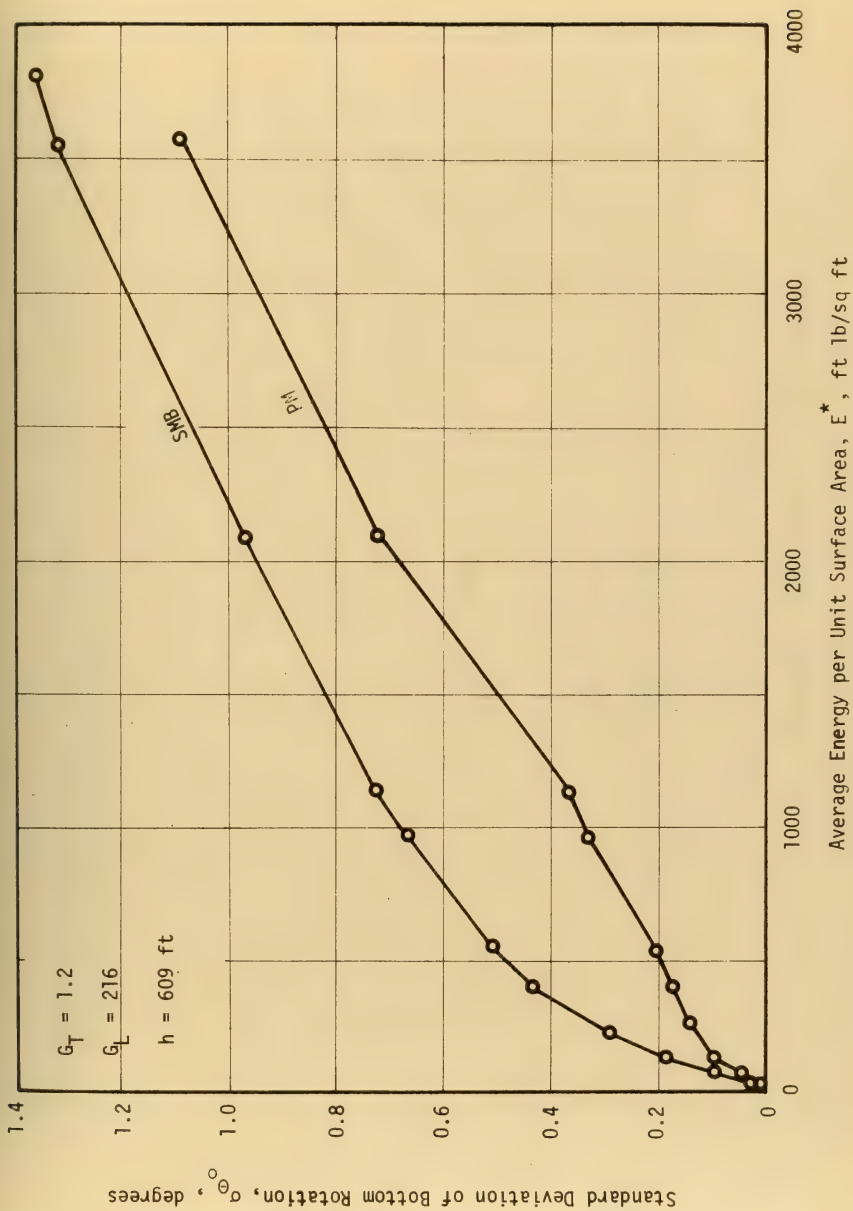


Fig. 6.11 Effect of Energy Density on Wave-Induced Bottom Rotation



Unless otherwise indicated,  $G_T = 1.2$  and input spectrum is Pierson-Moskowitz spectrum.

Standard Deviation of Maximum Moment, ft kips

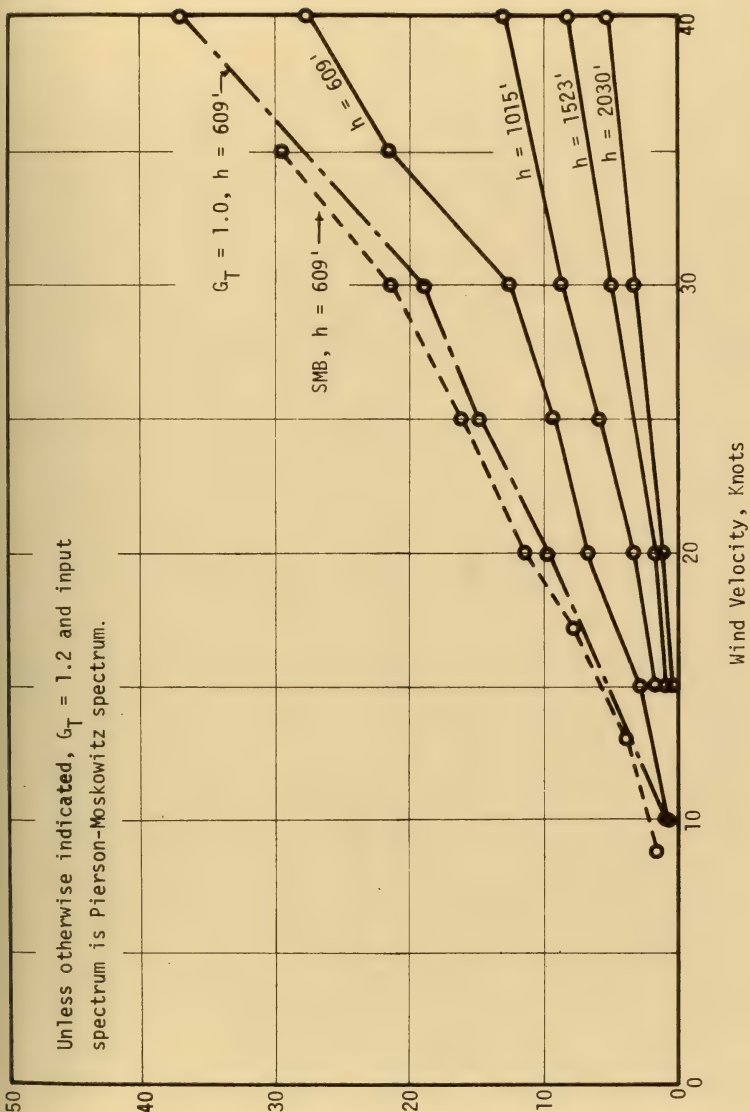


Fig. 6.12 Standard Deviation of Maximum Wave-Induced Bending Moment





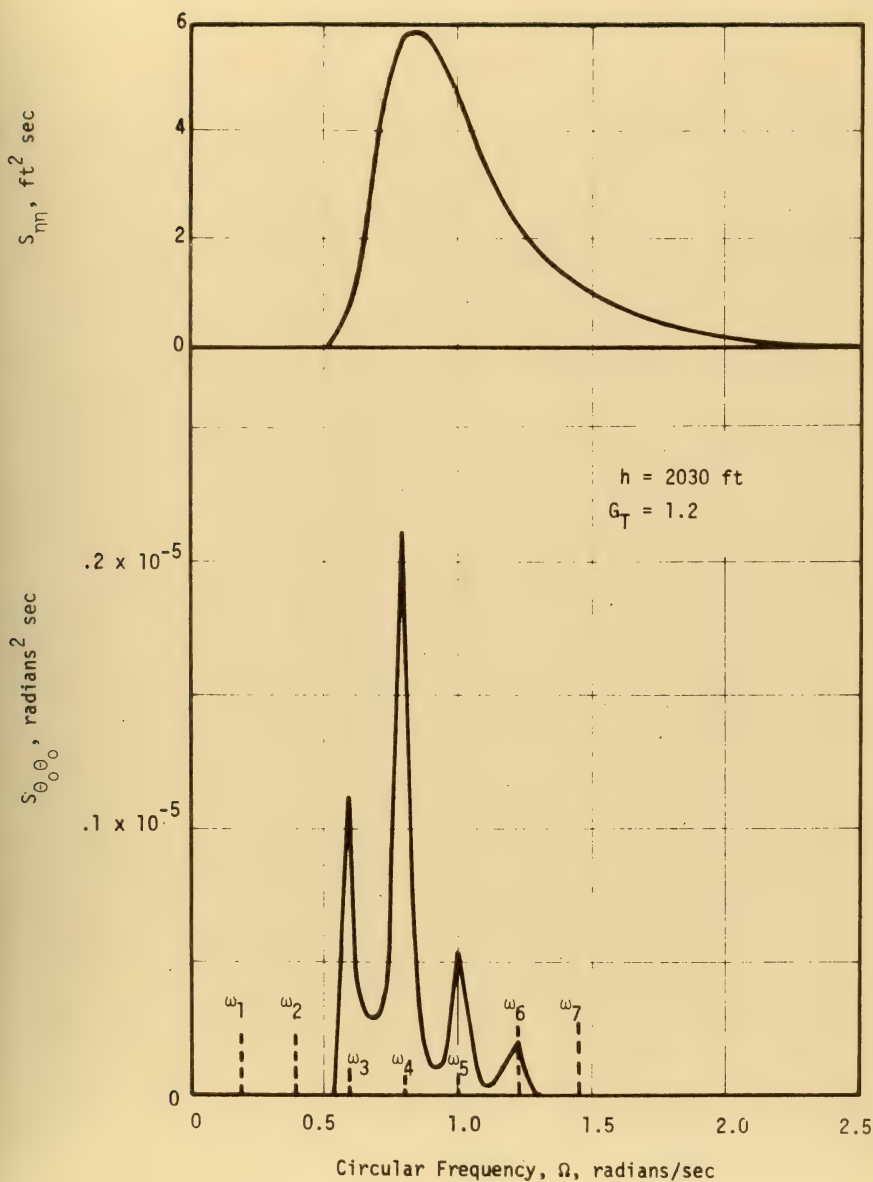


Fig. 6.13 Bottom Rotation Spectrum Produced by 20 Knot PM Spectrum



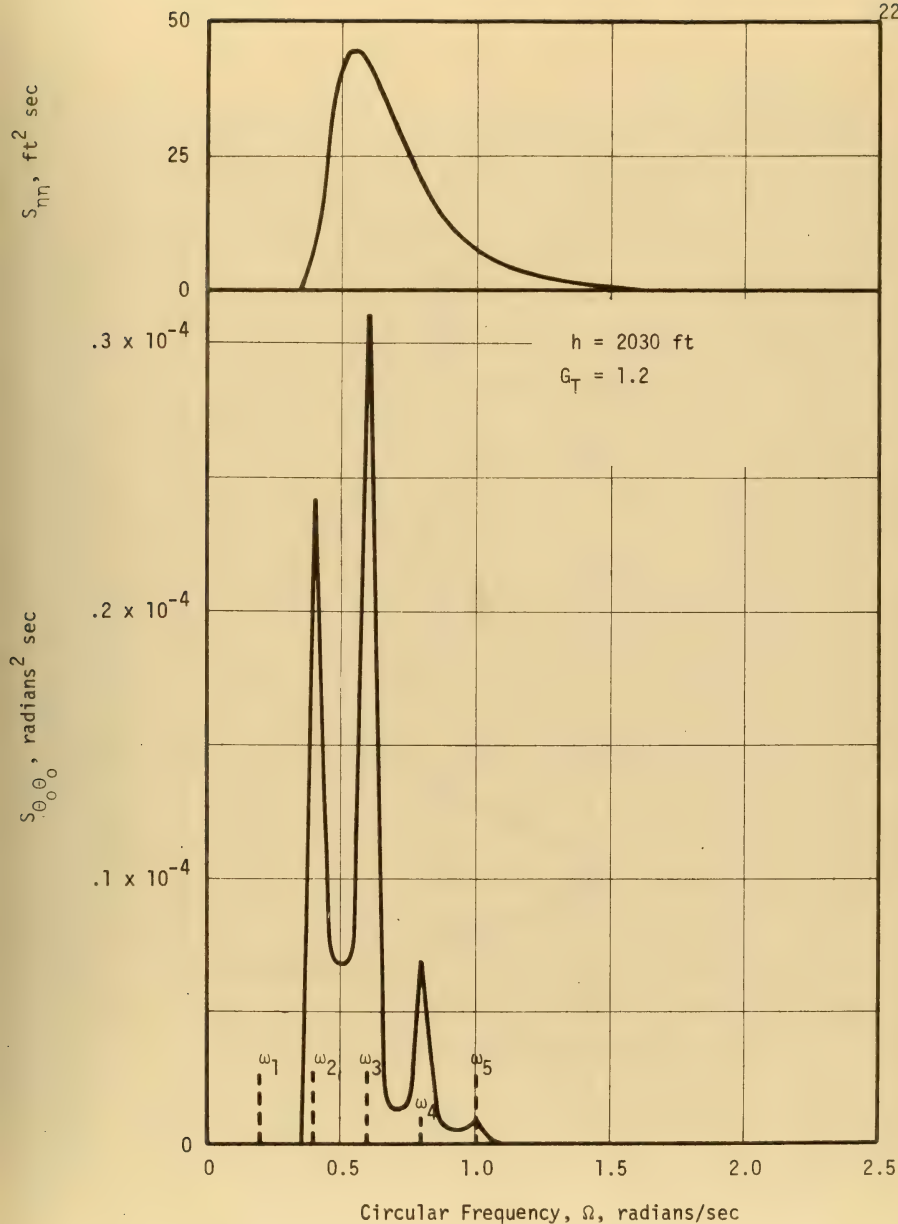


Fig. 6.14 Bottom Rotation Spectrum Produced by 30 Knot PM Spectrum



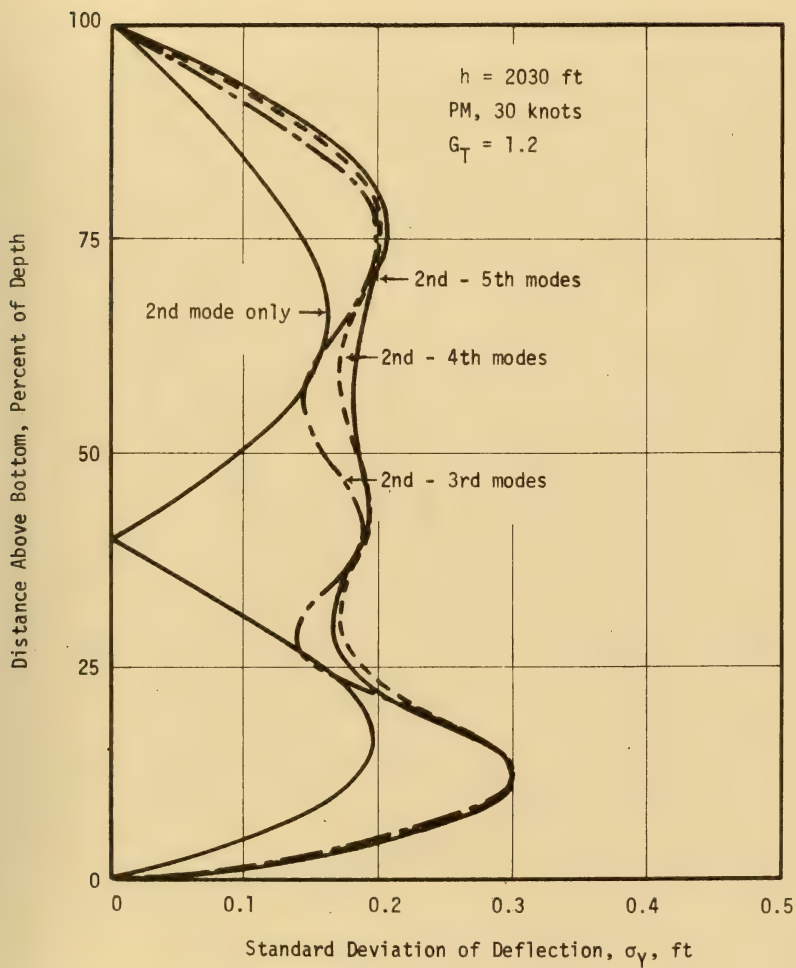


Fig. 6.15 Modal Contributions to Standard Deviation of Deflection



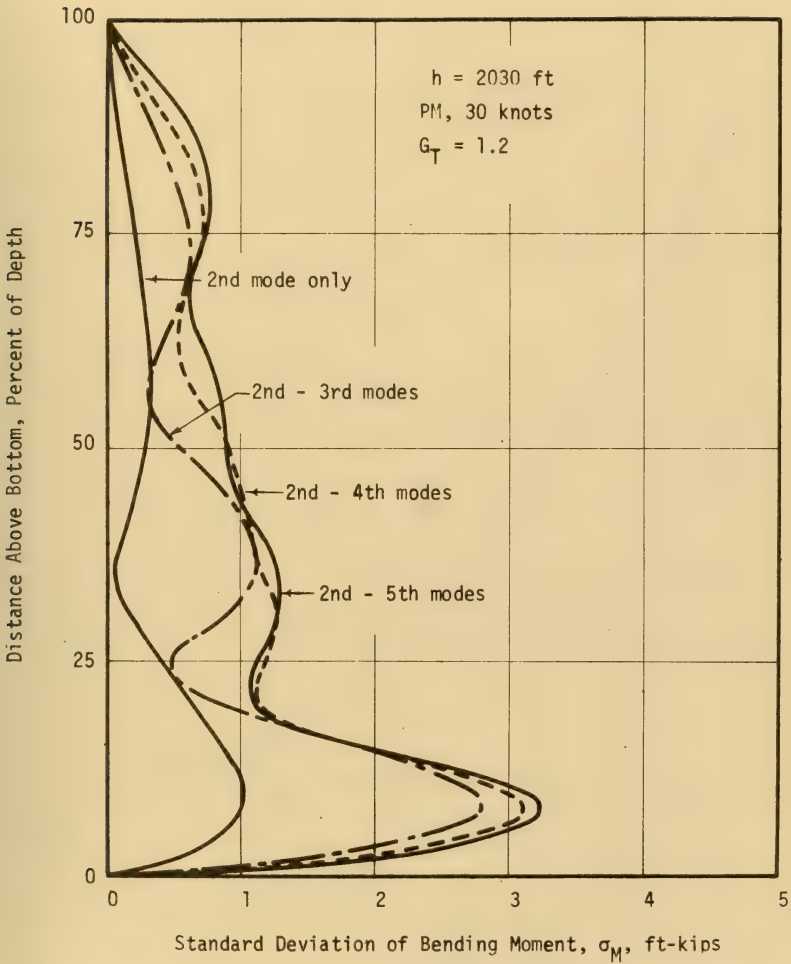


Fig. 6.16 Modal Contributions to Standard Deviation of Bending Moment





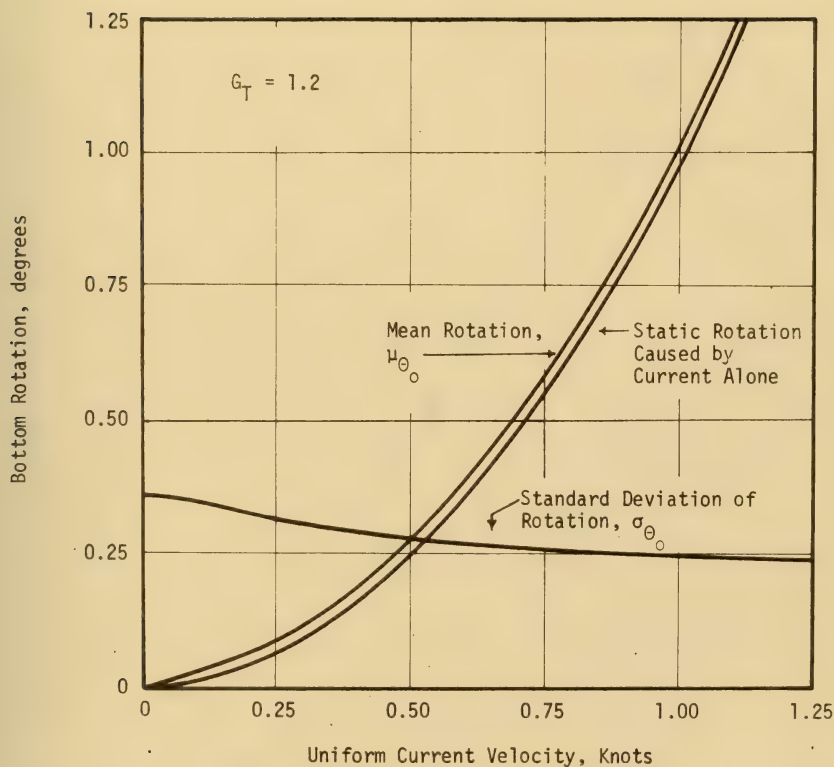


Fig. 6.17 Bottom Rotation Statistics for 609 ft Riser with 30 Knot, PM Waves and Uniform Current



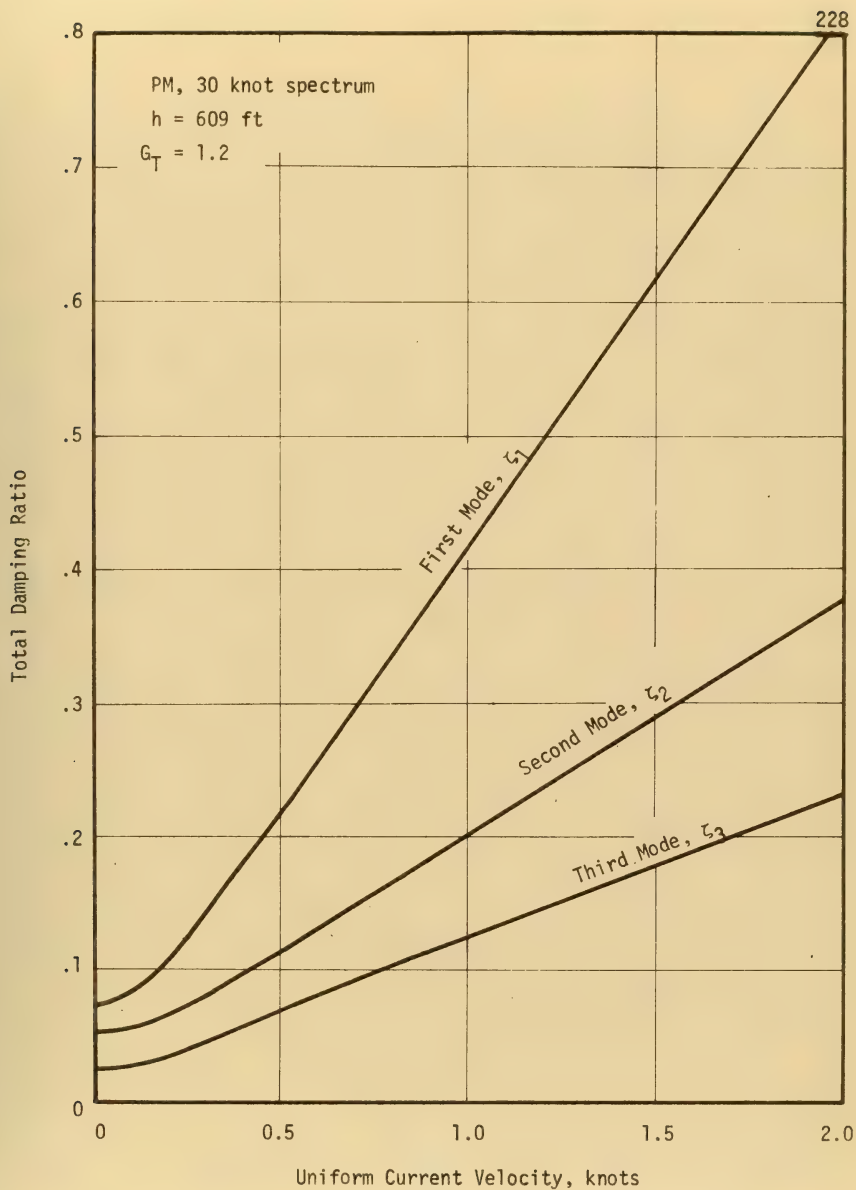


Fig. 6.18 Effect of Uniform Current Velocity on Damping Ratio



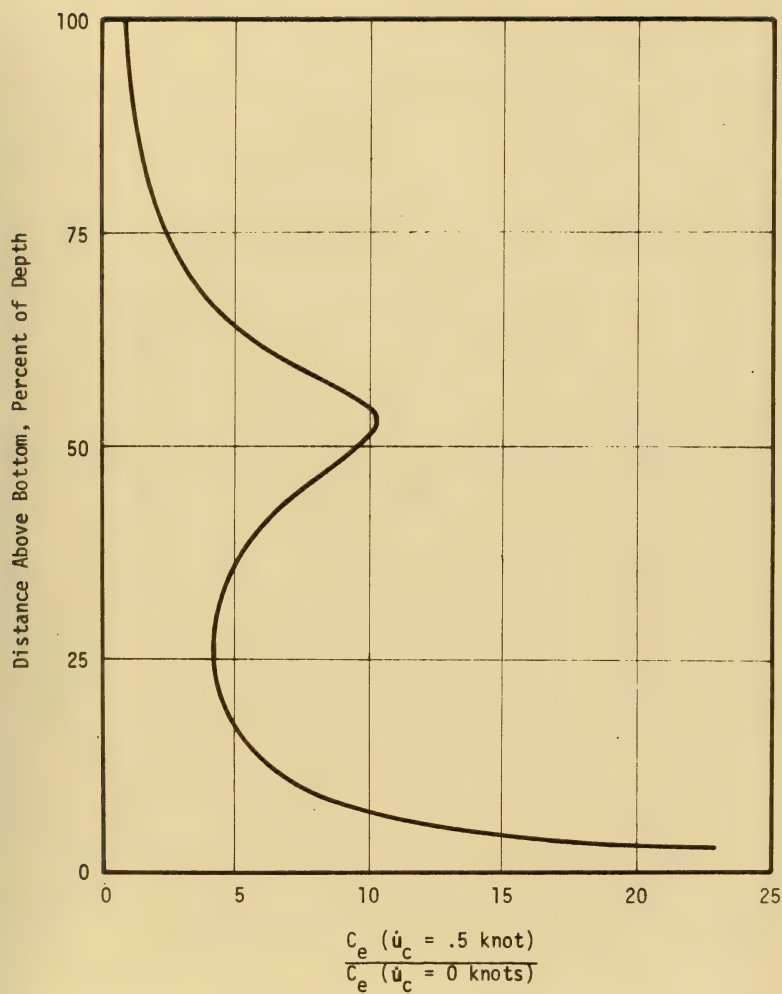


Fig. 6.19 Effect of Uniform Current on Hydraulic Damping Coefficients



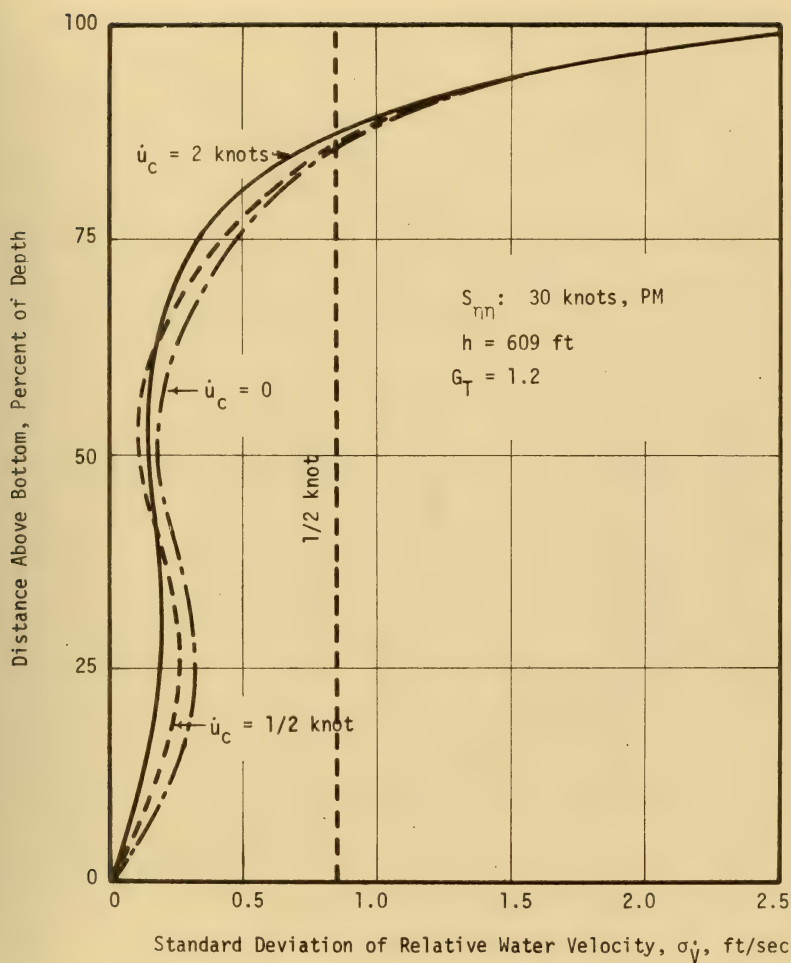


Fig. 6.20 Effect of Uniform Current on Standard Deviation of Relative Water Velocity





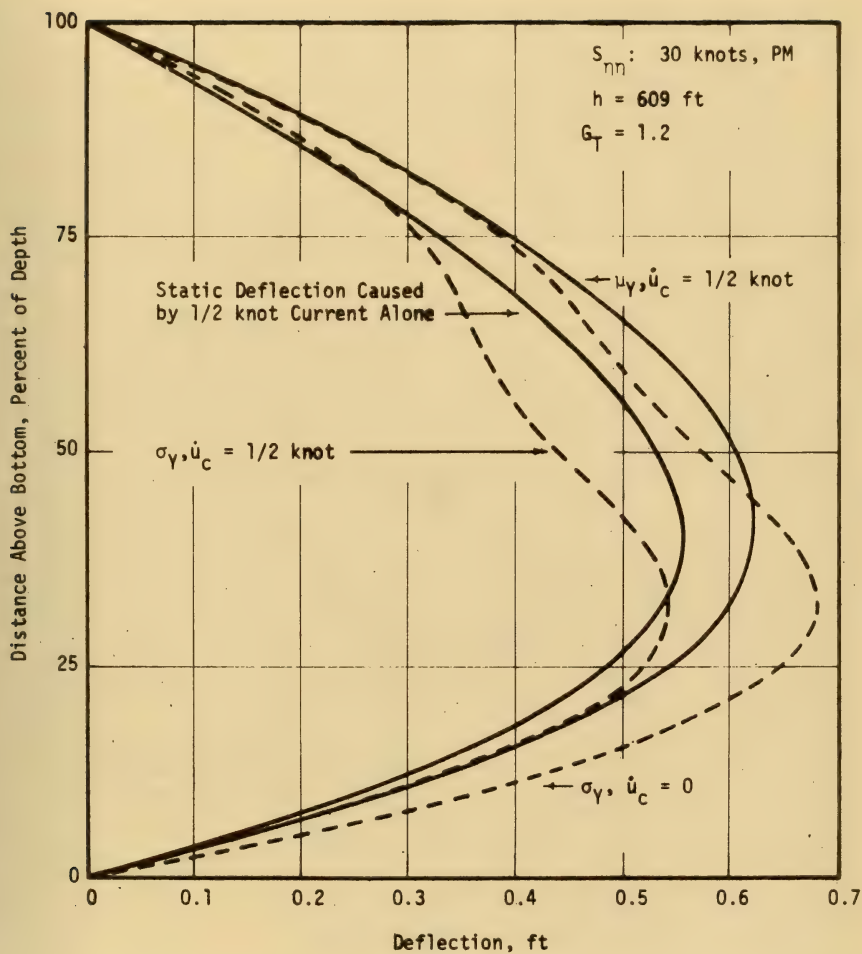


Fig. 6.21 Effect of Uniform Current on Deflection



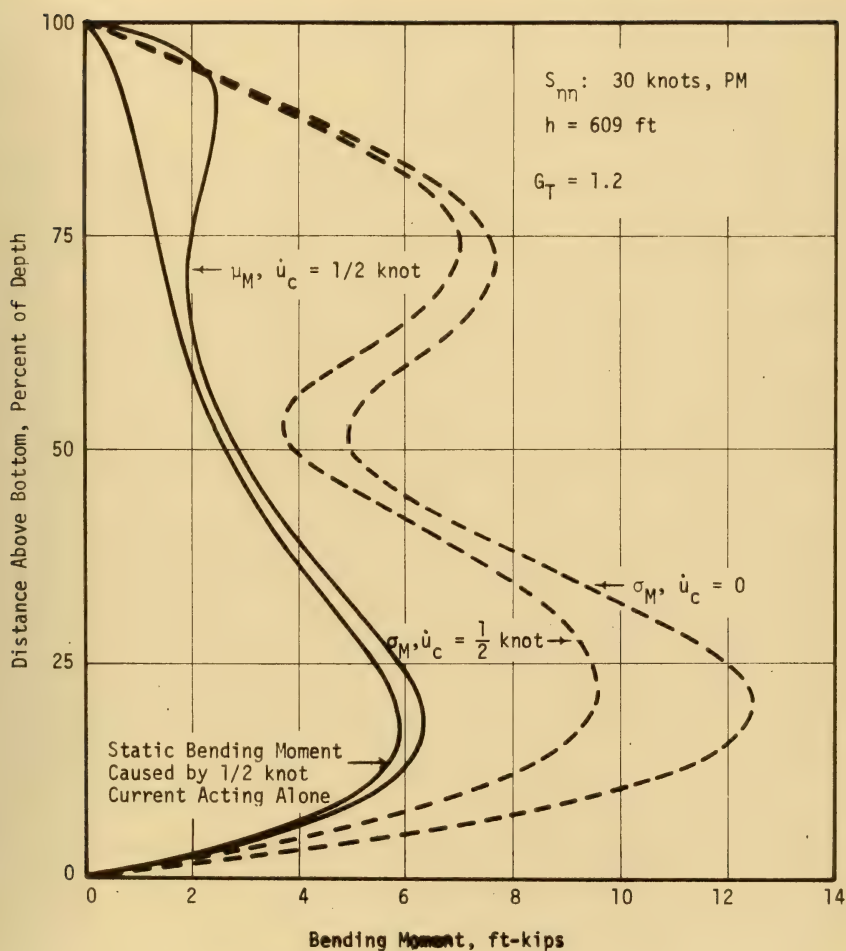


Fig. 6.22 Effect of Uniform Current on Bending Moments



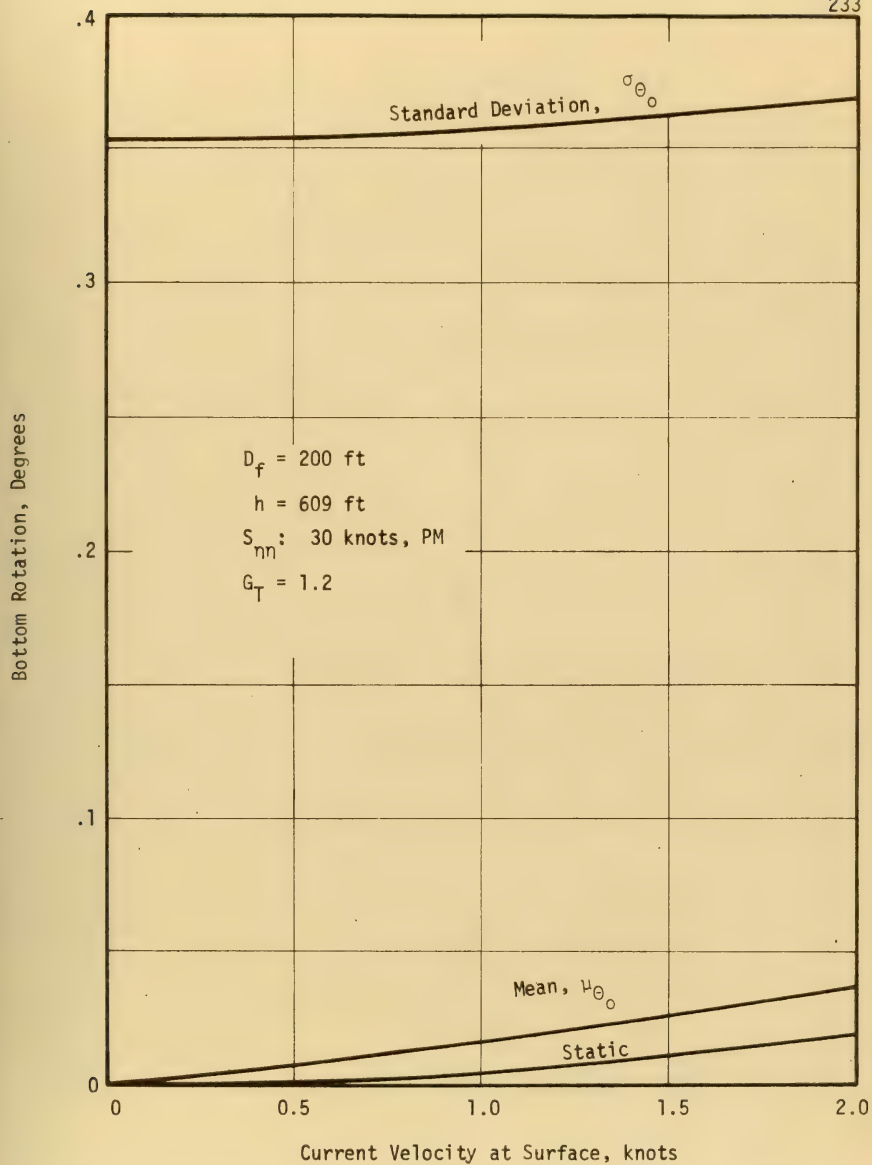


Fig. 6.23 Effect of Wind Driven Current on Bottom Rotation



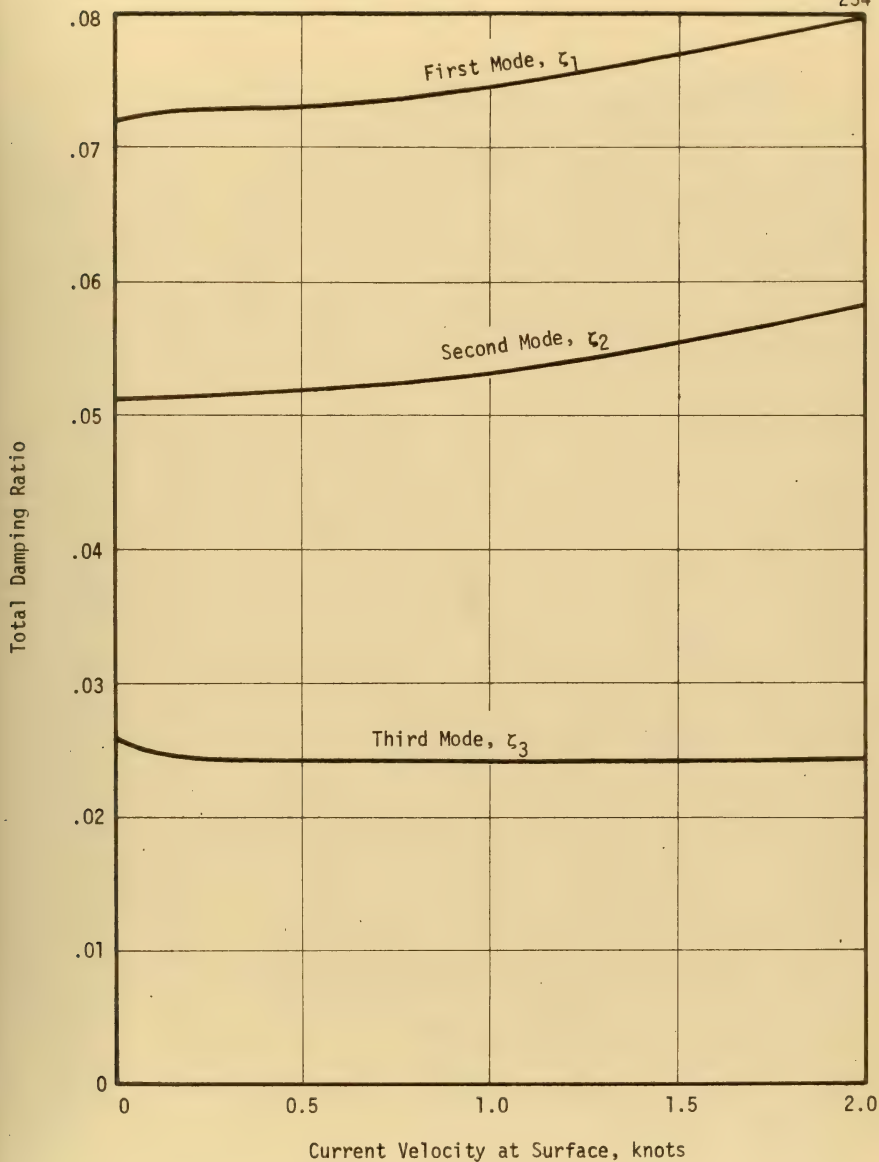


Fig. 6.24 Effect of Wind Driven Current on Damping Ratios





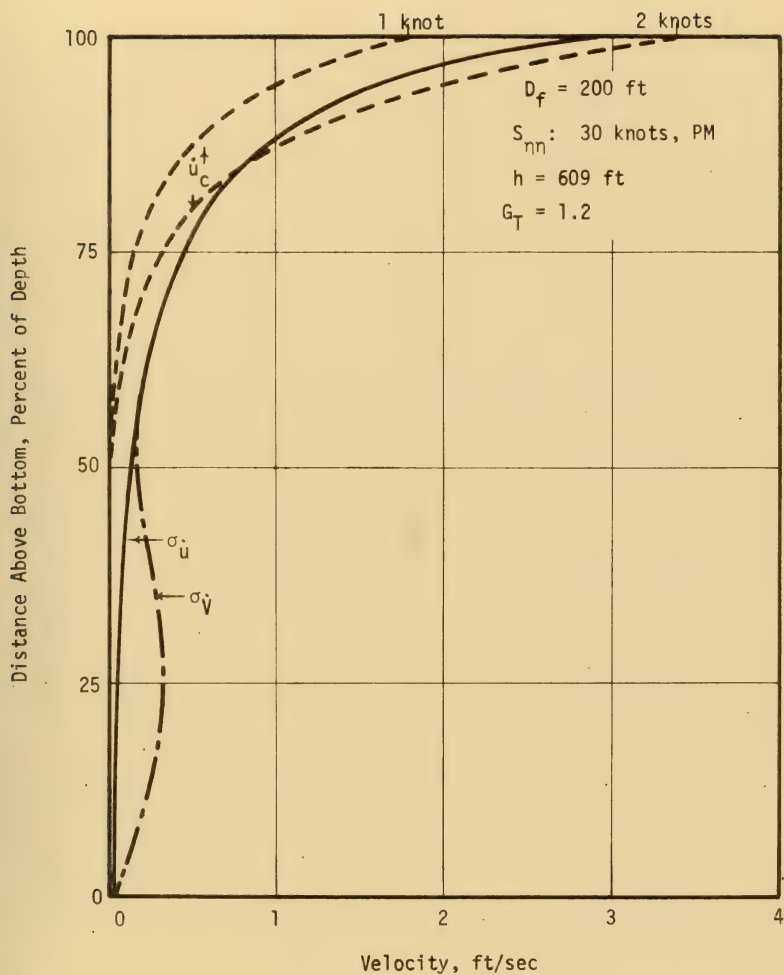


Fig. 6.25 Comparison of Velocity Profiles



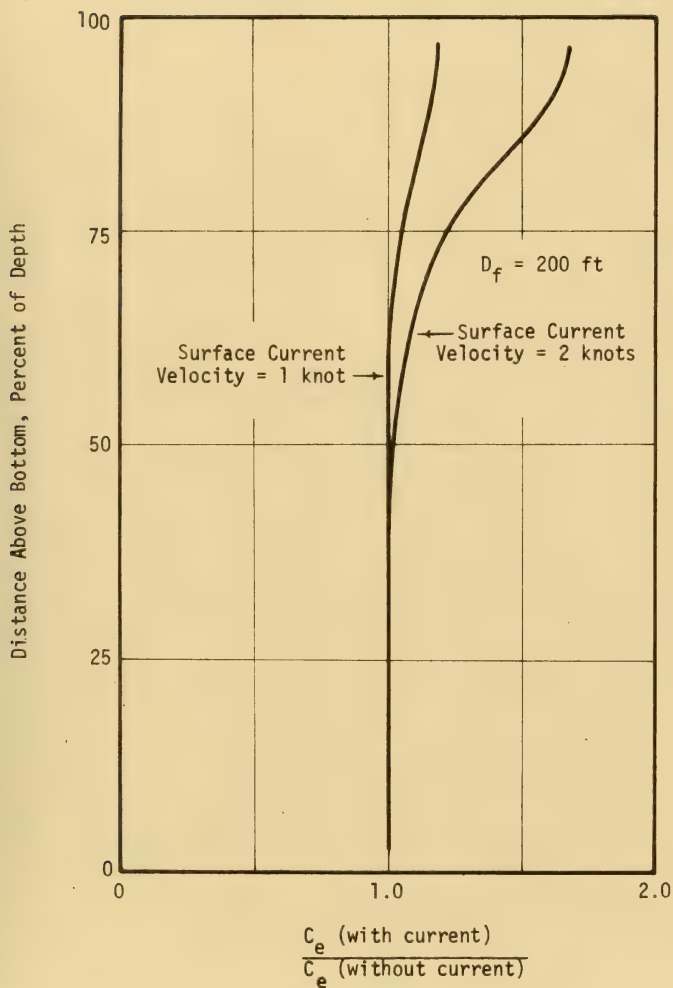


Fig. 6.26 Effect of Wind Driven Current on Hydraulic Damping Coefficients



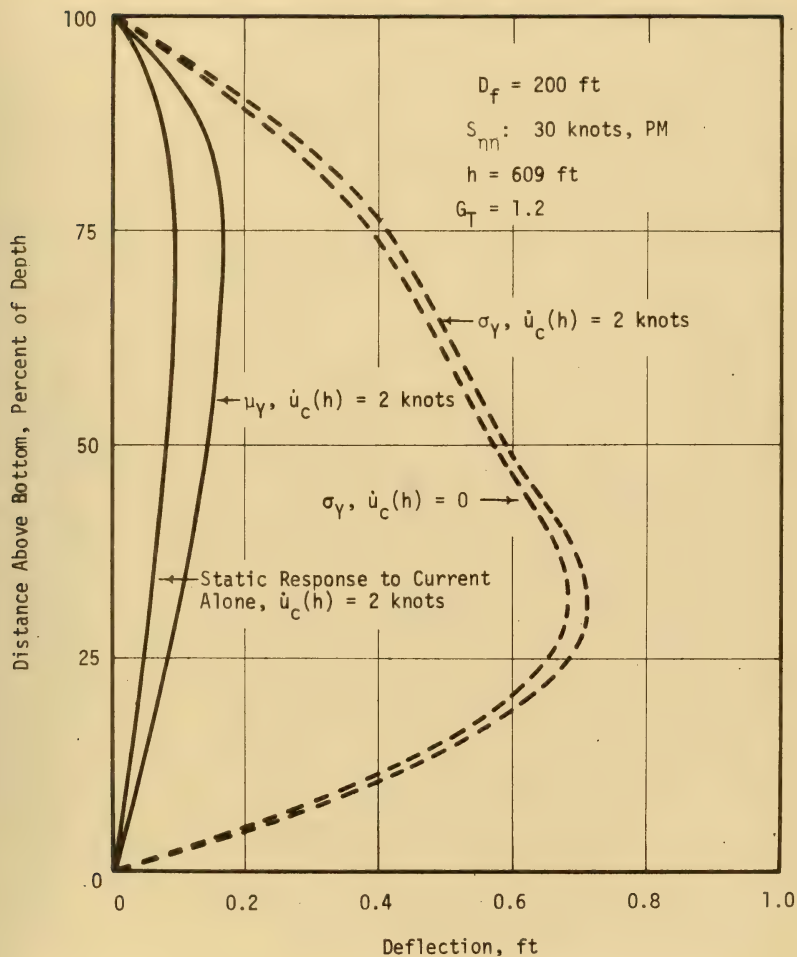


Fig. 6.27 Effect of Wind Driven Current on Deflection



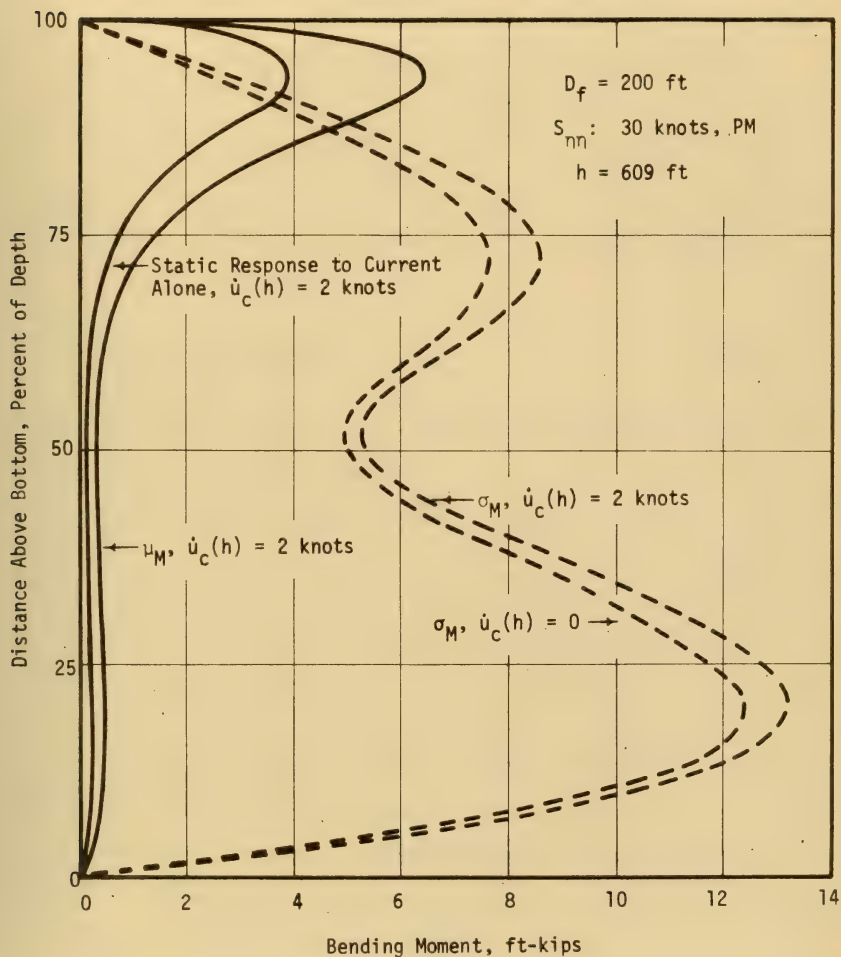


Fig. 6.28 Effect of Wind Driven Current on Bending Moment





## Appendix A

ANALYTICAL SOLUTION FOR THE DEFLECTED SHAPE OF A SIMPLE BEAM  
CAUSED BY A WAVE INERTIA FORCE DISTRIBUTION

Consider a simple beam subjected to a force distribution which is characteristic of the inertia force caused by water waves. The governing differential equation of the problem, which is depicted in Fig. 2.6, is

$$EI \frac{d^4 y}{dx^4} = \frac{\cosh(kx)}{\cosh(kh)} \quad (A.1)$$

The integration of Eq. A.1 four times results in the following expression for the deflected shape of the beam

$$y(x) = A_1 \left[ \cosh(kx) + C_1 \frac{x^3}{6} + C_2 \frac{x^2}{2} + C_3 x + C_4 \right] \quad (A.2)$$

where

$$A_1 = \frac{h^4}{(kh)^4 EI \cosh(kh)}$$

and  $C_1$ ,  $C_2$ ,  $C_3$ , and  $C_4$  are constants whose values are determined by the boundary conditions of the problem.

For a simply supported beam, the deflection and the curvature at the ends of the beam vanish. Application of the two boundary conditions at  $x = 0$  yields expressions for the constants  $C_4$  and  $C_2$ .

$$C_4 = -1 \quad (A.3)$$

$$C_2 = -k^2 \quad (A.4)$$



The condition of zero curvature at  $x = h$  leads to an expression for  $C_1$ .

$$C_1 = (kh)^2 [1 - \cosh(kh)] \frac{1}{h^3} \quad (A.5)$$

Finally, for zero deflection at  $x = h$ , the remaining constant must be

$$C_3 = [1 + \frac{(kh)^2}{3} - (1 - \frac{(kh)^2}{6}) \cosh(kh)] \frac{1}{h} \quad (A.6)$$

Substitution of Eqs. A.3 through A.6 into Eq. A.2 results in

$$\begin{aligned} y(x) = & \frac{h^4}{EI (kh)^4 \cosh(kh)} \{ [\frac{(kh)^2}{6} (1 - \cosh(kh))] (\frac{x}{h})^3 \\ & - [\frac{(kh)^2}{2}] (\frac{x}{h})^2 + [1 + \frac{(kh)^2}{3} - (1 - \frac{(kh)^2}{6}) \cosh(kh)] (\frac{x}{h}) \\ & + \cosh(kx) - 1 \} \end{aligned} \quad (A.7)$$

As the parameter  $kh$  approaches zero, the load approaches a uniformly distributed load of unit magnitude. By employing the infinite series representation of the hyperbolic cosine function, it can be shown that the limiting form of Eq. A.7 as  $kh$  approaches zero is

$$\lim_{kh \rightarrow 0} y(x) = \frac{1}{24 EI} [x^4 - 2x^3h + xh^3] \quad (A.8)$$

Equation A.8 is exactly the solution for the deflection of a simply supported beam under a unit uniformly distributed load.

For large values of  $kh$ , a simplified form of Eq. A.7 may be written by noting that as  $kh$  becomes large,



$\frac{1}{\cosh(kh)}$  approaches zero,

$\frac{(kh)^2}{\cosh(kh)}$  approaches zero,

and  $\frac{\cosh(kx)}{\cosh(kh)}$  approaches  $e^{k(x-h)}$ .

The resulting simplified expression is

$$y(x)_{\text{large } kh} = \frac{h^4}{EI} \left\{ \frac{e^{k(x-h)}}{(kh)^4} - \frac{1}{6(kh)^2} \left(\frac{x}{h}\right)^3 + \left[ \frac{1}{6(kh)^2} - \frac{1}{(kh)^4} \right] \left(\frac{x}{h}\right) \right\} \quad (\text{A.9})$$



## Appendix B

## ANALYTICAL SOLUTIONS FOR THE DEFLECTED SHAPES OF A CONSTANT TENSION BEAM CAUSED BY WAVE DRAG AND INERTIA FORCE DISTRIBUTIONS

## B.1 Inertia Force Deflections

Consider the constant tension beam shown in Fig. 2.2 with a force distribution which is characteristic of the inertia force caused by water waves. The governing differential equation of the problem is

$$EI \frac{d^4 y}{dx^4} - T \frac{d^2 y}{dx^2} = \frac{\cosh(kx)}{\cosh(kh)} \quad (B.1)$$

A general solution to Eq. B.1 is

$$y = A_1 \{ C_1 + C_2 x + C_3 \cosh(\mu x) + C_4 \sinh(\mu x) + A_2 \cosh(kx) \} \quad (B.2)$$

where

$$\mu = \sqrt{\frac{T}{EI}}$$

$$A_1 = \frac{h^4}{EI \cosh(kh) [kh]^4}$$

$$A_2 = \frac{A_3}{A_3 - 1}$$

$$A_3 = \frac{k^2}{\mu^2}$$

and  $C_1$ ,  $C_2$ ,  $C_3$ , and  $C_4$  are coefficients which are determined by the boundary conditions of the problem.





The four boundary conditions are that the deflection and moment (or curvature) at each end of the beam are zero. If the curvature at  $x = 0$  is zero, then

$$C_3 = -A_2 A_3 \quad (\text{B.3})$$

For the curvature to vanish at  $x = h$ , it is necessary that

$$C_4 = \frac{A_2 A_3}{\sinh(\mu h)} [\cosh(\mu h) - \cosh(kh)] \quad (\text{B.4})$$

The condition of zero deflection at  $x = 0$  implies that

$$C_1 = A_3 \quad (\text{B.5})$$

Finally, for the deflection to vanish at  $x = h$ , the remaining constant must be

$$C_2 = -\frac{A_3}{h} [1 - \cosh(kh)] \quad (\text{B.6})$$

Substitution of Eqs. B.3 through B.6 into Eq. B.2 yields

$$\begin{aligned} y = & \frac{h^4}{EI (kh)^4 \cosh(kh)} \left[ \frac{k}{\mu} \right]^2 \{ 1 - [1 - \cosh(kh)] \frac{x}{h} \\ & - \frac{k^2}{k^2 - \mu^2} \cosh \mu x + \frac{k^2}{k^2 - \mu^2} [\cosh(\mu h) - \cosh(kh)] \frac{\sinh \mu x}{\sinh \mu h} \\ & + \frac{\mu^2}{k^2 - \mu^2} \cosh kx \} \end{aligned} \quad (\text{B.7})$$

A simplified version of Eq. B.7 may be written for large values of  $kh$  where  $e^{-kh}$  approaches zero and  $\cosh(kh)$  approaches  $1/2e^{kh}$ . The resulting expression for deflection is



$$y = \frac{h^4}{EI} \frac{A_3}{(kh)^4} \left\{ \frac{x}{h} - A_2 e^{\mu x - kh} + \frac{A_2}{\sinh(\mu h)} \right. \\ \left. \cdot [e^{(\mu-k)h} - 1] \sinh(\mu x) + \frac{A_2}{A_3} [e^{k(x-h)}] \right\} \quad (B.8)$$

It is also of interest to examine the left end rotation of the constant tension beam. This rotation is analogous to the bottom rotation of a marine riser. The general solution for the left end rotation is obtained by evaluating the first derivative of Eq. B.7 with respect to  $x$  at  $x = 0$ .

$$y'(0) = \frac{A_1 A_3}{h} \left\{ \cosh(kh) - 1 + \frac{A_2 \mu h}{\sinh(\mu h)} [\cosh(\mu h) - \cosh(kh)] \right\} \quad (B.9)$$

A similar expression for the left end rotation when  $kh$  is large is obtained from the first derivative of Eq. B.8 with respect to  $x$ , evaluated at  $x = 0$ .

$$y'(0) = \frac{h^3}{EI} \frac{A_3}{[kh]^4} \left\{ 1 + \frac{A_2 \mu h}{\sinh(\mu h)} [e^{(\mu-k)h} - 1] \right\} \quad (B.10)$$

## B.2 Drag Force Deflections

The governing differential equation of a constant tension beam having an applied force distribution which is characteristic of the water wave drag force is

$$EI \frac{d^4 y}{dx^4} - T \frac{d^2 y}{dx^2} = \left[ \frac{\cosh(kx)}{\cosh(kh)} \right]^2 \quad (B.11)$$



The general solution to Eq. B.11 is given by

$$y = A_1 \{ C_1 + C_2 x + C_3 \cosh (\mu x) + C_4 \sinh (\mu x) \\ + A_2 \cosh (2kx) - 2A_3 (kh)^2 \left( \frac{x}{h} \right)^2 \} \quad (\text{B.12})$$

where

$$A_1 = \frac{h^4}{EI} \left[ \frac{1}{8 (kh)^4 \cosh^2 (kh)} \right]$$

$$A_2 = \frac{1}{4 - \left( \frac{\mu}{k} \right)^2}$$

and

$$A_3 = \left( \frac{k}{\mu} \right)^2$$

In order to satisfy the conditions of zero bending moment and zero deflection at  $x = 0$ , the coefficients  $C_3$  and  $C_1$  must be

$$C_3 = 4A_3[A_3 - A_2] \quad (\text{B.13})$$

and

$$C_1 = A_2[4A_3 - 1] - 4A_3^2 \quad (\text{B.14})$$

Because the bending moment at  $x = h$  is zero, the coefficient  $C_4$  is given by

$$C_4 = \frac{4A_3}{\sinh (\mu h)} [A_3 - A_2 \cosh (2kh) + (A_2 - A_3) \cosh (\mu h)] \quad (\text{B.15})$$

Finally, for the deflection to vanish at  $x = h$ , the remaining coefficient must be



$$C_2 = \frac{1}{h} \{A_2[4A_3 - 1][\cosh(2kh) - 1] + 2A_3(kh)^2\} \quad (B.16)$$

The substitution of Eqs. B.13 through B.16 into Eq. B.12 leads to

$$\begin{aligned} y = & A_1 A_3 \{-2(kh)^2 \left(\frac{x}{h}\right)^2 + [\cosh(2kh) - 1 + 2(kh)^2] \left(\frac{x}{h}\right) \\ & + [1 - 4A_3] + 4[A_3 - A_2] \cosh(\mu x) \\ & + \frac{4}{\sinh(\mu h)} [A_3 - A_2 \cosh(2kh) + (A_2 - A_3) \cosh(\mu h)] \sinh(\mu x) \\ & + \frac{A_2}{A_3} \cosh(2kx)\} \end{aligned} \quad (B.17)$$

Equation B.17 may be simplified somewhat for large values of  $kh$ , where

$$e^{-2kh} \approx 0$$

$$\cosh 2(kh) \approx \frac{1}{4} e^{2kh}$$

and

$$\cosh(2kh) \approx \frac{1}{2} e^{2kh}$$

The resulting simplified expression for the deflection is

$$\begin{aligned} y_{\text{large } kh} = & \frac{h^4}{EI} \frac{1}{4(kh)^4} \{A_3 \frac{x}{h} - [C_3 e^{(\mu-2k)h} + 4A_2 A_3] \frac{\sinh \mu x}{\sinh \mu h} \\ & + C_3 e^{(\mu x - 2kh)} + A_2 e^{2k(x-h)}\} \end{aligned} \quad (B.18)$$

where  $C_3$  is given by Eq. B.13.

The left end rotation for the general case is obtained from the first derivative of Eq. B.12 with respect to  $x$ , evaluated at  $x = 0$ .





$$y'(0) = A_1 \{C_2 + \mu C_4\} \quad (\text{B.19})$$

An expression for left end rotation when  $kh$  is large is obtained from Eq. B.18

$$y'(0)_{\text{large } kh} = \frac{h^3}{EI} \frac{1}{4(kh)^4} \left\{ A_3 - \frac{\mu h}{\sinh(\mu h)} \right. \\ \left. \cdot [C_3 e^{(\mu-2k)h} + 4A_2 A_3] \right\} \quad (\text{B.20})$$



## Appendix C

## SEA SURFACE ELEVATION SPECTRA

Oceanographic literature contains several formulas for the one-dimensional sea surface elevation spectral density function. These formulas have been derived by applying time series analysis techniques to ocean wave records. Each of the formulas differs somewhat from the others because of differences in the raw data analyzed as well as differences in methods of analysis.

Three of the more commonly used spectral density functions are those developed by Pierson, Neumann, and James<sup>14</sup> (PNJ); Sverdrup, Munk, and Bretschneider<sup>15</sup> (SMB); and Pierson and Moskowitz<sup>16</sup> (PM), each of which is defined somewhat differently. While the area under the PM spectrum is equal to the variance of the wave record,<sup>16</sup> the integral of the PNJ spectrum is equal to twice the variance of the wave record, and the integral of the SMB spectrum is eight times the variance of the wave record.<sup>11</sup> In this thesis, the sea surface elevation spectral density is defined in the same way as the PM spectral density function. Thus, the variance of the wave record is given by

$$\sigma_{\eta}^2 = \int_0^{\infty} S_{\eta\eta}(\Omega) d\Omega \quad (C.1)$$

Therefore, the PNJ and SMB spectral density functions given here are one-half and one-eighth, respectively, of the spectral density functions usually found in the literature.

The PNJ spectral density function for a fully developed sea, as given by Kinsman<sup>36</sup> and modified to satisfy Eq. C.1, is



$$S_{nnPNJ} = 25.8 \Omega^{-6} \exp \left[ -2 \left( \frac{g}{\Omega v_w} \right)^2 \right] \quad (C.2)$$

where  $S_{nnPNJ}$  is in feet<sup>2</sup>-seconds,  $\Omega$  is the circular frequency in radians per second, and  $v_w$  is the wind velocity. For a fully developed sea, the SMB spectrum,<sup>15</sup> modified to agree with Eq. C.1, is given by

$$S_{nnSMB} = 0.959 \Omega^{-5} \exp \left[ - \frac{6150}{(v_w \Omega)^4} \right] \quad (C.3)$$

where  $S_{nnSMB}$  is again in feet<sup>2</sup> seconds and the wind velocity is in knots.

The Pierson-Moskowitz spectrum<sup>16</sup> is given by

$$S_{nnPM} = 8.4 \Omega^{-5} \exp \left[ -0.74 \left( \frac{g}{v_w \Omega} \right)^4 \right] \quad (C.4)$$

Figures C.1, C.2, and C.3 show the three spectra for fully developed seas and wind velocities of 20, 30, and 40 knots. For a given wind velocity, the shapes of the three spectra are different. In particular, the peak of the SMB spectrum is sharper and is located at lower frequencies than the peaks of the other two spectra.

It can be shown that the energy density, or total average energy per unit surface area of the sea, is equal to the unit weight of the water multiplied by the variance of the sea surface elevation.<sup>26</sup> Thus, the area under the spectral density function is a measure of the energy density. Integration of Eqs. C.2, C.3, and C.4 leads to expressions for the energy density,  $E^*$ , in foot-pounds per square foot of sea surface, in terms of the wind velocity,  $v_w$ , in knots.

$$E_{PNJ}^* = 7.62 \times 10^{-5} v_w^5 \quad (C.5)$$



$$E_{\text{SMB}}^* = 2.51 \times 10^{-3} v_w^4 \quad (\text{C.6})$$

$$E_{\text{PM}}^* = 1.39 \times 10^{-3} v_w^4 \quad (\text{C.7})$$

In Fig. C.4, the variation of energy density with wind velocity is shown for the three spectra. Except at wind velocities of 18.25 knots and 32.9 knots, where the PNJ curve crosses the PM and SMB curves, each of the three spectral density formulas predicts a different energy density for the fully developed sea at a given wind velocity.





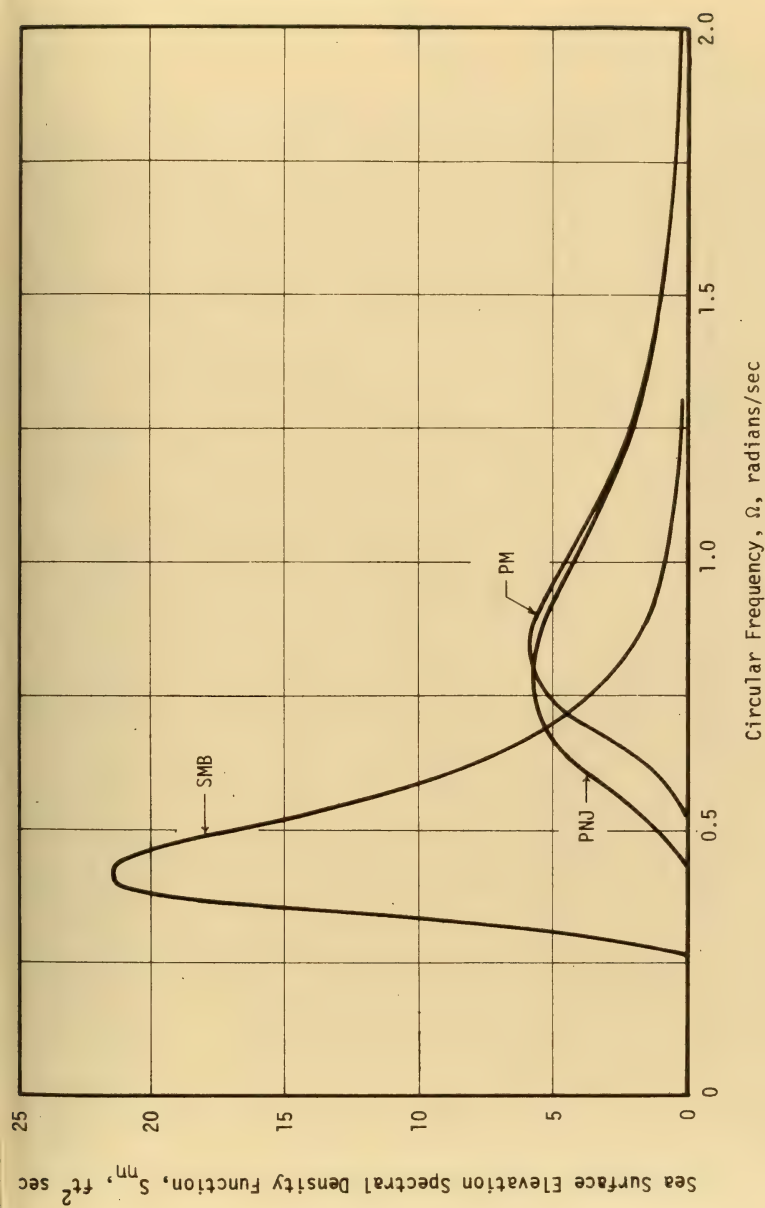


Fig. C.1 Sea Surface Elevation Spectra, 20 Knot Wind



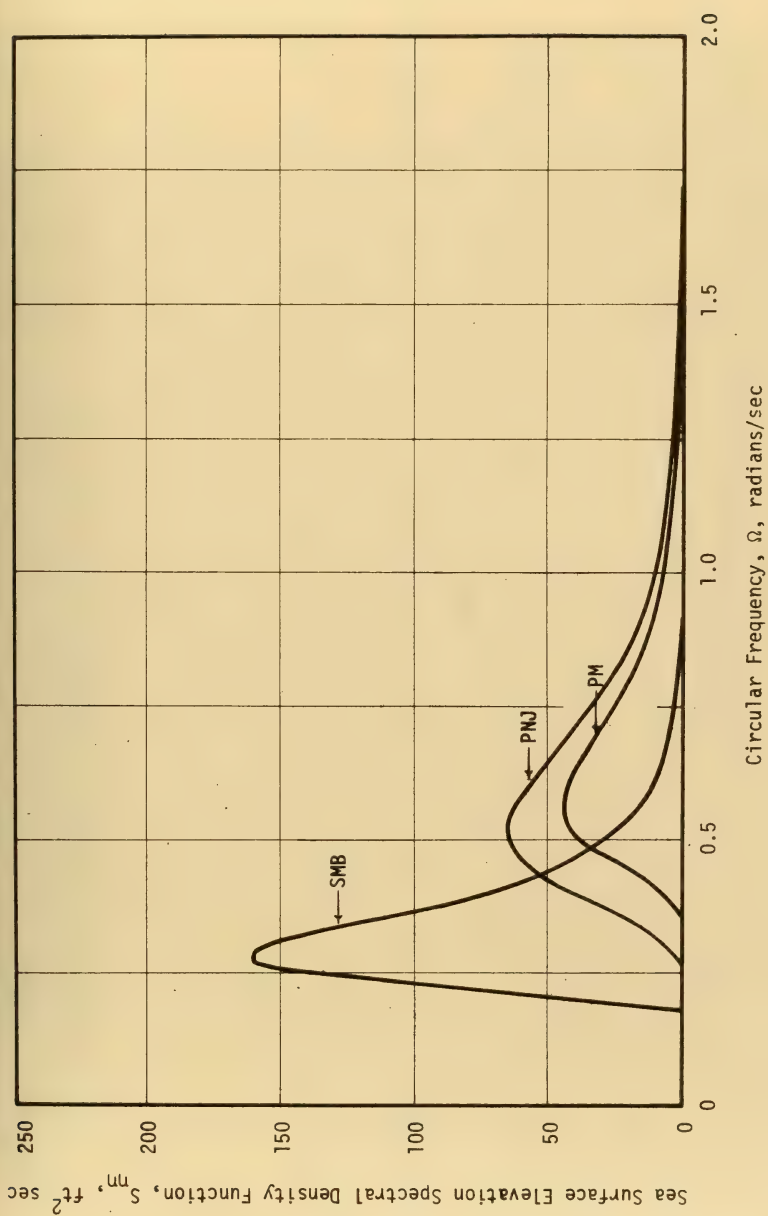


Fig. C.2 Sea Surface Elevation Spectra, 30 Knot Wind



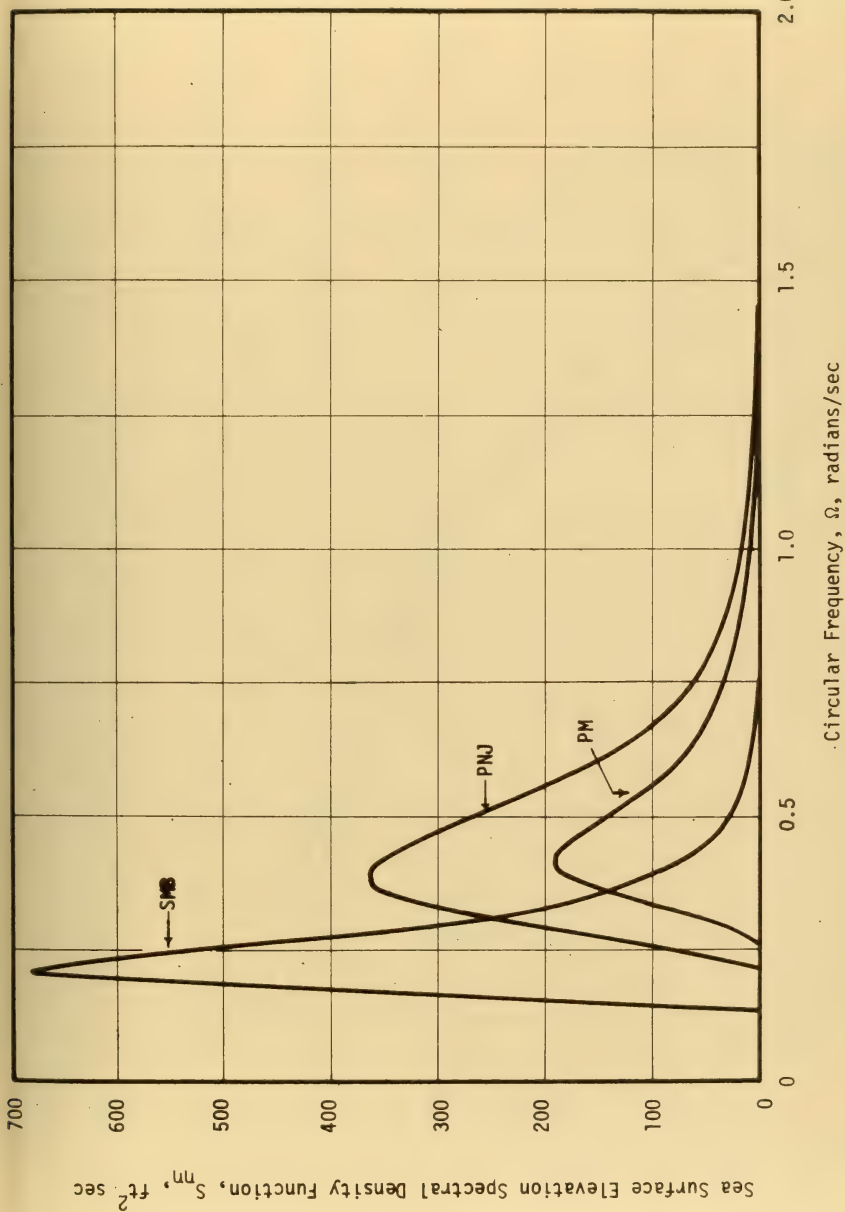


Fig. C.3 Sea Surface Elevation Spectra, 40 Knot Wind



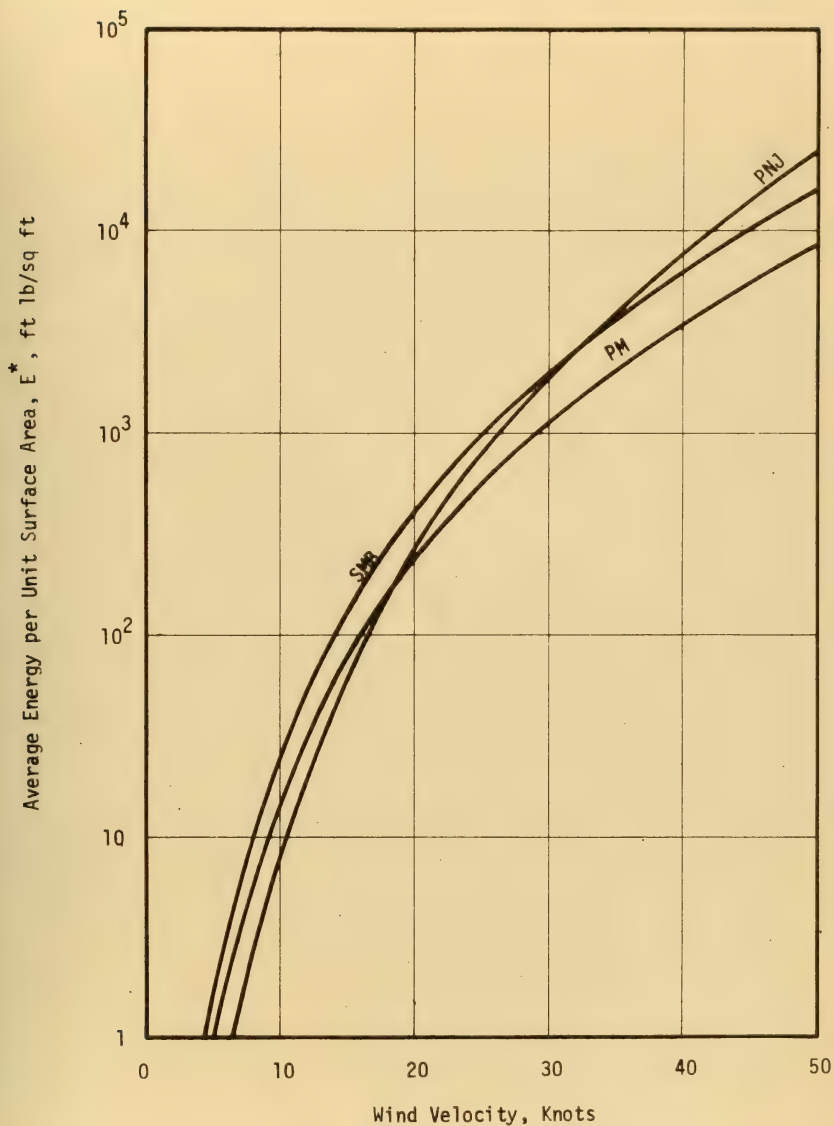


Fig. C.4 Average Energy Densities for Three Wave Spectra





## VITA

Tracy Clark Tucker was born in Silver Creek, New York, on April 21, 1939. Upon graduation from Silver Creek High School in 1956, he entered the United States Naval Academy, from which he graduated in 1960 with a Bachelor of Science degree and a commission in the Civil Engineer Corps, United States Navy. Following a year of duty in the Public Works Department at the Naval Air Station, Patuxent River, Maryland, he earned a Bachelor of Civil Engineering degree at Rensselaer Polytechnic Institute in 1962. After two years with the Atlantic Division, Bureau of Yards and Docks, he enrolled in the University of Illinois in 1964.

In 1966, his graduate education was interrupted by a two-year tour of duty with Naval Mobile Construction Battalion SEVEN serving in Vietnam, which was followed by a two-year assignment as an instructor at the Civil Engineer Corps Officers School, Port Hueneme, California. In 1970, he returned to the University of Illinois to complete his graduate studies.

He currently holds the rank of Lieutenant Commander, United States Navy, is a registered Professional Engineer in the state of Pennsylvania, and is a member of the American Society of Civil Engineers, Tau Beta Pi, Chi Epsilon, Phi Kappa Phi, and Sigma Xi.







REF ID: A61111  
BINDERY

Thesis  
T846

Tucker

134036

A mathematical model  
for the nondeterminis-  
tic analysis of a ma-  
rine riser.

19 SEP 72

BINDERY  
DISPLAY

Thesis  
T846

Tucker

134036

A mathematical model  
for the nondeterminis-  
tic analysis of a ma-  
rine riser.

thesT846

A mathematical model for the nondetermin



3 2768 001 88867 0

DUDLEY KNOX LIBRARY